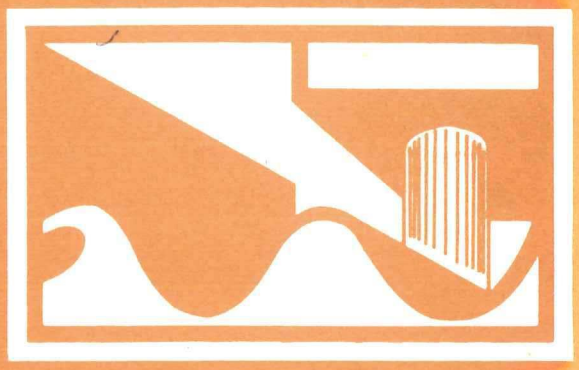

COASTAL ENGINEERING

Volume II
HARBOR AND BEACH PROBLEMS

Coastal Engineering Group
Department of Civil Engineering
Delft University of Technology
Delft, The Netherlands

COASTAL ENGINEERING

Volume II

Harbor and Beach Problems

edited by

W.W. Massie, P.E.

Coastal Engineering Group
Department of Civil Engineering
Delft University of Technology
DELFT
The Netherlands

Spring 1978.

I hear and I forget.

I see and I remember.

I do and I understand.

Confucius.

TABLE OF CONTENTS - Volume II

Harbor and Beach Problems

LIST OF TABLES

LIST OF FIGURES

1. INTRODUCTION

W.W. Massie

This second volume of the series on coastal engineering is intended as an amplification of certain topics mentioned in volume I. The organization is much the same as in the first book; two of the four main topic categories get emphasis here: harbors and coastal morphology.

Background material related to radiation stress is introduced briefly in chapter 9. Otherwise, background information is drawn from the first volume.

Again in this volume, we use an American rather than English spelling and the more difficult technical words are also included in the separately available word list.

Figures are drawn to scale unless otherwise noted, and we have sought to use consistent notation throughout this volume, at least, and as much as possible, throughout the entire set of notes.

Literature references are mentioned by author's name and year in the text; a complete listing is included in the back of the volume. Tables of symbols are also included in the back of the volume.

The technical topics to be treated in this volume are briefly summarized in the following chapter of this book. Contributing staff members are listed in table 1.1. Those responsible for the technical accuracy of each of the chapters are listed at the start of each chapter.

Table 1.1 Contributors to this volume.

Prof.dr.ir. E.W. Bijker, Professor
Ir. J.J. van Dijk, Senior Scientific Officer
Ir. J. van de Graaff, Scientific Officer
Ir. L.E. van Loo, Senior Scientific Officer
W.W. Massie, MSc., P.E., Senior Scientific Officer
J.D. Schepers, Student Assistant
Ir. P.J. Visser, Scientific Officer

All of the above persons are members of the Coastal Engineering Group, Delft University of Technology, Delft, The Netherlands.

Several example computations are presented in this book. They are intended to illustrate the process of a computation and the results which come from it. The reader should be careful not to become too involved with the details of the computational procedures; these can be quickly enough "re-discovered" by anyone having a sufficient insight. The development of this insight is the objective of this book.

2. SURVEY OF TOPICS TREATED

W.W. Massie

2.1 Purpose

The purpose of this volume is to treat certain coastal engineering topics specifically related to harbor approaches and to coastal morphology. Each of these subareas of coastal engineering is adequately defined in chapter 2 of volume I. Harbors and coastal morphology are presented together, here, because of their strong interdependence. The construction of a harbor entrance, or even only the dredging of an approach channel, can (and usually will) upset the existing bottom morphology in the area - along the coast or in the channel. The designer of an optimum harbor entrance, therefore, must consider both shipping and morphological aspects in his design.

2.2 Subdivision

Even though these topics are strongly interrelated, an attempt to separate the subtopics has been made. The following six chapters discuss the proper dimensioning of approach channels considering navigational aspects primarily: The following five chapters provide information on the movement of ships and the utilization of this information for a channel design. In chapter 8 the various aspects of channel design are brought together in order to attempt to make an optimum channel design. Morphological processes involving sediment movements along the coast and in channels are seen to influence this optimum design significantly.

The mechanics of water movement - longshore current - along a coast is carefully unraveled in chapters 9 through 16. Beach material movement along a sandy coast is treated in chapters 17 through 19. The better sediment transport determinations are built up from the knowledge of the longshore current studied in chapter 16. The result of the sediment transport determination is a relatively simple method to predict coastline changes presented in chapter 20. This simple model is refined and improved in chapters 21 through 23.

Two specific applications of sand transport conputations conclude this volume. The evaluation of coastal defense works is discussed in chapter 24 and the prediction of channel erosion and sedimentation - chapter 25 - completes this volume and completes a cycle back to harbor approach channel optimizations discussed in chapter 8.

Two other applications of sediment transport computations - prediction of erosion near offshore structures and pipelines on the sea bed - are considered to be a bit specialized for many users of this book; discussion of these topics is postponed till volume IV.

3. SHIP MOTIONS

W.W. Massie

3.1 Introduction

The displacements (movements) of a ship relative to its position when stationary in still water are of extreme importance in the design of a harbor entrance. Vertical relative movements are of importance for channel depth determinations while horizontal movements about a given desired course line are important for channel width and collision avoidance considerations.

3.2 Vertical movements

Vertical relative displacements of ships can be caused by waves but may also occur as a result of the ship's forward speed in still water. This latter displacement can be split into two components: squat and trim while waves give rise to vertical displacements via pitch, heave, and roll. All of these motion components are defined and described below.

Squat.

Squat is a uniform sinking of the ship - an apparent increase in draft - resulting from pressure changes in the surrounding water. As the ship moves forward, water flows in the opposite direction along the ship from bow to stern. Applying the Bernoulli Theorem reveals that the pressure at a given level in this return flow must be lower than at the same elevation in still water; the surface water level drops and the ship sinks along with it. This phenomonon occurs in all waters, both deep oceans and restricted channels. In restricted channels the return flow velocity will be relatively higher because the same return flow volume must pass through a smaller cross section; the water level lowering and squat are greater, thus, in restricted channels.

Trim.

Trim is a differential sinking of the stern of a ship relative to the bow. Thus, trim is the rotation of the ship about a horizontal crosswise (beam) axis; it results from asymmetry of the return flow patterns at bow and stern. The action of the propeller wil increase the effective return flow at the stern of a well streamlined ship form such as a container ship or fast cargo vessel; such ships will trim with their stern deeper than the bow. Bulk carrier or large oil tankers, on the other hand, have a very high block coefficient* and the blunt bow leads to return current concentrations near the bow. This results in a bow-down trim.

---

* The block coefficient is defined as the ratio of the displaced water volume to the product of length, beam, and draft of the ship.

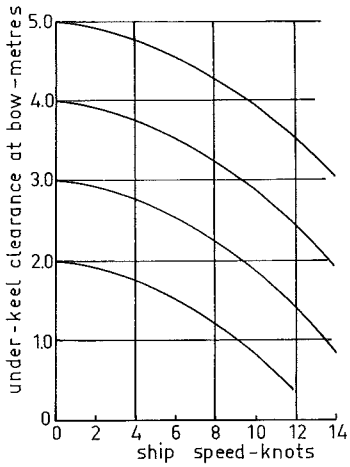

Figure 3.1
EFFECT OF SQUAT AND TRIM ON A VLCC

Figure 3.1 shows quantative results from model tests carried out at the British National Physical Laboratory reported in an anonymous article in the July 1974 issue of *The Motor Ship*. The curves show keel clearances at the bow of a 300 m long Very Large Crude Carrier as a function of speed and keel clearance at zero speed.

Wave Induced Motions.

Figure 3.2 illustrates the three wave induced vertical motions of a ship. The scale of this figure is distorted in order to clarify the illustration. The actual vertical motion of some point on the ship is determined by the superposition of heaving, pitching, and rolling motions.

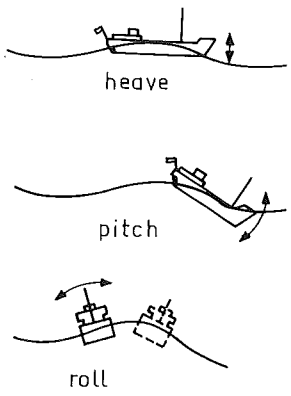

Figure 3.2
VERTICAL SHIP MOTIONS IN WAVES (not to scale)

The actual motion of the ship depends upon the size of the ship relative to the waves. In principle, heave, pitch and roll of a ship in waves can each be considered equivalent to a mass-spring dynamic system. We remember from dynamics that such systems have a natural or resonant frequency and at this frequency the displacements can be large even though the exciting forces (waves) are of small amplitude. A rowboat will respond much more violently to a wave 0.5 m high with a period of 2 seconds than will a large bulk carrier. In general, these latter ships are only slightly influenced by head seas. Beam seas, on the other hand, can excite roll motions which can be of significance for determining the maximum draft required. This results from the extreme width of such large ships. For example, if a large tanker with 60 m beam rolls only 3^o (a hardly noticable amount) its draft at one side will increase by:

$$\frac{60}{2} \sin 3^o = 1.6 \text{ m} \qquad (3.01)$$

3.3 Horizontal motions

Three horizontal ship motion components caused by waves are illustrated in figure 3.3. Additionally, use of the rudder while steaming in still water will cause a ship to yaw, sway, and roll. This last effect is most pronounced on large ships for which the center of mass is well above the center of lateral resistance. The centripetal acceleration combined with a lateral hydrodynamic resistance cause a roll moment.

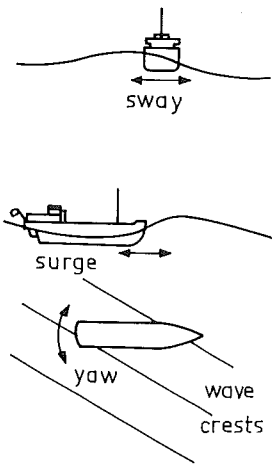

Figure 3.3
HORIZONTAL SHIP MOTIONS IN WAVES (not to scale)

Horizontal motion components yaw and sway caused by either rudder action or waves are most important for determining the required maneuvering areas and channel widths for ships underway. Surge, sway, and yaw components are important for mooring forces of ships and roll can be an additional factor in locating fenders on a quay.

3.4 Encounter frequency

A ship moving into head waves (against the direction of wave propagation) will encounter more waves per unit of time than would an observer at a fixed point. If, on the other hand, the ship were travelling with the waves, she would encounter relatively fewer waves per unit of time. A more general situation is shown in plan in figure 3.4. A formula for encounter frequency can be derived from the figure via kinematics:

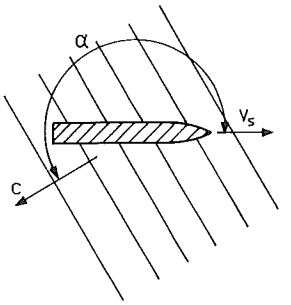

Figure 3.4
ENCOUNTER FREQUENCY DEFINITION SKETCH.

$$\omega_e = \omega \left(1 - \frac{V_s}{c} \cos \alpha \right) \qquad (3.02)$$

where c is the celerity of the wave,

V_s is the velocity of the ship,

α is the angle between the positive directions of V_s and c,

ω is the wave frequency, and

ω_e is the wave encounter frequency experienced by the ship.

Note that in figure 3.4, α is more than 90^o and thus, cos α is negative. The encounter period, T_e, can, of course, be computed from the general relation:

$$T_e = \frac{2\pi}{\omega_e} \qquad (3.03)$$

Usually, however, dynamic analyses are done using frequency as an independent parameter.

3.5 Determination of motions in waves

About 1860 Sir William Froude analyzed the motion of sailing warships of that era by assuming that the movement of the ship was the same as the average movement of the equivalent volume of water in the undisturbed wave. An equivalent form of his assumption is that the pressures exerted on the ship's hull surface are the same as those at the same location in an undisturbed wave. Many practical problems can be solved with acceptable accuracy using this simple and crude assumption. If, however, the ship's keel clearance is somewhat restricted or the ship is especially large relative to the wave length, then the disturbance (diffraction) of the on-coming wave by the ship becomes increasingly important and can no longer be neglected.

Naval architects have developed better theoretical models for computing ship motions since the time of Froude. The so-called strip theory is often used for computing heave and pitch in regular waves; the method is well documented by Comstock-editor (1967). These later methods make it possible to include wave diffraction effects and the generation of waves by the moving ship.

When the motion components of a ship are linear (all directly proportional to wave height) then it is possible to determine the total response to waves by superposition of the individual response components. Luckily, most ship response problems can be treated with linear models since the ship dimensions are usually large enough relative to the wave length - see volume IV.

The superposition principle makes it possible to determine the response of a ship to a spectrum of waves using a response function method; just as in many other problems in dynamics. We may remember from dynamics that the response functions needed to transform a force (wave) spectrum to a response (motion) spectrum can be determined by subjecting the ship to a series of constant frequency excitations (waves). Each wave frequency determines a single point in the response function. In many cases these responses can be computed. They can always be determined via model tests, and are usually obtained in the latter way except in deep water.

When the waterdepth becomes less than about 50 percent more than the ship draft, the ship response to a given wave condition becomes dependent upon the average keel clearance. As the keel clearance becomes smaller the flow pattern around the ship becomes more disturbed relative to the deep water conditions. In general, this results in a lower response function value for both horizontal and vertical motions; the ship moves less in response to a given force.

Computation of responses in real shallow water situations becomes very difficult; model tests yield the only reliable response data.

An example may make this principle more clear. Figure 3.5a illustrates a wave record and its associated spectrum, $A_\eta(\omega)$. In that figure:

$A_\eta(\omega)$ is the wave energy density (rate of change of wave energy per unit crest length with respect to frequency,

ω is the wave frequency, and

η is the water surface elevation at any instant of time.

If this spectrum, $A_\eta(\omega)$ is given for an observer at a fixed point - as it usually is -it must be replotted with a new horizontal scale based upon the encounter frequency, ω_e, using equation 3.02, and shown in figure 3.5b.

Figure 3.5c shows the response function $R(\omega)$ of a ship such as could be determined in a series of model tests using a series of regular waves of various periods.

The resulting spectrum representing the ship motion shown in figure 3.5d results from multiplying ordinates of the spectrum in figure 3.5b with corresponding ordinates in figure 3.5c. One of the many possible ship motion registrations corresponding to the determined spectrum is also shown. Since the extreme values of the original wave spectrum satisfied a Rayleigh Distribution, the extremes of the ship movement, s, can also be expected to satisfy this distribution.

Response functions will be used in the following two chapters to compute ship motions needed to determine channel depths and widths.

a. Wave record with spectrum

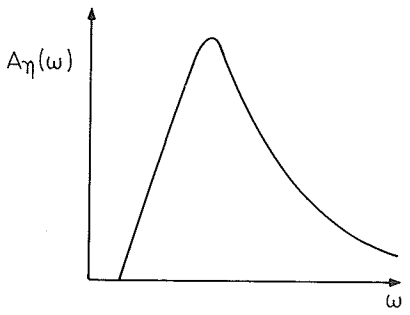

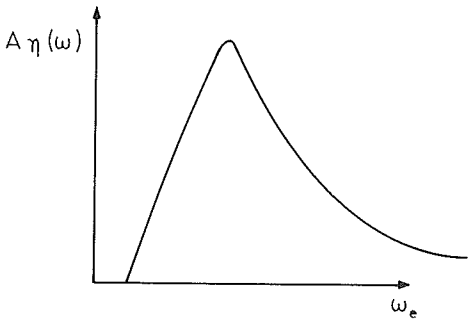

b. Transformed spectrum

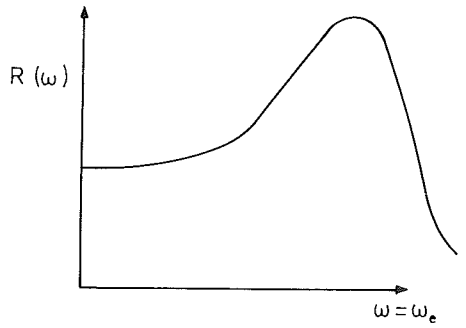

c. Response function

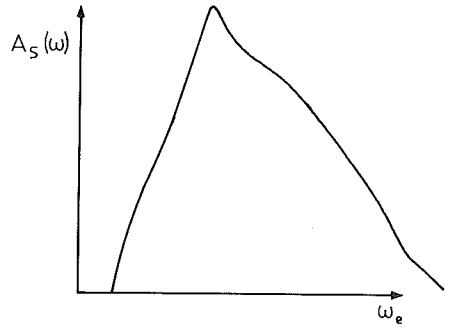

d. Resulting spectrum and motion

Figure 3.5
WAVE AND SHIP SPECTRUM

3.6 Useful Definitions and Approximations

It is often desirable to estimate approximate dimensions of a certain size ship for the purpose of preliminary harbor planning. The following definitions and approximate relationships can be handy for such work; detailed plans must be based upon more accurate data, however.

The deadweight tonnage (DWT) of a ship is its total capacity to carry cargo, supplies, and people. It thus includes the mass of crew, passengers, provisions, fuel, water, movable furniture and other supplies as well as cargo.

The lightweight tonnage of a ship includes the mass of the ship alone in a totally empty condition - all storage spaces empty.

The displacement of a ship is the mass of water displaced by the ship. Since Archimedes Principle applies to floating bodies, this displacement is also equal to the total mass of the loaded ship: the sum of lightweight and deadweight.

Further the following relationship holds:

$$\text{Displacement} = \rho\, C_B\, L\, B\, D \qquad (3.04)$$

where, B is the ship beam (width),

C_B is a so called block coefficient,

D is the ship draft,

L is the ship length, and

ρ is the mass density of water.

Normal block coefficient values for commercial ships range from about 0.4 for a fast destroyer to nearly 0.9 for a supertanker.

The gross register tonnage of a ship is a measure of its internal volume - with certain exceptions, see for example Baker (1953) - measured in units of 100 cubic feet (2.83 m^3).

The net register tonnage of a ship is a measure of the volume available for carrying revenue-earning cargo. Again, 100 cubic feet is the unit of volume used. Note that neither of the register tonnages just described are actual masses; they are actually volume measurements.

For most ships the DWT is about 1.5 times the gross register tonnage and about twice the gross register tonnage for very large crude carriers (VLCC). These relationships are dimensionally inconsistent and are valid for DWT in metric tons and register tonnages in the usual units.

Usually the displacement of a fully loaded ship is about 1.3 to 1.4 times its DWT. Further, the gross register tonnage varies from 1.7 (for freighters) to 1.3 (for VLCC) times the net register tonnage.

For most freighters, the ratio of length to beam varies between 5 and 8. Higher ratios are usually found on the faster ships. The ratio of beam to draft is usually about 2. Draft restrictions of very large ships, however, result in a somewhat higher ratio value; for them, a ratio nearer to 3 is common.

3.7 Example

The information in the previous section can be used to estimate the dimensions of a ship. Estimate, for example, the draft of a 250.000 DWT tanker.

The displacement is about 1.3 times DWT.

Displacement = 1.3 x 250.000 = 325.000 tons. (3.05)

The block coefficient is chosen as about 0.9. Since the ship will be draft limited, the beam will be about 3 times the draft:

$$B \approx 3D \tag{3.06}$$

Tankers are not fast ships; their beam is, thus, usually about 1/5 of their length or:

$$L \approx 5B \approx 15D \tag{3.07}$$

Substitution of all of this, with $\rho = 1.030$ tons/m^3 into (3.04) yields:

$$325.000 \approx (1.030)(0.9)(15D)(3D)(D) \tag{3.08}$$

$$\approx 41.72D^3 \tag{3.09}$$

or:

$$D \approx 19.8 \text{ m} \tag{3.10}$$

say, the draft is 20 meters.

4. CHANNEL DEPTH

E.W. Bijker
W.W. Massie

4.1 Factors influencing depth

The channel depth required, relative to some reference (datum) level, depends upon more than just the ship draft while floating in still water.

The actual water still water level relative to the datum is, of course, very important. Usually, the datum used for navigation charts is the long term average of the lowest measured spring low tide. It is thus Lower Low Water occurring at Spring tide (L.L.W.S.). The still water level (SWL) with reference to this datum is denoted by L in figure 4.1.

The draft of the ship floating in still water is obviously an important design parameter; it is denoted by D in the figure.

Squat and trim caused by the ship's speed through the water - see chapter 3 - also increase the channel depth required. The combined effect of these on the deepest point of the ship is denoted by Z in figure 4.1.

An additional depth, I, relative to the mean water level, will be needed to compensate for the instantaneous response of the ship, s, to the wave action.

This motion can be computed using the method described in chapter 3.

It is impossible to dredge a channel with a perfectly flat bottom. Some indication of attainable dredging tolerances is given in volume I chapter 16. The resulting bottom irregularity is a height, r, at some point relative to the mean bottom level. This is compensated by an allowance in depth, R'.

The necessary minimum maneuvering requirements of the ship dictate that a certain minimum extra depth (keel clearance) be available at all times. In general, ships become more difficult to maneuver as the keel clearance decreases. The allowance for this minimum keel clearance is indicated by c in figure 4.1.

Combining all of these as shown in the figure leads to the relationship:

$$h = R' + c + I + Z + D - L \tag{4.01}$$

where h is the mean depth* of the channel measured relative to the chart datum.

Most of the variables in equation 4.01 are time functions. For example, the allowance for this ship motion, I, is really related to the time dependent motion of the deepest point of the ship, s(t). The bottom irregularities, r, under the ship can be described by a function r(x(t)), relating the bottom irregularity to the time dependent position of the ship along the channel. Using these "new" definitions, and solving for the keel clearance yields:

$$c(t) = h + L(t) - Z - D - s(t) - r(x(t)) \tag{4.02}$$

* Actual sea charts often indicate the minimum rather than the mean depth.

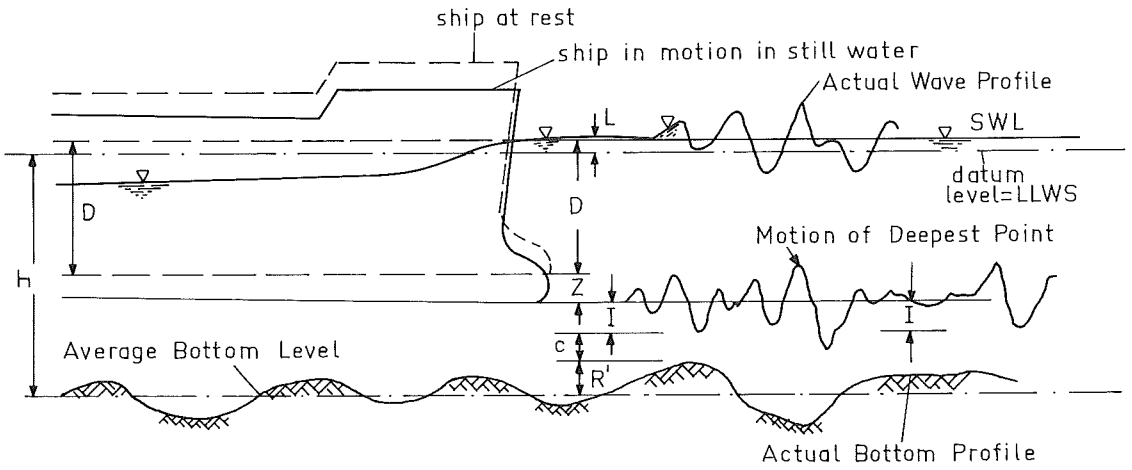

Figure 4.1
DEFINITION SKETCH FOR CHANNEL DEPTH PARAMETERS
(no scale)

4.2 Design still water level

The water level, L, relative to the chart datum chosen for channel design purposes is dependent upon many factors. One of the more important factors is the density of traffic of the design ship P. If these design ships enter the port only occassionally - every few days, for example - it is usually acceptable to delay their entry until sometime near high tide. This statement is valid, of course, only if other conditions such as currents allow safe navigation at those times.

The designer is often a bit conservative in selecting the high water level for the occasional design ship. If, for example there is a significant variation in high water levels during a month, he would choose a high water level that would be exceeded every normal day, the Higher High Water Neap (HHWN) as a basis. If shipping delays might still be too costly, a still lower level based upon the Lower High Water Neap (LHWN) might be selected. Further, dependent upon the time needed to traverse the channel, the designer should ultimately choose a design level sufficiently lower than the basis maximum so that that level will be equalled or exceeded during the passage of the ship.

Ships of extreme draft entering Rotterdam, for example, receive specific instructions advising them when to enter the outer approach channel relative to H.W. This advice is based upon the actual computed tide curve for the specific day and the ship characteristics.

The value of L in this case will usually be positive (depending upon the datum level, of course) and it will probably not vary too much during the passage of the ship. This water level variation can be included in our computations via a standard deviation, σ_L. For the problem described above this value of σ_L will be relatively low.

A problem of this type can be referred to as an "occasional ship problem" in contrast to that described below.

If, on the other hand, the design ship must enter the harbor channel very frequently - one can think of a ferry boat with a fixed time schedule entering many times each day - then the design water level must be one that can be guaranteed with almost perfect certainty. This level will probably be lower than even LLWS in order to allow for extra-ordinary conditions such as set down. This set down could be caused by a strong wind blowing from the shore, for example. Since such a low water level would be reasonably well defined, its associated value of σ_L would be small, just as with the "occasional ship problem". The choice of such a low design water level, while important for individual ship passages would be conservative for an overall channel optimization evaluation in this case; after all, most of the time a ship would be entering the channel when the water level was considerably higher. An overall channel evaluation could, then, better be based upon a water level equal to the mean sea level and a corresponding (large) standard deviation, σ_L, which included the entire tide as well as other influences. Such an approach will lead to a better overall evaluation of this "frequent ship problem" which is distinct from the "occasional ship problem", described previously.

4.3 Ship draft and movement

The draft of the ship in still water, D, depends upon more than the weight of the loaded ship. The draft depends as well upon the water density. From chapter 3 of volume I we remember that this density varies with both temperature and salinity. The draft increase of a large ship as it goes from salt to fresh water can be as much as 0.5 m.

Squat and trim of the ship have already been discussed in chapter 3, and will not be further elaborated here. Their effect must, of course, be included in the channel design, however.

The response of the ship to the wave spectrum present has been presented as well in the previous chapter. Since the maxima, I, of the downward movement, s, of the ship satisfy a Rayleigh Distribution (analogous to the waves which cause them), the probability of exceedance is given by:

$$P(I) = e^{-\frac{1}{2}\left(\frac{I}{\sigma_s}\right)^2} \qquad (4.03)$$

where: e is the base of natural logarithms,

I is the chosen ship motion peak value measured relative to the mean ship position,

P(I) is the chance that I is exceeded, and

σ_s is the standard deviation of the instantaneous ship motion, s.

Equation 4.03 resembles equation 10.02 in volume I, except that a significant value has been replaced with a standard deviation and I is measured relative to a mean. These changes change the constant in equation 4.03 - see Allersma, Massie (1973).

4.4 Channel bottom irregularities

The irregular character of the channel bottom can be caused by dredging inaccuracies as well as natural phenomona. Sediment deposition, and ripple and dune formation resulting from bed load transport along the channel are natural causes of bottom irregularity.

If the bottom irregularities, r, are schematized as a sine wave with "height" R, then the standard deviation of the bottom elevation is:

$$\sigma_r = \frac{1}{2\sqrt{2}} R = 0.3536\ R \tag{4.04}$$

It is appropriate, here, to remark about suitability of depth data. The most well-known sources of depth data are hydrographic charts published for mariners. Because these charts are for mariners, the charted depths are the shallowest depths in the vicinity; the actual sea bed lies below the surface defined by the charted depths. Thus, dredging quantities - especially initial dredging quantaties - estimated using such charts tend to be high. Generally, however, better information is also available from the various hydrographic services upon direct request. Data sheets, charting the depths used to draw the hydrographic chart, are often available. These charts show many more depth measurements, of course. Occasionally, the actual sounding records are available. Since these latter provide an extremely high density - every few meters along each profile measured - of soundings which are often uncorrected for tide, etc., they are usually more work than they are worth for our purposes.

4.5 Keel clearance

Since the water level, L, the instantaneous wave response, s, and the bottom elevation under the moving ship, r, are all variables, a statistical probability calculation seems to be appropriate in order to determine the remaining keel clearance, c. Since the standard deviations of each of the individual variables has been determined, the standard deviation of their total follows from an assumption that the variables are independent:

$$\sigma_{(L+s+r)} = \sqrt{\sigma_L^2 + \sigma_s^2 + \sigma_r^2} \tag{4.05}$$

$$= \sigma_c \tag{4.06}$$

using equation 4.02.
If the water level is assumed to be constant, then σ_L is zero. It should be emphasized that the standard deviation of the ship motions, σ_s, characterizes the response of the ship to the storm present during its passage through the channel. A whole variety of storms having different intensities can occur, however. Just as in chapter 11 of volume I, we shall choose N' different characteristic storms. Each will yield a different value for σ_s - say σ_{si}, and a related set of values σ_{ci} where i ranges from 1 to N'. We shall return to this in section 8. Until then, we shall work with a single storm - i is constant.

The standard deviation of the keel clearance is given in equation 4.06, but what minimum value, c_{min}, of this keel clearance is needed to guarantee adequate ship maneuverability? This can be determined from experience with actual ships or via model tests. These test results usually indicate that when a certain minimum keel clearance, c_{min}, is not maintained for more than a given portion of the time, damage will result. This damage will result either from a collision with other ships or from running aground alongside the channel. Methods to determine and influence this damage will be discussed in more detail in chapter 6 through 8. For now, we shall assume that c_{min} and the possible damage are known.

4.6 Channel depth optimization criteria

Two different criteria can be used to evaluate the suitability of a given channel for a given ship. The first of these has also been hinted at already in the last paragraph of the previous section - the keel clearance must be great enough to reduce the risk of collision or grounding to an acceptable level. Thus, the keel clearance, c, must be greater than the given value, c_{min}, for at least a certain percentage of the time. Equivalently, the keel clearance may be less than this given value no more than that given percentage of time. The proper value of this percentage will result from the optimization computation.

It is important to realize that this criteria depends upon the instantaneous values of the ship motion, s, rather than only their extreme values. We may remember from wave statistics, that water surface elevations are normally distributed around a mean value while the extreme values (wave heights) follow a Rayleigh Distribution. Ship motions and instantaneous keel clearances are analogous; since we are now interested in instantaneous elevations, we need to work with a Normal Distribution. This distribution is given by:

$$P(x) = \frac{1}{\sqrt{2\pi}} \int_{x}^{\infty} e^{-\frac{1}{2}q} \, dq \qquad (4.07)$$

where: P(x) is the chance that x is equalled or exceeded, and
x is the variable expressed in units of σ.
Some representative values of x and P(x) are given in table 4.1.

We need, now, to determine the chance that an instantaneous value of the keel clearance, c, is less than the minimum allowable keel clearance, c_{min}. This can be done by relating the maximum allowable displacement from the average keel clearance to the standard deviation of this keel clearance:

$$x_i = \frac{\overline{c} - c_{min}}{\sigma_{ci}} \qquad (4.08)$$

where $\overline{c}$ is the average keel clearance, provided,
c_{min} is the minimum allowable keel clearance,
σ_{ci} is the combined standard deviation from (4.06),
i is the index of the storm chosen, and
x_i is a factor corresponding to a chance $P(x_i)_i$ in table 4.1. or to x in equation 4.07.

As the channel becomes shallower, $\overline{c}$, and hence $\overline{c} - c_{min}$, decreases reducing the value of x_i. This, in turn increases the chance, $P(x_i)_i$ of a ship running into difficulty; this seems logical.

Table 4.1 Properties of Normal Distribution

P(x) (%)	x
10^{-5}	≈ 5.653
10^{-4}	4.754
10^{-3}	4.266
0.01	3.720
0.05	3.294
0.10	3.091
0.50	2.576
1.00	2.327
2.00	2.074
5.0	1.644
10.0	1.282
15.9	1.000
25.0	0.675
50.0	0.000

Note: x is made dimensionless by dividing its value by the standard deviation, σ.

The second of the two optimization criteria involves a risk that the ship hits the channel bottom. Thus, at that instant, the instantaneous keel clearance is zero. The effects of ship motion, water level variations, and bottom variations have been combined to a keel clearance variation characterized by σ_{ci}. The ship will hit the bottom, then, whenever a peak value of this variation exceeds the allowed average keel clearance. Thus, if the amplitude of the variation about the mean is denoted by c, then we need to determine the chance that c is greater than keel clearance provided, $\overline{c}$. Since extremes are now important, we can use the properties of the Rayleigh Distribution - see volume I chapter 10. The number of extremes of ship motion (and hence minima in

keel clearance) is equal to the number of waves encountered during the passage*. This can be easily computed knowing the ship speed, and wave direction and period - see section 3.4. The resulting number of waves encountered is:

$$N_i = \frac{L_c}{V_s} \frac{\omega_{ei}}{2\pi} \tag{4.09}$$

where L_c is the channel length,
i is the index of the chosen storm,
N_i is the number of waves encountered,
V_s is the velocity of the ship, and
ω_{ei} is the average wave encounter frequency.

The chance that an individual relative movement is greater than the allowed keel clearance, $\overline{c}$, is computed from the Rayleigh Distribution. In a way very similar to that in chapter 11 of volume I and equation 4.03, here:

$$P(\overline{c})_i = e^{-\frac{1}{2}(\frac{\overline{c}}{\sigma_{ci}})^2} \tag{4.10}$$

where: $\overline{c}$ is the keel clearance provided,
$P(\overline{c})_i$ is the chance that the keel clearance variation exceeds or equals $\overline{c}$,
i is the index of the chosen storm, and
σ_{ci} is the standard deviation of the keel clearance variation.

The chance that $\overline{c}$ *is not* exceeded is:

$$1 - P(\overline{c})_i \tag{4.11}$$

The chance that this is not exceeded in a series of N independent events is:

$$[\ 1 - P(\overline{c})_i\ ]^N \tag{4.12}$$

Finally, the chance that this keel clearance variation *does exceed* the clearance provided at least once during the ship's passage is:

$$E_{1i} = 1 - [\ 1 - P(\overline{c})_i\ ]^N \tag{4.13}$$

This chance, E_{1i}, corresponds in this second criterium, to the chance, $P(x_i)_i$, that a ship would be unable to maneuver adequately according to the first criterium. **

Obviously, both criteria are important for a design. A ship which cannot properly maneuver has a greater risk of drifting off course and either running aground at the edge of the channel or colliding with another ship. A ship which strikes the bottom, on the other hand, may spring a leak losing cargo which can pollute the environment or the ship may even sink in the channel blocking the passage of other ships.

---

* It has been assumed that there are many more bottom irregularities than waves.

** Although this statement is mathematically correct, the damage that can be associated with each is very different!

The chances just computed for each of the criteria above - $P(x_i)_i$ determined from the result of equation 4.08 and E_{1i} computed from equation 4.13 - are the chances that the chosen design criteria are exceeded during the passage of a single ship through the channel. This single ship passage also implies that a single given wave condition is present. This latter assumption is not immediately obvious, perhaps, but σ_{ci} includes the response of the ship to the waves and thus involves a wave height. Effects of long term wave height variations will be included in section 4.8 after we consider the effect of the number of ships present in the section 4.7.

4.7 Number of ships in channel

There is a chance, of course, that more than one, or even *no* ships are in the channel at any given instant. Information about the number of ships in the channel will be important because several ships may encounter the same storm or storms may occur when the channel is "empty" of ships. The influence of one ship on the behavior of another will not be included here.

For the "occasional ship problem" in which access to the channel is prohibited some of the time, we can guarantee that no ships will be in the channel during those prohibited times. How do we include this information on the number of ships present?

From queueing theory for a proposed harbor - see for example, Wanhill (1974) - or from observation of the traffic pattern in our (existing) harbor, we can determine the chance, p(m) that there are m design ships in our channel, where m is an integer between zero and some finite maximum value, M'. Since the values p(m) are related:

$$\sum_{m=0}^{M'} p(m) = 1 \qquad (4.14)$$

There are cases in which the values of p(m) may also be related to the storms, $p(H_{sig})_i$. Consider, for example, a fishing harbor into which an entire fleet flees as a severe storm approaches. The number and chance of ships in the channel peaks under certain storm conditions. Thus, since there were N' storm intensities in our characterization, we may need to subscript the values of p(m) and M' in (4.14) accordingly, thus:

$$\sum_{m=0}^{M'_i} p_i(m) = 1 \qquad (4.15)$$

This is not the only influence of the number of ships in the channel. From the previous section, we remember that E_{1i} is the chance that the safety margin *is not maintained for a single ship* in the channel. The chance that the safety margin *is* maintained for one ship is, thus,

$$(1 - E_{1i}) \qquad (4.16)$$

The chance that this margin is maintained for m ships is, then:

$$(1 - E_{1i})^m \qquad (4.17)$$

Notice that the chance of maintaining a safe margin for zero ships is always 1. This is logical. Also, as the number of ships, m, increases the chance that they *all* get through the channel safely gets smaller via relation 4.17; this seems proper as well.

The chance that at least one of these ships hits the bottom or cannot maneuver is, then:

$$1 - (1 - E_{1i})^{m} \tag{4.18}$$

assuming that these m ships are present.

The chance that at least one of these m ships hits *and* is present is:

$$[1 - (1-E_{1i})^{m}] \, p_i(m) \tag{4.19}$$

where $p_i(m)$ was defined early in this section.

The chance that all of this group of m ships gets through the channel without mishap is, then:

$$1 - [1 - (1-E_{1i})^{m}] \, p_i(m) \tag{4.20}$$

and the chance that all ships of this class coming through the channel in groups ranging from zero (no ships) to M' (maximum number of ships in channel at once) pass successfully is:

$$\prod_{m=0}^{M'} \left\{ 1 - [1-(1-E_{1i})^{m}] \, p_i(m) \right\} \tag{4.21}$$

and the chance that at least one of these ships runs into difficulty assuming that the i^{th} storm occurs is:

$$E'_{1i} = 1 - \prod_{m=0}^{M'_i} \left\{ 1 - [1-(1-E_1)^{m}] \, p_i(m) \right\} \tag{4.22}$$

Recapitulating, E'_{1i} is the chance that at least one ship of a given type hits the bottom or cannot maneuver properly during the predicted pattern of arrivals during one year assuming that the i^{th} type of characteristic storm occurred continuously.

4.8 Long term wave variations

Since σ_c includes the response of the ship to waves of given characteristics (described, for example, by a significant wave height, H_{sig}), the probability of occurrence of these waves should be included in our computation. If we were guaranteed that there would *always be one and only one* ship in the channel, then a computation exactly parallel to that listed in section 11.3 of volume I could be followed. We shall make this assumption for now and relax this restriction later. The chance E'_{1i} determined in the previous section using either criterium correspond to E_1 in volume I section 11.3. For convenience, we shall call E'_{1i} the chance that the required safety margin is not maintained.

The chance that *both* a given storm occurs and the safety margin *is not maintained* follows from equation 11.14 of volume I:

$$E_{2i} = p(H_{sig}) \cdot E'_{1i} \tag{4.23}$$

This can be determined for every specific characteristic significant wave height, $H_{sig\ i}$ and results in a series of values E_{2i}.

The chance that the safety margin *is maintained* during the entire year is:

$$E_3 = \prod_{i=1}^{N'} (1-E_{2i}) \qquad \text{(I-11.15)} \qquad (4.24)$$

when the entire long term wave height distribution has been divided into N' intervals as indicated in volume I.

The chance of a failure - ship difficulty - occurring during the year is then:

$$1 - E_3 \qquad (4.25)$$

4.9 Further optimization steps

Relation 4.25, just given, is the chance that our chosen design ship runs into difficulty in the proposed channel during a period of one year. In order to make an optimization as outlined in volume I chapter 13, we need to determine the annual cost of this damage. The annual cost of this damage to our chosen design ship is the chance of damage during the year multiplied by the cost of damage resulting from an accident. This cost may well include more than just the cost to the ship and cargo involved. For example, costs of delays to other ships which must wait for wreckage to be cleared and environmental consequences of resulting pollution should also be included in this cost.

It is possible that a somewhat different design ship with other characteristics and damage cost if failure occurs is also using the same channel. In principle,in fact, *every* ship using the channel has some probability of failure. In practice, however, smaller ships with a consequent large average keel clearance, $\bar{c}$, will have such a low chance of running into problems themselves that the annual cost of damage caused by these ships will be neglectable; we can, therefore, usually carry out the optimization by considering at most only a few different design ships. The total annual damage cost will then be the sum of the annual damage costs caused by each of the chosen ships.*

This annual damage cost can be thought of as a sort of insurance premium. In order to compare this to the original capital cost of the channel, it is necessary to transform this annual cost into an equivalent sum of money which, when set aside now at compound interest, would just pay for the total damage to be expected during the lifetime of the channel. This involves the determination of the present value of a series of future uniform withdrawals (payments) each equal to the annual damage cost for the entire lifetime of the channel. This present value of the future annual damage is found by multiplying the annual damage cost by the present worth factor, *pwf*. From finance,

*This damage includes much more than the direct cost to the ship causing the problem. For example, the cost of delays to other ships which must wait for a channel to be cleared of wreckage must also be included.

$$pwf = \frac{(1 + i)^{n} - 1}{i(1 + i)^{n}} \tag{4.26}$$

where: i is the interest rate per period expressed as a decimal, and
n is the number of payment periods.

The capitalized damage cost resulting from the product of the present worth factor and the annual damage cost can be added to the initial cost of building (dredging) the channel to determine the total capitalized cost of the chosen channel. Any periodic maintenance dredging of the channel could also be capitalized much like the damage costs and added to this total capitalized cost. Such an inclusion is necessary since the capitalized maintenance costs will usually depend upon the design parameters of the channel such as depth and width.

The optimum channel has the minimum capitalized cost. This minimum can be found only by repeating a whole series of the computations just outlined, each time changing *one* of the independent variables involved.

Since the number of independent variables is large - some will be listed in the next section - the number of combinations of independent variables possible is phenomonal - well above 1000. Obviously, such an optimization can only be carried out on a large digital computer.

4.10 Review

So many concepts and computation steps have been presented in the foregoing sections that it seems helpful, in review, to summarize the steps in sequence. This is done in table 4.2. The reader should be careful not to use these steps as a "cook book" for every problem. Many special cases can be conceived which are different.

Table 4.2. Channel depth optimization steps

step no.	task
1	Determine bottom irregularity and σ_r
2	Select design water level, L, and determine the associated value of σ_L.
3	Determine the wave conditions at the channel as a series of N' characteristic wave heights and periods each with an associated chance of occurrence, $p(H_{sig})$.
4	Select a design ship with an associated draft, D, squat and trim characteristics, and wave response transfer function.
5	Determine the maximum number of ships, M_i', to be expected in the channel at any one time and the probability, $p_i(m)$ of finding any number of ships, m, in the channel for each of the storms, i.

6 Select the design depth of the channel, h. This determines the keel clearance for the design ship at rest.

7 Select a ship speed. This determines the actual squat plus trim, Z, and the average keel clearance provided, $\overline{c}$, using average values in equation 4.02.

8 The ship speed and channel orientation determine the encounter frequency, ω_{ei}, for each of the N' characteristic waves. The number of waves encountered, N_i, can also be determined knowing the channel length using equation 4.09.

9 Determine the ship response standard deviations, σ_{si}, for each characteristic wave condition. This depends upon ship characteristics, speed, and average keel clearance, $\overline{c}$.

10 Compute the standard deviation of the keel clearance, σ_{ci} using equation 4.05.

*11a Compute x_i from equation 4.08 and determine $P(x_i)_i$, the chance that the ship cannot maneuver using table 4.1. Do this for each wave condition yielding N' values of $P(x_i)_i$ which are equivalent to E_{1i}.

*11b Compute the chance, E_{1i} that a single ship hits the channel bottom if always present in a continuous storm using equation 4.13 with $P(\overline{c})_i$ evaluated using equation 4.10. Do this for all N' characteristic wave conditions.

12 Compute the chance E'_{1i} that at least one ship has difficulty in the channel using equation 4.22 with i ranging from 1 to M'_i.

13 Include the long-term wave climate by computing N' values of E_{2i} using equation 4.23.

14 Compute the annual chance of damage to the shipping occurring using equation 4.25 with E_3 evaluated from equation 4.24.

15 Determine the annual damage cost for this design ship by multiplying the chance of failure - step 14 - by the total cost of one accident with this ship. This cost may be dependent upon the criterium used.

16 Determine the annual damage costs for other ships by repeating steps 4 through 15 for each ship using the channel - see text. Add all of these annual costs to get a total annual damage cost.

17 Determine the periodic channel maintenance costs.

18 Determine the initial capital investment cost of the channel as designed.

---

* Carry out either step a or step b as appropriate depending upon the criterium being used.

19 Capitalize the annual damage cost and the periodic maintenance costs using appropriate present worth factors - equation 4.26.

20 Determine the total capitalized cost of the project by adding the initial capital cost to the capitalized damage and maintenance costs.

21 Seek to minimize the resulting cost in step 20 by varying the design conditions.

There is a seemingly limitless number of possible interrelated parameter combinations which must be tested in order to find the optimum channel design. Several of these variables are listed below.

The most obvious design parameter is the depth, h. This changes the average keel clearance, $\overline{c}$, the squat plus trim, Z, and the ship motion, σ_{si}, which, in turn influences σ_{ci} and E_{1i}, etc.

Imposing an (additional) restriction upon the times during which certain ships are allowed in the channel will change L and σ_L, thus changing $\overline{c}$ and σ_c. Obviously, however, a certain minimum time must be available for the ship to traverse the length of the channel. Such a restriction is already implied in the description of the "occasional ship problem"; while it might reduce the chance of damage more dramatically in a "frequent ship problem" it would probably also increase the costs due to delayed traffic.

Reducing the speed of some of the ships would reduce the effect of squat plus trim, thus increasing $\overline{c}$. On the other hand, it would change σ_s and therefore σ_c as well as increase the number of waves encountered during the passage.

The channel alignment could be changed. This would change the ship's response to the waves and the number of waves encountered.

Ship scheduling changes or even ship delays might be imposed under certain wave conditions in order to change the number and frequency of ships in the channel.

The wave climate in the channel could be modified by constructing a breakwater. The cost of this breakwater would now have to be included in the cost of the channel, however. See volume III for details of breakwater design.

Increasing the width of the channel would reduce the damage associated with poor maneuverability while it would increase the capital cost of channel construction as well as maintenance costs.

Thousands of combinations of the above parameters can be conceived. The only possible way to conduct a true optimization will be by use of a rather large digital computer provided with sufficient quantative data. Only a small portion of such a computation is illustrated in the following section.

4.11 Example

A portion of the computations involved in a channel depth optimization are demonstrated below. While an attempt is made to keep the problem realistic looking, the actual data values are not taken from any particular harbor location. This is not, of course, detrimental to the illustrative nature of the problem.

Data

We wish to evaluate an approach channel 5 nautical miles (9266 m) long and 300 m wide. Its design depth relative to low water and measured to the average bottom level is 20 m. The design draft of the ship -a large tanker- is 18.5 meters in sea water. Waves, of which the statistical distribution is given in table 4.3 and figure 4.2, approach along the axis of the channel. The ship moves out the channel (into the waves) with a speed of 5 knots (2.573 m/s). Since we are dealing with an "occasional ship problem", the number of ships in the channel, m, and the associated chance of occurrance are:

m	$p_i(m)$
0	0.90
1	0.09
2	0.01

*

with the maximum number of ships, M', being 2. For simplicity, we shall initially assume that these conditions are true for all storm conditions given. A detailed hydrographic survey indicates that the bottom irregularities have a height of about 0.5 m.

Table 4.3 Wave and ship response data

H_{sig} (m)	$P(H_{sig})$ (storms/yr)	char. H_{sig} (m)	$p(H_{sig})$ (storms/yr)	Wave per. (sec)	σ_s (m)
10	0.33				
		9	0.97	19	1.13
8	1.30				
		7	4.0	15	0.78
6	5.3				
		5	16.7	11	0.50
4	22				
		3	70	6	0.27
2	92				
		1	1928	4	0.083
0	2020				

*A computation of the total number of ships involved yields a rather high result - more than 900 ships of this type in the channel per year. The computation procedure illustrated in this example remains valid, however.

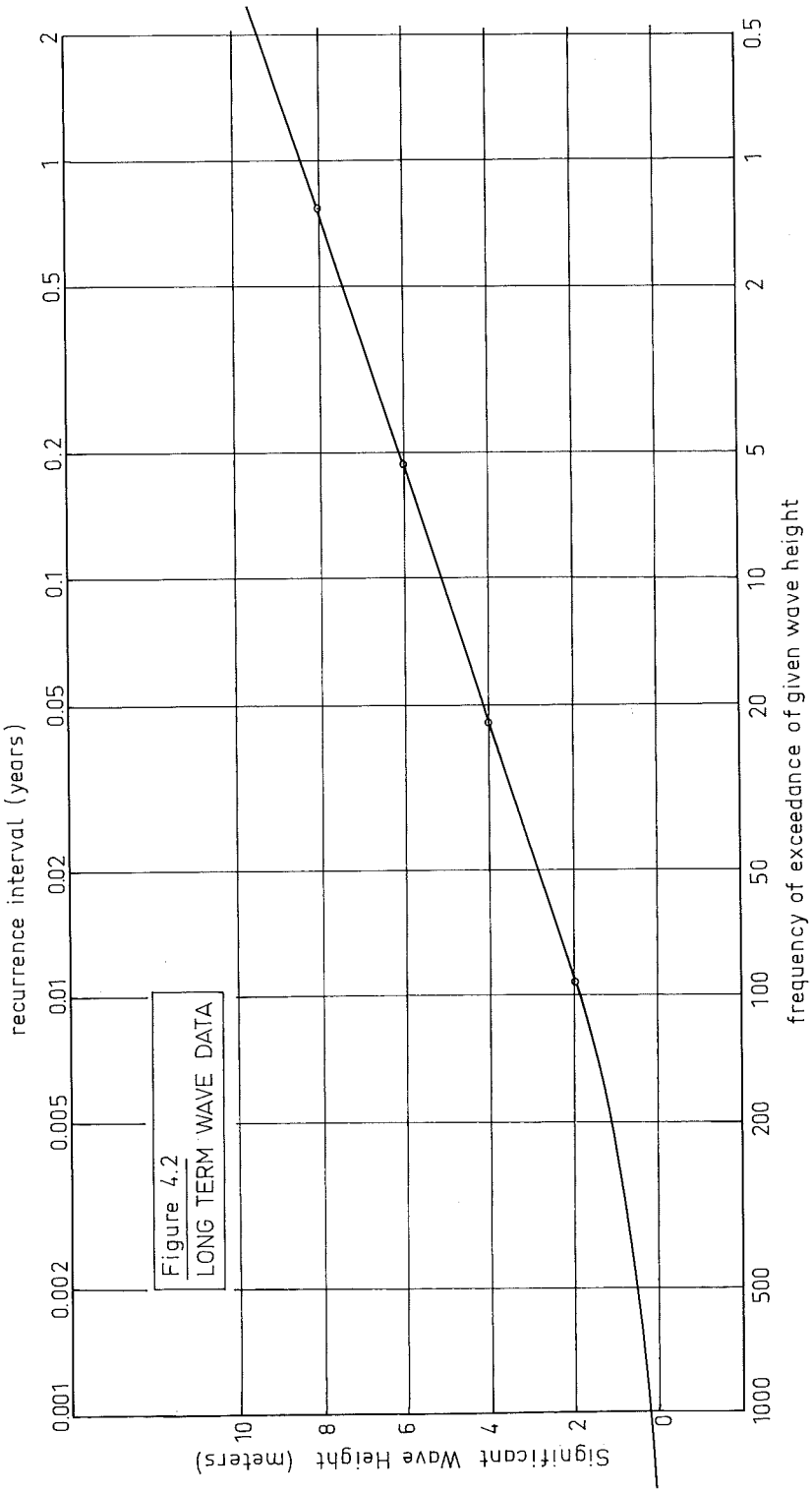

Figure 4.2
LONG TERM WAVE DATA

Ships are allowed to enter the channel only near high tide during a period when the average water level is +2.0 m and σ_L is 0.25 m. The data on squat plus trim in figure 3.1 are assumed to be valid for this ship. The standard deviation of the ship motion, σ_{si}, is listed in table 4.3 along with the wave data. Each of these values results from a computation such as that described in section 5 of chapter 3.

The design will be checked based upon a chance that the ship hits the bottom.

Solution

The calculations are outlined in table 4.4. The details of the computation for the second line, in particular, are described in more detail.

The data for the first 3 columns are given in table 4.3 and are simply repeated in table 4.4.

The deep water wave speed is calculated from the wave period using equation 5.05a of volume I:

$$c_o = \frac{g}{2\pi} T = (1.562)(15) = 23.43 \text{ m/s} \tag{4.27}$$

The actual water depth in the channel is:

$$h + L = 20 + 2 = 22 \text{ m} \tag{4.28}$$

This results in a wave speed in the channel of 13.73 m/s computed using equation 5.05 of volume I with wave length, λ, computed using a method outlined in chapter 6 of that volume.

The frequency of encounter for this wave follows from equation 3.02, in which α is now 180^0.

$$\omega_e = \frac{2\pi}{T} \left(1 - \frac{v_s}{c} \cos \alpha \right) \tag{3.02} \quad (4.29)$$

$$= \frac{2\pi}{15} \left(1 - \frac{2.574}{13.73} (-1) \right) \tag{4.30}$$

$$= 0.497 \quad \text{rad/sec} \tag{4.31}$$

The number of waves encountered is computed using equation 4.09 with the length of the channel and the ship speed coming from the given data.

$$N = \frac{9266}{2.574} \frac{0.497}{2\pi} = 285 \tag{4.32}$$

The standard deviation of the ship motion comes from the given data in table 4.3. The standard deviation of the bottom roughness can be computed from the given roughness using equation 4.04.

$$\sigma_r = (0.3536)(0.5) = 0.177 \text{ m} \tag{4.33}$$

The standard deviation of the keel clearance, σ_c, follows, then, from the data and equation 4.05.

$$\sigma_c = \sqrt{0.25^2 + 0.177^2 + 0.78^2} = 0.838 \text{ m} \tag{4.34}$$

Notice that for the higher waves in table 4.4, the influence of the ship motion - via σ_s - dominates σ_c, while for low waves, other factors dominate the standard deviation of the keel clearance.

The average keel clearance for the ship at rest can be found by putting average values in equation 4.02. The mean values of both r and s are zero, and Z is zero at rest:

$$c = 20.0 + 2.0 - 0 - 18.5 - 0 - 0 = 3.5 \text{ m} \tag{4.35}$$

Table 4.4 Ship channel evaluation computation

H_{sig} (m)	$p(H_{sig})$ (storms/yr)	Wave per. T (sec)	Deep water wave speed c_o (m/s)	Actual wave speed (m/s)	freq. of encounter ω_{ei} (rad/sec)	No. of waves N_i (-)	Ship motion std.dev. σ_s (m)	keel clear. std. dev. σ_c (m)	$P(\bar{c})$ (-)	E_1 (-)	No.of ships, m (-)	p(m) (-)	term (-)	E_1' (-)	E_{2i} (-)
											0	1.00	0.00		
9	0.97	19	29.67	14.09	0.391	224	1.13	1.171	2.39×10^{-2}	0.996	1	0	0.00	0.00	0.00
											2	0	0.00		
											0	0.90	0.00		
7	4.0	15	23.43	13.73	0.497	285	0.78	0.838	6.82×10^{-4}	0.177	1	0.08	1.42×10^{-2}	0.0205	0.0820
											2	0.02	6.45×10^{-3}		
											0	0.90	0.00		
5	16.7	11	17.18	12.90	0.685	392	0.50	0.586	3.35×10^{-7}	1.31×10^{-4}	1	0.09	1.18×10^{-5}	1.44×10^{-5}	2.40×10^{-4}
											2	0.01	2.62×10^{-6}		
											0	0.90	0.00		
3	70	6	9.37	9.24	1.339	767	0.27	0.408	4.39×10^{-14}	$<10^{-99}$	1	0.09	0.00	0.00	0.00
											2	0.01	0.00		
											0	0.90	0.00		
1	1928	4	6.25	6.25	2.218	1271	0.083	0.317	7.45×10^{-23}	$<10^{-99}$	1	0.09	0.00	0.00	0.00
											2	0.01	0.00		

Entering figure 3.1 with 3.5 m keel clearance and a speed of 5 knots yields a squat, Z, of about 0.3 meters yielding an actual average keel clearance underway, $\bar{c}$, of 3.2 meters. Values of $P(\bar{c})$ follow from equation 4.10:

$$P(\bar{c}) = e^{-\frac{1}{2}\left(\frac{3.2}{0.838}\right)^2} = 6.82\text{x}10^{-4} \tag{4.36}$$

and values of E_1 follow from equation 4.13:

$$E_1 = 1 - [\ 1 - 6.82 \times 10^{-4}\ ]^{285} = 0.177 \tag{4.37}$$

Remembering that E_1 is the chance that our ship runs aground if she happens to be sailing in the particular storm, we see that for the most severe storm listed in the table, the chance of running aground in that storm is more than 99%! Any responsible harbor master would close the channel under those conditions. We shall do so as well by changing the scheduling of the ships as indicated in the following two columns of table 4.4. We have increased the chance that two ships will be in the channel during the next most severe storm. The philosophy is that the ships may depart early if a heavy storm is approaching. Notice that equation 4.15 is still fulfilled by each set of values of p(m).

The "term" listed in the third column from the end of table 4.4 is really the term in relation 4.19. Note, for example, that each of the terms corresponding to H_{sig} = 9 m are zero because we have effectively closed the channel then by making p(m) = 0 for m > 0. Also note that these terms get smaller as E_1 gets smaller for equivalent values of p(m). (m = 0 is a special, degenerate case). The resulting values of E_1' are listed in the next to last column. For the second row in particular:

$$E_1' = 1 - (1\text{-}0)(1\text{-}1.42\text{x}10^{-2})(1\text{-}6.45\text{x}10^{-3}) \tag{4.38}$$

$$= 0.0205 \tag{4.39}$$

Note how the degenerate case, m = 0, does not influence the result.

The values of E_2 are the product of E_1' and $p(H_{sig})$ from column 2 of the table:

$$E_2 = (0.0205)(4.0) = 0.0820 \tag{4.40}$$

With this, E_3 can be evaluated using equation 4.24:

$$E_3 = (1\text{-}0)(1\text{-}0.0820)(1\text{-}2.40\text{x}10^{-4})(1\text{-}0)(1\text{-}0) \tag{4.41}$$

$$= 0.9178 \tag{4.42}$$

and the overall chance of a ship striking the bottom is-from (4.25):

$$0.0822 \text{ or } 8.2\% \tag{4.43}$$

per year. This does not seem too bad; indeed, it should not be. We chose an actual channel depth of 22 m, almost 20% more than the draft of our ship; this is a rather common rule of thumb.

This computation will not be carried further, here, even though several further steps have been indicated in section 4.9. Complete optimization computations for cases with many fewer independent variables are carried out in volume III for breakwater designs.

In the next chapter we examine the optimum width of a channel.

5. CHANNEL WIDTH

J.J. van Dijk

5.1 Introduction

In principle, an optimization technique similar to that suggested in the previous section - using a total cost basis - could be applied to the selection of an optimum channel width. Once again, the optimum would be sought by attempting to minimize the sum of construction, maintenance, and total damage costs; all of these costs should be interpreted broadly. For example, if a large tanker runs astray in a narrow channel, hits one edge and swings broadside to the channel grounding on the other edge and then sinks, the total damage cost will include the cost of:

clearing up wreckage of the tanker,
clearing up spilled oil,
possible damage to fisheries from the oil, and
costs to other ships, the harbor, and whole economy
resulting from blockage of the approach channel.

These last costs may be much greater than the first items on the list and be much more difficult to predict.

The cost determinations are not the only difficulty, however. The horizontal movements of a ship underway are determined to a large extent by the actions of the helmsman - by an unpredictable (in extreme cases) human control device. This makes a correct mathematical description of the problem even more difficult than for channel depth. Even so, some attempts have been made as are indicated in the remaining sections of this chapter.

5.2 An idealized problem

In order to arrive at a reasonable mathematical description of the phenomona involved, let us consider a ship moving up a channel of constant depth and infinite width; the sea bottom is a horizontal plane covered by a constant depth of water. The helmsman's orders are to hold the ship on a path along a given straight line. Currents will, of course, influence the ship, but there are no waves. Also, there are no other ships nearby. By eliminating the egdes of the channel and other ships we eliminate extraneous inputs to the pilot which might cause a panic type reaction.

The ship's position relative to the desired course line could probably be expected to follow a normal distribution, the same distribution used to describe the water surface elevation in irregular waves. The average position of the ship would correspond to the desired course line and the degree of variation in position relative to this line could be measured in terms of a standard deviation.

If a normal distribution adequately describes the ship's position, then, just as with waves, we can expect the distances between extremes of a ship's path to be described by a Rayleigh distribution. Thus, knowing the standard deviation of the ship's path and the number of extreme values to be expected during a given passage, we can calculate

the chance that a ship will exceed some given path width using the Rayleigh distribution. The mathematics follows that of equations 4.10 through 4.13 in the previous chapter. The chance that the ship's path goes more than a distance B away from the course line is:

$$P(B) = e^{-\frac{1}{2}\left(\frac{B}{\sigma_p}\right)^2} \tag{5.01}$$

where: B is the excursion from the course line, and
σ_p is the standard deviation of the ship's path.
The chance that B *is not* exceeded each time is:

$$1 - P(B) \tag{5.02}$$

and the chance that this *is not* exceeded in a series of N extreme values is:

$$[\ 1 - P(B)\ ]^N \tag{5.03}$$

Finally, the chance that the ship goes further than a distance B from the desired course line is:

$$E_1 = 1 - [\ 1 - P(B)\ ]^N \tag{5.04}$$

Oldenkamp (1977) has conducted an analysis of a limited amount of data available and found that for that limited data, the Rayleigh distribution *did not* describe the distribution of the extreme values exactly. He observed that the ships often tended to sail *close* and *parallel to* the desired course line rather than make the extra effort to reach the desired path exactly. For his data, a parameter $\varepsilon = 0.92$ described the best - fit distribution while $\varepsilon = 1.00$ for a Rayleigh distribution - see Allersma, Massie (1973).

How will the keel clearance influence the ship's behavior? In general, as the keel clearance becomes smaller, the ship becomes more difficult to turn. The implication of this is that the ship becomes more "course stable" as the keel clearance decreases - the ship has a greater tendency to maintain the path it happens to be on*.
This would, in turn, lead logically to a smaller number of course extremes during the passage of a given distance while these fewer extremes could be expected to be of greater magnitude as well. Thus, the standard deviation of the course would be greater, too.

This discussion has been limited to an extremely schematized problem. Factors which influence a real problem are described in the next section.

*This is true whether the path is correct or not!

5.3 A realistic problem

What are the factors influencing the actual path of a given ship under real conditions? Only after all of these influences are known and adequately described mathematically will it be possible to make meaningful statistical calculations based upon theory alone.

The most obvious unrealistic limitation of the problem in the previous section comes from the channel width. How does the edge of a channel influence the ship's path? First, as the ship nears a channel edge its hydrodynamic properties change in response to the proximity of the channel slopes; its steering characteristics change. This is in addition to changes in steering ability caused by changes in average keel clearance in the channel itself. Secondly, there can be a psycological human reaction - a panic - when the ship seems about to run aground by approaching too close to the channel markers.

Other ships either moving or moored in the vicinity will influence the behavior of our ship, again in both of the ways just described above. This problem is well known to the river engineers specialized in canal navigation.

Waves can also influence the horizontal movements of ships. Granted, their influence on the largest ships will probably be minimal, but their influence on a smaller ship such as a ferry or fishing boat can be appreciable.

Finally, a very important but unpredictable influence is the skill and disposition of the pilot.

The methods available to arrive at a somewhat resposible channel design in spite of all these difficulties are outlined in the following section and in chapter 6.

5.4 Design methods

In spite of the practical difficulties of an exact mathematical description of the physical processes involved in the determination of a ship's path, three methods have been developed which can help lead to a responsible channel design.

The oldest and most widely used technique for predicting the performance of a channel bases a prediction upon experience with similar ships in similar channels. Figure 5.1, based upon figure 7 by Eden, Jr. (1971) shows acceptable and unacceptable channel depth and width combinations for a 250.000 DWT tanker. This figure is based upon simulation data - see chapter 6. Kray (1973) summarizes the state of the art nicely. The figure gives some indication of the acceptable channel dimensions based upon the dimensions of the design ship. The method worked very well in the age when ship sizes did not increase rapidly. Extrapolation of data represented by graphs such as figure 5.1 is dangerous. In the past after a slight extrapolation had been made for a new, larger ship, new data on channel adequacy was obtained and added before a design for a still larger ship was needed. The accelerated growth of ship sizes in the last decades has made such an approach useless; the experience gained with large ships has not kept pace with the demand to design channels for even larger ones. Other

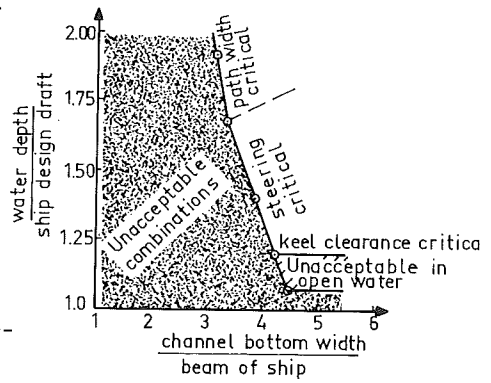

Figure 5.1
CHANNEL DESIGN PARAMETERS FOR 250000 DWT TANKER

methods have been sought and found to attack this large ship problem. There is, of course, enough data available to make it possible to design channels for smaller ships using past experience. The techniques described below will only be needed for small ships under special conditions.

A second method of approaching the design problem is, to reconstruct the actual proposed situation in a physical model. Such models, if large enough (scales of up to 1:50 are used), can reproduce the hydraulic situation almost exactly. The human pilot, however, cannot be reproduced on the proper scale. Both his time scale and scale of distance perception are distorted in a physical model. Even so, physical models have been used and will most likely continue to be used to at least determine the hydrodynamic characteristics of ships in channels. These characteristics may then be used as input to other analysis methods.

The third method available to evaluate a channel design makes use of a ship simulator, a device in which a pilot reacts with a computer in the same way that he would react with his environment in a real ship navigation situation. These ship simulators will be described in more detail in the following chapter.

5.5 Additional factors

So far, this discussion has been limited to the movement of the center of mass of a ship. Often, a ship sweeps out a path somewhat broader than the beam of the ship. For example,if a ship entered a harbor with a speed and cross current as indicated in figure 5.2, the actual swath of the ship would range - outside the breakwater - from a width of 110 m to a maximum of 232 m while the ship is only 60 m wide and 300 m long, itself.

For a large ship, the athwartships force from a cross current or wind can be substantial. The following orders of magnitude are realistic for a ship of about 120.000 deadweight tons.

A cross current of 1 knot can cause an athwartships force of about 14×10^5 N. A cross wind of 20 m/s (Beaufort force 8, from volume I, chapter 4) can cause an athwartsnips force of about 1.2×10^5 N on a loaded ship and 8×10^5 N on a empty ship.

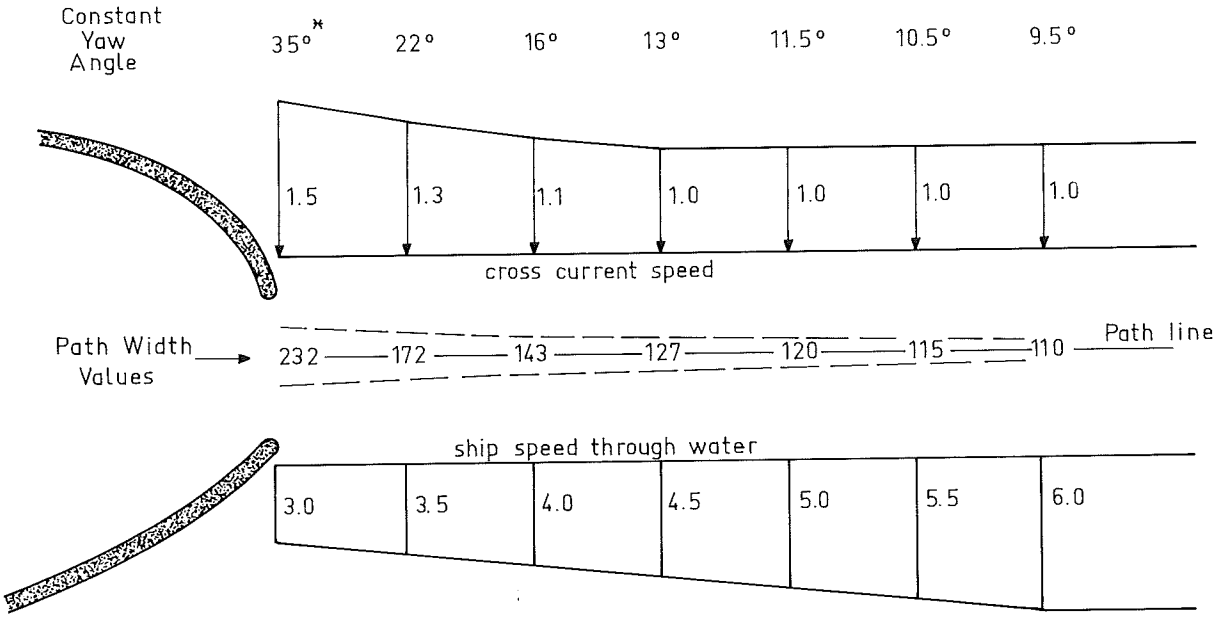

Figure 5.2
PATH WIDTH FOR SHIP 300M LONG, 60 M BEAM

* Value increased from 30° by moment resulting from current change.

6. SHIP MANEUVERING MODELS

E.W. Bijker
L.E. v. Loo
W.W. Massie

6.1 Physical models

The most obvious way to study the maneuverability of a ship at sea or in a harbor is with a full scale ship under natural conditions. Since this is often impractical for a proposed ship or harbor facility, physical models are often used. Some of the requirements for such models and their associated shortcomings are described below.

Since the time scale is distorted in any physical model, (time is not reproduced on a one-to-one basis) it is impossible to include this scale in the perceptive capability of the human pilot. Additionally, because of his size, the pilot cannot always be located in the proper relative position aboard his model ship. His visual impression will be different from that which he would experience standing on the bridge of a full scale ship. If he is located outside the model ship (on the shore, for example) he will not notice small course changes as easily but will have an advantage of having a better overall view of the total situation. Even when the pilot's head has been brought into the proper relative location on a ship model, he still has a relative advantage because his visual depth perception is more sensitive at the shorter distances encountered in the model. With normal binocular vision, distances can usually be estimated rather well up to about 200 m. Obviously, much more distance information is present within a range of 200 m on a model than in prototype*. This binocular vision benefit in a model can be compensated by covering one of the pilot's eyes.

Table 6.1 illustrates the characteristic dimensions of a model of the supertanker "Esso Atlantic". One sees that these ships are large - even on a model scale of 1:50, they have a higher displacement than many pleasure yachts. On the other hand, such supertankers have relatively little power, a yacht of size comparable to the 1:50 model would have a few hundred times as much power.

Ship models based at least partially upon computers will be described in the following sections.

Table 6.1 Characteristics of "Esso Atlantic" in prototype and in model.

scale	dead-weight (tons)	displ. (tons)	length (m)	beam (m)	depth (m)	draft (m)	power (kw)	speed (kt)
1	508731	≈670000	406.6	71.0	31.2	25.0	33570	16
25	32.56	42.88	16.2	2.84	1.25	1.0	.430	3.2
50	4.07	5.36	8.13	1.42	0.62	0.5	.038	2.26

*On a large tanker, even the bow of the ship is more than 200 m away!

6.2 The simulation approach

Ship simulators are machines upon which a pilot can experience the maneuvering of a given ship in a given situation. While physical models, just described in the previous section, satisfy this definition, we shall restrict ourselves, now, to machines upon which the human element can be handled on a natural time scale. A similar, perhaps better known simulator of the type of interest here, is the aircraft flight simulator used to train airline and military pilots. The basic property of all simulators of this type is that the pilot is made to think he is piloting an actual ship under real conditions. How this is accomplished with less than an actual ship is explained in the following section.

6.3 Description of ship simulator

The description which follows gives the general features of the more advanced ship maneuvering simulators available. There are as many differences in detail as there are individual simulators; no particular simulator is described here.

The most obvious part of a ship simulator is a full sized ship's bridge complete with all the amenities such as chart table, compass, radar, other navigation instruments, and perhaps even the coffee pot; all of the instruments work. For the moment, our pilot is on a real ship's bridge on a moored ship in a thick fog for nothing can be seen - yet - looking off from the bridge.

A second, much less obvious (in fact seldom seen), component of the simulator is a large computer. Both hybrid and pure digital computers have been used in the past; digital computers have developed sufficient computational speed recently to be winning the application contest at the moment. The computer is connected to all of the bridge instruments gathering input from the ships's bridge controls and guiding the read-out instruments accordingly. For example, when the helmsman turns the steering wheel to port, the rudder angle indicator is changed accordingly by the computer. Further, the control measures ordered by the pilot are used as input for the computation of changes in the speed and heading of the ship. These changes are also reported - at a proper time scale - to the pilot via his instruments on the bridge. The coordinates on the position determining system and the compass and speed indicator all reflect the ship's response to the pilot's orders. How is this response determined for a given ship in a given channel? This is just exactly the relationship or set of relationships needed for a direct statistical analysis suggested back in chapter 5! Because these relationships cannot, in general, be analytically predicted, the only hope is to determine them emperically based upon either prototype or physical model studies. Indeed, a series of standard tests, such as a zig-zag test, routinely carried out during trials of a new ship can be used to provide many of the necessary coefficients or relationships. More specific effects such as the influence of the proximity to the channel side slopes are best determined by conducting a series of "standard" maneuvers with a

physical model. With all of these relationships available, the computer can determine the path of the ship and change the instrument readings accordingly. The specific emperical nature of the resulting relationships makes theoretical statistical analysis unrewarding. The pilot is now navigating his ship but is still operating in a dense fog; he can see nothing looking out from the bridge.

Some use only the two components described above. The more sophisticated simulators, however, add a spatial dimension to the surroundings. The more succesful of these additions to the system project an image of the surroundings - buoys, coast, navigation lights, etc. on a screen surrounding the bridge. This projected image is, of course, also modified continuously to correspond to that seen by someone standing on an actual moving ship bridge. The best simulators generate this image of the surroundings by projecting the shadow image of a physical model on to the surrounding screen. A small but intense light source occupies the same position in the model as the ship's bridge. The light moves relative to the model (actually the model is moved relative to the fixed light) in order to modify the projected image. Thus, a turn of the ship results, in fact, in an opposite rotation of the model. Such a projected image removes the pilot from the "fog bank" and provides valuable extra visual data to the pilot. The realism is made even more complete by projecting an image of the bow of the ship - as seen from the bridge - onto the same surrounding screen. In principle, it is simple enough to project images of other ships in order to simulate various ship traffic conditions.

The computer controls this projection model as well, of course. In addition, the computer can compile statistics of the simulation run during its progress. The standard deviation of the actual ship's path relative to the described path can be determined, for example.

6.4 Ship simulator uses

Such a ship maneuvering simulator has many uses. The most obvious is probably the training of new harbor pilots just as the airlines use flight simulators. Unfortunately, the high expense of such a simulation facility have prevented its getting much use for this purpose.

The simulator can be used to evaluate ship movements during approaches to a proposed harbor. This is, indeed, how we as harbor designers can utilize the simulator most effectively. Alternatively, the behavior of a new type of ship approaching an existing harbor can be simulated. The data obtained from a number of "trials" with such a simulator can provide much valuable data for the evaluation of a whole harbor layout as well as the approach channel.

A simulator has even been used in the offshore industry to develop an optimum tugboat deployment and operation strategy to position a large gravity structure and hold it in position in the North Sea while it was sinking on to the sea bed.

Even situations not commonly ecountered (luckily) such as mechanical failures of the steering gear can be simulated. "What to do if." strategies can be developed from experience gained in this way.

The data reported by Oldenkamp (1977), referred to in the previous chapter, was even obtained on a simulator.

6.5 Critical remarks

Ship maneuvering simulators have made it possible to obtain much useful data on the behavior of a given ship under given conditions. This can be invaluable for the evaluation of harbor designs. Unfortunately, the simulation results still have some limitations.

Not *all* possible inputs to a simulation model are included. Effects of wave action, so important for smaller ships especially, are seldom if ever included, for example. Most simulators do not provide for the pilot to call on tugboats for assistance. It is doubtful whether the effects of, for example, varying the side slopes of an approach channel are accurately enough determined in a physical model for inclusion in successive simulation runs.

Even if their results do not represent the "absolute truth," simulations can, of course, still provide valuable information to the designer.

In some cases, a designer will be tempted to improve the handling characteristics of ships using his proposed harbor as an alternative to designing a much wider channel or harbor entrance. Data on what can be expected from tugboat assistance is provided in chapter 7.

7. MANEUVERABILITY IMPROVEMENT

L.E. v. Loo

7.1 Motivation

Often a harbor designer is faced with a decision concerning two design alternatives: A "modest" channel in which at least some ships will present too high a risk of mishap caused by maneuverability problems, or a "spaciously" dimensioned channel in which all ship can navigate safely. The second alternative may look very attractive until the capital costs of such an extensive harbor and channel area are computed and the port facilities planner starts protesting.

Methods to make the first of the above alternatives attractive are the subject of this chapter. A couple of methods have already been hinted at: modify the channel alignment to make maneuvering easier by, for example, reducing cross currents. A second, but expensive alternative solution is to construct breakwaters in order to block or re-direct cross currents in order to reduce their detrimental effects. In some places even special wind screens have been built - but only within a harbor - to reduce wind effects on maneuvering, slow-moving ships.

Why do ships encounter maneuvering difficulties? As has already has been pointed out in chapter 5, a cross current can cause a ship to sweep out a wider path than normal. As the ship speed through the water decreases, this influence becomes more pronounced. The relatively low forward speed of ships in and near harbors makes their rudders less effective as well. This reduction is even worse when the propeller is stopped in order to slow down the ship more rapidly. Since the rudder is often located just aft of the propeller, loss of its jet also reduces rudder effectiveness. If a ship throws the propeller into reverse to slow down even faster, there is a good chance that all steerability will be lost. Indeed, when a large tanker (200.000 DWT) makes an emergency stop from a speed of about 15 knots (7.7 m/s), it will have a stopping distance of about 2.5 nautical miles (4.6 km) and will most certainly *not* remain on course*. A much more practical alternative where there is adequate space, is for a tanker captain to call for full speed ahead and put the helm hard over making a controlled U turn. In this way, he can succesfully avoid an obstacle only a little more than a kilometer ahead. Obviously, such a maneuver is not practical in a channel.

*The stern of a ship equipped with a right-hand (clockwise turning) propeller will tend to swing to port when the propeller is turning in reverse. Thus, the bow of the ship swings to starboard if the ship is still moving ahead.

7.2 Tugboat assistance

One alternative open to a ship captain navigating in a restricted waterway is to enlist the assistance of tugboats. Only small ships can utilize tugboats as "brakes" effectively. For large ships (the definition of large depends somewhat on the tugboats available, but 50.000 DWT is always a large ship) tugboats can be most efficiently used to counteract cross-current influences and hold the ship on course, generally. With the steering task taken over by the tugs, the ship can reverse its propeller, if necessary, in order to decelerate more rapidly. Figure 7.1 shows stopping distance data for three types of tankers based upon field observations at Rotterdam.

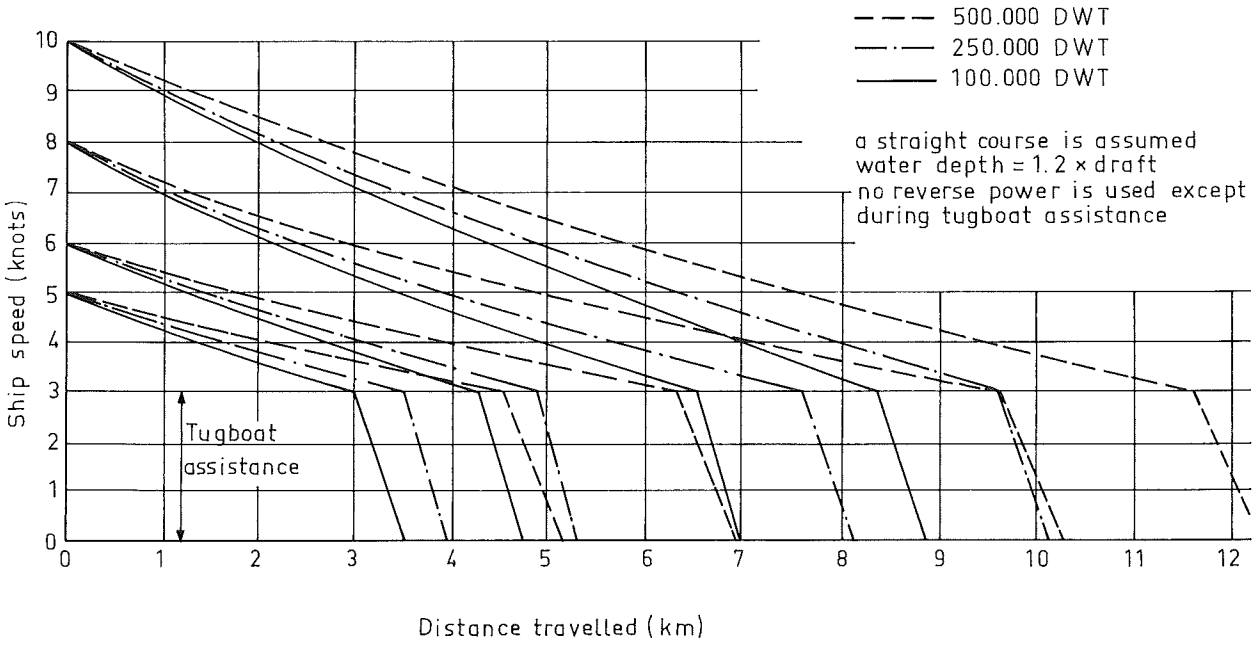

Figure 7.1
STOPPING DISTANCES FOR TANKERS IN SHALLOW WATER

How much tugboat power is needed? In Europoort, large tankers are usually supplied with a total of about 7×10^5 N total pulling force usually distributed over at least four tugboats. This means that the tugs will be rather large - as harbor tugs go - somewhat more than 2000 kw power. Table 7.1 lists some reference data on various types of tugboats. The data listed for a supertanker indicates how underpowered they are!

What are the operational problems with tugs? The most important handicap of most tugs is that a towing line must be passed between the ship and the tug underway. The highest possible speed at which a tugboat captain dares attempt such an operation is about 6 kt (3 m/s) under ideal conditions. The speed must be reduced still further to about 3 kt (1.5 m/s) before the tugs can assist the ship effectively. Because of their extreme maneuverability,tugboats with Voith-Schneider propellers are somewhat more effective at higher speeds. Indeed, such tugs can move at full speed or pull in any direction; this advantage offsets their relative inefficient use of power reflected in table 7.1.

Table 7.1 Tugboat and ship performance data

Type	Towing force power (N/kw)	Power displacement (kw/ton)
tug with normal propeller	170	
tug with propeller in tunnel	210	≈ 4
tug with Voith-Schneider Propeller	135	
large sea tug	170	≈ 5
"Smit Rotterdam"	-	3.76
supertanker	-	0.075
Navy Destroyer	-	11.5

The operation of transferring a towline to a tug also costs time which can be translated into distance progressed along the channel. A recent Japanese invention allows the tug to make fast directly to the side of the ship using a giant suction cup. It remains to be seen whether this will prove to be effective and sufficiently dependable.

The problem of reducing the necessary stopping distance within a harbor might be alleviated by extending tugboat assistance offshore so that deceleration could be started sooner. Unfortunately, wave action can handicap the operation of a harbor tug at sea. Not only is the transfer of a tow line more dangerous and time-consuming, the motion of the tug in the waves can impose undesirable shock loads on the towing cable and its hardware. Kruse and Niewenhuys (1974) have examined this problem in some detail.

Also, of course, tugboats must be available to be utilized and they cost money to rent. When the travel time of a ship is of high importance and harbor maneuvers are carried out frequently, an alternative to the use of tugs is often economical.

7.3 Bow thrusters

Fast ships carrying expensive cargos calling at many ports can find the delays and rental costs of tugboats to be too much of an economic burden on their overall operation. Container ships are an example of the type of ship involved.

Such ships often have bow thrusters in addition to twin propellers, both of which can improve maneuvering characteristics when compared to single screw sister ships. A bow thruster is a propeller mounted on an axle placed crosswise of the ship in a tube extending through the ship deep in the water well forward. Such a thruster can exert a direct crosswise force at the bow to help in maneuvering and berthing operations. Of course, such bow thrusters represent a capital investment for a ship; they are usually only economical on ships such as container ships.

In the following chapter, we re-examine the entire problem of optimum channel design working from the components presented in this and the previous chapters.

8. TOTAL CHANNEL OPTIMIZATION

W.W. Massie

8.1 Introduction

The previous four chapters have discussed aspects of harbor approach channel design with primary emphasis on depth in chapter 4 and on width in the remaining three chapters. In fact, the depth and width of a channel are very strongly interrelated; it is the purpose of this chapter to point out this interrelationship and develop the insight into a total channel optimization.

8.2 Definition of total optimum

In general in a competetive society, one seeks the cheapest supplier for particular goods and services on the market place. Wise investors consider more, however, than just initial cash expense, especially when an investment is at all substantial. Thus, an optimum channel design will be that one which is cheapest over a long term - its useful life - and not necessarily the design representing the lowest initial investment. As has, in fact, already been indicated the optimum design will involve a summation, on some legitimate basis such as capitalized value, of the costs of constructing, maintaining, and insuring against damage to shipping. Each of these topics is treated separately below with emphasis on the interrelationships between factors presented in chapters 4 through 7.

8.3 Construction costs

Construction costs of a particular channel are largely determined by the site conditions such as soil material, wave and tidal conditions, and method and location of dredge spoil disposal. While these factors are very important to a project, they usually do not vary significantly as alternative designs for the same project at the same site are being compared. Granted, the construction of a breakwater will make the wave climate in the channel more moderate and this in turn can reduce the unit cost of dredging, but such savings alone are not sufficient to justify the capital cost of the breakwater. Additional savings, accruing from reduced maintenance dredging or a smaller channel can, of course, justify the breakwater.

Even without a breakwater, both the depth and width of a channel influence its initial cost as well as its maintenance cost. It is conceivable that a relatively wide and shallow channel can be built for about the same initial investment as a deeper but narrower channel.

8.4 Damage costs

The insurance model for damage costs has been adequately described in chapter 4. Of importance, here, is only the realization that these costs, too, are related to channel width and depth in a rather complex way.

The relatively wide shallow channel suggested in the last sentences of the previous section would need its extra width, perhaps, to compensate for the poor maneuverability of the ships resulting from the low average keel clearance. Increasing the depth of the channel would improve maneuverability most likely making a width reduction possible while maintaining the same annual damage cost.

8.5 Maintenance costs

In addition to the construction and damage costs - the only two mentioned in chapter 13 of volume I - we must, for a channel, include the costs of routine dredging necessary to maintain the channel dimensions. Since we can intuitively feel that the quantity of maintenance dredging will be related to the channel geometry, a prediction of this maintenance dredging will be necessary in order to complete the evaluation of particular channel alternatives.

The prediction of such sedimentation is an extremely complex problem in itself. If we consider a sediment-laden current crossing a channel the abrupt change in hydraulic conditions - waves, currents, depth, perhaps even water salinity near a river mouth - will cause some sort of time dependent morphological change in the channel. Local sedimentation or perhaps even erosion can be expected. It should be obvious that the classical sediment transport formulas used by river engineers will be insufficient to predict channel bottom changes in a marine approach channel. Most of the remainder of this book is devoted to the proper prediction of coastal morphological changes in general. Chapter 25 will discuss the state of the art relative to channel sedimentation.

It would be a mistake to conclude from the above that the dredging and sedimentation of an approach channel are the only morphological factors influencing a harbor design; the construction of a new harbor on anything but a solid rock coast will trigger morphological changes along a whole segment of coast. While it is not usually necessary to involve all of these changes and associated costs in an evaluation of an approach channel design, they must most certainly be included in the evaluation of the total harbor project.

Extra Notes

9. COASTAL SAND TRANSPORT

J. v.d. Graaff

9.1 Introduction

Sediment transports are of utmost importance in coastal engineering. In many coastal engineering problems the quality of a proposed solution is dependent upon quantatative estimates of erosion and accretion.

Waves and currents along with the physical properties of the bottom material, together, determine the rate of material transport in the coastal zone. This transport rate, its variations and resulting coastal changes, are of importance for the prediction of both natural coastline changes and the influence of man-made structures on the coastal zone. Even away from the coastal zone, sediment transport problems can be important; scour occurring near offshore structures or pipelines can play a significant role in their stability.

The sediment transport process may, in general, be divided into three steps:

a. The stirring-up of bottom material bringing it into suspension in the water above, or to loosen this material from the bottom.
b. The horizontal displacement of these particles by the water, and
c. The sedimentation of these particles once again.

Usually, of course, we are interested in the effects of sediment transport on some given bottom area. It should be obvious that a continuity principle can be applied to a volume extending from the given bottom area to the water surface as shown in figure 9.1. The resulting erosion or accretion of the bottom can be determined once the resulting sediment transport through the vertical boundary of the volume is known. Combining this knowledge with the steps a to c mentioned above, we see that only step b is really important; in principle we need not concern ourselves with either of the other two steps as separate problems. Our main interest is, then, the horizontal displacement of individual material particles through a given cross section in a given time.

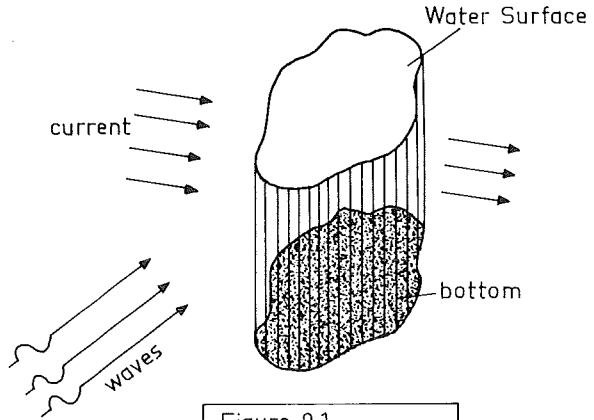

Figure 9.1
PRINCIPLE SKETCH OF CONTINUITY.

For many problems the distribution of the sediment transport over a vertical profile is immaterial for the resulting bottom changes; then, knowing the material properties such as void ratio as well, a sediment transport can be expressed in terms of volume of material per unit width per unit time - $[L^3/LT]$.

It would be wonderful to get a simple theoretical expression for such a sand transport in terms of physical wave, current, and material parameters. Unfortunately, no one has yet (1977) been entirely successful at this; we can, however, develop a conceptual model via which sediment transport formulas can be derived.

9.2 Concept of formulas

Figure 9.2 illustrates the problem to be solved. We wish to determine the volume rate of sediment transport through a unit width of the y-z plane extending from the bottom, $z = -h$, to the water surface, $z = \eta$. In general, neither the wave nor the current direction need coincide with the given axes.

The sediment transport through the plane shaded in figure 9.2 can be expressed as:

$$S_x = \frac{1}{t'} \int_{-h}^{\eta} \left[\int_{0}^{t'} c(z,t) \cdot u_p(z,t)\, dt \right] dz \qquad (9.01)$$

where $c(z,t)$ is the instantaneous concentration of material in suspension expressed in units of volume of deposited bottom material per unit volume of (flowing) water. Wave action causes rapid variations in c, while bottom elevation changes affect it more slowly,

h is the local water depth,

S_x is the sediment transport rate expressed in units of volume per unit width and time,

t is the time,

t' is a period over which the integration is carried out, and

$u_p(z,t)$ is the instantaneous x component of the velocity of the sediment particles passing through the plane; this results from both wave and current influences, and

$\eta(x,y,t)$ is the instantaneous water surface elevation.

In the above, any variations in the parameters over the unit width have been averaged out. The time, t, used in equation 9.01 should be long enough to average out the effects of irregularities in the waves and is, thus, much longer than a single wave period.

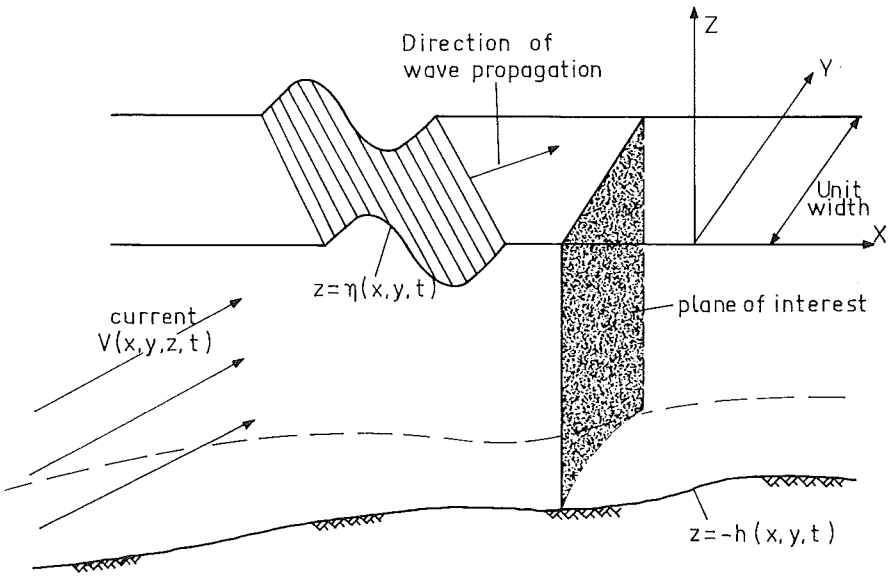

Figure 9.2
SEDIMENT TRANSPORT PRINCIPLE SKETCH
(no scale)

The principle just expressed is simple enough; major difficulties arise , however, when we try to evaluate the functions $c(z,t)$ and $U_p(z,t)$ for substitution into equation 9.01. Indeed, much of the rest of this book will be devoted to the determination of acceptable means of predicting the two above functions in terms of known, measurable parameters.

9.3 Plan of attack

It may seem to the unitiated reader that we shall be wandering far from our objective in the course of the next few chapters. This is not really so as we point out here below.

Cnapters 10 deals with radiation stress, a wave phenomona which contributes significantly to the hydrodynamics in tne coastal zone. After tne general discussion of chapter 10, a specific radiation stress component is examined in chapter 11; it is responsible primarily for an increase in the still water level along a beach. In special cases, however, this wave set-up can also result in a longshore force component which influences a current along the coast in the breaker zone - the longshore current. The discussion of these special cases is posponed to chapter 16, however.

Chapter 12 treats another radiation stress component which is nearly always a significant contributor to the driving force of the longshore current. Other, usually less significant force components, needed for dynamic equilibrium of the water in the breaker zone are discussed briefly in chapters 13 and 14.

Chapter 15 details how the bed friction force under a combination of waves and currents can be evaluated. This resulting friction force is especially important in the breaker zone.

Chapter 16 attempts to solve the problem of determining the longshore current in the breaker zone via an equilibrium using the results of chapters 12 through 15. This current velocity is essentially the u_p needed for equation 9.01.

Chapters 17 and 18 provide historical and background information for the determination of sand transport presented in chapter 19. It should be obvious from equation 9.01 that currents found in chapter 16 will appear again in chapter 19 which finally answers the question posed in the previous section of this chapter.

10. RADIATION STRESS AND ITS COMPONENTS

E.W. Bijker

10.1 Introduction

This chapter is devoted to a presentation of the concept of radiation stress and its components which play a significant role in coastal morphological processes. This presentation will be brief; more detailed descriptions are available in the literature - Longuet-Higgins and Stewart (1962, 1964), Dorrestein (1961), and Battjes (1977).

The theoretical results presented here will be applied to particular coastal problems in the following chapters.

10.2 Principal radiation stresses

Radiation stress is a pressure force in excess of the hydrostatic pressure force caused by the presence of waves. In reality, the radiation stress is neither a true stress (force/area) nor a true force (as implied in the previous sentence) but a force per unit length. (This results from the integration of a force per unit area over the water depth). Even so, transformations applicable to true stresses can still be used on the radiation stress; this will be demonstrated in section 10.4. Unlike hydrostatic pressure, the radiation stress is not isotropic; indeed, just as with stresses, it is associated with a given direction or plane. In this discussion, these planes will be vertical and perpendicular to the two horizontal axes, X oriented in the direction of wave propagation and Y along the wave crest. This will yield the principal stresses.

According to Newton's second law of motion, a force is equivalent to a rate of change of momentum. A stress is equivalent to a momentum flux, and the radiation stress is determined by integrating this momentum flux of the waves over the depth. When we carry out this integration - it is a considerable task - over the depth on a plane perpendicular to the X axis, then the result is:

$$S_{XX} = \left(\frac{2kh}{\sinh 2kh} + 1/2 \right) E \qquad (10.01)$$

where :

S_{XX} is the principal radiation stress component in the direction of wave propagation,

h is the water depth,

k is the wave number = $2\pi/\lambda$,

λ is the wave length, and

E is the wave energy given by (from volume I chapter 5):

$$E = 1/8\ \rho\ g\ H^2 \qquad (I\text{-}5.09) \qquad (10.02)$$

in which:

g is the acceleration of gravity,

H is the wave height, and

ρ is the density.

Using equation 5.07 of volume I, equation 10.01 can be expressed in an equivalent form:

$$S_{XX} = (2n - 1/2)\ E \tag{10.03}$$

where $n = \frac{c_g}{c}$ is the ratio of wave group velocity to wave celerity. This latter form is often more convenient in practical use.
Computation of the second principal radiation stress component acting on a vertical plane perpendicular to the wave crests yields:

$$S_{YY} = \frac{kh}{\sinh 2kh}\ E \tag{10.04}$$

or, expressed in terms of n,

$$S_{YY} = (n - 1/2)\ E \tag{10.05}$$

Application of the usual approximations for deep water explained in volume I chapter 5 yields:

$$S_{XX} = \frac{1}{2}\ E \tag{10.03a}$$

and

$$S_{YY} = 0 \tag{10.05a}$$

In shallow water these stresses become:

$$S_{XX} = \frac{3}{2}\ E \tag{10.03b}$$

and

$$S_{YY} = \frac{1}{2}\ E \tag{10.05b}$$

10.3 Radiation stress changes

What are the factors that influence the radiation stress? Obviously, the most important parameter is the wave height, via the wave energy. In deep water, this is the only influencing factor. In intermediate water depths, the water depth, h, and wave length, λ, (via k) or simply n are important as well. In shallow water, it appears that the radiation stress depends, once again, only upon the wave energy. This is not the whole story, however, since the wave energy is now very dependent upon the water depth when wave breaking occurs.

If we now consider a rectangular element of water enclosed by four vertical principal planes shown in plan in figure 10.1, then, if the wave conditions and depth at all four planes 1, 2, 3, 4 are identical, the radiation stress components on opposite sides of the "block" shown in the figure are identical and there is no resulting force. Only if the wave conditions vary between planes 1 and 2 or 3 and 4 in that figure will there be a resultant force. Thus, we can expect the radiation to influence physical processes only in areas where wave conditions change. Such areas would, therefore, be at locations where wave refraction, diffraction, shoaling, or breaking occur.

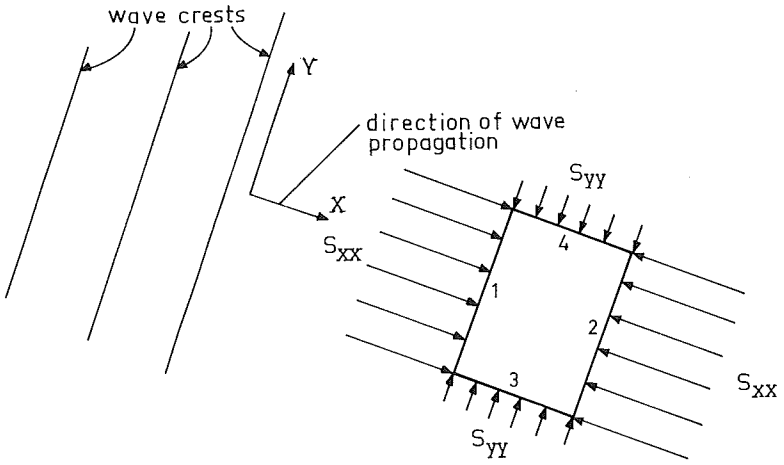

Figure 10.1 PLAN SHOWING PRINCIPAL STRESSES

The following example illustrates these changes in the principal radiation stresses caused, in this case, only by shoaling and breaking of the waves as they approach a coast.

A constant bottom slope, m, of 1:100 will be assumed and a wave with a deep water height, H_o, of 5 m will be assumed to approach with its crest parallel to the coast. (refraction and diffraction do not enter the computation). The wave period is 12 seconds.

The wave period yields a deep water wave length of 225 m. The breaker type parameter (chapter 8, volume I) is:

$$\frac{H_o}{\lambda_o m^2} = 222$$

so that the breaking parameter, p, is small, implying that spilling breakers will be present. A breaker index, γ, of about 0.5 is used, therefore.

Table 10.1 shows the computations for a series of depths.

Notice how the stresses "grow" as the waves approach the coast outside the breaker zone, and how breaking limits and reverses this growth process.

10.4 Radiation stress components

If we wish to know the radiation stress components upon a plane other than a principal plane, the usual methods of plane stress analysis can be used. The graphical Mohr's Circle analysis or its equivalent mathematical form is such a method. Such transformations will be very useful when it becomes necessary to determine stress components on planes parallel to a coastline approached obliquely by waves.

Table 10.1 Radiation stress values

H_o = 5.00 m, T = 12 sec, γ = 0.50

h	$\frac{h}{\lambda_o}$	$\frac{H}{H_o}$	H	E	n	S_{XX}	S_{YY}	dist. from coast	
(m)	(-)	(-)	(m)	(N/m)	(-)	(N/m)	(N/m)	(m)	
150	0.6670	0.9983	4.99	31325.	0.5019	15782.	60.	15000	
125	0.5558	0.9945	4.97	31087.	0.5064	15941.	199.	12500	
100	0.4447	0.9839	4.92	30428.	0.5203	16449.	618.	10000	
80	0.3557	0.9656	4.83	29307.	0.5476	17443.	1395.	8000	
60	0.2668	0.9380	4.69	27655.	0.6020	19469.	2821.	6000	
40	0.1779	0.9142	4.57	26270.	0.6947	23364.	5115	4000	
30	0.1334	0.9160	4.58	26373.	0.7569	26737.	6775.	3000	
25	0.1112	0.9250	4.62	26894.	0.7917	29137.	7845	2500	
20	0.0889	0.9434	4.72	27974.	0.8292	32406.	9209.	2000	
15	0.0667	0.9778	4.89	30052.	0.8688	37192.	11083.	1500	
12.5	0.0556	1.005	5.02	31747.	0.8993	41227.	12677.	1250	
10	0.0445	--	5.00	31432.	0.9105	41522.	12903	1000	*
8	0.0356	--	4.00	20116.	0.9278	27270.	8606.	800	*
6	0.0267	--	3.00	11315.	0.9454	15738.	5040.	600	*
4	0.0178	--	2.00	5029.	0.9633	7175.	2330.	400	*
3	0.0133	--	1.50	2829.	0.9724	4087.	1336.	300	*
2.5	0.0111	--	1.25	1964.	0.9770	2856.	937.	250	*
2	0.0089	--	1.00	1257.	0.9815	1839.	605.	200	*
1.5	0.0067	--	0.75	707.	0.9860	1041.	344.	150	*
1.0	0.0044	--	0.50	314.	0.9908	466.	154.	100	*

Figure 10.2a shows the Mohr's Circle for the stresses at some intermediate water depth for the element shown in figure 10.2b. Those, familiar with the pole method of using the Mohr's Circle will recognize that the pole is at S_{XX} and the stresses on a plane located at an angle Θ can be found by passing a line having the same relative orientation through the pole. The mathematical description can more easily be obtained either from a force equilibrium on the element in figure 10.2b or from the geometry of the circle. In either case, the results are:

$$S_{xx} = \frac{S_{XX} + S_{YY}}{2} + \frac{S_{XX} - S_{YY}}{2} \cos 2\Theta \qquad (10.06)$$

$$S_{yy} = \frac{S_{XX} + S_{YY}}{2} - \frac{S_{XX} - S_{YY}}{2} \cos 2\Theta \qquad (10.07)$$

$$S_{xy} = \frac{S_{XX} - S_{YY}}{2} \sin 2\Theta \qquad (10.08)$$

The Mohr's Circles corresponding, associated with the principal stresses computed in table 10.1 are shown in figure 10.3. The numbers adjacent to the circles give the water depth for which the circle is valid. Some of the circles are shown dashed in order to assist in differentiating them in the figure.

* Wave height governed by breaking!

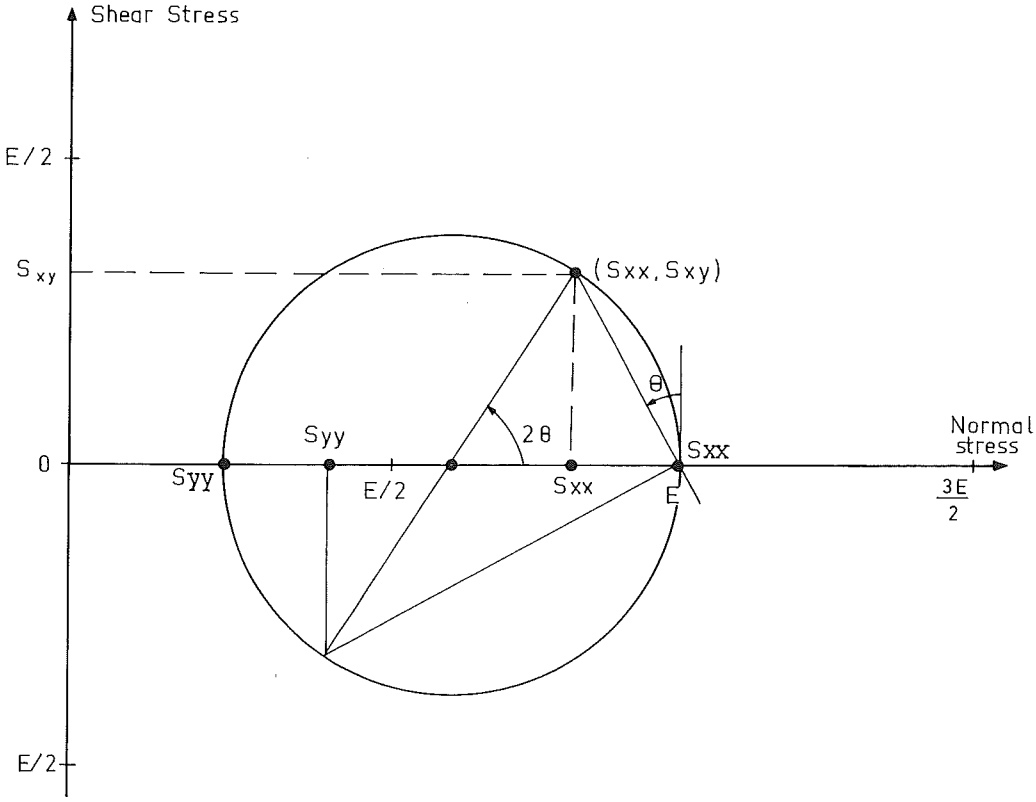

a. MOHR'S CIRCLE

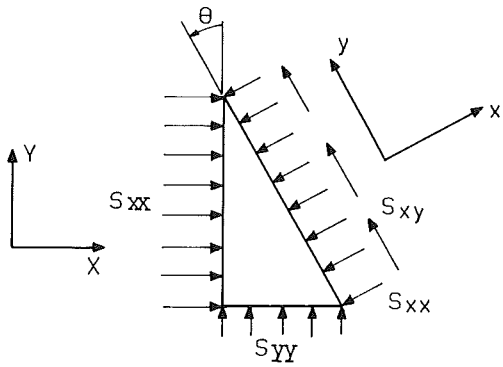

b. STRESS ELEMENT

Figure 10.2
MOHR'S CIRCLE ANALYSIS

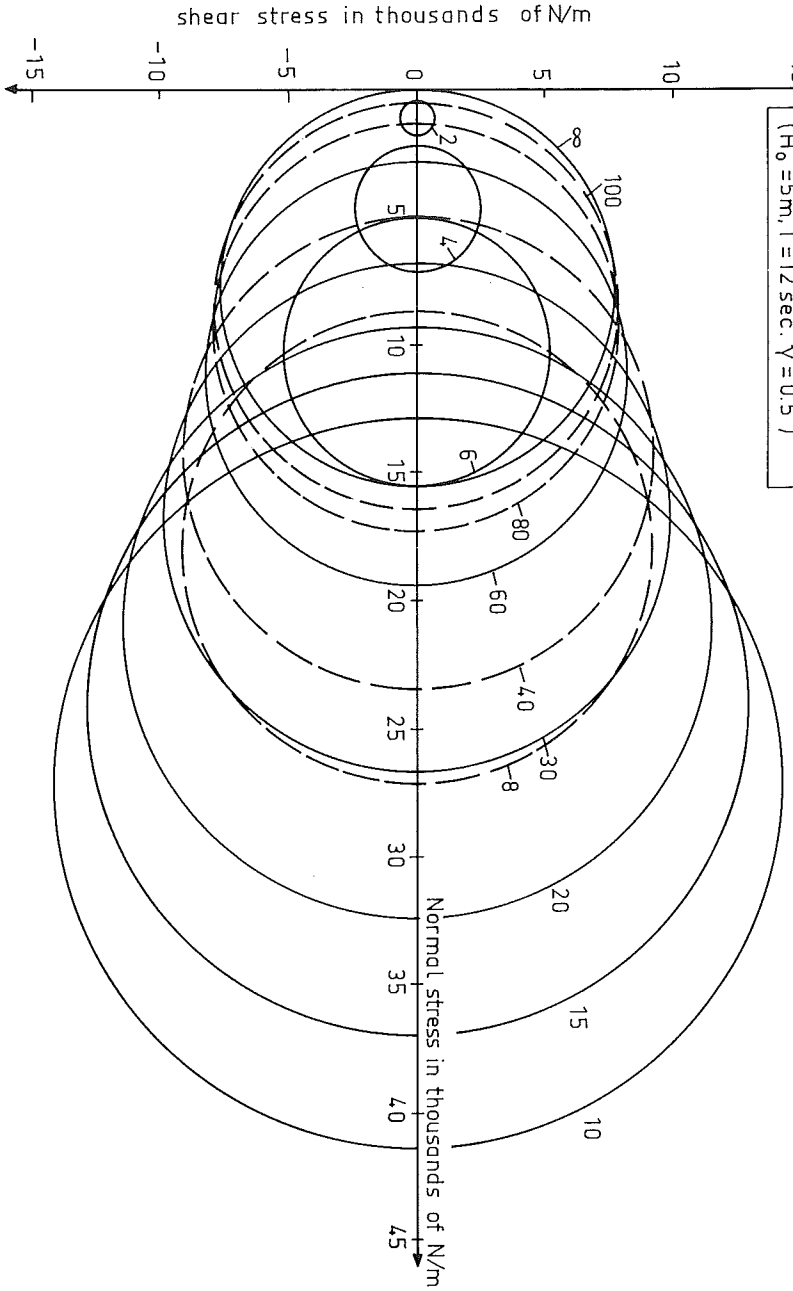

Figure 10.3
MOHR'S CIRCLES
FOR VARIOUS WATER DEPTHS
(H_o =5m, T=12 sec. γ = 0.5)

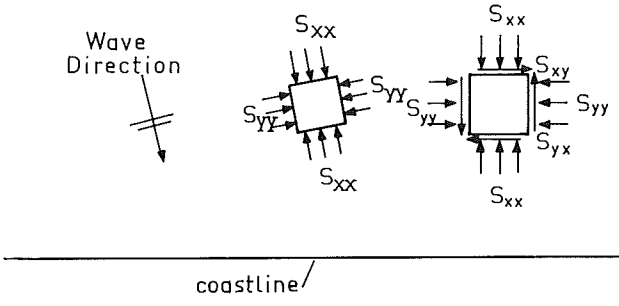

Figure 10.4
COASTAL PLAN WITH STRESS ELEMENTS

10.5 Application to coastal engineering problems

Since the coastal processes to be studied in later chapters of this book can be split into components parallel and perpendicular to the coastline, it is convenient to work with radiation stress components along these axes. Figure 10.4 shows a plan view of a coastal area with principal stresses acting on an element oriented parallel to the wave crests, and normal and shear stresses on an element parallel to the coastline.

In the following few chapters various individual radiation stress components will be examined in more detail in order to explain certain specific coastal phenomona.

Extra Notes

11. WAVE SET-UP

E.W. Bijker
P.J. Visser

11.1 The phenomonon

Waves approaching a coast undergo changes resulting from refraction, diffraction, shoaling, and breaking. Since the radiation stress components are directly expressed in terms of wave parameters, we can also expect radiation stress changes and some influences of these changes. One of the simpler influences of the radiation stress changes is a change in the average water level along a profile perpendicular to the coast.

Figure 11.1 shows such a profile in which the waves approach from the left with crests parallel to the coast. (Consideration of such a special approach direction makes the mathematics considerably simpler and illustrates the principles equally well.) With this restriction, the radiation stress component of interest will be the larger principal stress, S_{XX}. Changes in this principal stress will exert a net resultant force on a vertical water element shown in figure 11.1. This radiation stress resultant is counteracted by a static horizontal pressure gradient resulting from a water surface slope just as a Coriolis force was held in equilibrium in volume I chapter 3. This equilibrium between radiation stress change and average water level slope yields the following first order ordinary differential equation:*

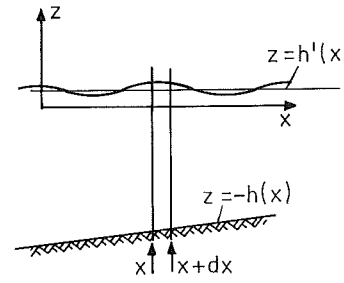

Figure 11.1
ELEMENT OF COASTAL WATER
(not to scale)

$$\frac{d\,S_{XX}}{dX} + \rho g\,(h + h')\,\frac{dh'}{dX} = 0 \qquad (11.01)$$

where:

- g is the acceleration of gravity,
- h is the water depth relative to still water at point X,
- h' is the average water level change at point X caused by the waves,
- S_{XX} is the principal radiation stress component,
- X is the horizontal coordinate in the direction of wave propagation, and in this case, perpendicular to the coast, and
- ρ is the mass density of water.

11.2 Solutions to the differential equation

How, then, does the principal radiation stress component S_{XX} vary as waves proceed from deep water to a shore? Since *changes* in this component are of interest, we examine the derivative of S_{XX} with respect to X. Direct differentiation of equation 10.01 is difficult since all three variables, k, h and E can be dependent upon the horizontal coordinate X for this problem. Battjes (1977) shows the algebra involved and finds the following solution for 11.01 provided that the waves have not yet broken:

* The normal force from the sloping bottom must be included!

$$h' = - \frac{k\,E}{\rho g \sinh 2kh} = - \frac{1}{8} \frac{k\,H^2}{\sinh 2kh} \qquad (11.02)$$

where:

k is the wave number.

Equation 11.02 is valid for the region outside the breaker zone. The resulting water level change at the outside of the breaker zone follows from the substitution of shallow water approximations and breaking conditions into (11.02) - see volume I chapter 5:

$$h'_{br} = - \frac{1}{16} \frac{H^2_{br}}{h_{br}} \qquad (11.03)$$

where the subscript br refers to conditions at the outer edge of the breaker zone. The wave height and mean water depth are often proportional in the breaker zone:

$$H_{br} = \gamma\, h_{br} \qquad (11.04)$$

Where the influence of the set-down h'_{br} has been neglected since $h'_{br} << h_{br}$. With (11.04), (11.03) becomes:

$$h'_{br} = - \frac{1}{16} \gamma\, H_{br} \qquad (11.05)$$

Thus, at the outer edge of a breaker zone there is an average water level reduction - a wave set-down - proportional to γ and H_{br}. See figures 11.2 and 11.3. For a given deep water wave height, H_o, the exact value of this set-down will still depend upon several parameters such as beach slope and wave period via the breaker index, γ - see volume I chapter 8.

11.3 Spilling breaker solution

When spilling breakers occur, the direct relationship between wave height and water depth remains valid throughout the breaker zone. The energy decrease of the waves due to breaking must be included, however. Using the shallow water approximation for S_{XX} (equation 10.03b), and defining E as:

$$E = \frac{1}{8} \rho g\, \gamma^2\, (h + h')^2 \qquad (11.06)$$

the derivative of the principal radiation stress becomes:

$$\frac{d\,S_{XX}}{dX} = \frac{3}{8} \rho g\, \gamma^2\, (h + h') \frac{d(h + h')}{dX} \qquad (11.07)$$

where: $\frac{d(h + h')}{dX}$ is the slope of the water surface relative to the beach.

Substitution of (11.07) into (11.01) and integration over the width of the breaker zone yields:

$$\Delta h' = \frac{3}{8} \gamma\, H_{br} \qquad (11.08)$$

where $\Delta h'$ is the change in average water level across the breaker zone.

Since $\Delta h'$ is positive, a water level increase toward the shore can be expected. Remembering that the average water level at the outer edge of the breaker zone is lowered(equation 11.05), the absolute average water level at the beach line relative to the condition without waves is:

$$h'_{bs} = \frac{5}{16} \gamma H_{br} \qquad (11.08)$$

for spilling breakers, where h'_{bs} is the wave set-up at the beach caused by spilling breakers. This is shown in figure 11.2.

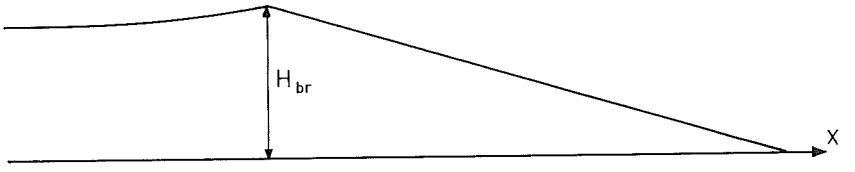

a. Wave Height changes

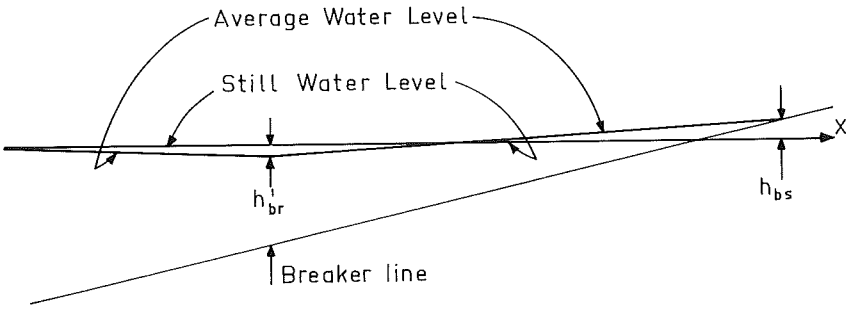

b. Shore Profile

Figure 11.2
WAVE SET-UP WITH SPILLING BREAKER
(vertical scale distorted)

11.4 Plunging breaker solution

Swart (1974) studied the form of breaking waves near a coast. He found that a "pure" plunging breaker seldom if ever occurred and introduced a parameter, p, to describe breakers which are partially spilling and partially plunging - see volume I chapter 8.

If we assume as a limit case that a complete plunging breaker does exist, then the entire energy of the approaching wave is transformed at once as the breaker plunges at the outer edge of the breaker zone. Just as with spilling breakers, the change in principal radiation stress is counteracted by a water level change. This time, however, this level change occurs abruptly at the plunge point (in this ideal case). A simple equilibrium yields:

$$\Delta h' = \frac{3}{16} \gamma H_{br} \qquad (11.10)$$

Again including the water level drop outside the breaker zone, we find the absolute set-up at the beach line to be:

$$h'_{bp} = \frac{1}{8} \gamma H_{br} \qquad (11.11)$$

where h'_{bp} is the wave set-up at the beach caused by plunging breakers. Note that this value is lower than that found for spilling breakers - equation 11.08. Figure 11.3 shows an average water level profile.

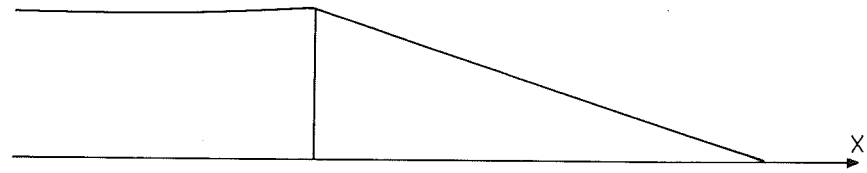

a. Wave Height Variation

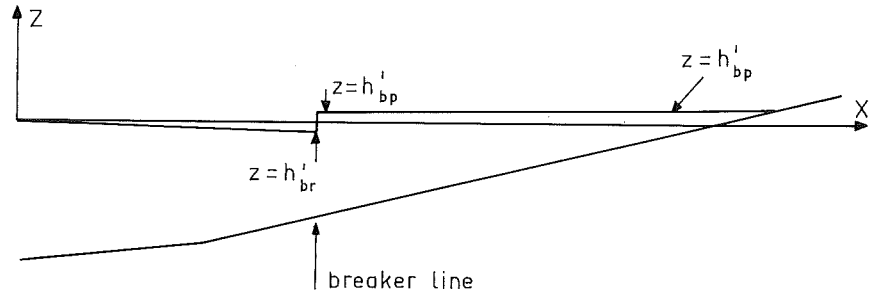

b. Shore Profile

Figure 11.3

WAVE SET-UP WITH PLUNGING BREAKER ACCORDING TO SWART.
(vertical scale distorted)

As already been indicated, a pure plunging breaker is essentially non-existant in nature. More usually, a less pronounced plunging will occur and a breaking wave will continue to propagate toward the coast from the plunge point. This will yield a wave set-up pattern more like that described for spilling breakers described in the previous section and illustrated in figure 11.2.

11.5 Special remarks

The wave set-up just discussed should not be confused with the wind set-up discussed in chapter 3 of volume I. The two phenomona are entirely different and may or may not occur simultaneously. As the names imply, wind set-up is dependent upon the presence of a wind field (with or without waves) while waves alone - on ocean swell, for example - cause a wave set-up. Further, wind set-ups occur over a longer fetch of the wind while wave set-up is purely a coastal phenomona.

If the wave conditions vary along a coast, then, of course, the wave set-up will also vary along the coast. The variation in wave conditions along the coast could be caused by refraction or diffraction or even by differences in breaker type caused, for example, by coastal slope variations. The water level differences between points on the coast will yield, obviously, a pressure gradient along the coast. This pressure gradient can form an important contribution to the driving force for the longshore current at locations where the wave conditions vary rapidly along the beach. See, also, Bakker (1971).

In addition to a wave set-up, the breaking waves set up a circulation current in the breaker zone. This phenomona is exposed by examining the distribution of the momentum flux which yields the radiation stress over a vertical profile. Since the orbital wave motion is maximum at the surface, we can expect the momentum flux there to be greater than at the bottom. The resisting hydrostatic pressure is evenly distributed over the depth on the other hand. This yields a net coastward force at the surface and a net seaward force near the bottom. The resulting circulation is shown in figure 11.4.

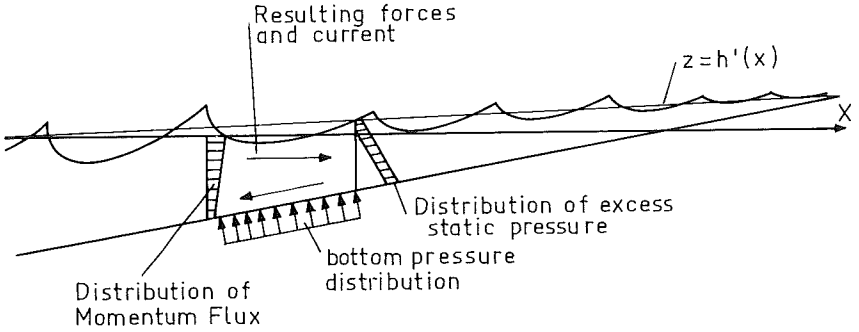

Figure 11.4

CIRCULATION CURRENT IN BREAKER ZONE
(not to scale)

Many experimental measurements of wave set-up have not agreed well with theoretically predicted values. Several explanations have been offered. Battjes (1974) ascribes some of the discrepancy to the influence of the air entrained in the water by the breaking waves. The resulting mixture of air and water has, therefore, a lower density.

Another possible influencing factor is a friction force acting between the bottom and moving water. Even though the circulation currents mentioned above are low, *instantaneous friction forces*, resulting from the wave orbital motion, can have a non-zero time average*, and thus, can contribute an additional net horizontal force component.

The approach to the wave set-up problem solution with waves approaching at an angle to the coast is, in principle, the same as that for the case without refraction influences. Instead of the principal radiation stress component, S_{XX}, the normal stress component on a plane parallel to the coast, S_{xx}, will be needed in equation 11.01. In the solution of that equation, one must also remember that the angle of attack, ϕ, is also a function of distance to the shore; this makes the algebra a bit more complicated.

11.6 Example

Compute the wave set-up generated by the waves used to compute table 10.1 and figure 10.3. The regular waves had a deep water height, H_o, of 5.0 m, a period, T, of 12 seconds, and approached parallel to the coast. The breaker index, γ, was found to be about 0.5.

A bit of trial and error work** with tables of wave functions is needed in order to determine the location of the breaker line. The results are:

$$h_{br} = 10.4 \text{ m} \tag{11.12}$$

and:

$$H_{br} = 5.2 \text{ m} \tag{11.13}$$

Knowing these values, the wave set-up at the outer edge of the breaker zone can be computed using equation 11.05:

$$h'_{br} = - \left(\frac{1}{16}\right) (0.5) (5.2) = - 0.163 \text{ m} \tag{11.14}$$

The resulting water level change is a set-down of 16.3 cm.

The water level change across the breaker zone follows from equation 11.08 for a spilling breaker.

$$\Delta h' = \left(\frac{3}{8}\right) (0.5) (5.2) = 0.975 \text{ m}. \tag{11.15}$$

The absolute water level at the coastline relative to a condition without waves is, then, about 87 cm.

Battjes (1974) gives a method to compute set-ups caused by irregular waves.

This concludes for now our discussion of phenomona occurring in a profile perpendicular to a coast.
In the next chapters we concentrate attention on forces working along a coast and the longshore currents and sand transports which result.

* In real situations, the waves will be asymetrical leading to the non-zero average.

** An iterative program can be conceived for a small programmmable pocket calculator to simplify the computations. A generalized version of this procedure is presented in section 16.5.

12. RADIATION SHEAR STRESS GRADIENT

E.W. Bijker

12.1 Introduction

In this and following three chapters we consider force components which act parallel to a coast and, as such, define the dynamic equilibrium of a water mass moving along the coast - the longshore current. The first of these force components arrises out of changes in the shear stress component of the radiation stress. As was pointed out in chapter 10, we shall be interested in *changes* in this shear stress as the waves approach the coast under some angle, ϕ. Expressed in equation form, we are interested in:

$$\frac{d\, S_{xy}}{dx} = f\,(x, H_o, T, \phi_o) \qquad (12.01)$$

where: H_o is the deep water wave height,
T is the wave period,
x is the horizontal coordinate perpendicular to the coast*
ϕ_o is the angle of attack in deep water, and
$f\,(\ )$ denotes some function of $(\ )$.

The exact nature of changes in S_{xy} will be discussed in the following sections.

12.2 Changes outside the breaker zone

Since the waves approaching a coast first begin to change in intermediate water depths, we shall first examine the changes in the shear stress component outside the breaker zone. Bowen (1969) did this and shows the algebra involved in more detail; the basic steps will be shown here in order to develop our insight into the problem.

Adaptation of the results of chapter 10 yields:

$$S_{xy} = \frac{S_{XX} - S_{YY}}{2} \sin 2\phi \qquad (10.08) \qquad (12.02)$$

Using trigonometry and substituting for S_{XX} and S_{YY} from (10.03) and (10.05) yields:

$$S_{xy} = E\, n \sin\phi \cos\phi \qquad (12.03)$$

From refraction theory:

$$E\, n\, c\, b = \text{constant} \qquad (I\text{-}9.02) \qquad (12.04)$$

or, in particular:

$$E\, n\, c\, b = E_o\, n_o\, c_o\, b_o \qquad (12.05)$$

where c is the phase velocity, b is the distance between orthogonals, and the subscript o refers to deep water conditions which are known and constant. Equations 12.04 and 12.05 are valid only in the region outside the breaker zone. See volume I chapter 9. Also from that chapter, equations 9.05 and 9.06:

* This convention will be changed later. See chapter 13.

$$bc = \frac{b_o c_o}{\sin \phi_o \cos \phi_o} \sin \phi \cos \phi \qquad (12.06)$$

Substituting (12.06) in (12.05) and comparing that to (12.03) yields the startling result:

$$S_{xy} = E_o n_o \sin \phi_o \cos \phi_o = \text{constant!} \qquad (12.07)$$

and hence, the driving force component proportional to $\frac{\partial S_{xy}}{\partial x}$ is identically zero even though the wave conditions change outside the breaker zone. Since equations 12.04 and 12.05 are valid only outside the breaker zone, we must make a new analysis for the breaker zone; this is done in the next section.

12.3 Changes within the breaker zone

Within the breaker zone we shall begin, again, with the general relationship expressed in equation 12.03:

$$S_{xy} = E n \sin \phi \cos \phi \qquad (12.03)$$

Using equation 9.05 of volume I, this becomes:

$$S_{xy} = E n c \cos \phi \frac{\sin \phi_o}{c_o} \qquad (12.08)$$

Remembering the definition of E - equation I - 5.09- and that equation 11.04 now governs the wave breaker height, (12.08) becomes:

$$S_{xy} = \frac{1}{8} \frac{\sin \phi_o}{c_o} \rho g \gamma^2 [h^2 n c \cos \phi] \qquad (12.09)$$

Since only the terms within the brackets are dependent upon x, a brute force differention can be carried out:

$$\frac{\partial S_{xy}}{\partial x} = \frac{1}{8} \frac{\sin \phi_o}{c_o} \rho g \gamma^2 \left[2h n c \cos \phi \frac{dh}{dx} + h^2 c \cos \phi \frac{dn}{dx} + h^2 n \cos \phi \frac{dc}{dx} - h^2 n c \sin \phi \frac{d\phi}{dx} \right] \qquad (12.10)$$

This result holds only *within* the breaker zone. It can be simplified, however, by making the usual substitutions for shallow water parameters described in section 5.5 of volume I. These are summarized as follows:

$$\begin{aligned} n &= 1 \quad ; \quad \frac{dn}{dx} = 0 \\ \cos \phi &= 1 \; ; \quad \frac{d\phi}{dx} = 0 \\ c &= \sqrt{gh} \end{aligned} \qquad (12.11)$$

From the last line of (12.11):

$$\frac{dc}{dx} = \frac{1}{2} \sqrt{g} h^{-1/2} \frac{dh}{dx} \qquad (12.12)$$

With (12.11), the second and fourth terms in the brackets in (12.10) are zero. Substitution of (12.11) and (12.12), then yields:

$$\frac{\partial S_{xy}}{\partial x} = \frac{1}{8} \rho g \gamma^2 \frac{\sin \phi_o}{c_o} \left[2 h \sqrt{gh} \frac{dh}{dx} + \frac{1}{2} h^2 \frac{g}{\sqrt{gh}} \frac{dh}{dx} \right] \quad (12.13)$$

or, with a bit of algebra:

$$\frac{\partial S_{xy}}{\partial x} = \frac{1}{8} \rho g \gamma^2 \frac{\sin \phi_o}{c_o} \left[2{,}5 h \sqrt{gh} \frac{dh}{dx} \right] \quad (12.14)$$

$$= \frac{5}{16} \rho \gamma^2 (g h)^{3/2} \frac{\sin \phi_o}{c_o} m \quad (12.15)$$

where m is the beach slope, $\frac{dh}{dx}$.*

This last equation gives, then, the contribution of the radiation stress to the driving force parallel to the coast on an element of water of differential thickness, dx, and height, h.

In later chapters we shall be using a different coordinate system in order to better agree with literature on coastal morphology. This, however, will have no fundamental influence on the right hand side of equation 12.15.

* Note that $\frac{dh}{dx}$ is negative, here, since x is positive toward the beach.

Extra Notes

13. TIDAL FORCES ALONG A COAST

E.W. Bijker

13.1 Coordinates used

In this and the following chapters, processes occurring *along* a coastline will be of especial significance. Until this point, however, attention has primarily been focused on phenomona occurring along a profile *perpendicular* to a coast or in the direction of wave propagation. A new coordinate system is chosen for the remainder of this book in order to achieve better agreement with the reference literature. The axis system can therefore be described as follows:

The x axis is horizontal and parallel to the shore line. It is directed positively to the right for an observer standing on the beach looking out at the sea.

The y axis is also horizontal, perpendicular to the shore line and positive in the direction of the sea. Waves approaching with crests parallel to the coast are travelling along the y axis in the negative direction, therefore. The x-y plane is usually placed at the still water level.

The z axis is directed upward from the still water level; its definition has not changed.

Axis-dependent equations picked up from earlier work will be transformed to the new coordinate system; a note reminding us of this will be included.

13.2 The one-dimensional tidal force component

The equation of motion of a tidal wave propagating along a coast line follows from long wave theory:

$$-\frac{\partial V}{\partial t} - V\frac{\partial V}{\partial x} - g\frac{\partial Z}{\partial x} = \frac{g\,V|V|}{C^2\,h} \qquad (13.01)$$

where: C is the Chézy friction factor,
g is the acceleration of gravity,
h is the water depth,
V is the average velocity over the depth,
x is the ordinate along the coast,
Z is the tidal elevation, and
t is time.

In this equation, the first three terms represent driving forces while the fourth term is a frictional resistance term.

The driving force component to be included in a longshore current determination comes from the integration of the first three terms of equation 13.01 over the depth, h, and multiplied by the density, ρ:

$$F_{tide} = -\rho\,(h\frac{\partial V}{\partial t} + V\,h\frac{\partial V}{\partial x} + g\,h\frac{\partial Z}{\partial x}) \qquad (13.02)$$

Continuing this one-dimensional approximaton, the tidal elevation can be written as:

$$Z = \hat{Z} \cos (\Omega t - Kx) \tag{13.03}$$

where: $\hat{Z}$ is the tidal amplitude,
K is the wave number = $2\pi/\lambda_{tide}$,
λ_{tide} is the wave length of the tide,
Ω is the tidal frequency = $2\pi/T'$, and
T' is the tidal period.

Similarly, the tidal velocity can be written as:

$$V = \hat{V} \sin (\Omega t - Kx - \phi) \tag{13.04}$$

where: $\hat{V}$ is the amplitude of the pure tidal current, and
ϕ is the phase angle between vertical and horizontal tide - see volume I chapter 20 for an example of this phase shift.

The necessary partial differentiations of equations 13.03 and 13.04 can be carried out easily. These results can be substituted into 13.02 yielding:

$$F_{tide} = - \rho h \hat{V} [\Omega - K\hat{V} \sin (\Omega t - Kx - \phi)] \cos (\Omega t - Kx - \phi)$$
$$- \rho g Kh \hat{Z} \sin (\Omega t - Kx) \tag{13.05}$$

Since this is a bit complicated, it can be simplified in an approximation by retaining only the first and last terms which are usually an order of magnitude greater than the other terms. Thus, the influence of the water surface slope along the coast and inertia are usually the most important of the tidal force terms, and (13.05) becomes:

$$F_{tide} \approx - \rho h [g K\hat{Z} \sin (\Omega t - Kx) - \hat{V}\Omega \cos (\Omega t - Kx - \phi)] \tag{13.06}$$

The parameters involved in equation 13.06 cannot be evaluated from tidal height measurements at a single location. Simultaneous measurement of tide level and tidal current will yield the necessary parameters. One must be careful with tidal current measurements in the coastal zone, however; as will be shown in chapter 15, the presence of waves will influence the bottom friction force acting on a steady current. This implies that the only dependable measurements of tidal currents - influenced only by tidal forces - can be made when no waves are present, or a correction procedure must be used.

The tidal force which then results from the analysis of tidal elevation and current data can be one of the driving* force components for a coastal longshore current. After considering other force components in the following two chapters, several of these components will be combined in chapter 16 to determine the resulting current velocity along a coast.

---

* This force may be positive or negative at any given moment dependent upon the actual flow direction at that instant.

14. TURBULENT FORCES

E.W. Bijker

14.1 Introduction

The previous two chapters have discussed driving force components for the longshore current; chapter 15, on the other hand discusses a resistance force component. This current chapter concentrates on the action of turbulent forces which both drive and resist fluid motion; they tend to smooth out sharp, steep velocity profiles. We will concern ourselves, here, with a horizontal, turbulence-caused dispersion of momentum through a vertical plane parallel to the coast (the x axis) resulting from a gradient of the velocity in the y-direction, $\frac{\partial u}{\partial y}$, where u is the x component of the velocity. This momentum transfer may be expressed as a shear stress acting on this plane.

14.2 Mathematical description

Using the theory of turbulent momentum diffusion one can express the turbulent shear stress as:

$$\tau_{yx} = \rho \, u' \, v' = \rho \, \varepsilon_y \frac{\partial u}{\partial y} \qquad (14.01)$$

where: u is the velocity component along the x axis parallel to the coast,

u' is the turbulent velocity fluctuation in the x direction,

v' is the turbulent velocity fluctuation in the y direction,

y is the coordinate perpendicular to the coast,

ε_y is the turbulent diffusion coefficient, sometimes called the "eddy viscosity", and

ρ is the mass density of water.

The "eddy viscosity" is often defined in terms of a so-called mixing length:

$$\varepsilon_y = v' \, \ell_y \qquad (14.02)$$

where ℓ_y is the horizontal mixing length.

Thornton (1970) explains the whole problem in much more detail. He relates both v' and ℓ_y to the wave motion - the horizontal wave orbital velocity and particle displacement, respectively. (In the surf zone, both of these lie approximately along the y axis). Battjes (1975, 1976), on the other hand, relates ε to the normal viscosity of a current having velocity, v.

Model measurements carried out by Swart (1974) indicate, in any case, that ε_y should have a value in the order of 10^{-2} m^2/s for model conditions. Using model scale laws, it is, in principle, possible to convert this to a prototype value.

Extra Notes

15. BOTTOM FRICTION FORCES

E.W. Bijker
J. v.d. Graaff

15.1 Introduction

This fourth force component acting on the water in the longshore current results from the bottom friction of the beach on the water element above it; this friction force is related to the velocity in the element. However, in a breaker zone, the instantaneous velocity of the water there is dependent upon both the more or less constant longshore current and the rapidly varying velocity components in the breaking waves.

The proper description of these wave velocity components is, in itself, an impossible task; every mathematical description is only an approximation, at best. We shall later assume that the orbital velocity components can be described by simple sine functions. Even with this (probably crude) assumption it proves difficult to describe the bottom friction phenomona accurately. An attempt is made, here, to explain this rather complex phenomona. First, we shall examine the development of friction under a constant current without waves. Later in this chapter we look at friction under waves alone and finally, using the insight gained, attack combined waves and currents.

15.2 Friction in constant currents

The normally encountered expression for bottom friction in steady flow is, from elementary fluid mechanics:

$$\tau_c = \rho g \frac{V^2}{C^2} \qquad (15.01)$$

where C is the Chézy friction factor,
g is the acceleration of gravity,
V is the current velocity averaged over the flow cross-section,
ρ is the mass density of the fluid, and
τ_c is the (constant) bottom shear stress acting against the flow,

More generally, the shear stress acting across any horizontal plane in the fluid is:

$$\tau = \rho \ell_z^2 \left[\frac{d\, V(z')}{dz'} \right]^2 \qquad (15.02)$$

where ℓ_z is the mixing length,
z' is a vertical coordinate axis with origin at the bottom*, and
V(z') is the current velocity at elevation z'.

By making the special assumption that:

$$\ell_z = \kappa z' \sqrt{\frac{h-z'}{h}} \qquad (15.03)$$

Prandtl (1926) and Von Kármán (1930) were able to solve equation 15.02 to get the well known Prandtl - Von Kármán logarithmic velocity distribution law:

---

* This represents a change of vertical axis origin. z' = 0 corresponds to z = -h.

$$V(z') = \frac{1}{\kappa} V_* \ln\left(\frac{z'}{z'_o}\right) \tag{15.04}$$

where: V_* is a velocity often called the "shear velocity" at some elevation (see below),

z'_o is the elevation at which the velocity is zero, and

κ is the Von Kármán constant which has been found by experiment to be equal to 0.4.

V_* is somewhat difficult to interpret physically.
It is the velocity occurring at elevation:

$$z' = z'_o e^{\kappa} \tag{15.05}$$

having magnitude:

$$V_* = V \frac{\sqrt{g}}{C} \tag{15.06}$$

which is of no special significance. Another relationship involving V_* is:

$$V_* = \sqrt{\frac{\tau_c}{\rho}} \tag{15.07}$$

and appears quite often. We shall attempt to avoid further use of V_*.

The elevation z'_o has been related to the bottom roughness, r, experimentally:

$$z'_o \approx \frac{r}{33} \tag{15.08}$$

Below this elevation, equation 15.04 yields negative - very unrealistic! - values. Therefore, velocities near the bottom are usually described by a linear velocity profile from the origin ($z' = 0$, $V(0) = 0$) tangent to the profile described by equation 15.04; the result is shown in figure 15.1. The elevation of the point of tangency, z'_t, turns out to be:

$$z'_t = e\, z'_o = \frac{er}{33} \tag{15.09}$$

where e is the base of natural logarithms. For convenience, we shall denote the velocity at this elevation by V_t. From the figure, the velocity gradient at an elevation z'_t above the bottom is:

$$\left.\frac{d\,V(z')}{d\,z'}\right|_{z' = z'_t} = \frac{V_t}{z'_t} \tag{15.10}$$

At this same elevation, the mixing length is:

$$\ell_{z_t} = \kappa\, z'_t \sqrt{\frac{h - z'_t}{h}} \tag{15.11}$$

using equation 15.03.
Since $z'_t \ll h$, equation 15.11 is approximately:

$$\ell_{z_t} \approx \kappa\, z'_t \tag{15.12}$$

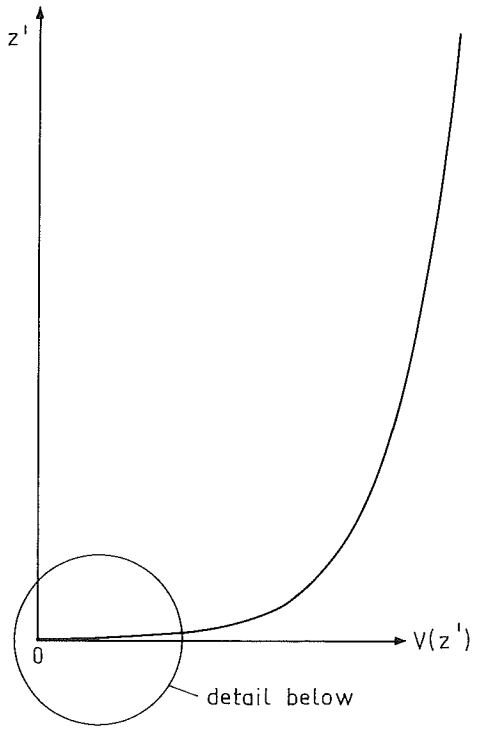

a. TOTAL LOGARITHMIC VELOCITY PROFILE

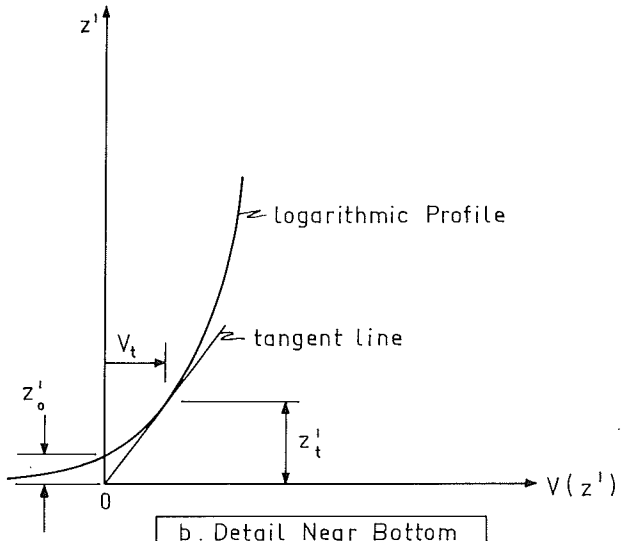

b. Detail Near Bottom
(vertical scale extended)

Figure 15.1 LOGARITHMIC VELOCITY PROFILE
(no absolute scale)

Substitution of (15.12) and (15.10) into equation 15.02 yields an alternate expression for the bottom* shear stress:

$$\tau_c = \rho \kappa^2 V_t^2 \qquad (15.13)$$

* This is actually the shear stress at an elevation $z' = z'_t$ above the bottom. This is universally accepted as equivalent to that at the actual bottom, however.

This equation expresses the bottom shear stress in terms of the velocity occurring very near the bottom. This will be useful for current determination both with and without waves as well as for sediment transport determinations - chapter 19.

Of course, we can express V_t in terms of V in this case if we wish. Using equation 15.06 in 15.04 yields, ultimately:

$$V_t = \frac{\sqrt{g}}{\kappa C} V \tag{15.14}$$

15.3 Friction with waves alone

Jonsson (1966) carried out experiments to determine bed shear stresses under waves. He found that this shear stress, τ_w, could be described by:

$$\tau_w = \frac{1}{2} f_w \rho u_b^2 \tag{15.15}$$

where: f_w is a dimensionless coefficient, and
u_b is the instantaneous water velocity near the bottom.

Jonsson derived an emperical relation for f_w in terms of more readily measurable parameters: the bottom roughness, r, and the amplitude of the water displacement near the bottom, a_b. His relationship as rewritten by Swart (1974) is:

$$f_w = \exp\left[-5.977 + 5.213 \left(\frac{a_b}{r} \right)^{-0.194} \right] \tag{15.16}$$

This relation is also shown graphically in figure 15.2 and is only valid for $1.47 < \left(\frac{a_b}{r} \right) < 3000$. For values of $\frac{a_b}{r} \leq 1.47$, f_w has a constant value of 0.32.

Both u_b and a_b are easily evaluated using short wave theory. The velocity at the bottom, u_b, follows from a substitution of z = -h into equation 5.01 of volume I:

$$u_b = \frac{\omega H}{2} \frac{1}{\sinh kh} \sin \omega t \tag{15.17}$$

Similarly, a_b - denoted by $\hat{\xi}$ in volume I* - follows from equation 5.03 of that volume:

$$a_b = \frac{H}{2} \frac{1}{\sinh kh} \sin \omega t \tag{15.18}$$

Sometimes it is acceptable to use the shallow water approximations for the two above equations. The effects of the use of the shallow water approximations will be demonstrated in the example in this chapter and again in chapter 19.

* The reason for this notation change will become obvious in section 15.4.

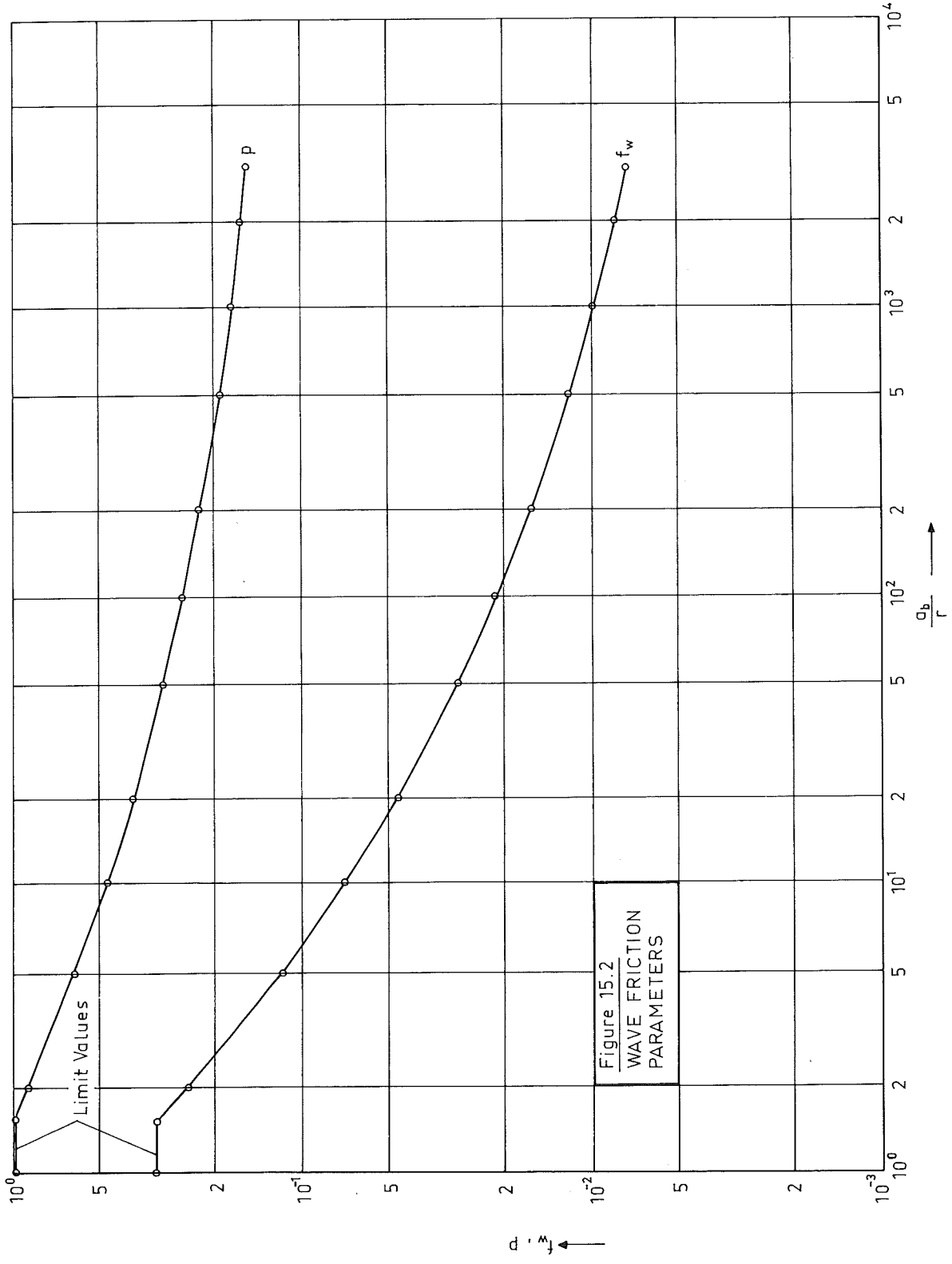

Figure 15.2
WAVE FRICTION PARAMETERS

The computations of u_b and a_b just carried out neglect boundary layer effects. According to boundary layer theory we should expect the actual velocity to be zero at the bottom. A boundary layer can be expected to develop in a thin region near the bottom; the fact that it does not have time enough to develop a velocity profile over the entire depth is not important to us.* Jonsson (1966), thus measured logarithmic velocity profiles in his experiments and assumed that a linear portion would develop near the bottom just as with constant currents in this same region. Continuing with an approach entirely parallel to that in the previous section, we can assume that the actual water velocity in the wave at an elevation z'_t above the bottom will be directly proportional to the bottom velocity computed in equation 15.17:

$$u_t = p\, u_b \tag{15.19}$$

where p is a dimensionless parameter discussed further below.

Bijker (1967) plugged this into an equation like (15.13) and found:

$$\tau_w = \rho\, \kappa^2\, (p\, u_b)^2 \tag{15.20}$$

where τ_w is the bottom shear stress under the wave. This shear stress has amplitude $\hat{\tau}_w$.

Bijker (1967) assumed that p was constant and, from a series of model tests, he indeed found a nearly constant value of 0.45 for p. Later, comparison of the work of Bijker to that of Jonsson (1966) indicated that p should be a variable. It can be evaluated by equating (15.15) and (15.20):

$$p = \frac{1}{\kappa} \sqrt{\frac{f_w}{2}} \tag{15.21}$$

Additionally, the maximum value of p physically possible is 1.00.** Values of p as a function of $\frac{a_b}{r}$ are also shown in figure 15.2.

15.4 Friction with combined current and waves

In the two previous sections we have developed expressions for the bottom shear stress under currents and waves in terms of the velocities at a distance z'_t above the bottom - equations 15.13 and 15.20 respectively. Bijker (1967) extended this to include combinations of currents and waves. He let the wave crests approach the constant current direction under an angle ϕ. Figure 15.3 shows the constant current velocity, V_t and the wave particle velocity, $p\, u_b$, in the plane $z' = z'_t$. Bijker simply added these velocities as vectors to obtain a time dependent resultant velocity, V_r, also shown. From the figure:

$$V_r = \sqrt{V_t^2 + (p\, u_b)^2 + 2\, p\, u_b\, V_t \sin \phi} \tag{15.22}$$

and:

---

* We need only to assume that it develops in the region $0 \leq z' \leq z'_t$.

** $p = 1$ corresponds to the maximum value of $f_w = 0.32$ given above.

$$\cos \Theta = \frac{V_t + p\, u_b \sin \phi}{V_r} \qquad (15.23)$$

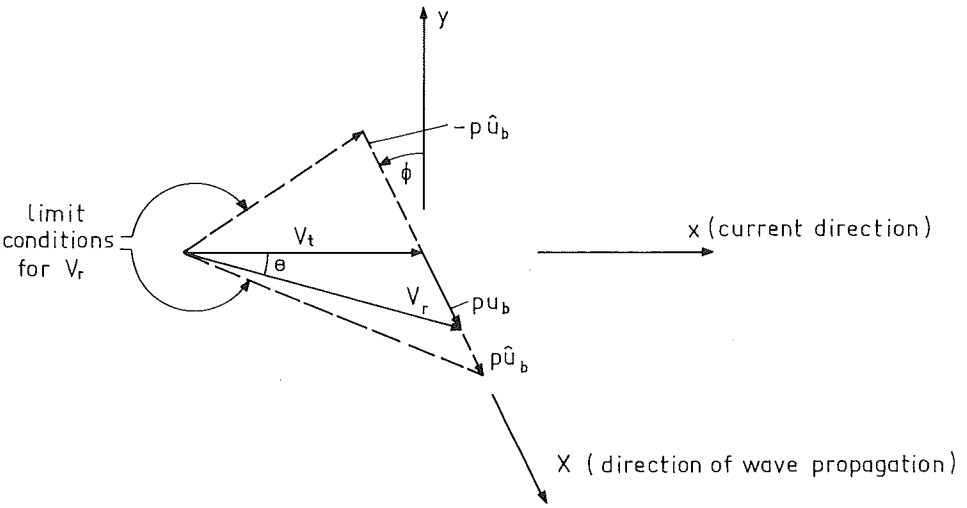

Figure 15.3
GEOMETRY OF VELOCITY COMPONENTS AT ELEVATION z'_t ABOVE BOTTOM

Proceeding just as in the previous sections, we can now determine the shear stress under the combination of currents and waves, τ_{cw}:

$$\tau_{cw} = \rho\, \kappa^2\, V_r^2 \qquad (15.24)$$

This shear stress is now directed along the time-varying line of action of V_r. The current, flowing in the x direction will be influenced primarily by the x component of this stress, τ_{cwx}. In chapter 19 the total shear stress, τ_{cw}, will be important for the sediment transport; for now, however, we shall concentrate exclusively on the friction shear stress component τ_{cwx}, important for the current. This component can be expressed as:

$$\tau_{cwx} = \tau_{cw} \cos \Theta \qquad (15.25)$$

or, using (15.22) through (15.24) in (15.25):

$$\tau_{cwx} = \rho\, \kappa^2 \sqrt{V_t^2 + (p\, u_b)^2 + 2p\, u_b\, V_t \sin \phi}\; [V_t + p\, u_b \sin \phi] \qquad (15.26)$$

in which u_b is a function of time. For our purposes, however, it is sufficient to determine the time average of τ_{cwx}. We do this by first writing out u_b:

$$u_b = \hat{u}_b \sin \omega t \qquad (15.27)$$

and for convenience introducing equation 15.14 for V_t. Doing this and carrying out a lot of algebra yields the following expression for the time average x component of the bottom shear stress:

$$\overline{\tau_{cwx}} = \frac{2\,\tau_c}{T} \int_{-T/4}^{T/4} \left[\left(1 + \xi \frac{\hat{u}_b}{V} \sin \omega t \sin \phi \right) \sqrt{1 + \left(\xi \frac{\hat{u}_b}{V} \sin \omega t \right)^2 + 2\xi \frac{\hat{u}_b}{V} \sin \omega t \sin \phi} \right] dt \qquad (15.28)$$

where ξ is a collection of parameters:

$$\xi = \frac{p\,\kappa\,C}{\sqrt{g}} = \frac{C\sqrt{f_w}}{\sqrt{2g}} \qquad (15.29)$$

Equation 15.28 is an elliptic integral and is, as such, not conducive to analytical solution. Bijker (1967) used a numerical procedure to evaluate the above integral for various realistic values of the independent variables, V, $\hat{u}_b$, ξ and ϕ. Then, by fitting an equation to the results obtained, he determined that for $|\phi| < 20^o$:

$$\overline{\tau_{cwx}} = \tau_c \left[0.75 + 0.45 \left(\xi \frac{\hat{u}_b}{V} \right)^{1.13} \right] \qquad (15.30)$$

or, introducing the definition of τ_c from equation 15.01:

$$\overline{\tau_{cwx}} = \frac{\rho g}{C^2} V^2 \left[0.75 + 0.45 \left(\xi \frac{\hat{u}_b}{V} \right)^{1.13} \right] \qquad (15.31)$$

Equation 15.31 is the relation between bed shear stress and velocity that should be used in the dynamic equilibrium of - for example - a wave-driven longshore current. Unfortunately, equation 15.31 is rather inconvenient* for this since V is then an unknown.

In order to arrive at a handier solution, we introduce a restriction that the angle between wave crests and the current be small. This is usually not too bad an assumption within the breaker zone. With this basis a still cruder assumption is made, namely:

$$\sin \phi = 0 \qquad (15.32)$$

instead of the more common one:

$$\sin \phi = \phi \qquad (15.33)$$

Introduction of equation 15.32 into 15.28 yields:

$$\overline{\tau_{cwx}} = \frac{2\,\tau_c}{T} \int_{-T/4}^{T/4} \sqrt{1 + \left(\xi \frac{\hat{u}_b}{V} \sin \omega t \right)^2}\, dt \qquad (15.34)$$

which can be further simplified by making the assumption (usually valid in the breaker zone) that:

$$\xi\, u_b >> V \qquad (15.35)$$

---

* This inconvenience will be demonstrated in chapter 16; it will lead to solutions by successive approximations.

Doing this allows us to carry out the integration directly yielding:

$$\overline{\tau_{cwx}} = \frac{2}{\pi} \tau_c \xi \frac{\hat{u}_b}{V} \qquad (15.36)$$

Equation 15.36 can be expressed in another form by introducing equations 15.01 and 15.29 into 15.36 yielding:

$$\overline{\tau_{cwx}} = \frac{\rho}{\pi C} \sqrt{2 g f_w} V \hat{u}_b \qquad (15.37)$$

A still further simplification can be introduced by using a shallow water approximation to evaluate $\hat{u}_b$ - see volume I chapter 5. Such an approximation yields:

$$\hat{u}_b = \frac{\omega H}{2kh} \qquad (I\text{-}5.01b) \qquad (15.38)$$

Using the relation between breaker height and water depth:

$$H = \gamma h \qquad (15.39)$$

and:

$$\frac{2\pi}{k} = \lambda = \sqrt{gh}\, T = \sqrt{gh}\, \frac{2\pi}{\omega} \qquad (15.40)$$

equation 15.38 becomes:

$$\hat{u}_b = \frac{\gamma}{2} \sqrt{gh} \qquad (15.41)$$

Substituting this relationship into equation 15.37 then results in:

$$\overline{\tau_{cwx}} = \frac{\rho g}{\sqrt{2}\, \pi\, C} \gamma \sqrt{h}\, \sqrt{f_w}\, V \qquad (15.42)$$

Equation 15.42 can be used in a dynamic equilibrium balance in order to derive a simple equation for the longshore current in the breaker zone. As already mentioned earlier, equation 15.31 would yield a more accurate result assuming that equation 15.17 were used to evaluate $\hat{u}_b$. Comparative results are shown in section 16.5.

15.5 Additional remarks

The equations and philosophy just presented has been used with reference to a longshore current in the breaker zone. Except for certain limitations imposed as a simplification - $\phi \ll 1$, $\xi \hat{u}_b \gg V$ - the procedure is general. Other important applications can be found wherever waves influence the local current velocities near the bottom. Thus, for example, the wave influence on currents in wide river mouths can also be studied using the procedure presented. The influence of waves on tidal currents in shallow seas or bays can also be evaluated; the validity of the simplifying assumptions made must, of course, be checked in each case.

In the previous sections we concerned ourselves only with the component of the bottom shear stress in the x direction indicated in figure 15.3 It is perhaps suprising that, in general, the resulting time-averaged bottom shear stress also has a component in the y direction. Only for the special cases where ϕ is an integer multiple of $\pi/2$ is this not the case.

The reason for this resultant y component of the bottom shear stress follows from the time average of τ_{cw} based upon V_r^2. Since the velocity vector pattern in figure 15.3 is not symmetrical about the x axis (unless ϕ is an integer multiple of $\pi/2$), the pattern of V_r^2 and hence τ_{cw} is also unsymmetrical and the stress component parallel to the y axis has a non-zero average. As a result of this phenomenon, the current direction will change relative to a no wave condition. In the breaker zone, where the angle ϕ is usually small, this effect is not noticable. Outside the breaker zone where, for example, a river current intersects a wave field, ϕ is no longer limited in value and a wave influence on the current direction can sometimes be observed.

In the following chapter various force components will be combined to predict the longshore current in the breaker zone.

16. LONGSHORE CURRENT COMPUTATION

E.W. Bijker
J. v.d. Graaff

16.1 Introduction

The previous four chapters have been devoted to discussions of various force components acting on an element of water in the breaker zone. As long as the wave conditions and shore geometry remain constant along the coast, these are the only force components acting on this water element; additional force components which can result when this limitation is not applied will be discussed in a later section of this chapter.

Rather than attempt to formulate a general current formula based upon a dynamic equilibrium of all four of the force components involved, we begin more simply by formulating an equilibrium between only two force components which are nearly always present in the breaker zone. This solution is expanded in succeeding sections of the chapter.

16.2 Basic force equilibrium

Since the bottom friction and the radiation stress gradient are always present in the breaker zone, it seems appropriate to begin a prediction of the resulting longshore current velocity with an equilibrium of these two forces.

From chapter 12, the driving force is:

$$\frac{\partial S_{yx}}{\partial y} = \frac{5}{16} \rho \gamma^2 (gh)^{3/2} \frac{\sin \phi_o}{c_o} m \qquad (12.15)^* \qquad (16.01)$$

where c_o is the wave velocity in deep water,
g is the acceleration of gravity,
h is the water depth,
m is the beach slope $= \frac{dh}{dy}$, *
γ is the breaker index,
ρ is the mass density of water, and
ϕ_o is the angle of wave approach in deep water.

The stress component from the friction force follows from equation 15.31 if we wish to be precise:

$$\overline{\tau_{cwx}} = \frac{\rho g}{C^2} V^2 \left[0.75 + 0.45 \left(\xi \frac{\hat{u}_b}{V} \right)^{1.13} \right] \qquad (15.31) \qquad (16.02)$$

where C is the Chézy coefficient,
$\hat{u}_b$ is the wave-caused water velocity amplitude near the bottom,
V is the (unknown) current velocity averaged over the depth, and
ξ is a coefficient defined in equation 15.29.

---

* Note that the notation has been changed to correspond to the new axis notation introduced in chapter 13. Thus, both $\frac{\partial S_{yx}}{\partial y}$ and m are now positive.

Equation (16.01) to (16.02) and solving for V yields the desired expression for the velocity at a given point in the breaker zone. Unfortunately, because of the nature of (16.02) an explicit solution is impossible; the best that can be achieved is:

$$0.75\ V^2 + 0.45\ (\xi\ \hat{u}_b)^{1.13}\ V^{0.87} = \frac{5\sqrt{g}}{16}\ \frac{\gamma^2\ C^2\ \sin\phi_o\ m}{c_o}\ h^{3/2} \qquad (16.03)$$

which can only be solved iteratively for V. (A Runge-Kutta method is sufficient).

In order to obtain more insight into the velocity distribution in the breaker zone, we shall start again, however this time using the simpler, more approximate friction stress relation (15.42):

$$\overline{\tau_{cwx}} = \frac{\rho g}{\sqrt{2}\ \pi\ C}\ \gamma\ \sqrt{h}\ \sqrt{f_w}\ V \qquad (16.04)$$

where f_w is the wave friction factor evaluated using equation 15.16 or figure 15.2.

The approximate velocity distribution as a function of distance from the coast, y, can be determined equating (16.01) and (16.04):

$$\frac{\sqrt{2}\ \rho g}{2\ \pi\ C}\ \gamma\ \sqrt{h}\ \sqrt{f_w}\ V = \frac{5}{16}\ \rho\ \gamma^2\ (gh)^{3/2}\ \frac{\sin\phi_o}{c_o}\ m \qquad (16.05)$$

Solving this for V yields:

$$V = \frac{5\ \pi\ \sqrt{g}}{8\ \sqrt{2}}\ \frac{\sin\phi_o}{c_o}\ \gamma\ \frac{C}{\sqrt{f_w}}\ h\ \ m \qquad (16.06)$$

In this equation:

$\frac{5\ \pi\ \sqrt{g}}{8\ \sqrt{2}}$ is a constant,

$\frac{\sin\phi_o}{c_o}$ depends only upon the deep water wave conditions,

γ depends upon wave conditions and beach slope,

$\frac{C}{\sqrt{f_w}}$ is a friction term dependent upon bottom roughness, water depth, and the local wave conditions.

h and m are functions of the distance to the shore.

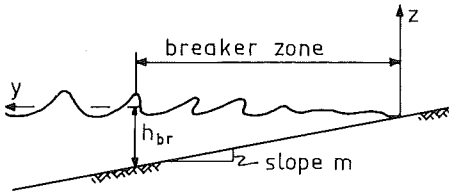

a. Cross Section

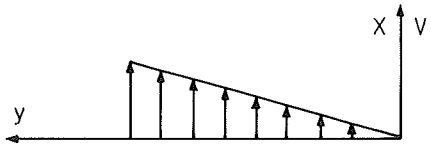

b. Velocity Profile

Figure 16.1
SIMPLIFIED VELOCITY PROFILE IN BREAKER ZONE

The dependence of the friction term, above, upon the water depth - even for constant roughness—complicates the problem a bit; therefore, many investigators have assumed that this friction term is constant throughout the breaker zone.

If we accept the above simplifying assumption and further stipulate that the beach is of uniform slope, then the longshore current velocity turns out to be a linear function of the water depth, h, within the breaker zone; the maximum velocity in the profile shown in figure 16.1b occurs at the outer edge of the breaker zone shown in figure 16.1a. The fact that the velocity outside the breaker zone is zero follows directly from the fact that $\frac{\partial S_{yx}}{\partial y} = 0$, there, as shown in section 12.2.

16.3 Effect of turbulence

In chapter 14 the effect of turbulent forces was found to be dependent upon the velocity gradient, thus upon $\frac{dV}{dy}$ in the notation of this section. Since the velocity gradient is infinite at the outside of the breaker zone in figure 16.1 , we can expect the velocity profile to be most influenced there. Indeed, the horizontal transfer of momentum will decrease the velocities within the outer portion of the breaker zone and provide the driving force for a current in the same direction just outside the breaker zone. Longuet-Higgins (1971) and Battjes (1974) have recently theoretically predicted the velocity distribution resulting from including the turbulent forces in a dynamic equilibrium along with the radiation shear stress gradient and friction.

16.4 Effect of irregular waves

All of the discussion presented so far has been based upon an assumption that regular waves are present. In practice, this will, of course, not be the case; the wave heights will vary and the outer edge of the breaker zone will not be as well defined as is suggested in figure 16.1. The largest waves will break in deeper water than the smaller waves. Battjes (1974) attacked the problem of computing the longshore current distribution by starting with a reasonable description of the irregular wave field within the breaker zone. He computed the resulting radiation shear stress gradient from the (known) wave height distributions at various locations within the breaker zone. Then, he determined the lateral velocity profile from the distribution of this radiation stress component. The effect of this wave irregularity is much like that of the lateral turbulence; the velocity profile becomes wider and less sharply peaked than that shown in figure 16.01. A quantatative comparison will be made in the next section.

Longshore current velocity profiles on real coasts can vary significantly - see figure 16.2. Tidal influences, width of the wave spectrum, variations in bottom roughness, irregular bottom slopes and variations in wave direction and height all contribute to modifying the velocity profile.

16.5 Example

Determine the distribution of the average (over the depth) longshore current velocity in a breaker zone as a function of distance from the shore. Regular waves with a period of 7 seconds approach the coast from deep water with a wave height, H_o, of 2.0 m and an approach angle, ϕ_o, of 30^o. A breaker index, γ, of 0.8 and a beach slope, m, of 1:100 are to be used. The bottom roughness, r, is assumed to have a constant value of 0.06 m across the entire beach. The first step of the solution is to define the outer edge of the breaker zone. The non-linear character of the problem makes a direct analytical solution impossible; instead, the following iterative scheme can be used, however.

1. Guess a breaker depth, h_{br}, and compute h_{br}/λ_o.
2. Using tables of wave functions (or computations) determine the shoaling coefficient, K_{sh} and the ratio of wave speeds, c/c_o.
3. Determine the angle ϕ_{br} using:

$$\sin \phi_{br} = \frac{c}{c_o} \sin \phi_o \tag{16.07}$$

4. Compute the breaker height, H_{br} from:

$$H_{br} = H_o K_{sh} \sqrt{\frac{\cos \phi_o}{\cos \phi_{br}}} \tag{16.08}$$

5. Compute a new value of h_{br} from the known values of γ and the computed H_{br}. Return to step 1.

Applying the above procedure to the problem at hand and using tables of wave functions for step 2 yields:

$$\left.\begin{aligned} H_{br} &= 2.07 \text{ m}, \\ h_{br} &= 2.59 \text{ m, and} \\ \phi_{br} &= 13.3^o \end{aligned}\right\} \tag{16.09}$$

Table 16.1 shows computations for a series of points within the breaker zone. The computation is illustrated below for the point 259 m from the shore; the outer edge of the breaker zone.

The wave length follows from:

$$\lambda = c\,T \approx \sqrt{gh}\;T = \sqrt{(9.81)(2.59)}\;(7) = 35.3 \text{ m}^* \tag{16.10}$$

The amplitude of the motion on the bottom, a_b - see chapter 15, follows equation 5.03b of volume I, with (16.10) and results in:

$$a_b = \frac{\gamma}{4\pi} \lambda = \frac{0.8}{(4)(\pi)} 35.3 = 2.25 \text{ m} \tag{16.11}$$

The friction term can then be computed from equation 15.16 or taken from figure 15.2 knowing that the bottom roughness, r, is 0.06 m.

$$f_w = \exp\left[-5.977 + 5.213 \left(\frac{2.25}{0.06} \right)^{-0.194} \right] = 0.034 \tag{16.12}$$

The Chézy coefficient, C, is determined in the usual way using:

$$C = 18 \log \left(\frac{12\,h}{r} \right) \tag{16.13}$$

$$= 48.9 \text{ m}^{\frac{1}{2}}/\text{s} \tag{16.14}$$

Then, V follows by substitution in equation 16.06:

$$V = \frac{5\,\pi\,\sqrt{g}}{8\,\sqrt{2}} \frac{\sin 30^o}{(1.56)(7)} (0.8) \left(\frac{48.9}{\sqrt{0.034}} \right) (2.59) \left(\frac{1}{100} \right) \tag{16.15}$$

$$= 1.09 \text{ m/s} \tag{16.16}$$

This value can be found in the column labeled V_1 in table 16.1.

---

* The shallow water approximations are being used throughout the rest of this computation. This is in keeping with the approximations made earlier in the determination of $\overline{\tau_{cwx}}$.

Table 16.1 Longshore current determination

H_o = 2.0 m, T = 7 sec., $\phi_o = 30^o$

distance y	water depth h	wave height H	wave length λ	bottom amplitude a_b	f_w	C	V_1	V_2	V_3	V_4	V_5	V_6
(m)	(m)	(m)	(m)	(m)	(-)	($m^{\frac{1}{2}}/s$)	(m/s)	(m/s)	(m/s)	(m/s)	(m/s)	(m/s)
0	0	0	0.	0.	-	-	0.00	0.0	0.00	0.00	0.00	0.00
25	0.25	0.20	11.0	0.70	0.065	30.6	0.48	0.04	0.11	0.12		0.04
50	0.50	0.40	15.5	0.99	0.052	36.0	0.126	0.11	0.21	0.24		0.11
75	0.75	0.60	19.0	1.21	0.047	39.2	0.216	0.20	0.31	0.36		0.19
100	1.00	0.80	21.9	1.40	0.043	41.4	0.318	0.28	0.42	0.45		0.26
125	1.25	1.00	24.5	1.56	0.040	43.2	0.430	0.37	0.53	0.53		0.33
150	1.50	1.20	26.9	1.71	0.039	44.6	0.539	0.46	0.63	0.58		0.38
175	1.75	1.40	29.0	1.85	0.037	45.8	0.663	0.55	0.73	0.59	0.55	0.42
200	2.00	1.60	31.0	1.97	0.036	46.8	0.785	0.65	0.82	0.57		0.43
225	2.25	1.80	32.9	2.09	0.035	47.8	0.915	0.74	0.84	0.51		0.43
250	2.50	2.00	34.7	2.21	0.034	48.6	1.05	0.83	0.65	0.40		0.42
259	2.59	2.07	35.3	2.25	0.034	48.9	1.09	0,86	0.50	0.35		0.41
275							0.00	0.00	0.21	0.27		0.39
300									0.06	0.18		0.35
350									0.01	0.09		0.24
415										0.04	0.00	0.12
450										0.03		0.07
500												0.03

Several different resulting velocity profiles are listed in this table; each is described below. V_1 is found from the tabulated computations basing each velocity value on a locally computed friction term. The approximate friction term (15.42) and shallow water wave approximations are used throughout. V_2 includes none of the simplifying assumptions inherent in the shallow water approximations. Thus, equation 12.10 is used instead of equation 12.15 to determine the driving force, and the friction force is determined using the more exact relation equation 15.31. Also, intermediate depth wave theory is used for all computations. Only the resulting values are shown; they are seen to be lower by as much as 20%.

V_3 in the table results from including a turbulent friction force in the velocity equation. The use of Battjes (1974) approach for regular waves yields the results shown within the breaker zone. The technique may not be applied officially outside the breaker zone, but has been applied there for comparison purposes.

Longuet-Higgins (1971) uses a different approach which includes a larger turbulent lateral friction force than does Battjes. The results of his approach are denoted by V_4 in table 16.1.

Still another approximate attempt at reality schematizes the velocity profile by a triangle extending over a width equal to 1.6 y_{br}. Its peak value occurs at $y = \frac{2}{3} y_{br}$ from the shore, and its peak value is found by stipulating that:

$$\int_0^{1.6\, y_{br}} \overline{\tau_{cwx}}\, dy = S_{yx}\Big|_{y = y_{br}} \qquad (16.17)$$

Carrying out the integration yields a peak value of 0.55 m/s denoted by V_5 in the table. This type of velocity distribution can be assumed to include some lateral turbulent friction effects.

Finally, if an irregular wave having the same total energy as the regular wave ($H_{rms\ o} = 2.0$ m in this case) is used, then the method suggested by Battjes (1974) neglecting lateral friction yields the velocities denoted by V_6.

All of these profiles are compared in figure 16.2.

16.6 Additional driving forces

In the work so far in this chapter variations in wave conditions between places along the coast have not been considered; all wave properties have been assumed to be independent of the location, x, along the coast. This is seldom the case in a real situation.

Since the depth contours along a coast are seldom parallel, variation in refraction will cause the wave height to vary as we travel along some depth contour. Partial obstructions such as capes, spits, or even breakwaters will cause additional wave height and direction changes as we again follow a given depth contour along the coast.

The necessity of including a $\frac{\partial H}{\partial x}$ and a $\frac{\partial \phi}{\partial x}$ in the longshore current computations should be obvious. Perhaps less obvious is that two additional driving forces need some explanation; both result from the longshore gradient of the wave height and angle of approach.

In chapter 11 we examined the wave set-up, h', resulting from waves approaching a coast. This was found to be dependent upon the wave height, H.* If the wave height and angle now vary along the coast then we can expect the wave set-up and set-down to vary as well resulting in a slope of the average water level along the coast, $\frac{\partial h'}{\partial x}$. This water surface slope will then provide an additional driving force for the dynamic equilibrium of a water element.

---

* In general, it is also dependent upon ϕ.

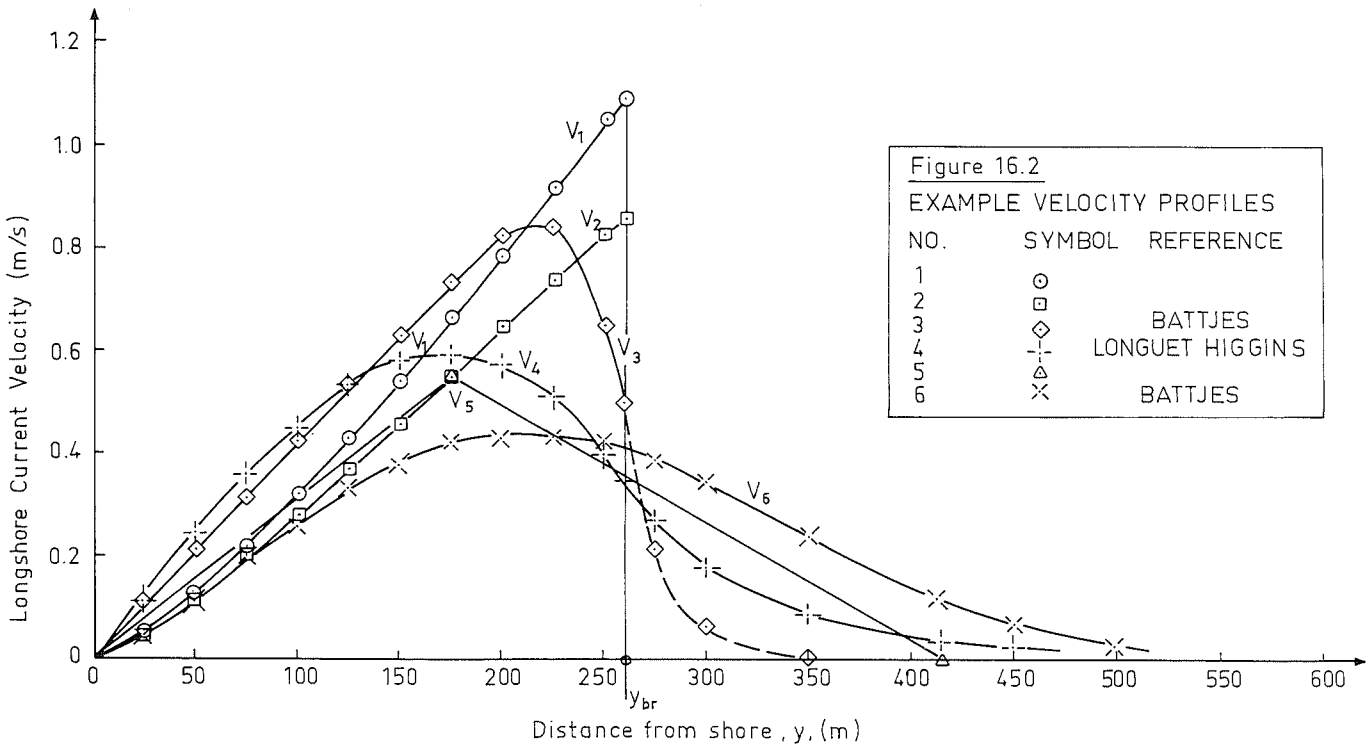

Figure 16.2

EXAMPLE VELOCITY PROFILES

NO.	SYMBOL	REFERENCE
1	⊙	
2	⊡	
3	◇	BATTJES
4	⊹	LONGUET HIGGINS
5	△	
6	×	BATTJES

The second additional driving force results from a gradient in the normal stress acting on a plane perpendicular to the coastline. This would be denoted by S_{xx} using the notation of this chapter; in chapter 10 it was denoted by S_{yy} - see figure 10.2. Our element of water experiences a driving force proportional to $\frac{\partial S_{xx}}{\partial x}$ (back in currently popular notation) which is dependent upon both $\frac{\partial \phi}{\partial x}$ and $\frac{\partial H}{\partial x}$

While both of the forces indicated above have been called driving forces, this does not imply that they always both act in the same direction or in the same direction as $\frac{\partial S_{yx}}{\partial y}$. Obviously, their proper directions must be assigned in a force balance and these directions must be determined for each case separately.

Tides, discussed in chapter 13, can also, of course, influence the longshore current velocity. Because of their more universal occurrence, tidal influences can be found in more and larger areas than the other influences just mentioned above. Indeed, because of tidal phase and amplitude differences occurring along the Dutch coast, for example, tidal influences play an important role in the coastal sand transport process, especially in the region immediately outside the breaker zone.

This concludes our discussion of longshore currents. In the next three chapters we focus attention upon the prediction of sediment movements along the coast.

17. EARLY COASTAL TRANSPORT FORMULAS

J. v.d. Graaff

17.1 Introduction

This chapter begins a new phase of our study of coastal changes. The previous five chapters have been devoted to the determination of the coastal current, one of the input parameters for a general sediment transport formula such as was suggested in chapter 9.

Here, we begin to consider the movement of sediment instead of water. Before attacking sediment transport via a prediction of sediment concentration and sediment velocity - the method suggested in chapter 9 - we sharpen our insight by first considering one of the first coastal sediment transport formulas.

Since most coastal sediments are sands, most formulas have been developed for sand beaches. Luckily, sand is one of the more predictable soil materials; it has negligible cohesion and a fairly constant shear strength property (angle of internal friction). Finer materials, silts and clays, on the other hand, do not have such simple properties. Because of its simplicity and common occurrence the sediment transport formulas are usually derived for sand; they are even often called sand transport formulas.

The formula presented in the remainder of this chapter was developed from prototype and model measurements long before much of the longshore current theory was available. Indeed, the formula - the so-called CERC formula - was apparently developed soon after World War II by the Beach Erosion Board, the predecessor of the U.S. Army Coastal Engineering Research Center.

17.2 The CERC formula

Observations in both prototype and models made in the decade following World War II indicated a correlation between the volumetric sand transport rate along a coast [L^3/T] and a "component of the approaching wave energy".* This sand transport was found to be more or less concentrated in the breaker zone. Expressed as a formula, this sand transport rate, S, is:

$$S = A\,U' \tag{17.01}$$

where A is coefficient and units conversion factor, and
U' is a component of the energy flux or power entering a unit length of the breaker zone.

The power or energy flux in a unit crest length of wave train approaching the coast was given in volume I:

$$U = E\,c_g \qquad \text{(I-5.10)} \tag{17.02}$$

where E is the wave energy, and
c_g is the wave group velocity.

* It is a mystery how scalar quantities, energy and power, can have components. Both Longuet-Higgings (1971) and Battjes (1974) show that this concept has no physical interpretation.

U is a perfectly valid scalar physical parameter.
Its component - invalid parameter! - along the coast (in the x direction) at the outer edge of the breaker zone is:

$$U_x = U \sin \phi_{br} \tag{17.03}$$

where ϕ_{br} is the angle between the wave crests and the coast at the outer edge of the breaker zone. Similarly - and just as incorrectly - the power component perpendicular to the coast is:

$$U_y = U \cos \phi_{br} \tag{17.04}$$

This yield a similarly non-interpretable parameter:

$$U' = \frac{U_x U_y}{U} = U \sin \phi_{br} \cos \phi_{br} \tag{17.05}$$

or equivalently:

$$U' = E c_g \sin \phi_{br} \cos \phi_{br} \tag{17.06}$$

Using refraction theory (volume I, chapter 9) and appropriate approximations:

$$U' = \frac{1}{16} \rho g H_o^2 c_o K_{rbr}^2 \sin \phi_{br} \cos \phi_{br} \tag{17.07}$$

where: c_o is the deep water wave speed,
g is the acceleration of gravity,
H_o is the deep water wave height,
K_{rbr} is the refraction coefficient at the outer edge of the breaker zone, and
ρ is the mass density of water.

Substituting (17.07) into (17.01) and substituting a (not dimensionless) value for A (determined from both model and prototype measurements) yields:

$$S = 0.014 H_o^2 c_o K_{rbr}^2 \sin \phi_{br} \cos \phi_{br} \tag{17.08}$$

which is exactly the same as equation 26.04 in volume I. If consistent units are used, the coefficient, 0.014, is dimensionless. However, it is often convenient to express S in volume per year while c_o remains units of length per second. In such a case, the coefficient is not dimensionless and the equation becomes:

$$S = 0.44 \times 10^6 H_o^2 c_o K_{rbr}^2 \sin \phi_{br} \cos \phi_{br} \tag{17.09}$$

which also appears in volume I as equation 26.05.

There remains some disagreement as to the proper wave height to use to represent an irregular wave train and the proper value for the coefficient in the two equations immediately above. This will be discussed in detail in section 17.5 after a better physical explanation for the CERC formula is presented in the following section.

17.3 Modern justification of the CERC formula

More recent developments such as the formulation for the radiation stress make it possible to give a more reasonable explanation for the CERC formula in terms of "correct" physical phenomona.

The radiation shear stress for all points outside the breaker zone is constant - see chapter 12. This shear stress, sometimes called lateral wave thrust, is equal to:

$$S_{yx} = E\, n \sin \phi \cos \phi \qquad (12.03)^{*} \qquad (17.10)$$

where n is the ratio $\frac{c}{c_g}$.
Since S_{yx} is constant outside the breaker zone, we can choose to evaluate it using wave conditions at the outer edge of the breaker zone:

$$S_{yx} = E_{br}\, n_{br} \sin \phi_{br} \cos \phi_{br} \qquad (17.11)$$

In the previous chapter, this radiation shear stress provided the driving force for the longshore current within the breaker zone.

Beginning again on a new tack, we can reasonably accept the hypothesis that the waves are the primary factor in stirring sand into suspension for transport by a current. A reasonable characterizing parameter for this stirring can be the wave orbital velocity amplitude near the botton, $\hat{u}_b$. If we use shallow water approximations, $\hat{u}_b$ can be expressed in terms of the wave speed in the breaker zone:

$$\hat{u}_b = \frac{\gamma}{2} c_{br} \qquad (17.12)$$

In more general terms, $\hat{u}_b$ is directly proportional to c_{br} within the breaker zone, thus, c_{br} is a legitimate parameter for characterizing the stirring action and hence the sand concentration within the breaker zone.

Now, using the concept expressed in chapter 9, we can develop a sand transport formula by taking a product of S_{yx} (a measure of velocity) with c_{br} (a measure of sand concentration):

$$S_{yx}\, c_{br} = E_{br}\, n_{br}\, c_{br} \sin \phi_{br} \cos \phi_{br} \qquad (17.13)$$

This is equivalent to equation 17.06.

17.4 Variation with angle of approach

How do changes in the angle between the approaching wave crests and the coastline influence the longshore sediment transport? This can be studied via equation 17.08, but it is more convenient to express the relationship between S and angle of approach, ϕ, in terms of the deep water angle, ϕ_o.

---

* Remember the change of axes!

Using refraction theory from volume I, chapter 9:

$$K_{rbr}^{\ 2} \cos \phi_{br} = \cos \phi_o \tag{17.14}$$

and:

$$\sin \phi_{br} = \frac{c_{br}}{c_o} \sin \phi_o \tag{17.15}$$

Equation 17.08 then becomes:

$$S = 0.014\ H_o^2\ c_{br} \sin \phi_o \cos \phi_o \tag{17.16}$$

In order to investigate the effect of changes in ϕ_o on S, we need to determine which parameters depend upon ϕ_o. Obviously sin ϕ_o and cos ϕ_o do, but c_{br} does as well, since the wave height at the edge of the breaker zone depends upon the refraction coefficient. This variable wave height means that the outer edge of the breaker zone shifts as ϕ_o changes. The fact that c_{br} is dependent upon h_{br} completes the argument.

Thus, the behavior of:

$$f(\phi_o) = c_{br} \sin \phi_o \cos \phi_o \tag{17.17}$$

must be studied. Unfortunately, this function, $f(\phi_o)$, cannot be written out in a simple algebraic form.

Rather than present a rather cumbersome numerical procedure to evaluate $f(\phi_o)$, we shall be content only to discuss the results of such a study of $f(\phi_o)$ found by evaluating the function for a whole series of values of ϕ_o and the wave period*. The factor sin ϕ_o cos ϕ_o is by far the most important in the function $f(\phi_o)$. Thus, a graph of $f(\phi_o)$ looks much like one of sin ϕ_o cos ϕ_o. Just as sin ϕ_o cos ϕ_o, $f(\phi_o)$ is zero for $\phi_o = 0^o$ and $\phi_o = 90^o$. In contrast to sin ϕ_o cos ϕ_o which is symmetrical about the line $\phi_o = 45^o$, $f(\phi)$ is asymmetric; values of $f(\phi_o)$ for $0 < \phi_o < 40^o$ are generally higher than corresponding values of $f(90^o-\phi_o)$. This is most pronounced for relatively small values of ϕ_o. Lastly, the peak value of $f(\phi_o)$ occurs for $\phi_o < 45^o$ - usually somewhere between 40^o and 45^o.

17.5 CERC formula coefficient

As was already indicated in section 17.2, certain disagreements exist with regard to the proper coefficient value to use in equation 17.08 or 17.09. The choice of the proper wave height (H_{sig} or H_{rms}) introduces an additional complication.

The early model tests used to determine equation 17.09 were conducted using regular waves for which U' can easily be evaluated. The significant wave height, H_{sig}, was most likely used to characterize the waves in the prototype upon which the equation was checked even though the physically proper characterizing wave height is the root-

* The wave period enters the computation via the value, c_o, used in the refraction computation.

mean-square wave height, H_{rms}. This error leads to an error of a factor 2* in U' and hence the coefficient - see volume I chapter 10.

Additionally, there is further discussion about the proper coefficient value stemming from the various sets of model and prototype data. Study of the literature on this topic is confusing since a given set of data is often presented in various different hopefully equivalent manners by different investigators.

Figure 17.1 shows some experimental data relating S to U', with U' based upon H_{rms}. If a linear relationship between these parameters is assumed as in the CERC formula, then a least-squares fit using all of the data points results in line 1 plotted in the figure**. If, on the other hand, the one point given by Moore and Cole is neglected, line 2 results which indicates that the sand transport, S, should be nearly four times as great for the same wave conditions!

The disagreement is further illustrated in table 17.1 where coefficients for the CERC formula determined by various investigators are compared. When all coefficients are related to the same characteristic wave, the Shore Protection Manual gives a coefficient yielding a sand transport nearly 6 times that suggested by line 1 in figure 17.1!

The discussion is far from ended.....

Table 17.1 CERC formula coefficients

Investigator	Coefficient in equation 17.08	Characterizing Wave Height	Corresponding coefficient in (17.09)
Original CERC	0.014	H_{sig}	0.44×10^6
	0.028	H_{rms}	0.88×10^6
Shore Protection Manual (1973)	0.025	H_{sig}	0.79×10^6
Komar (1976)	0.049	H_{rms}	1.55×10^6
Svašek (1969)	0.039	H_{rms}	1.23×10^6
figure 17.1:			
line 1	0.008	H_{rms}	0.25×10^6
line 2	0.036	H_{rms}	1.13×10^6
Delft Univ. of Tech. Computer Program	0.039†	H_{rms}	1.23×10^6†

* $H_{sig}^2 = 2\, H_{rms}^2$

** The data in the figure is plotted on a logarithmic scale for convenience, only.

† These coefficients are really variables in this computer program. Commonly used values of these coefficients are listed.

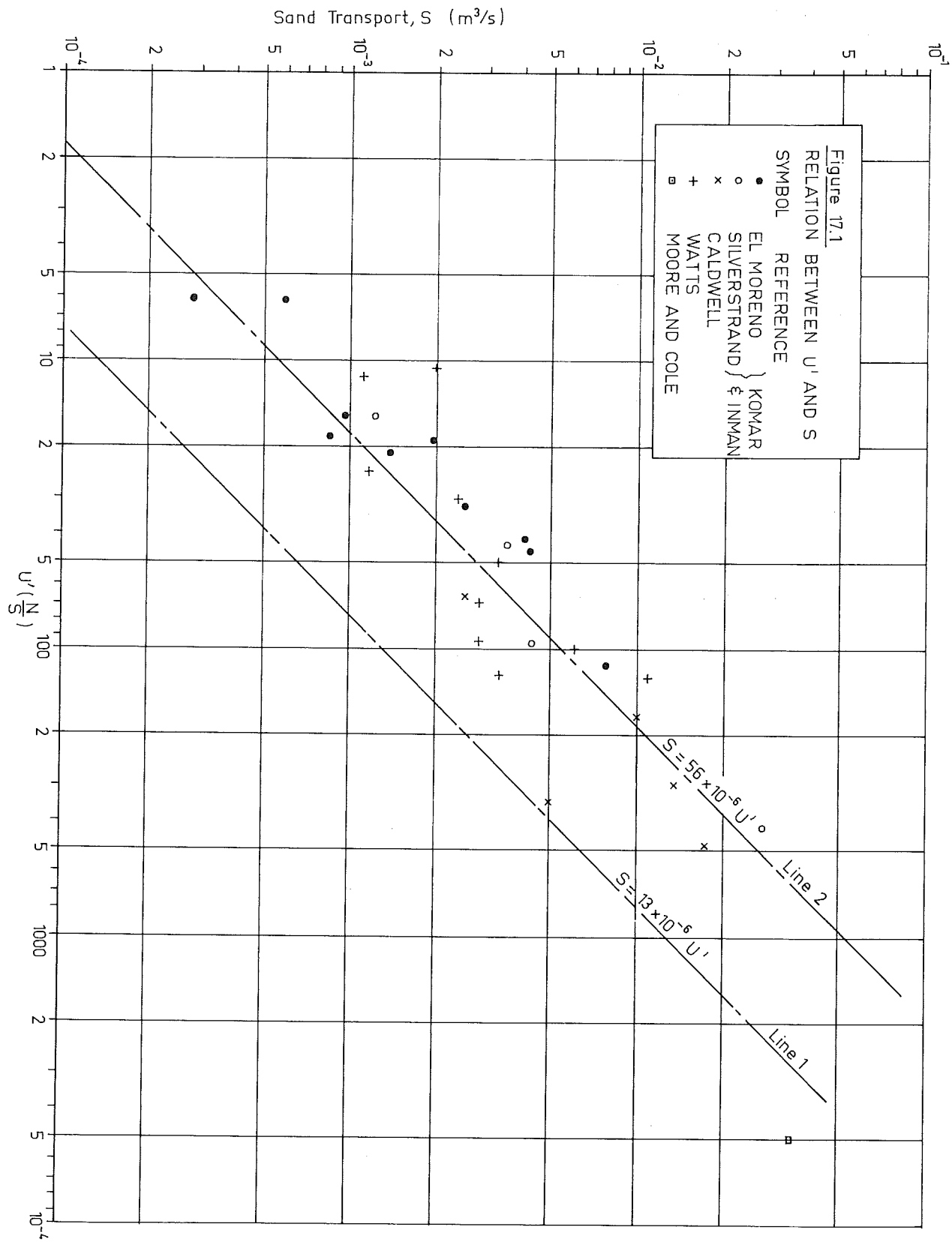
Sand Transport, S (m³/s)
10⁻⁴
2
5
10⁻³
2
5
10⁻²
2
5
10⁻¹
1
2
5
10
2
5
100
2
5
1000
2
5
10⁻⁴
U' (N/S)
Figure 17.1
RELATION BETWEEN U' AND S
SYMBOL REFERENCE
EL MORENO } KOMAR
SILVERSTRAND } & INMAN
CALDWELL
WATTS
MOORE AND COLE
S = 56 × 10⁻⁶ U'²
Line 2
S = 13 × 10⁻⁶ U'
Line 1

17.6 Example of use of CERC formula

Since a computation of sand transport using the CERC formula is so straightforward it is not deemed necessary to illustrate its use here. Instead, a computation using the CERC formula is postponed until section 11 of chapter 19 where the results are compared to those of other sand transport determinations.

17.7 Limitations of the CERC formula

The CERC formula with proper coefficient (whatever that is) is suprisingly trustworthy for many more or less routine applications. It does, however, have some limitations which make it unsuitable for certain problems.

Only a total sand transport rate is computed. No information on the distribution of this transport over the width of the breaker zone is obtained. This can be a serious limitation when coasts having several offshore bars or short groins are being studied.

The formula takes no account of the bottom material properties. It was derived for beaches having rather uniform sand with average diameters ranging 175 μm to 1000 μm (1 mm). The presence of similar beach sand is a prerequisite to the use of this formula.

The beach slope or breaker zone width do not enter the CERC formula.

Only driving forces resulting from waves which have the same properties at all points along the coast are considered. The formula will then fail where other driving forces play a significant role - see chapter 16 for a further discussion of this.

The CERC formula is not applicable to shoals, dumping grounds, or near dredged channels.

Svašek (1969) has attempted to overcome the first limitation and has modified the CERC formula to yield a distribition of the sand transport across the breaker zone. His approach is to assume that the sand transport occurring across some element of width of breaker zone, is directly proportional to the loss of power by the waves crossing that same width. This assumption, although plausible, has not been proven rigorously.

In another attempt to eliminate most all of these limitations of the CERC formula Bijker (1967) attacked the problem afresh modifying a sediment transport formula for constant currents to include wave effects. The details of this will be presented in chapter 19; first, however, we need to review the physical sand transport phenomona in the next chapter.

Extra Notes

18. SAND TRANSPORT MECHANISM

J.D. Schepers

18.1 Introduction

An insight into the physical process of stirring up of bottom material, its transport and re-deposition by waves and currents will be helpful for the understanding of the philosophy of the more modern coastal sediment transport formulas. In this chapter, we examine these physical processes occurring near a sandy bottom over which waves are propagating.

18.2 Basic concepts

Waves travelling in all except deep water cause a horizontal oscillating water movement near the bottom. The water there moves with a time-dependent velocity, u_b.

As has already been shown in chapter 15, the shear stress near the bottom increases as the velocity near the bottom increases. This is true universally - for waves or currents or a combination of them. When this shear stress exceeds a certain critical value (corresponding to a velocity u_{bcr} at the bottom) sand grains on a plane bed will begin to move with the water. Since the individual sand grains have so little mass they usually attain a velocity essentially equal to that of the water very quickly. Thus, the grains can be assumed to remain at rest when $u_b < u_{bcr}$ and to move with velocity u_b when $u_b > u_{bcr}$. This assumption becomes invalid, however, if in a special case, $u_b \approx u_{bcr}$ for an extended time period.

If a graph of the bottom velocity, u_b, versus time, t, is a bit asymmetrical with respect to its zero value, a resultant transport of bottom material could be expected. Such a transport is suggested by figure 18.1.

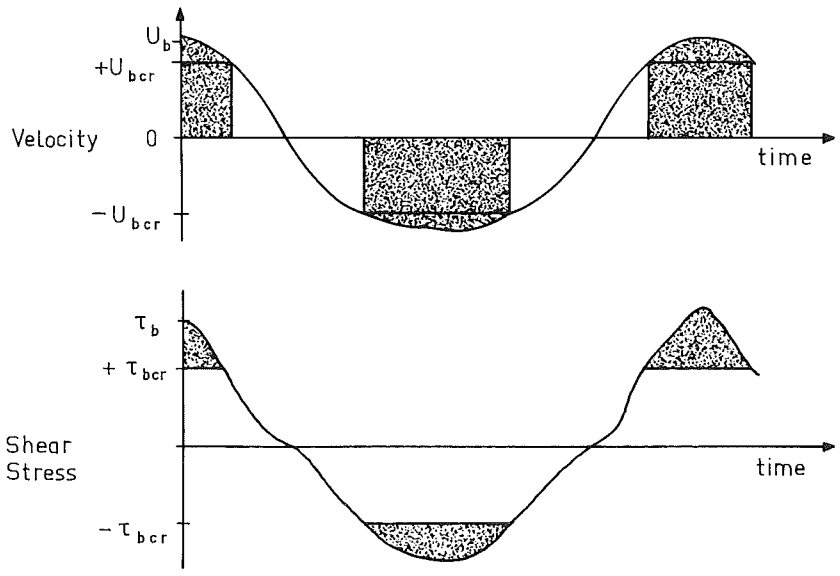

Figure 18.1

BOTTOM VELOCITY AND SHEAR STRESS VARIATION. SEDIMENT MOTION TAKES PLACE IN THE SHADED PORTIONS.

The velocity diagram shown in the figure would lead to a net bottom transport in the positive u_b direction. Sand grains will move back and forth, as suggested in figure 18.2, with a net forward movement. The asymmetry of the velocity diagram shown in figure 18.1 is nearly always present in shallow water. The simple linear wave theory is totally inadequate to describe the water motions accurately even though it is often used because of its relative simplicity.

Figure 18.2
SCHEMATIC REPRENSENTATION OF SEDIMENT MOVEMENT

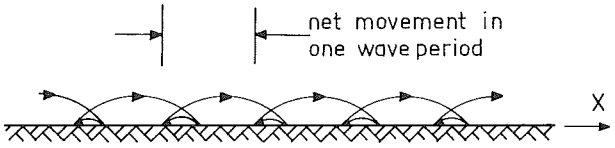

18.3 Bottom roughness

Slight irregularities of a sandy plane bed will initiate the formation of a wave-like rippled bottom profile. This rippled bottom disturbs the flow pattern near the bottom; separations occur at various points on each ripple profile at different times in the wave period. For example, when the bottom velocity is positive - defined as the direction of wave propagation in this chapter - a separation and resulting eddy will occur on the front of the ripple as shown in figure 18.3a. The opposite pattern - figure 18.3b - will be generated one half wave period later. This discussion implicitly defines the front and back of a ripple as shown in figure 18.3.

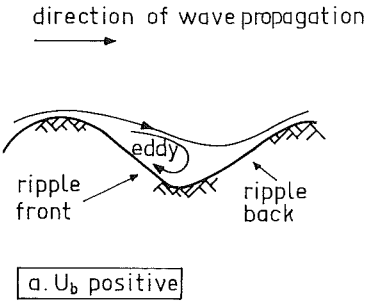

Figure 18.3
EDDY FORMATION NEAR BOTTOM RIPPLES

It seems obvious that the sand transport will be strongly influenced by these ripples and resulting eddies. Two separate mechanisms of sand transport can be distinguished; the first of these results directly from the presence of the eddies.

As has been indicated above, a primary eddy will form on the front side of a ripple when the bottom velocity, u_b, is positive - figure 18.3a. The high local velocities resulting from this eddy cause local erosion as is indicated in figure 18.4a; this sand remains in suspension within the eddy. A short time later, indicated in figure 18.4d, the flow stops and the eddy "explodes" dispersing the entrained sand upward - figure 18.4b.
Still later, this sand falls back to the bottom on the "upstream" side of the ripple from which it was eroded as indicated in figure 18.4c. This last process is very dependent upon the details of the water motion, the exact shape of the ripples, and the bottom material properties.

Obviously a mirror-immage situation with a secondary eddy exists during the other half of the wave period. Again, asymmetry of the ripples as well as the wave motion will guarantee that a net sand transport results. Note that the material eroded by the primary eddy during the presence of positive velocities is moved in the negative direction and vice-versa.

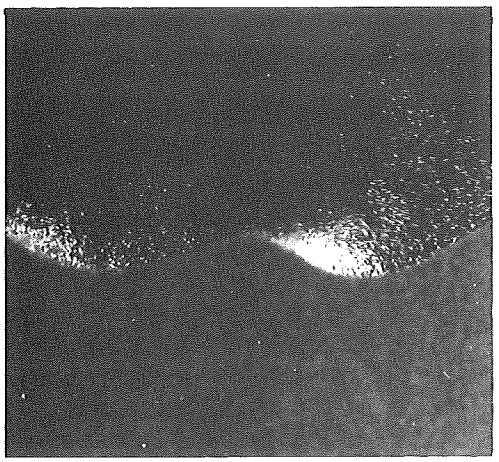

a. Sand Eroded to Eddy

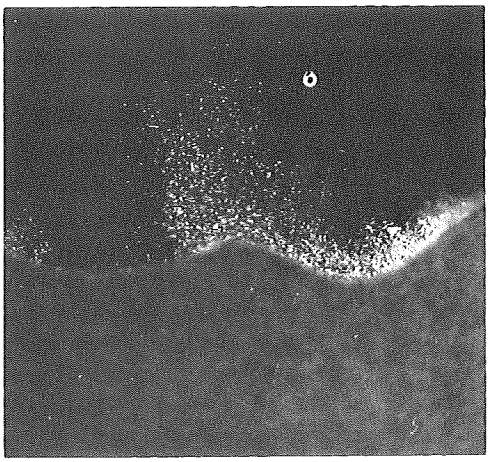

b Eddy "Explodes"

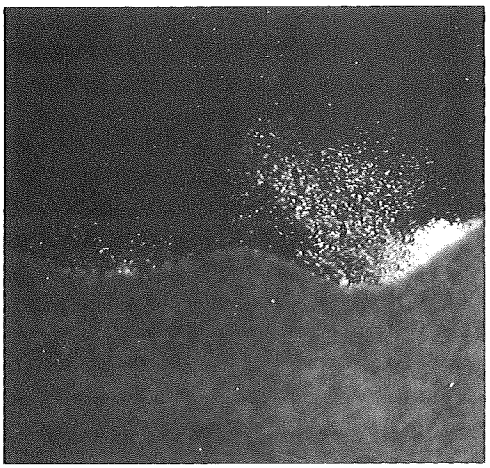

c. Sand Deposited

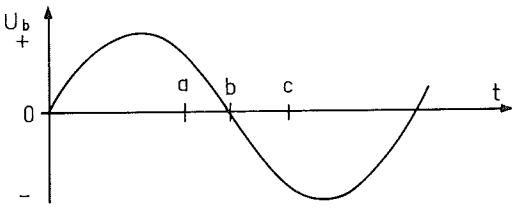

d. Times in wave period corresponding to above figures.

Figure 18.4
STEPS IN EROSION AND DEPOSITION

The irregularities in the waves are usually such that the maximum positive velocity - generating the primary eddy - is greater than the maximum magnitude of the negative velocities - generating the secondary eddy. This, in turn, can lead us to expect a relatively strong primary eddy having a higher eroded sand concentration than the secondary eddy. From the discussion of figure 18.4, then, we can conclude that a negative net sand transport will result - see Bijker et al (1976). In some cases it is even possible that a small positive resulting water movement (current) superimposed on the waves will increase the magnitude of the negative sand transport. How can this happen? The constant current component strengthens the effect of the primary eddy and thus erodes more material during phase a in figure 18.4. As long as a negative velocity is still present during phase c of that figure, a large volume of material will be moved in the negative direction. Conversely, the positive average current weakens the secondary eddies and reduces the positive transport of sand; an increased net transport in the negative direction results.

The above discussion also points out one of the significant difficulties in carrying out experimental sand transport investigations of this type: the net sand transport (usually the important item) results from the difference between two other absolute sand transport quantities which are much larger than the value we are seeking. As one may remember from numerical analysis, small errors in either of these large quantities can change the value of their difference (the net sand transport) drastically.

It would seem that in order to make much progress with studies of sediment transport, it is essential to determine the exact eddy pattern and sediment concentration, both as a function of time. While this is easily suggested, it is extremely difficult to determine these items even in a laboratory situation. Kennedy and Locher (1972) were among the first to measure such sediment concentrations successfully in a model; an example of their results is shown in figure 18.5. The unequal peaks in the sediment concentration are easily explained in the light of the asymmetry of the wave and ripples.

A second influence of the presence of the ripples is a local contraction of the streamlines near the ripple crests. The higher resulting current velocities near the ripple crests can cause local erosion of material which is "deposited" where the streamlines are more widely spaced - in the following valley.

These two processes just outlined may not be seen separately. Certainly some of the material eroded from the ripple crest will be caught in the eddy just downstream(whatever direction the water is flowing at that instant). That portion of the crest material caught in the eddy will then be transported in a direction opposite to that described in the above paragraph. Generally speaking, when waves are present, the eddy formation and its consequences dominate the sand transport process; the ripple crest erosion usually plays only a relatively minor role.

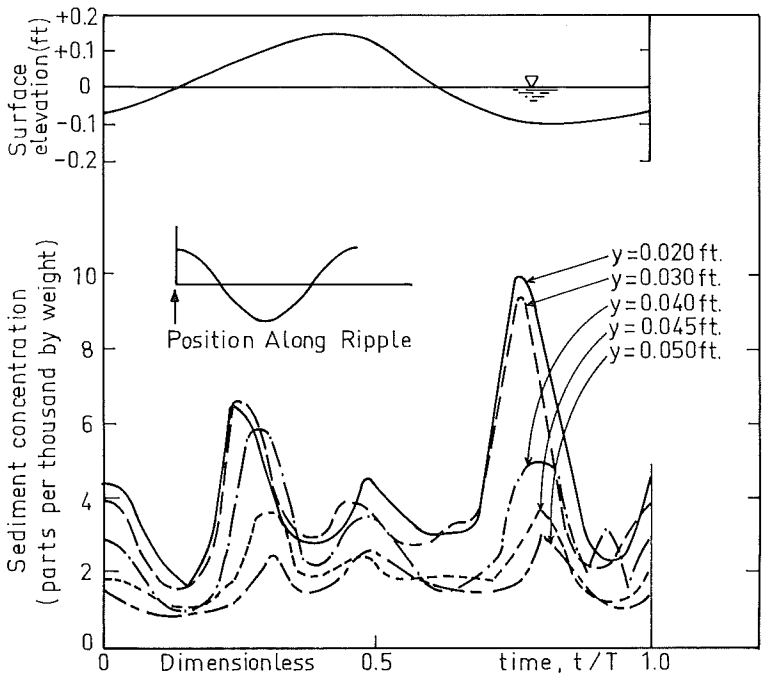

Figure 18.5
SEDIMENT CONCENTRATIONS VERSUS TIME ABOVE RIPPLE CREST

18.4 Concluding remarks

It should be obvious from the previous section that a sediment transport concept based exclusively on a principle of exceedance of a critical bottom shear stress will most likely run into difficulty. A newer theoretical/experimental approach is to attempt to predict the eddy and ripple formations and local sediment concentrations in terms of more readily measured or predicted parameters such as water velocities above the ripples and the bed material properties. It is even possible that the bed shear stress may remain an adequate parameter for the description of the net effect of the much more complex phenomona occurring in the immediate vicinity of the bottom ripples. Detailed studies of the phenomona involved are just beginning. The literature already cited in this chapter represents some of the first results. Research is continuing on a rather intensive basis; members of the Coastal Engineering Group of the Delft University of Technology are among the investigators.

This chapter has concentrated on a very detailed examination of the sand transport in a very small region near a portion of an individual ripple on a sandy bed. Our more immediate concern in practice, however, is the prediction of sand movements on a much larger scale - within a portion of a coastal breaker zone, for example. In the remaining chapters, therefore, we return to this much larger scale problem, and in the next chapter, for example, consideration of individual eddies is completely neglected; the best large scale sediment movement description available now (1977) relates this transport to a bed shear stress.

19. MODERN COASTAL SAND TRANSPORT FORMULAS

J. v.d. Graaff

19.1 Introduction

Now that some of the details of the sand transport mechanism have been considered, we can attempt to formulate the more modern sand transport formulas for transport caused by waves plus currents. As one might expect from the introduction presented way back in chapter 9, the modern formulas, in general, determine a concentration of material, $c(z,t)$, multiply this by a particle velocity, $u_p(z,t)$, integrate over the depth and average over time in order to determine a sediment (sand) transport, S_x. Equation 9.01 expresses this in a mathematical form. As was indicated in the previous chapter, it is universally assumed that sediment particles in motion move with essentially the same horizontal velocity component as the surrounding water. (This certainly is not so in the vertical direction, however, because of gravity influences.)

Since the water velocities in a breaker zone have already been determined, the main emphasis of this chapter will be on the determination of a sediment concentration profile $c(z,t)$ in the most general sense.

Many sediment transport formulas make a distinction between sediment transported along the bottom - bed load transport, S_b - and sediment transport carried in suspension well above the bottom, S_s. The total transport is obviously the sum of these two terms.

Before discussing coastal sediment transport formulas, we shall first review some formulas developed for steady currents alone such as might be found in rivers.

19.2 Transport formulas for currents alone

Most of the sediment transport formulas reviewed here are also discussed in detail in courses and literature on (river) sediment transport. This will not be duplicated here; only results will be presented along with some insight into their meaning for our coastal application.

One of the earlier of the modern formulas was formulated by Frijlink (1952) using data and concepts of Kalinske (1947). In its most convenient form, the Kalinske-Frijlink formula for a unit channel width is:

$$S_b = B\, D\, \frac{V}{C}\, \sqrt{g}\, \exp\left[-0.27\, \frac{\Delta\, C^2 D}{\mu\, V^2}\right] \qquad (19.01)$$

where:
- B is a dimensionless coefficient,
- C is the Chézy friction factor,
- D is mean sediment grain size,
- exp [ ] denotes the exponential function, $e^{[\ ]}$,
- g is the acceleration of gravity,
- S_b is the bed load transport,
- V is the average - constant - velocity,
- μ is a so-called "ripple factor", and
- Δ is the relative sediment density defined by:

$$\Delta = \frac{\rho_s - \rho}{\rho} \qquad (19.02)$$

where: ρ_s is the mass density of the sediment particles, and
ρ is the mass density of water.

In this formula, the coefficient, B, usually has a value of about 5. Bijker (1967) in contrast to Frijlink did not include the ripple factor, μ, in the first part of the equation. This emerical factor indicates the influence of the form of the bottom roughness on the bed load transport; the actual roughness, r, is incorporated in the Chézy coefficient, C, of course.

The relation between equation 19.01 and the movement of bed material can be made more obvious by changing some parameters in equation 19.01. Expressing the Chézy coefficient in terms of the bed shear stress:

$$\frac{C^2}{V^2} = \frac{\rho g}{\tau_c} \qquad (19.03)$$

where τ_c is the bed shear stress - see equation 15.01. The exponential term in equation 19.01 then becomes:

$$\exp \left[- 0.27 \frac{\Delta D \rho g}{\mu \tau_c} \right] \qquad (19.04)$$

which is often referred to as the "stirring parameter" in the Kalinske-Frijlink formula. Note, as well, that this term is dimensionless.

The remaining terms in equation 19.01:

$$B D \frac{V}{C} \sqrt{g} \qquad (19.05)$$

are often collectively called the "transport parameter" which has units of volume per unit width per unit time.

A more or less physical explanation for the appearance of the dimensionless parameter $\frac{\sqrt{g}}{C}$ in the transport parameter is that the bed load transport is related to the velocities near the bed, and

$$V \frac{\sqrt{g}}{C} = V_* \qquad (15.06) \qquad (19.06)$$

is the velocity occurring at elevation:

$$z' = z'_o e^k \qquad (15.05) \qquad (19.07)$$

- see section 15.2. Thus, V_* is more typical of the velocities near the bottom in the layer where the bed load transport takes place. The bottom roughness, r, influences this velocity via its influence on C:

$$C = 18 \log \frac{12h}{r} \qquad (16.13) \qquad (19.08)$$

where h is the water depth.

The Kalinske-Frijlink formula was developed for rivers in which the major portion of the sediment transport took place in a small zone near the bed - as bed load transport. As such, the formula neglects the influence of sediment carried in suspension. Along a beach, however, we can expect the high turbulence in the breaking waves to hold a relatively large quantity of sand in suspension; we cannot generally neglect suspended sediment transport in the breaker zone.

Einstein (1950) approached the problem of sediment transport in a river having both suspended and bed load transport. He approached the problem in the same fundamental way as was expressed in chapter 9 by determining a total transport:

$$S = \int_0^h c(z')\, V(z')\, dz' \qquad (19.09)$$

where: $c(z')$ is the concentration* of sediment at an elevation z', and

$V(z')$ is the horizontal velocity at that same elevation.

He split this total transport into two parts: a bed transport occurring in a layer of thickness, a,** near the bed:

$$S_b = \int_0^a c(z')\, V(z')\, dz' \qquad (19.10)$$

and a suspended transport:

$$S_s = \int_a^h c(z')\, V(z')\, dz' \qquad (19.11)$$

Einstein (1950) used the Prandtl-Von Kármán logarithmic velocity distribution - see section 15.2 - to describe $V(z')$. He described the concentration, $c(z')$, using a diffusion equation modified to include the effects of gravity on the particles:

$$W\, c(z') + \varepsilon_z \frac{d\, c(z')}{dz'} = 0 \qquad (19.12)$$

where: W is the fall velocity of the particles in water, and

ε_z is a diffusion coefficient (eddy viscosity).

This diffusion coefficient can be related to the same parameters as those used in the logarithmic velocity distribution. The result is that ε_z is a specific function of z':

---

* This concentration, c, is expressed in terms of *volume of deposited sediment* per unit volume of water. As such, it includes the voids in the deposited sediment. This is of extreme importance when caculating sediment transports based upon measured sediment concentrations expressed in units of *mass* per unit volume.

** This thickness was in the order of 2 to 3 times the bed material grain diameter.

$$\varepsilon_z = \kappa V_* z' \left(\frac{h-z'}{h} \right) \tag{19.13}$$

where κ is the Von Kármán coefficient = 0.4. Substitution of (19.13) into (19.12) and solving for c(z') - not too easy a task! yields:

$$c(z') = c(b) \left(\frac{h-z'}{z'} \frac{a}{h-a} \right)^{z_*} \tag{19.14}$$

where: c(b) is the concentration at some chosen elevation z' = b above the bottom, and

z_* is a dimensionless parameter:

$$z_* = \frac{W}{\kappa V_*} \tag{19.15}$$

By choosing b in (19.14) to be the elevation of the boundary between bed and suspended transport layers, z' = a, and combining (19.14) and (15.04) in (19.11) yields:

$$S_s = \int_a^h c(a) \left(\frac{h-z'}{z'} \frac{a}{h-a} \right)^{z_*} \frac{V_*}{\kappa} \ln \frac{z'}{z'_0} \, dz' \tag{19.16}$$

Einstein determined c(a) from the bed load transport using his own bed load transport formula. As will be shown later, Bijker (1968) applied the same principle, but used the Frijlink-Kalinske bed load transport formula instead.

Einstein further solved the integral in equation 19.16 in terms of two other integrals, I_1 and I_2. This resulted in a suspended transport formula looking like:

$$S_s = 11.6 \sqrt{\frac{\tau_c}{\rho}} a \, c(a) \left[I_1 \ln \frac{33h}{r} + I_2 \right] \tag{19.17}^*$$

where:

$$I_1 = 0.216 \frac{A^{(z_*-1)}}{(1-A)^{z_*}} \int_A^1 \left(\frac{1-\zeta}{\zeta} \right)^{z_*} d\zeta \tag{19.18}$$

$$I_2 = 0.216 \frac{A^{(z_*-1)}}{(1-A)^{z_*}} \int_A^1 \left(\frac{1-\zeta}{\zeta} \right)^{z_*} \ln(\zeta) \, d\zeta \tag{19.19}$$

in which: A is a dimensionless roughness, $\frac{r}{h}$, and

ζ is a dimensionless elevation $\frac{z'}{h}$.

Einstein (1950) provided graphs and tables of the functions I_1 and I_2 for various values of z_* and A. Later investigators - Bakker and Bogaard (1977) for example - have evaluated the entire term in brackets in equation 19.17 instead of working with the two integrals I_1 and I_2. Values of this term:

$$Q = \left[I_1 \ln \left(\frac{33h}{r} \right) + I_2 \right] \tag{19.20}$$

are listed in table 19.1 as a function of $\frac{r}{h}$ and z_*.

---

* Some investigators substitute the "shear velocity", V_*, for $\sqrt{\frac{\tau_c}{\rho}}$.

(The significance of other parameters listed there will be explained later).

Figure 19.1 shows an example of a concentration profile, c(z') for $z_* = 1$, r = a = 0.06 m and h = 3 m. The associated logarithmic velocity profile and resulting transport profile are also shown. All three profiles have been made dimensionless by dividing by appropriate parameters as indicated on the axis of the figure.

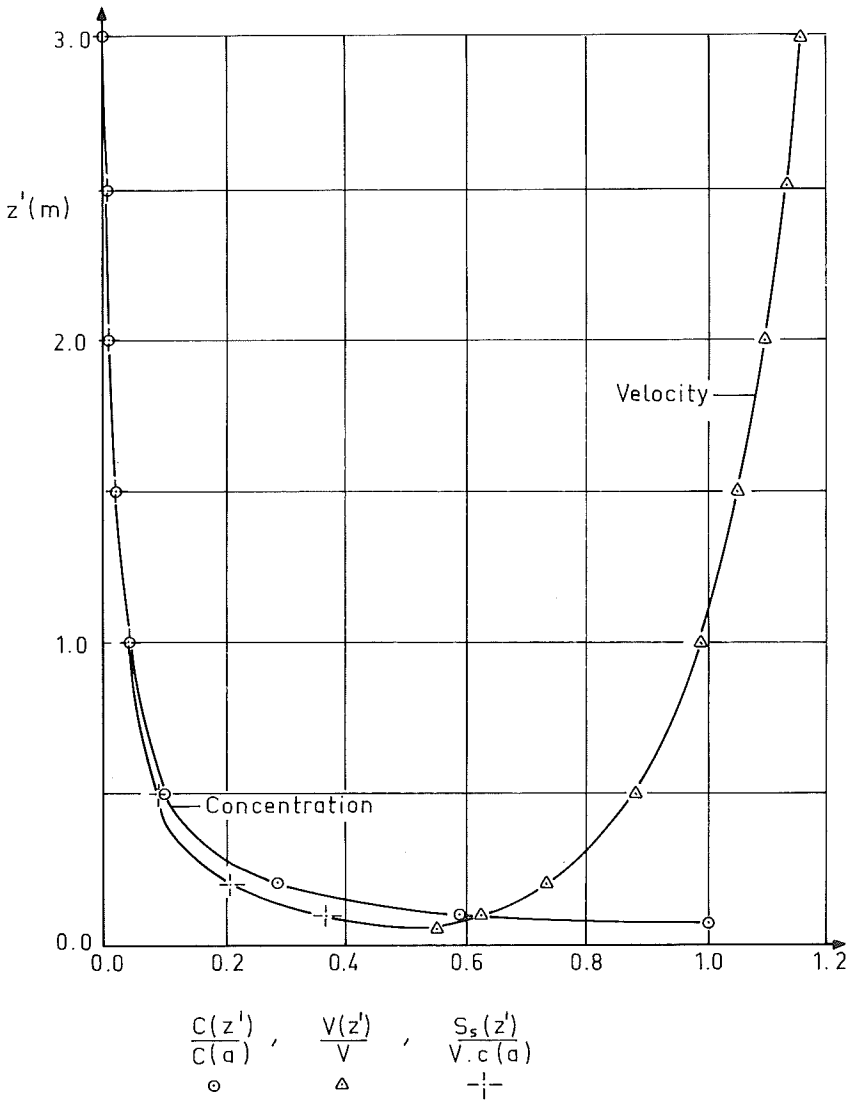

Figure 19.1
EXAMPLE CONCENTRATION, VELOCITY AND TRANSPORT PROFILES
($z_* = 1$, r = a = 0.06 m, h = 3 m)

Table 19.1 Values of Einstein integral factors (all items are dimensionless)

r/h	$z_* = 0$			$z_* = 0.20$			$z_* = 0.40$			$z_* = 0.60$			$z_* = 0.80$			$z_* = 1.00$		
	Q	S_s/S_b	S_t/S_b	Q	S_s/S_b	S_t/S_b	Q	S_s/S_b	S_t/S_b	Q	S_s/S_b	S_t/S_b	Q	S_s/S_b	S_t/S_b	Q	S_s/S_b	S_t/S_b
$1x10^{-5}$	$3.03x10^5$	$5.54x10^5$	$5.54x10^5$	$3.28x10^4$	$6.00x10^4$	$6.00x10^4$	$3.88x10^3$	$7.10x10^3$	$7.10x10^3$	527.	964.	965.	88.0	161.	162.	20.0	36.6	37.6
$2x10^{-5}$	$1.44x10^5$	$2.63x10^5$	$2.63x10^5$	$1.79x10^4$	$3.27x10^4$	$3.27x10^4$	$2.43x10^3$	$4.44x10^3$	$4.44x10^3$	377.	689.	690.	71.6	131.	132.	17.9	32.8	33.8
$5x10^{-5}$	$5.36x10^4$	$9.80x10^4$	$9.80x10^4$	$7.98x10^3$	$1.46x10^4$	$1.46x10^4$	$1.30x10^3$	$2.37x10^3$	$2.37x10^3$	239.	438.	439.	53.6	98.0	99.0	15.4	28.2	29.2
$1x10^{-4}$	$2.53x10^4$	$4.63x10^4$	$4.63x10^4$	$4.32x10^3$	$7.90x10^3$	$7.90x10^3$	803.	$1.47x10^3$	$1.47x10^3$	169.	310.	311.	42.7	78.2	79.2	13.6	24.9	25.9
$2x10^{-4}$	$1.19x10^4$	$2.18x10^4$	$2.18x10^4$	$2.33x10^3$	$4.26x10^3$	$4.26x10^3$	496.	907.	908.	119.	218.	219.	33.9	62.0	63.0	11.9	21.8	22.8
$5x10^{-4}$	$4.36x10^3$	$7.98x10^3$	$7.98x10^3$	$1.02x10^3$	$1.87x10^3$	$1.87x10^3$	260.	475.	476.	74.3	136.	137.	24.6	45.0	46.0	9.78	17.9	18.9
$1x10^{-3}$	$2.03x10^3$	$3.72x10^3$	$3.72x10^3$	545.	998.	999.	158.	290.	291.	51.2	93.7	94.7	19.1	34.9	35.9	8.36	15.3	16.3
$2x10^{-3}$	940.	$1.72x10^3$	$1.72x10^3$	289.	529.	530.	95.6	175.	176.	35.1	64.2	65.2	14.6	26.7	27.7	6.99	12.8	13.8
$5x10^{-3}$	336.	615.	616.	123.	226.	227.	48.5	88.7	89.7	20.8	38.1	39.1	10.0	18.3	19.3	5.38	9.84	10.8
0.01	153.	280.	281.	63.9	117.	118.	28.6	52.3	53.3	13.8	25.2	26.2	7.32	13.4	14.4	4.28	7.84	8.84
0.02	68.9	126.	127.	32.8	60.0	61.0	16.5	30.2	31.2	8.91	16.3	17.3	5.21	9.54	10.5	3.30	6.04	7.04
0.05	23.2	42.4	43.4	13.1	24.0	25.0	7.70	14.1	15.1	4.78	8.74	9.74	3.13	5.73	6.73	2.18	3.99	4.99
0.10	9.84	18.0	19.0	6.28	11.5	12.5	4.12	7.54	8.54	2.81	5.14	6.14	1.99	3.64	4.64	1.48	2.70	3.70
0.20	3.90	7.13	8.13	2.80	5.13	6.13	2.04	3.73	4.73	1.51	2.77	3.77	1.15	2.10	3.10	0.896	1.64	2.64
0.50	0.836	1.53	2.53	0.716	1.31	2.31	0.601	1.10	2.10	0.492	0.900	1.90	0.396	0.724	1.72	0.312	.571	1.57
1.00	0.00	0.00	1.00	0.00	0.00	1.00	0.00	0.00	1.00	0.00	0.00	1.00	0.00	0.00	1.00	0.00	0.00	1.00

r/h	$z_* = 1.50$			$z_* = 2.00$			$z_* = 3.0$			$z_* = 4.0$			$z_* = 5.0$		
	Q	S_s/S_b	S_t/S_b	Q	S_s/S_b	S_t/S_b	Q	S_s/S_b	S_t/S_b	Q	S_s/S_b	S_t/S_b	Q	S_s/S_b	S_t/S_b
$1x10^{-5}$	2.33	4.26	5.26	0.973	1.78	2.78	0.432	0.790	1.79	0.276	0.505	1.50	0.202	0.370	1.37
$2x10^{-5}$	2.31	4.23	5.23	0.973	1.78	2.78									
$5x10^{-5}$	2.28	4.17	5.17	0.967	1.77	2.77									
$1x10^{-4}$	2.25	4.11	5.11				0.432	0.790		0.276	0.505				
$2x10^{-4}$	2.21	4.04	5.04	0.967	1.77	2.77	0.431	0.789		0.275	0.504				
$5x10^{-4}$	2.13	3.90	4.90	0.962	1.76	2.76	0.431	0.788		0.275	0.504				
$1x10^{-3}$	2.05	3.76	4.76	0.951	1.74	2.74	0.430	0.787	1.79	0.275	0.503			0.370	
$2x10^{-3}$	1.96	3.58	4.58	0.940	1.72	2.72	0.428	0.784	1.78	0.274	0.502		0.202	0.369	
$5x10^{-3}$	1.78	3.26	4.26	0.907	1.66	2.66	0.424	0.776	1.78	0.273	0.499	1.50	0.201	0.367	1.37
0.01	1.62	2.96	3.96	0.869	1.59	2.59	0.417	0.763	1.76	0.270	0.494	1.49	0.199	0.364	1.36
0.02	1.42	2.59	3.59	0.809	1.48	2.48	0.404	0.740	1.74	0.264	0.483	1.48	0.195	0.357	1.36
0.05	1.10	2.02	3.02	0.694	1.27	2.27	0.374	0.684	1.68	0.249	0.456	1.46	0.186	0.341	1.34
0.10	0.836	1.53	2.53	0.568	1.04	2.04	0.339	0.620	1.62	0.236	0.432	1.43	0.181	0.332	1.33
0.20	0.552	1.01	2.01	0.414	0.758	1.76	0.317	0.580	1.58	--	--	--	--	--	--
0.50	0.174	0.319	1.32	--	--	--	--	--	--	--	--	--	--	--	--
1.00	0.00	0.00	1.00	--	--	--	--	--	--	--	--	--	--	--	--

Many other investigators have proposed sediment transport formulas. Engelund and Hansen (1967), for example, suggest the following formula which they based upon certain prototype river measurements:

$$S = 0.05\ V \frac{\tau_c^2\ C}{\rho^2\ g^{5/2}\ \Delta^2\ D_{50}} \qquad (19.21)$$

where: D_{50} is the grain size exceeded by 50% (by weight) of the bed material sample, and

S is the total sediment transport - sum of bed and suspended transports.

Another sediment transport formula was proposed by White and Ackers (1973). Details of this formula can be found in the literature or in more specifc courses on sediment transport.

19.3 Influence of waves on bed transport

It would seem logical to include the influence of waves on sediment transport in a manner more or less analogus to the way their influence was included in the longshore current friction force determination - see chapter 15. Indeed, Bijker (1967) has done this in a way which demonstrates a clear insight into the phenomona involved. The approach of Bijker was to introduce the wave influence via a modification of the bottom shear stress in a sediment transport formula already available for currents. He chose the Kalinske-Frijlink formula - equation 19.01-for the bed load transport and coupled this on the Einstein formula for suspended sediment transport - equation 19.17.

The instantaneous velocity component caused by the waves can be significant in the breaker zone even though the time average of this component is small relative to the longshore current velocity. This observation leads to an hypothesis that the waves contribute primarily to the stirring up of material from the bottom rather than the transport. Working out this idea, Bijker modified the bottom shear stress term in the stirring parameter of the Kalinske-Frijlink formula. The details of this modification of τ_c in this stirring term are presented in the following section.

19.4 Bed shear stress modification

It was indicated in chapter 18 that the bed shear stress is important for the movement of sediment on a shore or in a channel. The influence of waves on the bed shear of a longshore current has also already been explained in chapter 15; there, the component of the bed shear stress in the current direction was averaged in order to determine a resultant steady state equivalent shear stress.

Without thinking, we might substitute this same bed shear stress into our sediment transport formulas. The error in such an approach is revealed by the answer to the question: what bed shear stress component determines when a bottom material particle starts to move? Expressed less formally: In what direction must we "kick" a

bottom material particle in order to stir it loose so that it may be transported? The answer to these questions is that it does not matter one bit in which direction the force - bed shear stress - acts in the stirring term of the Kalinske-Frijlink formula.

The shear stress which must be used in this stirring term has already come up in chapter 15; it is:

$$\tau_{cw} = \rho \kappa^2 V_r^2 \qquad (15.24) \qquad (19.22)$$

where V_r is the instantaneous resultant velocity.
The background of this term can be found in section 15.4. In contrast to the further work in that chapter, we shall continue working with τ_{cw} instead of its x component, τ_{cwx}. No absolute value has been taken in equation 19.22 since all terms are non-negative, anyway.

Just as in chapter 15, we shall need to compute an average value $\overline{\tau_{cw}}$ of this instantaneous shear stress. Its direction no longer plays a role; we need only consider the magnitude of the (vector) quantity. Since the only time variable in equation 19.22 is V_r, it is sufficient to compute the average magnitude of the square of the resultant velocity, $\overline{V_r^2}$ *.

Recalling the definition of V_r from chapter 15:

$$V_r^2 = V_t^2 + (p\, u_b)^2 + 2\, p\, u_b\, V_t \sin \phi \qquad (15.22) \qquad (19.23)$$

where $p\, u_b$ is the wave current velocity at height z_t' above the bottom,

V_t is the constant current velocity at the same elevation, and

ϕ is the angle between the wave crests and (constant) current.

A more complete discussion of these can be found in chapter 15.

The value of ϕ will not be restricted since it is desirable to derive a formula for general application in any combination of waves and current.

In equation 19.23 only u_b is a function of time. Picking up:

$$u_b = \hat{u}_b \cos \omega t \qquad (15.27) \qquad (19.24)$$

and remembering that:

---

* We should be aware that we are making a potentially serious fundamental error here; we are proposing the substitution of an *average* value of an independent variable, $\overline{\tau_{cw}}$, into a *non-linear* relationship, the stirring term of the Kalinske-Frijlink formula, in order to obtain an "average" result. This is fundamentally wrong. In order to be fundamentally correct we must first substitute the instantaneous value of τ_{cw} into the stirring term and *then* take the average. This fundamental error has been accepted in the interest of avoiding a monumental problem in mathematics.

$$\frac{1}{2\pi}\int_0^{2\pi} \cos x \, dx = 0 \tag{19.25}$$

and:

$$\frac{1}{2\pi}\int_0^{2\pi} \cos^2 x \, dx = \frac{1}{2}\,, \tag{19.26}$$

(19.23) becomes, simply:

$$\overline{V_r^2} = V_t^2 + \frac{1}{2}(p\,\hat{u}_b)^2 \tag{19.27}$$

$$= V_t^2 \left[\,1 + \frac{1}{2}\left(\frac{p\,\hat{u}_b}{V_t}\right)^2\right] \tag{19.28}$$

Substituting this last result into (19.22) yields:

$$\overline{\tau_{cw}} = \rho\,\kappa^2\,V_t^2\left[\,1 + \frac{1}{2}\left(\frac{p\,\hat{u}_b}{V_t}\right)^2\right] \tag{19.29}$$

in which we recognize:

$$\rho\,\kappa^2\,V_t^2 = \tau_c \qquad (15.13) \tag{19.30}$$

as the shear stress under a current alone. Substituting (19.30) and equation 15.20 into (19.29) yields a very simple form:

$$\overline{\tau_{cw}} = \tau_c + \frac{1}{2}\hat{\tau}_w \tag{19.31}$$

Another convenient form expresses the ratio of $\overline{\tau_{cw}}$ to τ_c in terms of common parameters. Using equations 15.14 and 15.29 along with 19.30 in equation 19.29 yields the desired result:

$$\overline{\tau_{cw}} = \tau_c\left[\,1 + \frac{1}{2}\left(\xi\,\frac{\hat{u}_b}{V}\right)^2\right] \tag{19.32}$$

which is somewhat different from equation 15.30.

19.5 Bed load transport by waves and current

The result of the previous section can be substituted directly into the stirring term of the Kalinske-Frijlink formula shown in (19.04). Using (19.32) to modify τ_c in (19.04) and multiplying by (19.05) yields:

$$S_b = \frac{B\,D\,V\,\sqrt{g}}{C}\exp\left[\frac{-0.27\,\Delta\,D\,\rho\,g}{\mu\,\tau_c\left[1 + \frac{1}{2}\left(\xi\,\frac{\hat{u}_b}{V}\right)^2\right]}\right] \tag{19.33}$$

or equivalently using equation 19.03:

$$S_b = \frac{B\,D\,V\,\sqrt{g}}{C}\exp\left[\frac{-0.27\,\Delta\,D\,C^2}{\mu\,V^2\left[1 + \frac{1}{2}\left(\xi\,\frac{\hat{u}_b}{V}\right)^2\right]}\right] \tag{19.34}$$

It is obvious from these relationships that the presence of the waves ($\hat{u}_b$) increases the sediment transport. Further, since ϕ does not enter the equation, the increase in sediment transport is independent of the wave direction provided the current velocity is maintained. This seems logical in light of the earlier remarks concerning the direction of the bed shear stress relative to the stirring of bed material.

Bijker (1967) assumed that the bottom transport occurred in a bottom layer having thickness equal to the bottom roughness, r. The concentration of bed material in this layer, c_b, (assumed to be constant over the thickness) is, then:

$$c_b = \frac{S_b}{\int_0^r V(z')\, dz'} \qquad (19.35)^*$$

The integral is evaluated from the velocity profile of the current - see chapter 15, especially figure 15.1b:

$$\int_0^r V(z')\, dz' = \frac{1}{2} z_t' V_t + \frac{1}{\kappa}\sqrt{\frac{\tau_c}{\rho}} \int_{z_t'}^r \ln \frac{z'}{z_t'}\, dz' \qquad (19.36)$$

Using the definitions of z_t', etc. in terms of r and carrying out the integration yields:

$$\int_0^r V(z')\, dz' = 6.34 \sqrt{\frac{\tau_c}{\rho}}\, r = 6.34\, V_* r \qquad (19.37)$$

With this result equation 19.35 becomes:

$$c_b = \frac{S_b}{6.34 \sqrt{\frac{\tau_c}{\rho}}\, r} \qquad (19.38)$$

This concentration is assumed to be constant over the entire thickness, r, of the bed transport layer. Also, as pointed out earlier, this concentration is expressed in units of volume of deposited sediment per unit volume of water and thus includes the voids in the deposited sediment.

---

* We are here converting this modified Frijlink bed load formula to a form corresponding to equation 19.10. This may seem strange at first sight.

19.6 Influence of waves on suspended transport

Since the concentration distribution of the suspended sediment depends upon the bed shear stress - via z_* (equation 19.15) in equation 19.14 - Bijker (1968) simply accounted for the influence of waves by modifying the shear stress term. Reasoning that the shear stress in (19.14) acts in the same physical way as in the stirring term of the bed transport formula, he modified the shear stress via equation 19.32. Also, choosing a = r and selecting c(a), then, equal to c_b yields:

$$c(z') = c_b \left[\frac{r}{h-r} \; \frac{h-z'}{z'} \right] \frac{W \sqrt{\rho}}{\kappa \sqrt{\tau_c} \sqrt{1 + \frac{\xi^2}{2} \left(\frac{u_b}{V}\right)^2}} \qquad (19.39)$$

lekop de wortels

The suspended load transport then follows from:

$$S_s = \int_r^h c(z') \, V(z') \, dz' \qquad (19.11) \qquad (19.40)$$

where: c(z') is determined in equation 19.39, and
V(z') is defined in equation 15.04.

The result, after substitution of (19.38), (19.39) and (15.04) in equation 19.40, succesful completion of a lot of algebra, and use of (19.20) is:

$$S_s = 1.83 \; Q \; S_b \qquad (19.41)$$

which shows that the suspended load transport is directly proportional to the bed load transport. This is logical, considering the direct relationship between c_b and both S_b and S_s. Values of:

$$\frac{S_s}{S_b} = 1.83 \; Q \qquad (19.42)$$

have been included in table 19.1 and are plotted in figure 19.2 as a function of the two independent parameters, A and z_*. Of course, the shear stress used to compute z_* must be modified ; equation 19.15 becomes:

$$z_* = \frac{W \sqrt{\rho}}{\kappa \sqrt{\tau_c \left[1 + \frac{1}{2} \left(\xi \frac{\hat{u}_b}{V} \right)^2 \right]}} \qquad (19.43)$$

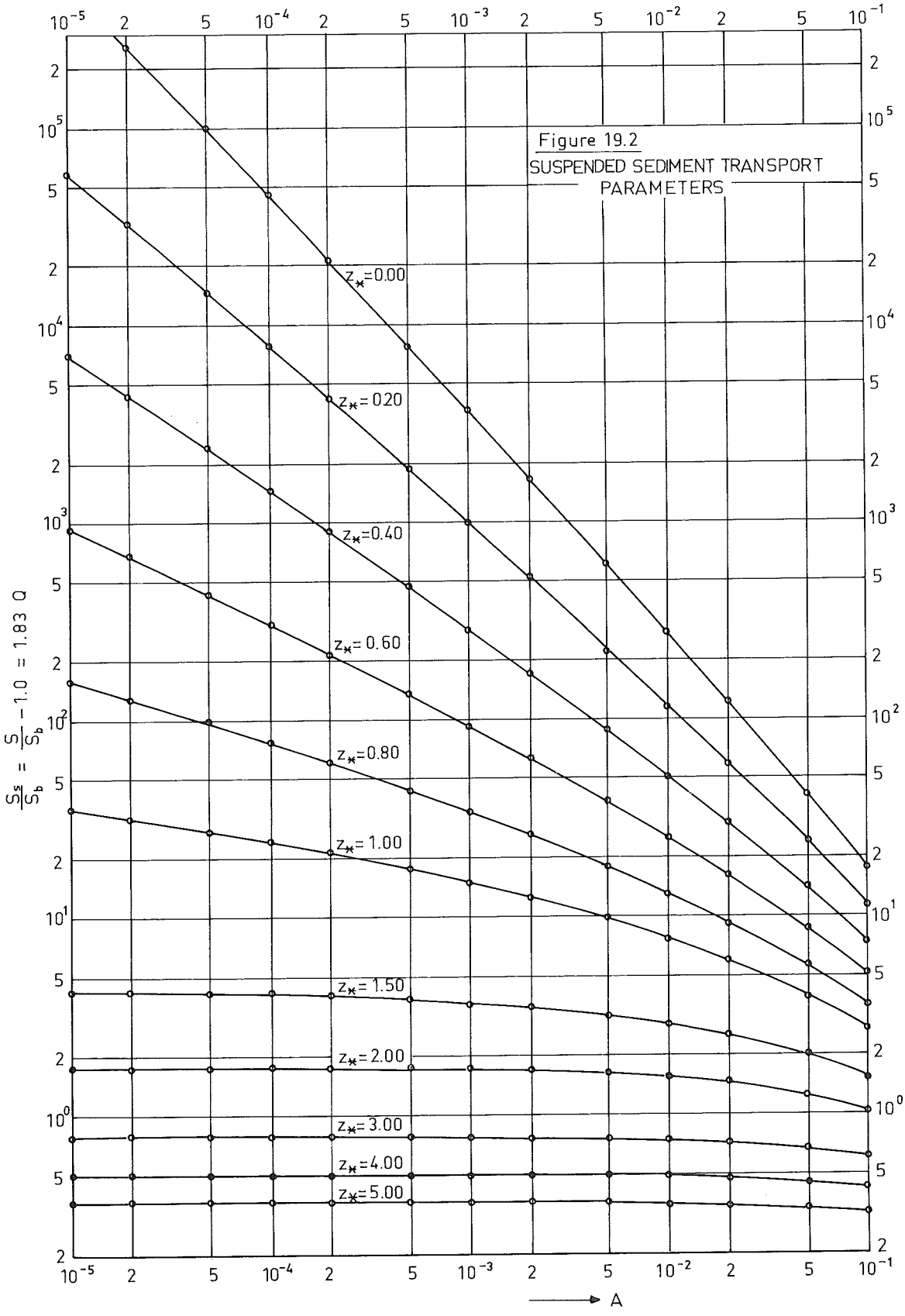
Figure 19.2
SUSPENDED SEDIMENT TRANSPORT PARAMETERS
$\frac{S_s}{S_b} = \frac{S}{S_b} - 1.0 = 1.83\ Q$
A
z_*=0.00
z_*=0.20
z_*=0.40
z_*=0.60
z_*=0.80
z_*=1.00
z_*=1.50
z_*=2.00
z_*=3.00
z_*=4.00
z_*=5.00

19.7 Total sediment transport

Now that both the bed load transport, S_b, and the suspended load transport, S_s, are known, the total transport, S, follows by addition. Additionally, since S_s is directly related to S_b, an especially simple relationship results:

$$S = S_b + S_s = S_b\ (1 + 1.83\ Q) \tag{19.44}$$

In this equation, S_b is evaluated using either equation 19.33 or 19.34, and Q must be evaluated using the modified value of z_* given in equation 19.43. Values of the term in parantheses in equation 19.44 - $\frac{S}{S_b}$ - are also included in table 19.1 and can also be found by adding 1.0 to the values in figure 19.2.

The procedure just outlined is often referred to as the Bijker formula since he was the one who first modified the bottom shear stress in the way just outlined.

The theoretical work is now completed. The only remaining problem is that of evaluating all the parameters involved in terms of known or measurable quantities.

It turns out that only the ripple factor, μ, needs further definition. It is usually defined via an emperical relation:

$$\mu = \left(\frac{C}{C'} \right)^{3/2} \tag{19.45}$$

where: C is the Chézy coefficient evaluated via equation 19.08, and
C' is another Chézy coefficient based upon the bed material properties:

$$C' = 18 \log \frac{12\ h}{D_{90}} \tag{19.46}$$

in which D_{90} is the soil grain diameter allowing 90% (by weight) of the soil to pass.

Table 19.2 shows the steps necessary to compute the sediment transport occurring along a unit width of beach with water depth, h.* The distribution of the sand transport across the breaker zone can be determined by carring out steps 7 through 19 in that table for various chosen values of h ranging up to the depth at the outer edge of the breaker zone, h_{br}. Such a computation, obviously involves a lot of work; digital computer programs are available. If necessary, the computations could be carried out using a series of programs for a pocket computer. A sample computation will be shown in section 19.9.

* Some variation in the sequence of steps may be appropriate depending upon the nature of the given data or perhaps the computation method used.

Table 19.2 Steps in coastal sand transport computation

Step	Determination/evaluation	equation	Parameter
1	Determine deep water wave conditions H_o, T, ϕ_o		
2	Compute deep water wave speed, c_o and wave frequency, ω		T
3	Determine oceanographic and hydrographic data: bathymetry, soil sample, water density, ρ		
4	Laboratory analysis of soil: ρ_s, D, W, D_{90}		soil sample
5	Compute relative density, Δ	(19.02)	ρ_s , ρ
6	Determine breaker index, γ	(Vol I)	H_o, T, bath.
7	Choose water depth, h		
8	Compute local wave conditions H, λ, k, $\hat{u}_b$, a_b (include refraction, diffraction)	(Vol I) (15.18)	H_o, ω h, ϕ_o bath.
9	Estimate roughness, r		
10	Compute: $A = \frac{r}{h}$		h, r
	C	(19.08)	h, r
	C'	(19.46)	h, D_{90}
11	Compute f_w	(15.16) or fig. 15.2	a_b, r
12	Compute p *	(15.21) or fig. 15.2	f_w
13	Compute V (only for wave driven longshore current; otherwise, field measurement or other computation method.)	(16.03) or (16.06)	ϕ_o, c_o, γ, bath., C, f_w
14	Compute μ	(19.45)	C, C'
15	Compute ξ	(15.29)	p, C
	τ_c	(19.03)	ρ, V, C
16	Compute z_*	(19.43)	ρ, W, $\hat{u}_b$, V, τ_c
17	Compute bed transport S_b	(19.33) or (19.34)	Δ, D, C, V, μ, ξ, $\hat{u}_b$
18	Determine: Q	table 19.1 or fig. 19.2	A, z_*
19	Compute S	(19.44)	S_b, Q

* In his original work, Bijker (1967) assumed that p was a constant equal to 0.45.

19.8 Critical comments on Bijker formula

The whole method of adjusting the bed shear stress to account for the wave presence is based upon relationships for a constant current. In particular, the mixing length distribution (15.03) has been assumed leading to the logarithmic Prandtl-Von Kármán velocity distribution (15.04). This velocity distribution has been assumed to be valid for the current alone as well as for the combination of waves and current.

As already indicated, Bijker assumed that the bed transport layer had a thickness equal to the bottom roughness, r, and that the sediment concentration in that layer is constant. For practical problems where the actual roughness is unknown, Bijker suggested using a roughness equal to one half the height of the ripples on the bottom. These ripples could often be measured directly, especially in a model.

More recent studies have indicated that the bottom roughness is often much more than that suggested by Bijker; roughness values of two to four times the bottom ripple height are more acceptable at present.

This drastic increase in bottom roughness then increases the thickness of the bed load transport layer. This, in turn, makes it less acceptable to assume that the bed load material concentration remains constant over the entire thickness of this layer. Recent measurements in the laboratory indicate that concentration variations do exist in this layer. This has consequences, of course, for the reference concentration in the suspended sediment concentration equation.

Further, there is even some doubt about the validity of the diffusion - type concentration relationship used by Einstein when applied to waves. Indeed, it neglects any mixing that might occur as a result of the vertical velocities under the wave. Measurements by Kennedy and Locher (1972) and in an anonymous report from the Delft Hydraulics Laboratory (1976) indicate that several concentration distribution models more or less adequately fit the measured data.

In spite of these limitations - some of which are of very principle nature - the Bijker formula usually gives good results. When, for example, it is applied to beaches having rather uniform sand and a wave-driven longshore current, it yields total results which usually agree rather well with those of the CERC formula presented in chapter 17. This is not necessarily true of other formulas.

The principle of modifying the shear stress in a sediment transport formula can be applied, in principle. to any sediment transport formula. Often times, however, the insight into the physical process involved is difficult to detect making a correct shear stress modification difficult.

The Bijker-Kalinske-Frijlink formula takes no account of a critical shear stress as defined in chapter 18. In the above mentioned formula, the existance of any current and bed shear stress will lead to a sediment transport while in chapter 18 bed transport could exist only during times when a certain critical shear stress was exceeded.

For field conditions, the suspended sediment transport usually far exceeds the bed load transport - ratios of suspended to bed load of 50 to 1 are normal.

There is much discussion about the proper value of the coefficient, B, to be used in the bed load transport formula. Values ranging between 1 and 5 have been suggested. This disagreement reflects the possible inaccuracy of such a sand transport computation. Even though many parameters are involved in the final resulting formulas, errors of more than ten percent are common in practice; in other words, computed sediment transports are often wrong even in the first significant figure! Unfortunately, no great improvement of this situation can be expected until a mass of trustworthy field data with actual measured sediment transports is available. The example, following, illustrates this as well.

19.9 Example of Bijker formula

The following example is intended to demonstrate several principles: First, a computation such as is outlined in table 19.2 is illustrated. Second, the influence of the longshore current velocity distribution is demonstrated by computing sand transport distributions for the various longshore current distributions illustrated in chapter 16. Third, the influence of other parameters such as beach slope and particle grain size is investigated for a given wave and current distribution model. Lastly, a comparison computation using the CERC formula is presented.

The same offshore wave and beach bathymetry conditions assumed in section 5 of chapter 16 will be retained here. These are:

Wave period, T : 7.0 s
Wave height, H_o : 2.0 m
Approach angle, ϕ_o : 30^o
Breaker index, γ : 0.8
Beach slope, m : 1:100
Bottom roughness, r : 0.06 m

Additionally a sand bed consisting of sand with a mean diameter, D, of 200 μm is used. The diameter passing 90% of the sample is D_{90} = 270 μm. Further laboratory analysis yields that the water density, ρ, is 1000 kg/m^3 * and that of the sand, ρ_s, is 2650 kg/m^3. The particle fall velocity is W = 0.0252 m/s.

The computations involved follow more or less the procedure outlined in table 19.2, although some short cuts will be taken. Table 19.3 lists the computation values. Six columns of values - y, h, a_b, c, f_w, and V_1 - have been taken directly from table 16.1. The computations for the row y = 259 m will again be illustrated in detail just as was done in section 16.5. Results from that section will be freely used here.

The orbital velocity amplitude at the bottom can be computed using equation 5.01b of volume I, but can more quickly be found from:

$$\hat{u}_b = \omega a_b \tag{19.47}$$

$$\hat{u}_b = \left(\frac{2\pi}{7} \right) (2.25) = 2.02 \text{ m} \tag{19.48}$$

* Apparently the beach in question is on a large lake!

The parameter A is simply:

$$A = \frac{r}{h} = \frac{0.06}{2.59} = 0.0232 \tag{19.49}$$

The value of C' comes directly from equation 19.46:

$$C' = 18 \log \frac{(12)(2.59)}{270 \times 10^{-6}} = 91.1 \text{ m}^{\frac{1}{2}}/\text{s} \tag{19.50}$$

Since f_w and V_1 are taken from table 16.1, the next parameter to calculate is the ripple factor. Using its emperial definition (19.45) directly yields:

$$\mu = \left(\frac{48.9}{91.1} \right)^{3/2} = 0.39 \tag{19.51}$$

The parameter ξ can be computed using equation 15.29:

$$\xi = \frac{48.9 \sqrt{0.034}}{\sqrt{(2)(9.81)}} = 2.04 \tag{19.52}$$

The parameter z_* is computed with equation 19.43. τ_c must be computed first, however, using (19.03):

$$\tau_c = \frac{(1000)(9.81)(1.09)^2}{(48.9)^2} = 4.88 \text{ N/m}^2 \tag{19.53}$$

$\overline{\tau_{cw}}$ is then, from (19.32):

$$\overline{\tau_{cw}} = \tau_c \left[1 + 1/2 \left(\frac{\xi \hat{u}_b}{V} \right)^2 \right] \tag{19.32}$$

$$= 4.88 \left[1 + \frac{1}{2} \left(\frac{(2.04)(2.02)}{1.09} \right)^2 \right] = 39.75 \text{ N/m}^2 \tag{19.54}$$

The parameter z_* is then simply:

$$z_* = \frac{W \sqrt{\rho}}{\kappa \sqrt{\overline{\tau_{cw}}}} \tag{19.55}$$

$$= \frac{(0.0252)(\sqrt{1000})}{(0.40)(\sqrt{39.75})} = 0.316 \tag{19.56}$$

Knowing $\overline{\tau_{cw}}$, S_b can most conveniently computed using equation 19.33 instead of 19.34:

$$S_b = B D \sqrt{g} \frac{V}{C} \exp \left[\frac{-0.27 \Delta D \rho g}{\mu \overline{\tau_{cw}}} \right] \tag{19.33}$$

Using the currently (1977) popular value of 5.0 for B,

$$S_b = (5.0)(200\text{x}10^{-6}) \sqrt{9.81} \frac{(1.09)}{48.9} \exp \left[\frac{-0.27 (1.65)(200\text{x}10^{-6})(1000)(9.81)}{(0.39)(39.75)} \right] \tag{19.57}$$

$$= 6.600\text{x}10^{-5} \text{ m}^3/\text{s/m} \tag{19.58}$$

Table 19.3 Sediment transport computations and results

(1) y (m)	(1) h (m)	(1) a_b (m)	u_b (m/s)	A (-)	(1) C ($m^{\frac{1}{2}}/s$)	C' ($m^{\frac{1}{2}}/s$)	(1) f_w (-)	(1) V_1 (m/s)	μ (-)	ξ (-)	z_* (-)	S_{b1} (m^2/s)	Q (-)	S_1 (m^2/s)	S_2 (m^2/s)	S_3 (m^2/s)	S_4 (m^2/s)	S_5 (m^2/s)	S_6 (m^2/s)
0	0	0.00	0.00	--	--	--	--	0.00	--	--	--	0.00	--	0.00	0.00	0.00	0.00	0.00	0.00
25	.25	0.70	0.63	.240	30.6	72.8	.065	.048	0.272	1.76	.783	2.99×10^{-6}	0.945	8.16×10^{-6}	1.29×10^{-6}	2.54×10^{-6}	2.56×10^{-5}	2.18×10^{-6}	--
50	.50	0.99	0.89	.120	36.0	78.2	.052	.126	0.312	1.85	.618	8.37×10^{-6}	2.32	4.39×10^{-5}	2.14×10^{-5}	4.14×10^{-5}	5.03×10^{-5}	3.08×10^{-5}	3.2×10^{-5}
75	.75	1.21	1.09	.0800	39.2	81.4	.047	.216	0.334	1.92	.527	1.44×10^{-5}	3.88	1.17×10^{-4}	7.27×10^{-5}	1.23×10^{-4}	1.41×10^{-4}	8.64×10^{-5}	9.1×10^{-5}
100	1.00	1.40	1.26	.0600	41.4	83.7	.043	.318	0.348	1.94	.474	2.09×10^{-5}	5.53	2.32×10^{-4}	1.57×10^{-4}	2.41×10^{-4}	2.61×10^{-4}	1.74×10^{-4}	1.8×10^{-4}
125	1.25	1.56	1.40	.0480	43.2	85.4	.040	.430	0.360	1.95	.439	2.77×10^{-5}	7.25	3.95×10^{-4}	2.78×10^{-4}	4.09×10^{-4}	4.09×10^{-4}	2.93×10^{-4}	2.69×10^{-4}
150	1.50	1.71	1.53	.0400	44.6	86.8	.039	.539	0.368	1.99	.404	3.43×10^{-5}	9.18	6.11×10^{-4}	4.37×10^{-4}	6.12×10^{-4}	5.58×10^{-4}	4.44×10^{-4}	3.75×10^{-4}
175	1.75	1.85	1.66	.0343	45.8	88.0	.037	.663	0.375	1.99	.379	4.17×10^{-5}	11.21	8.97×10^{-4}	6.35×10^{-4}	8.59×10^{-4}	6.78×10^{-4}	6.18×10^{-4}	4.68×10^{-4}
200	2.00	1.97	1.77	.0300	46.8	89.1	.036	.785	0.381	2.00	.359	4.88×10^{-5}	13.37	1.24×10^{-3}	8.71×10^{-4}	1.14×10^{-3}	7.60×10^{-4}	6.33×10^{-4}	5.39×10^{-4}
225	2.25	2.09	1.88	.0267	47.8	90.0	.035	.915	0.387	2.02	.339	5.62×10^{-5}	15.76	1.68×10^{-3}	1.14×10^{-3}	1.33×10^{-3}	7.72×10^{-4}	6.30×10^{-4}	5.80×10^{-4}
250	2.50	2.21	1.98	.0240	48.6	90.8	.034	1.05	0.391	2.02	.324	6.38×10^{-5}	18.19	2.19×10^{-3}	1.46×10^{-3}	1.13×10^{-3}	6.76×10^{-4}	6.24×10^{-4}	5.88×10^{-4}
259	2.59	2.25	2.02	.0232	48.9	91.1	.034	1.09	0.393	2.04	.316	6.60×10^{-5}	19.26	2.39×10^{-3}	1.59×10^{-3}	--	--	--	
275	2.75							0.00								3.63×10^{-4}	4.69×10^{-4}	5.39×10^{-4}	5.61×10^{-4}
300	3.00															1.02×10^{-4}	3.07×10^{-4}	4.45×10^{-4}	5.02×10^{-4}
350	3.50																1.47×10^{-4}	2.29×10^{-4}	3.59×10^{-4}
400	4.00																7.70×10^{-5}	4.62×10^{-5}	2.11×10^{-4}
450	4.50																4.29×10^{-5}		9.6×10^{-5}
500	5.00																		4.0×10^{-5}

Note: (1) Data taken directly from table 16.1.

The value of Q can be found approximately by entering figure 19.2 with a value of A and by interpolating between curves of z_* values. Alternatively, an interpolation can be carried out in table 19.1. With either method, this yield Q = 19.26.

Knowing Q, the total transport can be found using equation 19.44:

$$S = 6.60\text{x}10^{-5} \; [\; 1 + 1.83 \; (19.26) \;] \tag{19.59}$$

$$= 2.39\text{x}10^{-3} \; m^3/s.m \tag{19.60}$$

The total sediment transport can be found by integrating the values of S across the width of the breaker zone. Integrating the values of S_1 using the trapezoidal rule and remembering that the last interval, Δy, is only 9 m. yields:

$$S_1 = 0.179 \; m^3/s \tag{19.60}$$

$$= 5.64\text{x}10^{6} \; m^3/\text{year} \tag{19.61}$$

This resulting value seems high on a yearly basis, but on the other hand, a deep water wave height of 2.0 m is about twice as high as a year-averaged North Sea wave. Secondly, one has the erronious tendency to compare the figure in equation 19.61 to *net* sand transport along the Dutch Coast which is much smaller.

Values of sediment transport rates computed using the other longshore current profiles listed in table 16.1 are also listed in table 19.3.

Values of S_2 are found by applying the technique just described for S_1, except that intermediate water depth wave theory is used throughout the sand transport computation. (It had already been used along with a more exact force balance to determine the longshore current velocity, V_2, in chapter 16).

The remaining sand transports, S_3 through S_6, all result from the use of the Bijker formula with the correspondingly numbered velocity profile from table 16.1.

All of these results as well as their associated velocity profiles from chapter 16 are compared in figure 19.3. Note that when an intermediate peak in the velocity profile occurs such as with V_3 through V_6, the corresponding peak in the sediment transport occurs seaward of the velocity peak.

Also, from the computations shown in table 19.3, we can conclude that the suspended transport becomes relatively more important as the water depth increases. This follows from the higher values of Q associated with greater depths in the table.

The local variations in sand transport between the various transport profiles seems rather great. However, when the total sand transports are computed by integrating the curves shown in figure 19.3b, remarkably consistent results are obtained. These are indicated in table 19.4.

A computation using the CERC formula is shown in section 19.11. for comparison. In the following section we investigate the sensitivity of the Bijker formula.

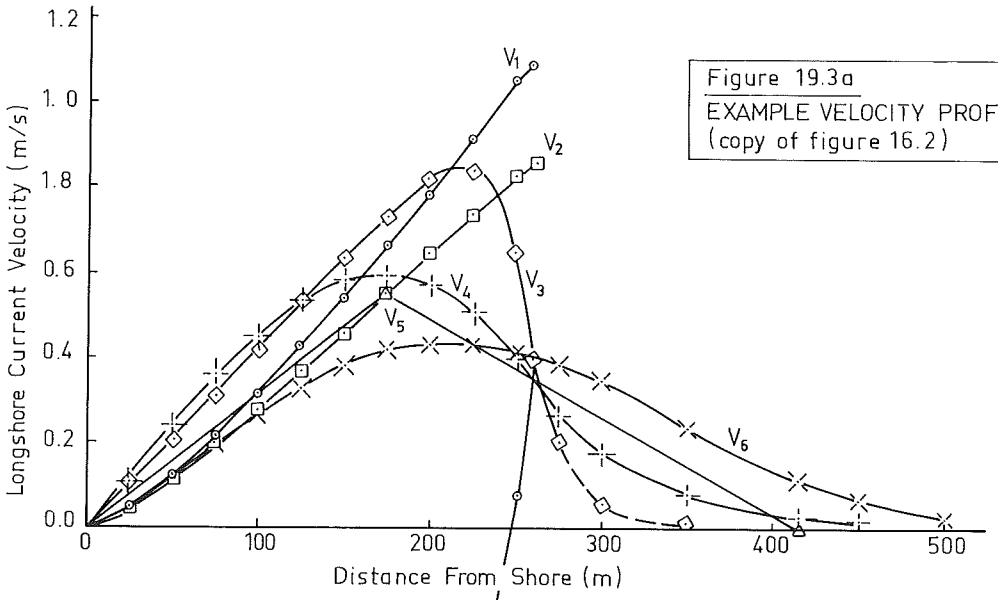

Figure 19.3a
EXAMPLE VELOCITY PROFILES
(copy of figure 16.2)

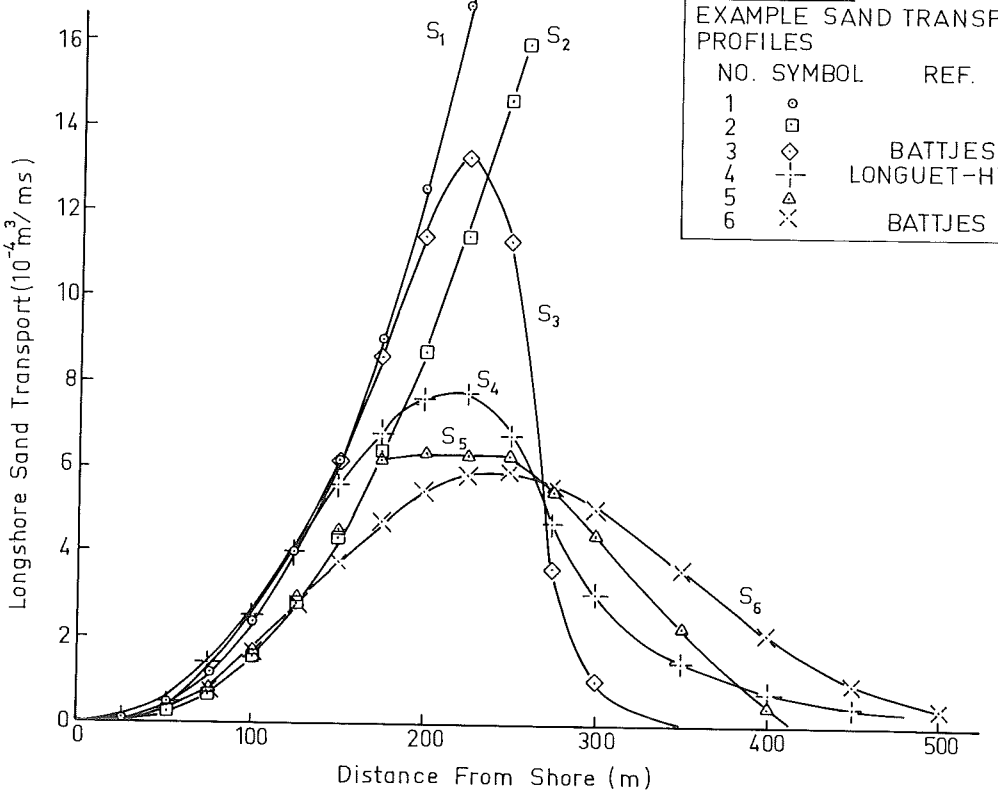

Figure 19.3 b
EXAMPLE SAND TRANSPORT PROFILES

NO.	SYMBOL	REF.
1	⊙	
2	⊡	
3	◇	BATTJES
4	⊹	LONGUET-HIGGINS
5	△	
6	✕	BATTJES

Table 19.4 Total sand transports

Profile no.	Total transport m^3/s
1	0.179
2	0.123
3	0.132
4	0.159
5	0.143
6	0.146
CERC Coef. = 0.036	0.314 *
CERC Coef. = 0.008	0.070 *

19.10 Sensitivity of the Bijker formula

In the previous example specific values of such parameters as bottom roughness, r, particle grain size, D, beach slope, m, and breaker index, γ, have been used. Figure 19.4 shows the total sand transport found using the Bijker formula in combination with the velocity distribution denoted by V_6, as a function of bottom roughness, r, for various grain sizes and beach slopes. Offshore wave conditions were held constant and the same as in the previous section. Once again, the results from the CERC formula are shown for comparison. Note that the CERC formula is completely insensitive to the parameters being discussed here.

The bottom roughness influences the total sand transport in 2 ways: As the bottom roughness increases, the longshore current velocity decreases - see chapter 16; secondly, for a given current velocity, the Bijker formula usually gives a lower sediment transport as the roughness is increased. These two influences reinforce each other to yield the decreasing total sediment transport with increasing roughness.

The influence of increasing the average bed material grain size is also obvious from figure 19.4. Increasing the bottom material grain size has decreased the total sediment transport in this example. This may seem suprising in light of the direct relationship between D and S_b in the transport term of equation 19.34. The error in this oversimplified examination is that the grain size, D, also influences the fall velocity, W, (for the suspended load transport) and even the ripple factor, μ, indirectly. Thus, the influence of the bed material gradation on the sediment transport is complex, indeed.

Increasing the beach slope tends to increase the longshore current velocity. (This is demonstrated in a very simple case by equation 16.06.) This increased velocity will yield a higher sediment transport per unit width. The increasing beach slope narrows the breaker (and transport) zone, however, so that the total sediment transport on a steep, narrow beach is little different from that on a flatter, wider beach.

* These results are shown in section 19.11.

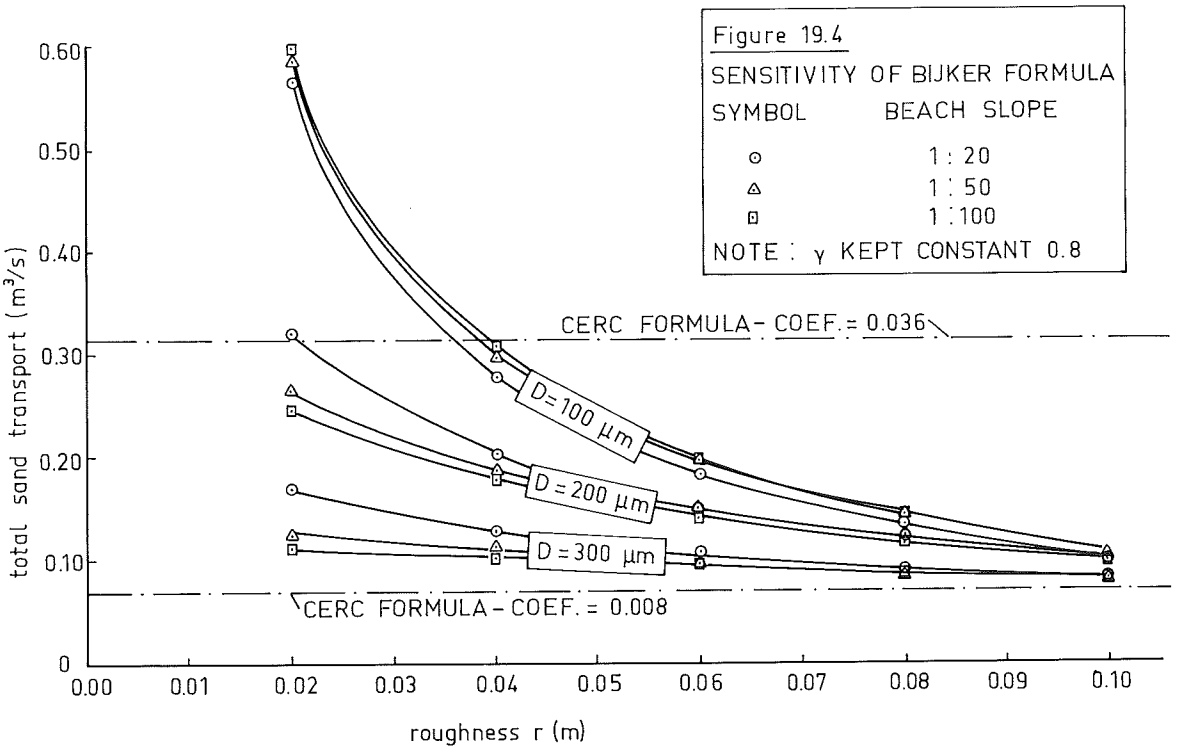

19.11 Comparison to CERC formula

The application of the CERC formula is illustrated here in order to compare its results to those found using the Bijker formula. The same conditions and parameter values used in sections 16.5 and 19.9 will be used here as well.

The CERC formula - from chapter 17 - is:

$$S = 0.014\, H_o^2\, c_o\, K_{rbr}^2 \sin \phi_{br} \cos \phi_{br} \qquad (17.08) \qquad (19.62)$$

Instead of using the original coefficient in equation 19.62, we shall use the coefficients associated with lines 1 and 2 in figure 17.1 which are listed in table 17.1. These coefficient values are 0.008 and 0.036 respectively. line 1 is not recommended

The necessary data are:

$H_o = 2.0$ m

$\phi_o = 30^o$

$\phi_{br} = 13.3^o$

$T = 7.0$ s

From volume I chapter 5:

$$c_o = \frac{9}{2\pi} T \qquad (I\text{-}5.05a) \qquad (19.63)$$

$$= (1.56)(7) = 10.93 \text{ m/s} \qquad (19.64)$$

and from volume I chapter 9:

$$K_r^2 = \frac{\cos \phi_o}{\cos \phi_{br}} \tag{19.65}$$

$$= \frac{\cos 30^o}{\cos 13.3^o} = 0.890 \tag{19.66}$$

Substituting values into (19.62) with the larger coefficient yields:

$$S = (0.036)(2)^2 (10.93)(0.890)(\sin 13.3^o)(\cos 13.3^o) \tag{19.67}$$

$$= 0.314 \text{ m}^3/\text{s} \quad = 9,902,304 \text{ m}^3/\text{yr} \tag{19.68}$$

and with the smaller coefficient:

$$S = 0.070 \text{ m}^3/\text{s} \quad = 2,207,520 \text{ m}^3/\text{yr} \tag{19.69}$$

The results from this CERC formula have already been compared to those of the Bijker formula in table 19.5 and figure 19.4. Note that it brackets the other results rather well. Thus, one can conclude - correctly - that the Bijker formula will solve any problem which the CERC formula will also solve. Why bother, though? The CERC formula is much simpler to apply as has just been demonstrated.

Indeed, the power of the Bijker formula lies in its adaptability to any current condition. The concept of the Bijker formula - the adjustment of the bottom shear stress to account for the waves - can be applied much more universally. Alternatively, the current, V, included in the Bijker formula may be driven by any combination of forces and subjected to all sorts of local influences. For example, the Bijker formula can be used to predict sedimentation in shipping channels in which there are no breaking waves; the CERC formula would yield no result in such a case. This specific problem of channel sedimentation comes up again in chapter 25.

Now that we can compute longshore sediment transport rates for a given set of conditions, we are in a position to attack the problem of predicting coastal changes. The first application of sediment transport computations to predict coastal changes is the topic of chapter 20.

20. COASTAL CHANGES WITH SINGLE LINE THEORY

E.W. Bijker

20.1 Introduction

The previous chapters have been devoted to the determination of the sediment transport at a given location on the coast. In this chapter we shall apply the knowledge of sediment transport rates to the prediction of coastal changes. As has been pointed out in section 1 of chapter I-28, only a *change* in sediment transport as we progress along a coast will cause erosion or accretion of a coast.

The method to be presented here was, in principle, developed by Pelnard-Considère (1954). Although it is old and poorly suited for many problems - it involves some very limiting assumptions - it is one of the few methods available suitable for hand computation. As such, it retains its value.

The profile characterizing the beach to be studied is assumed to move horizontally over its entire height as a result of accretion or erosion. The beach slope does not change, therefore. Such a beach and its schematization have already been illustrated in volume I, figure 26.1. That figure is reproduced here from completeness. The area between and the horizontal displacement of the solid and dashed lines is the same for the schematization and the actual profile. In practice, this profile usually extends somewhat farther seaward than the breaker zone and includes the entire nearshore area. Often, the toe of the profile can be defined as the point where the beach slope becomes essentially horizontal.

Two equations will be necessary in order to predict the coastal changes: an equation of motion and a continuity equation; these will be discussed in the following sections.

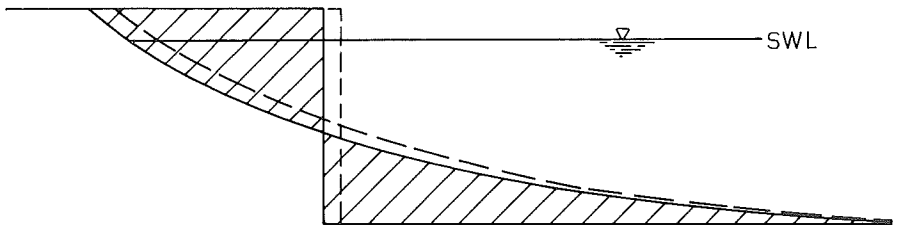

Figure 20.1 BEACH PROFILE AND ITS SCHEMATIZATION. THE SHADED AREAS ARE EQUAL (no scale)

20.2 Equation of continuity

Consider a segment of a beach which is changing - either eroding or accreting. If we examine a portion of length dx for a time dt, we shall find that the coastline has moved a distance dy. From figure 20.2, we see that if the depth over which the coastal changes take place is h, then:

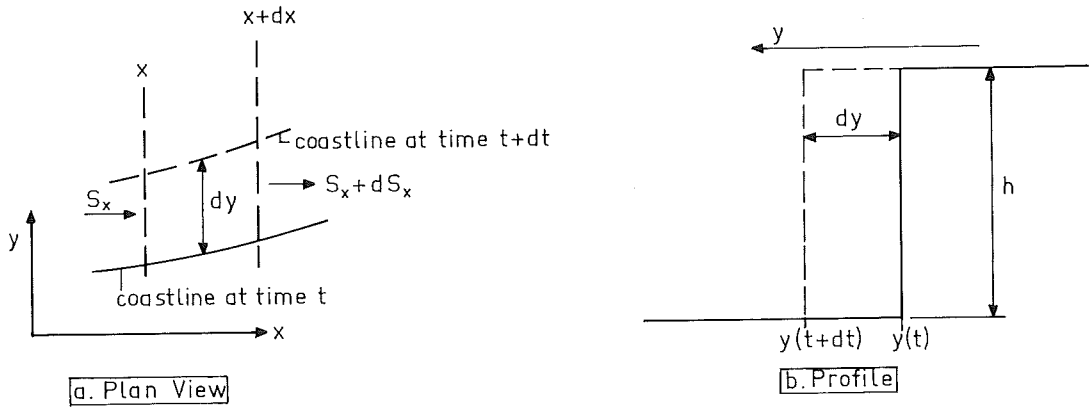

Figure 20.2
CONTINUITY EQUATION RELATIONSHIPS

$$S_x\, dt - (S_x + d\, S_x)\, dt = dx\, dy\, h \qquad (20.01)$$

where: h is the depth over which the change takes place,
S_x is the sand transport along the coast at location x, and
$S_x + d\, S_x$ is the sand transport along the coast at location x + dx.

In words, the inflow minus the outflow is the volume of material accumulated.

Also:

$$d\, S_x = \frac{\partial\, S_x}{\partial x}\, dx \qquad (20.02)$$

and

$$dy = \frac{\partial y}{\partial t}\, dt \qquad (20.03)$$

Substitution of these last two relationships into equation 20.01 yields, after simplification:

$$\frac{\partial\, S_x}{\partial x} + h\, \frac{\partial y}{\partial t} = 0 \qquad (20.04)$$

which is the resulting equation of continuity.

Our primary practical interest is in the change in the coastline as a function of time, thus indirectly in $\frac{\partial y}{\partial t}$. If we can evaluate $\frac{\partial\, S_x}{\partial x}$ in equation 20.04, then we can determine the coastal changes via an integration. This necessary first term of (20.04) is examined in the following section.

20.3 Equation of motion

In the previous section, we were left with the problem of evaluating $\frac{\partial S_x}{\partial x}$. What changes along a coast will cause S_x to change? The most important variables which can change as we proceed along a coast are the wave height and the angle of wave attack relative to the coastline. Of these, we shall restrict ourselves, here, to changes in the angle of wave attack; this implies that there is no diffraction and the offshore wave conditions do not change along the coast*.

In section 17.4 we carried out an investigation of the relationship between changes in the angle of wave approach relative to the coast and the resulting sand transport, S_x. There, we examined S_x for various values of wave attack relative to a fixed coast. We could just as well have examined S_x for a fixed wave direction and a varying coastline orientation relative to the waves. Thus, by varying ϕ slightly in a sand transport equation, we can then emperically determine $\frac{\partial S_x}{\partial \phi}$. (This can be done with any longshore sand transport formula). Also, if we restrict our changes in angle of attack relative to a changing coastline to small changes, we can assume $\frac{\partial S_x}{\partial \phi}$ to be constant:**

$$\frac{\partial S_x}{\partial \phi} = A S_x \qquad (20.05)$$

This is our desired equation of motion.

We can transform this known function $\frac{\partial S_x}{\partial \phi}$ to our unknown function $\frac{\partial S_x}{\partial x}$ via the Chain Rule:

$$\frac{\partial S_x}{\partial x} = \frac{\partial S_x}{\partial \phi} \frac{\partial \phi}{\partial x} \qquad (20.06)$$

If, as we have assumed, $\partial\phi$ is small, then $\partial\phi$ is equivalent to $-\frac{\partial y}{\partial x}$ and:

$$\frac{\partial \phi}{\partial x} = -\frac{\partial^2 y}{\partial x^2} \qquad (20.07)$$

The negative sign results from the fact that a positive (increase in) $\frac{\partial y}{\partial x}$ results in a decrease in ϕ.

---

* We shall discuss the location at which the wave conditions should be taken in more detail in a later section.

** Such an assumption implies that a segment of the entire function relating S_x to ϕ has been replaced by a straight line. This is not too bad an assumption as long as the changes in ϕ are not too large. In the following it will be obvious that $\phi=0$ should be included in the solution. We are thus restricted in our analysis to small values of ϕ

The angle ϕ used here has not been specifically defined; it is the angle of wave attack in some water depth before the coast. This depth must correspond to the depth at the toe of portion of the coast which is modified by the longshore sand transport. This corresponds, thus, to the depth, h, in figure 20.2. We denote this angle by ϕ' as shown in figure 20.3 when it is measured relative to the original coast (x axis). The angle we need in the equation of motion is, however, the angle between the wave crest at depth h and the instantaneous shoreline at some time, t. Thus, also from figure 20.3, we can define ϕ as:

$$\phi = \phi' - \frac{\partial y}{\partial x} \tag{20.08}$$

Figure 20.3
SHORE PLAN SHOWING $\frac{\delta y}{\delta x}$

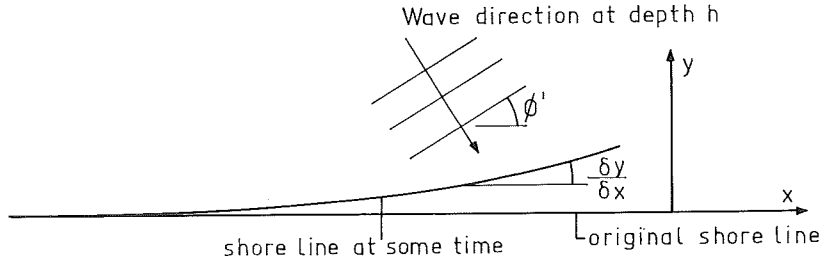

Note that the result above - that ϕ must be measured at a depth h - is in contrast to that presented in chapter 17 where ϕ_0 was used in the CERC formula. That was valid, there, because we implicitly assume that the beach slope continued to deep water, thus $\phi' = \phi_0$ in that case. The present definition, using ϕ', is more general; it is also valid, for example, when the toe of the beach slope is on a horizontal sandbank.

What about the wave height we are going to use to determine the sand transport? (The wave height enters any coastal sand transport formula in some way). Just as with the angle of attack, it is safest to evaluate the wave height (or heights) in the area where the coastal changes are to be predicted. Use of deep water wave data will yield incorrect results if breaking occurs on intermediate offshore bars.

20.4 Equation solution, boundary and initial conditions

Equation 20.05, the equation of motion, and 20.04, the continuity equation, can be combined by substitution of (20.05) and (20.07) into (20.05):

$$\frac{\partial S_x}{\partial x} = - s_x \frac{\partial^2 y}{\partial x^2} \tag{20.09}$$

and substituting this into (20.04), yielding:

$$- s_x \frac{\partial^2 y}{\partial x^2} + h \frac{\partial y}{\partial t} = 0 \tag{20.10}$$

which can be reduced to a standard form by substituting:

$$a = \frac{s_x}{h} = \frac{S}{\phi' h} \qquad (20.11)$$

so that the final result is:

$$a \frac{\partial^2 y}{\partial x^2} - \frac{\partial y}{\partial t} = 0 \qquad (20.12)$$

The last step in equation 20.11 follows from equation 20.05.

Both initial conditions and boundary conditions are needed in order to solve equation 20.12 for a specific problem. One initial condition - the coast form at time t = 0 - and two boundary conditions - sand transports as a function of time at two different places - are usually specified. Initial and boundary conditions for a specific problem, that of accretion against an impermeable (for sand) breakwater, are given in the following section along with the resulting shore line solution.

20.5 Application to breakwater accretion

The construction of a breakwater to protect a harbor approach channel from wave action also upsets the equilibrium of coastal sediment transport. Figure 20.4 shows a sketch plan of such a breakwater. Coastlines for various times, t, are shown.

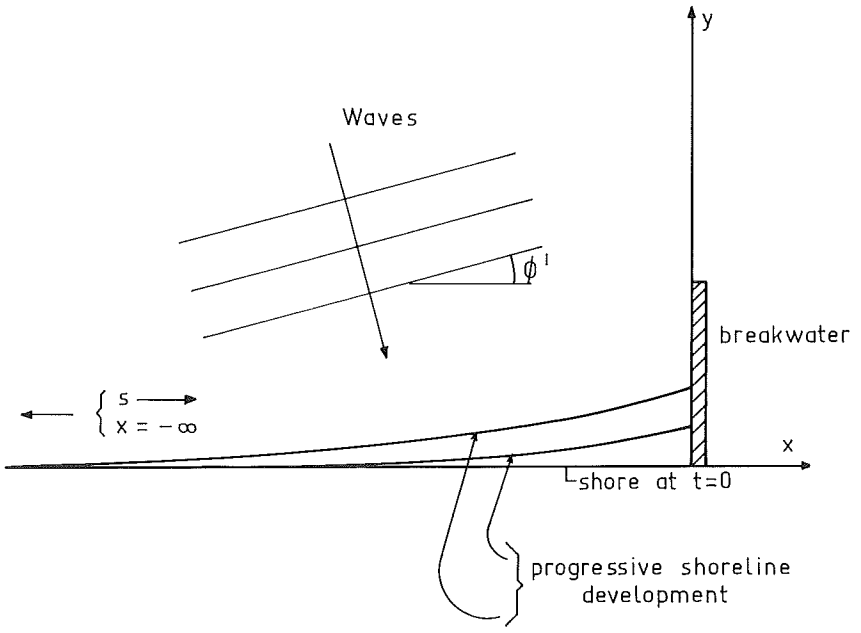

Figure 20.4
ACCRETION OF SHORE NEAR BREAKWATER

The initial condition is the shape of the coastline at time t = 0. This is expressed by:

$$\text{at } t = 0\text{: } y = 0 \text{ for all } x \qquad (20.13)$$

One boundary condition is that at a great distance from the breakwater, $x = -\infty$, the sand transport remains constant and equal to its value initially on the undisturbed coast:

$$\text{at } x = -\infty\text{: } S_x = S \text{ for all } t \tag{20.14}$$

The second boundary condition is imposed by the breakwater; it is impervious to sand. Thus:

$$\text{at } x = 0\text{: } S_x = 0 \text{ for all } t > 0 \tag{20.15}$$

This last boundary condition implies, using (20.08) and remembering the dependence of S_x on ϕ that:

$$\text{at } x = 0\text{: } \frac{\partial y}{\partial x} = \phi' \text{ for all } t > 0 \tag{20.16}$$

In other words, the beach accretion progresses seaward always making an angle ϕ' with respect to the x axis at the breakwater.

The resulting solution to equation 20.12 is:

$$y = \phi' \sqrt{\frac{4at}{\pi}} \left[e^{-u^2} - u\sqrt{\pi}\,\Theta \right] \tag{20.17}$$

where: $u = -\dfrac{x}{\sqrt{4at}}$, (20.18)

x is the distance along the beach - fig. 20.4, and

$$\Theta = \frac{2}{\sqrt{\pi}} \int_u^\infty e^{-u^2}\,du \tag{20.19}$$

Θ has the form of a probability integral.

$$\Theta = \frac{2}{\sqrt{\pi}} \left[\int_0^\infty e^{-u^2}\,du - \int_0^u e^{-u^2}\,du \right] \tag{20.20}$$

$$\Theta = 1 - \frac{2}{\sqrt{\pi}} \int_0^u e^{-u^2}\,du \tag{20.21}$$

This last parameter can be evaluated using tables of the normal probability distribution*. Some values of Θ and $e^{-u^2} - u\sqrt{\pi}\,\Theta$ are listed in table 20.1.

Since $\Theta \approx 0$ for $u > 2.5$ we can conclude, using equation 20.18, that the breakwater has little influence at distances more than $5\sqrt{at}$ "upstream". ($x = -5\sqrt{at}$).

The outward growth of the coastline at the breakwater, $L(t)$, at $x = 0$ is:

$$L(t) = \phi' \sqrt{\frac{4at}{\pi}} = 2\sqrt{\frac{\phi' S}{\pi h}}\sqrt{t} = 2\varphi'\sqrt{\frac{St}{\pi h}} \tag{20.22}$$

from (20.17) using (20.11). The progress of the coast is proportional to the square root of time; all other parameters in equation 20.22 are constant for a given problem.

---

* See, also, equation 4.07 and table 4.1.

Table 20.1 Shoreline accretion parameters

u	Θ	$e^{-u^2} - u\sqrt{\pi}\,\Theta$
0	1.000	1.000
0.10	0.8875	0.8327
0.20	0.7773	0.6852
0.30	0.6714	0.5569
0.40	0.5716	0.4469
0.50	0.4795	0.3538
0.60	0.3962	0.2764
0.70	0.3222	0.2128
0.80	0.2579	0.1616
0.90	0.2031	0.1209
1.00	0.1573	0.0890
1.25	0.0771	0.0388
1.50	3.389×10^{-2}	1.529×10^{-2}
1.75	1.333×10^{-2}	5.418×10^{-3}
2.00	4.680×10^{-3}	1.726×10^{-3}
2.50	4.084×10^{-4}	1.208×10^{-4}
3.00	2.216×10^{-5}	5.581×10^{-6}
3.50	7.430×10^{-7}	1.759×10^{-7}
∞	0	0

Some handy geometrical relations, valid if ϕ' is sufficiently small, are listed below and shown in figure 20.5.

$$\frac{\text{distance OB}}{\text{distance OC}} = \phi' \qquad (20.23)$$

$$\frac{\text{distance OA}}{\text{distance OC}} \approx 2.5\pi = 7.85 \qquad (20.24)$$

Also, obviously, from continuity, the total surface area, OAB is:

$$\frac{St}{h} = a\,\phi' t \qquad (20.25)$$

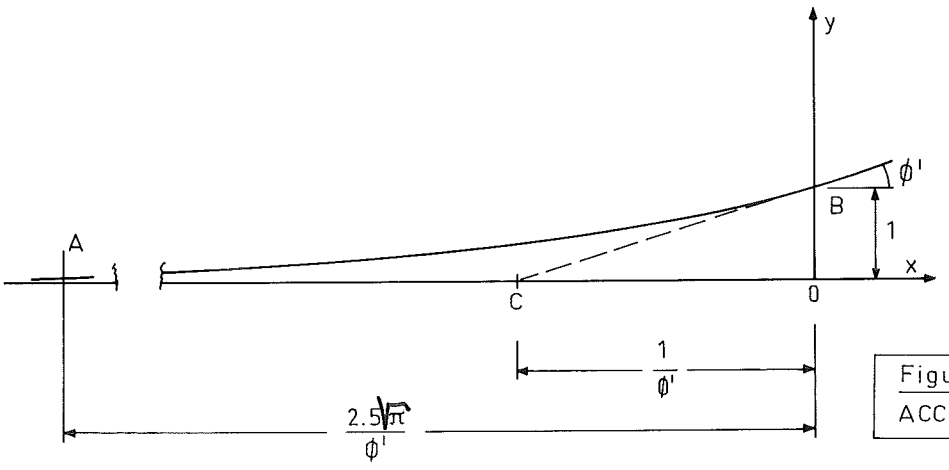

Figure 20.5
ACCRETION GEOMETRY

20.6 Non-parallel accretion

In the previous analysis it was assumed that the entire beach profile at any given point, x, moved forward uniformly. While this assumption simplifies the mathematics, it is often difficult to justify in practice. It would be handy, therefore, to have a solution usable for a situation where the accreting beach profile slope differed from that of the original profile.

Van Hijum (1972) attacked the problem for which the accretion at the toe of the slope progressed more slowly than at the top. In the schematized profile in figure 20.6, the original beach has a slope m while the accretion zone moves forward at slope m'. Here, m and m' are the tangents of the slope angles.

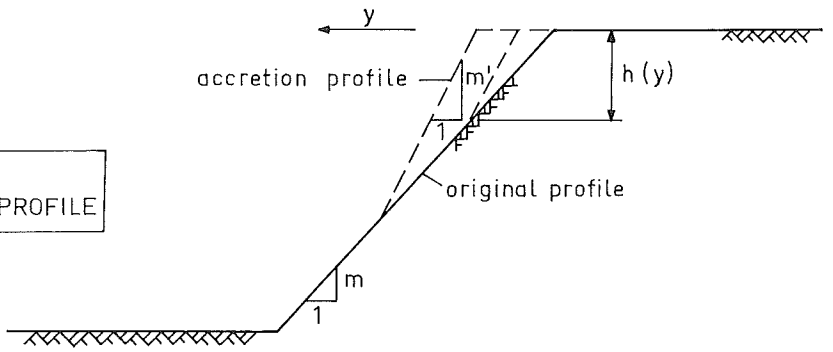

Figure 20.6
NON-PARALLEL ACCRETION PROFILE

From figure 20.6:

$$h(y) = \frac{m\,m'}{m' - m}\,y \tag{20.26}$$

The equation of continuity (20.04) now gets the form:

$$\frac{\partial S_x}{\partial x} + \frac{m\,m'}{m' - m}\,y\,\frac{\partial y}{\partial t} = 0 \tag{20.27}$$

which results in an equation for the coastline (corresponding to equation 20.10) of:

$$-S_x\,\frac{\partial^2 y}{\partial x^2} + \frac{m\,m'}{m' - m}\,y\,\frac{\partial y}{\partial t} = 0 \tag{20.28}$$

After much work, van Hijum was only able to find an approximate solution to the above equation:

$$y \approx 1.59\,M^3\,\phi'\,\frac{(0.72M - x)^2}{(M - x)^4} \tag{20.29}$$

where: $$M = \left[\frac{6(m' - m)S\,t}{m\,m'\,(\phi')^2}\right]^{1/3} \tag{20.30}$$

At the breakwater (x = 0):

$$L = \left[\frac{1.5\,(m' - m)S t\,\phi'}{m\,m'}\right]^{1/3} \tag{20.31}$$

Comparison of (20.31) with (20.22) shows that accretion at the breakwater progress faster in the initial stages with the non-parallel accretion. This is logical in view of figure 20.6; less sand is needed to form the initial stages of the accretion.

The solution method just presented is, of course, only valid as long as the toe of the accreting slope continues to progress along the original slope. When this accreting toe reaches the bottom of the original slope, the situation reverts to that of parallel accretion outlined in the previous section.

20.7 Transport Past Breakwater Tip

The shoreline development equations in the previous sections were dependent upon an impervious boundary condition at the breakwater. Assuming once again that there is parallel beach accretion, the accretion at the breakwater is given by equation 20.22 in which y increases indefinitely as long as t increases. Since it is uneconomical and even irresponsible to build an infinitely long breakwater, a breakwater of a given, finite length can only be expected to stop the longshore sand transport for a finite time. Two important questions can be asked: "How long will a given breakwater completely obstruct the longshore sediment transport?", and "What happens after that time?"

Figure 20.7 shows a shore profile immediately on the accretion side of the breakwater. Since the major portion of the sand transport takes place in the breaker zone, no appreciable transport will take place arround the end of the breakwater as long as the breakwater extends through the breaker zone. This implies, in the figure, that transport around the breakwater tip can be expected to start when the depth on the accreted slope at the end of the breakwater has decreased to h_{br}, the depth at the outer edge of the breaker zone.

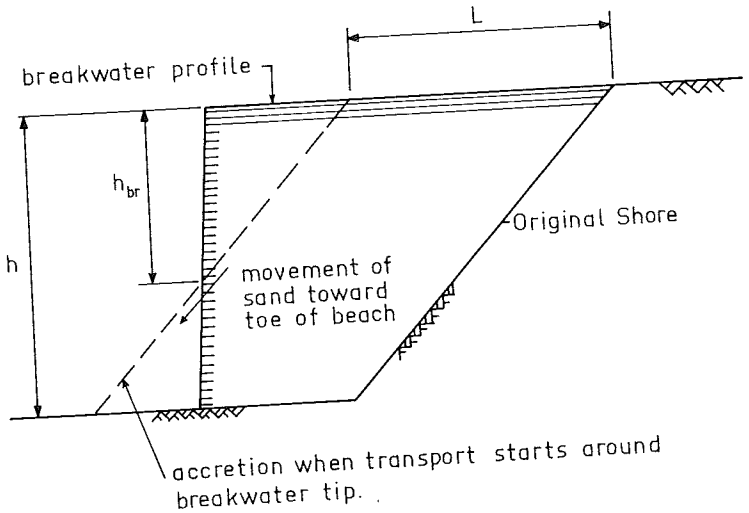

Figure 20.7
PROFILE AT START OF SAND PASSAGE

The accretion shown in figure 20.7 at depths greater than h_{br} has been transported along the coast within (or very close to) the breaker zone and then moved down the slope of the beach to the toe. This transverse transport along the beach profile will be treated in detail in chapter 21.

The accretion distance, L in the figure, can be computed knowing the breaker depth and the slopes of the beach and breakwater. Knowing this length, L, the time, t_1, before sand escapes around the breakwater tip can be computed using equation 20.22:

$$t_1 = \frac{\pi}{4} \frac{L^2}{S} \frac{h}{\phi'} = 0.785 \frac{L^2}{S} \frac{h}{\phi'} \qquad (20.32)$$

For the non-parallel accretion - equation 20.31:

$$t_1' = \left[\frac{m\, m'\, L^3}{1.5\,(m' - m)\, \phi' S} \right]^3 \qquad (20.33)$$

In practice, L will probably be so long that a solution using equation 20.33 will not be valid; the water will not be deep enough for this non-parallel accretion to extend so far.

The above equations answer the first of the two questions posed earlier. Note that at this time, t_1, the toe of the accretion slope extends beyond the breakwater tip! Because there is little longshore sand transport so deep on the profile, this will not lead to noticable transport around the breakwater tip, however.

In order to answer the second question about the sand transport around the breakwater tip after time t_1, we need to formulate a new set of boundary and initial conditions and generate a new solution to the differential equation.

When material is passing around the breakwater tip, our boundary condition:

$$\text{at} \quad x = 0\text{: } S_x = 0 \text{ for all } t > 0 \qquad (20.15)$$

is no longer valid. Instead, this boundary condition should now become:

$$\text{at} \quad x = 0\text{: } y = L \text{ for all } t \geq t_1 \quad * \qquad (20.34)$$

The other boundary condition:

$$\text{at } x = -\infty,\ S_x = S \text{ for all } t \qquad (20.14)$$

remains perfectly valid, of course.

The most convenient initial condition would now be:
at $t = t_1$, y is given by equation 20.17 evaluated as a function of x for $t = t_1$. This is the actual coastline profile determined using the previous solution.

---

* Strictly speaking y must be greater than L for sand transport to take place past the breakwater tip.

Unfortunately, a workable analytic solution to the differential equation with boundary and initial conditions outlined above has not yet been found; the problem cannot be conveniently solved. This forces us to modify the conditions so as to make an analytic solution possible.

An initial condition which does allow analytical solution of equation 20.12 is:

$$\text{at } t = 0,\ y = 0 \text{ for } x < 0 \tag{20.35}$$

with:

$$\text{at } t = 0,\ y = L \text{ for } x = 0 \tag{20.36}$$

This is an initial condition following AOB in figure 20.5 instead of AO as in section 20.5 and curve AB as suggested above. The present initial condition (20.35 and 20.36) implies that the beach bends sharply at x = 0 and proceeds perpendicular to the coast along the breakwater! Further, the angle between the waves and the "breakwater beach" at the end of the breakwater is initially negative and we can expect sand to be transported to the *left* around the breakwater tip in the initial stages of shoreline development! Since no supply for this sand exists, this solution approach seems rather unrealistic; we can, however, salvage the situation by restricting ourselves by agreeing to use this new solution only when there is a *positive* transport to the *right* around the breakwater tip.

With (20.14), and (20.34) through (20.36) the solution to equation 20.12 is:

$$y = L\,\Theta \tag{20.37}$$

where Θ is defined just as in equation 20.19.

In order to compute the sand transport, S_x, at points along the accretion coast, we need to evaluate $\frac{\partial y}{\partial x}$ for substitution into equation 20.08 to determine ϕ, and hence S_x. Using (20.19) and (20.18) in (20.37) and differentiating:

$$\frac{\partial y}{\partial x} = \frac{L}{\sqrt{\pi a t}} \exp\left[-\frac{x^2}{4at}\right] \tag{20.38}$$

In particular, at the breakwater, x = 0:

$$\left.\frac{\partial y}{\partial x}\right|_{x=0} = \frac{L}{\sqrt{\pi a t}} = \beta \tag{20.39}$$

where the notation β has been introduced for convenience.

The sand transport at the tip of the breakwater is, now:

$$S_{tip} = S\left(1 - \frac{\beta}{\phi'}\right) = S\left(1 - \frac{L}{\phi' \sqrt{\pi a t}}\right) \tag{20.40}$$

Indeed, as long as β is larger than ϕ', there is a sand transport in the negative direction at x = 0 (to the left around the end of the breakwater). This confirms our earlier observation based upon the initial conditions.

How, then, must we compute the entire coastal development? We split the solution into two phases. The first phase begins when the breakwater is built, is described in section 20.5, and is valid until time $t = t_1$ from equation 20.32. The volume of sand accretion at that time will be:

$$v_1 = S\, t_1 = \frac{\pi\, L^2\, h}{4\, \phi'} \tag{20.41}$$

from equations 20.25 and 20.32 knowing that there is parallel accretion.

The equations for the second phase are developed in this section. The volume of sand accumulated is now:

$$v_2 = \int_0^{t_2} (S - S_{tip})\, dt \tag{20.42}$$

which, with (20.40) works out to be:

$$v_2 = \frac{S}{\phi'} \int_0^{t_2} \beta\, dt \tag{20.43}$$

$$= 2\, L\, h \sqrt{\frac{a\, t_2}{\pi}} \tag{20.44}$$

after a bit of algebra. The subscript, 2, has been added to v and to t to emphasize that it results from the second coastline solution.

The proper time, t_2, to start using the second coastline solution may be found by stipulating that the volumes of accreted material be equal when the shift is made.* This does not mean that t_2 will be equal to t_1; indeed, $t_2 < t_1$ since the second model allows (fictitious) sand supply from the tip of the breakwater.

Equating v_1 and v_2 yields:

$$\frac{\pi\, L^2\, h}{4\, \phi'} = 2\, L\, h \sqrt{\frac{a\, t_2}{\pi}} \tag{20.45}$$

This yields:

$$t_2 = \frac{\pi^3}{64}\, \frac{L^2\, h}{S\, \phi'} \tag{20.46}$$

Introducing t_1 from (20.32) yields:

$$t_2 = \frac{\pi^2}{16}\, t_1 = 0.617\, t_1 \tag{20.47}$$

---

* Another, different solution would result by stipulating $\beta = \phi'$ at time t_2; in other words, there is no sand transport at the tip.

This confirms our observation about the relative values of t_1 and t_2. This means, in practice, that we must "start" the second solution at some time later than the time t = 0 when the phase 1 solution started. This is shown diagrammatically in figure 20.8. In that figure data pertaining to the first model is indicated above the time axis, that for the second model is below the axis. As we can see from the figure, the time axis for the second solution model is shifted to the right relative to the origin of the original time axis. Since this time origin shift can be inconvenient, we can make an appropriate correction to the equations for phase 2 to allow substitution of times based upon the original time scale. The time scale for phase 2 is found by shifting times from the original scale by 0.383 t_1 as shown in the figure. Making this time origin shift in equation 20.40 yields:

$$S_{tip} = S \left[1 - \frac{L}{\phi' \left(\pi a \left(t - 0.383\ t_1\right)\right)^{1/2}} \right] \qquad (20.48)$$

or, using (20.32):

$$S_{tip} = S \left[1 - \frac{2}{\pi \sqrt{\frac{t}{t_1} - 0.383}} \right] \qquad (20.49)$$

which describes the sand transport past the breakwater tip for all times $\geq t_1$ using the original time scale.

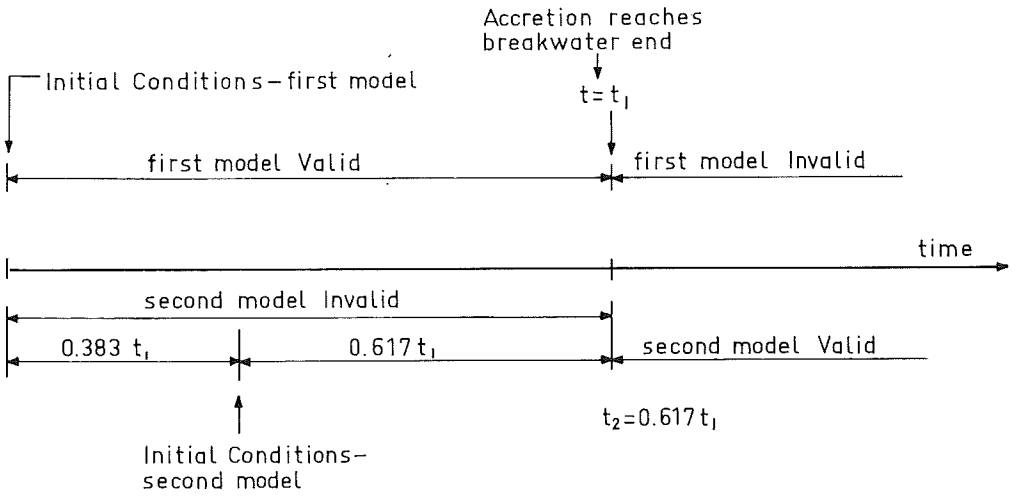

Figure 20.8
VALIDITY ZONES OF MODELS

As a check, we might well determine the sediment transport past the breakwater at time t = t_1; this should be zero. With t = t_1 (20.49) yields:

$$S_{tip} = S \left(1 - \frac{2}{\pi \sqrt{1-0.383}}\right) \qquad (20.50)$$

$$= 0.189\ S \quad ! \qquad (20.51)$$

This error results from the fact that the details of the shorelines are different for each of the models even when the total volumes of accumulated sediment are equal. The differences can be seen by plotting the two coastline profiles - equations 20.17 and 20.37.

Bakker has determined a correction to be applied to the computed values of transport at the breakwater tip. These are listed in table 20.2.

The merits of all of this work will be discussed in the following section; an example of its application is given in section 20.9.

Table 20.2 Corrections to breakwater tip transport computations

$\frac{t}{t_1}$	$\frac{S_{tip}}{S}$ equation 20.[illegible]51	$\frac{S_{tip}}{S}$ corrected value
1.00	0.189	0.000
1.25	0.316	0.298
1.50	0.398	0.394
2.00	0.499	0.499
3.0	0.606	0.606
4.0	0.665	0.665
5.0	0.704	0.704

20.8 Critical evaluation

The method of Pelnard-Considère has one major strong feature - it makes a hand computation of coastal changes possible. It can be used for accretion, as done here, and also for erosion on the lee side of a coastal sediment obstruction. Application in such a case will yield a coastal profile that is a mirror immage relative to the origin of those found for accretion.

In the development just presented we have allowed the beach to change (accrete in this case) even outside the breaker zone. The motivation for this was not given; it shall become obvious in a later chapter when sediment movements along a beach profile are discussed.

The development of the transfer of phases between the two coastline profile models is quite arbitrary. The assumption that the length of the accretion at the breakwater, L in figure 20.7, remains constant after time $t = t_1$ will not be exactly true in practice; some continued growth in the second phase should be expected.

The assumptions made in order to get an equation of motion are, at best, so restrictive that the approach is primitive. Wave height and direction variations along the coast, tidal influences, and many of the other more sophisticated points of the Bijker formula have had to be neglected. The assumption about the angle of wave attack, ϕ', being very small can be very crude, especially since the toe of the zone affected by longshore transport - where ϕ' is measured - can be well outside the breaker zone.

The inclusion of an arbitrary coastline profile as an initial condition - as opposed to the straight line used here - is difficult, if not impossible. This makes the modeling of many "real" coasts rather arbitrary. Indeed, we have assumed a straight coast for $\frac{7.85}{\phi'}$ times the length of the breakwater - equation 20.24. If, for example, $\phi' = 10^{o} = 0.175$ rad. and the breakwater is 1000 m long, then we assume a straight coast extending over 45 km!

20.9 Example

A harbor entrance is to be built upon a straight sandy coast which is subjected to waves having a period of 13 seconds and a deep water height, H_{sig_o}, of 1.8 meters. The angle of approach of the waves in deep water, ϕ_o, is 25^{o}. (Such a situation can often be found in tropical seas; this example is not too different from the situation on the coast of Ghana. The waves are of very constant period, height and direction throughout the year).

For simplicity, we shall assume that the breaker index, γ, is 0.8 and that the beach contour lines are parallel.

A harbor entrance is to be built with a breakwater which is curved in plan - a circle with a radius of 1650 m with center at the existing straight beach line. The breakwater slopes are 1:3 and the natural beach slope is 1:100 to a depth of 7.0 m beyond which the sea bottom is considered to be horizontal for a considerable distance. See figure 20.9.

Before we can begin actual sand transport computations, we must determine the wave angle at the toe of the beach slope. This is a straightforward refraction computation:

$$\lambda_o = (1.56)(13)^2 = 264 \text{ m} \tag{20.52}$$

$$\frac{h}{\lambda_o} = \frac{7}{264} = 0.02652 \tag{20.53}$$

Using the tables in volume III of the *Shore Protection Manual*:

$$\frac{h}{\lambda} = 0.06683 \tag{20.54}$$

$$\frac{c}{c_o} = 0.4199 \tag{20.55}$$

and thus:

$$\sin \phi' = 0.4199 \sin 25^o \tag{20.56}$$

which yields $\phi' = 10.2^o$ (20.57)

see figure 20.9.

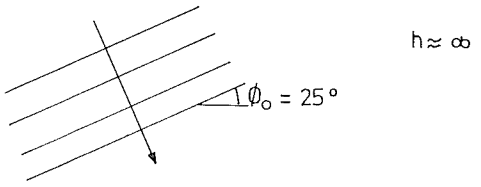

Figure 20.9
HARBOR ENTRANCE PLAN
scale 1 : 50 000

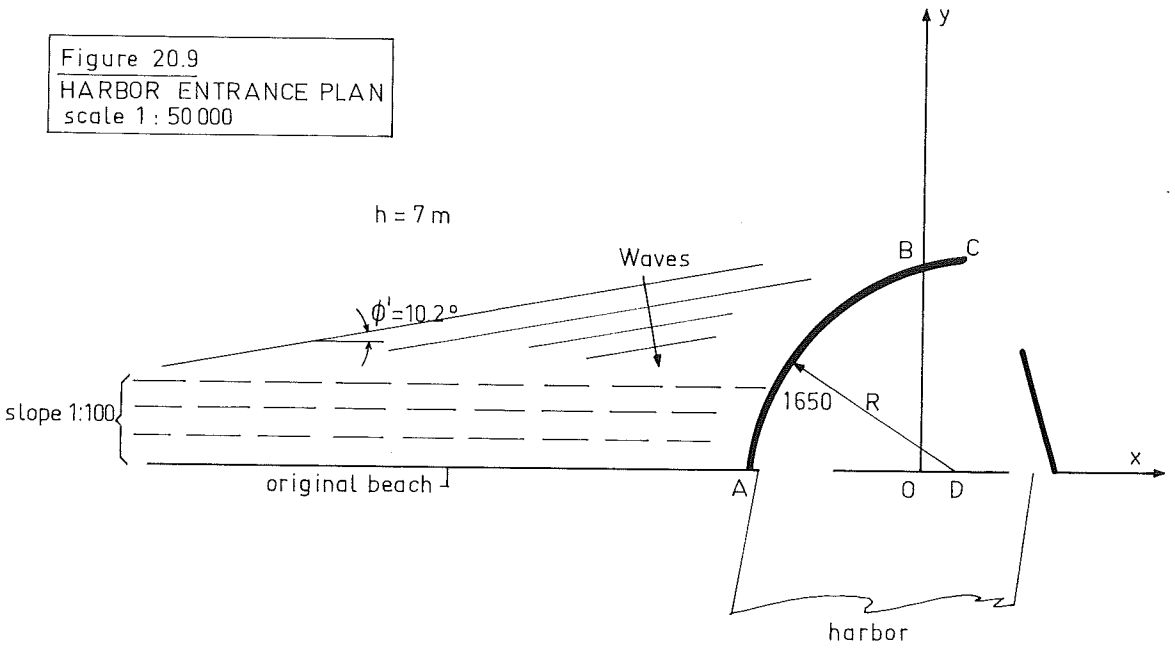

In order to use the CERC formula to determine the longshore sand transport along the undisturbed coast, we must also determine the angle of wave attack at the breaker line. This breaker line is located at the depth at which the root-mean-square wave breaks.

From equation 10.03 of volume I:

$$H_{rms_o} = \left(\frac{1}{\sqrt{2}}\right)(1.8) = 1.27 \text{ m} \tag{20.58}$$

We can now determine the breaker angle, ϕ_{br}, using the iterative procedure outlined in section 5 of chapter 16. This results in:

$$\left.\begin{aligned} H_{rms\ br} &= 1.80 \text{ m} \\ h_{br} &= 2.26 \text{ m} \\ \phi_{br} &= 5.6^o \end{aligned}\right\} \tag{20.59}$$

The CERC formula (17.09) (with improved coefficient) then yields:

$$S = 1.23 \times 10^6 \ (1.27^2)(1.56 \times 13)\left(\frac{\cos 25^o}{\cos 5.6^o}\right)^2 (\sin 5.6^o)(\cos 5.6^o)$$

$$= 3.24 \times 10^6 \text{ m}^3/\text{yr}. \quad * \tag{20.60}$$

* This rather high value results from a combination of relatively high characteristic wave height and respectable angle of attack.

Before this question can be answered directly, we must determine the effective length of the breakwater shown in figure 20.9. A naive approach is to begin assuming the breakwater extends 850 m (the distance CD) from the coast. However the correct approach is to realize that sand passing point B on the breakwater will be transported further by the waves. Thus, the breakwater should be schematized by one of length OB where B is located at the point where the approaching waves are tangent to the circle. The distance OB is:

$$OB = 1650 \cos 10.2^{o} = 1624 \text{ m} \tag{20.61}$$

Construction of a figure such as that shown in figure 20.7 with the appropriate length, breaker depth, and slope values yields:

$$L = 1624 - (100-3)(2.26) = 1405. \text{ m} \tag{20.62}$$

Knowing L, the time needed for the sand to accumulate to the point that it is no longer obstructed by the breakwater is found using equation 20.32:

$$t_1 = 0.785 \frac{(1405)^2(7)}{(3.24\text{x}10^6)(0.178)} = 18.8 \text{ years} \tag{20.63}$$

Note that the angle ϕ' has been expressed in radians in the above expression.

One may argue that this result must be corrected for the fact that a portion of the space to the left of the y axis in figure 20.9 has been occupied by the harbor instead of accumulated sand. The volume occupied by the harbor to the left of the y axis is about 10^7 m^3 which means that the time t_1 will actually be:

$$t_1' = 18.8 - \frac{10^7}{3.24\text{x}10^6} = 15.7 \text{ years.} \tag{20.64}$$

Note that for further computations, a time t_1 of 18.8 years must be used. This time corresponds to the computed time; the differential equation solution is not aware of the area occupied by the harbor.

The form of the coast after 10 years, at the time sand starts bypassing, and after 30 and 100 years can be plotted using equation 20.17 for the first two cases and equation 20.37 for the last two cases. Since the times are known, we are to plot y as a function of x; all other parameters are known. The computations are listed in table 20.3. The computations for t = 18.8 years are illustrated.

Three constant factors can be evaluated. From equation 20.11:

$$a = \frac{S}{\phi' h} = \frac{3.24\text{x}10^6}{(0.178)(7)} = 2.60\text{x}10^6 \tag{20.65}$$

From equation 20.18:

$$\sqrt{4at} = \sqrt{(4)(2.60\text{x}10^6)(18.8)} = 13980. \tag{20.66}$$

These values are listed under table 20.3.

Table 20.3 Coastline form computations

x	t = 10 years			t = t_1 = 18.8 years			t = 18.8 years			t = 30 years			t = 100 years		
	u	Θ	y	u	Θ	y	u	Θ	y	u	Θ	y	u	Θ	y
(km)	(-)	(-)	(m)	(-)	(-)	(m)	(-)	(-)	(m)	(-)	(-)	(m)	(-)	(-)	(m)
-40										2.597	2.6×10^{-4}	0.4	1.287	0.068	99.5
-30	2.941	2.7×10^{-5}	0.03	2.146	0.002	0.9	2.732	1.2×10^{-4}	0.2	1.948	0.006	8.3	0.966	0.172	242.
-20	1.961	0.006	2.0	1.431	0.043	26.9	1.821	0.010	14.3	1.299	0.067	93.6	0.644	0.363	510.
-15	1.471	0.038	16.3	1.073	0.129	98.6	1.366	0.053	75.0	0.974	0.169	237	0.483	0.495	695.
-10	0.980	0.166	96.	0.715	0.311	288.	0.911	0.197	277.	0.649	0.358	503.	0.322	0.650	913.
-8.	0.784	0.268	172.	0.572	0.418	417.	0.729	0.304	427.	0.519	0.462	649.	0.257	0.716	1006.
-6.	0.588	0.403	294.	0.429	0.546	585.	0.546	0.440	618.	0.390	0.584	821.	0.193	0.790	1110.
-4.	0.392	0.579	466.	0.286	0.685	806.	0.364	0.607	853.	0.260	0.714	1003.	0.129	0.856	1203.
-3.	0.294	0.678	577.	0.215	0.762	935.	0.273	0.700	984.	0.195	0.784	1102.	0.097	0.891	1252.
-2.	0.196	0.782	707.	0.143	0.841	1077.	0.182	0.797	1120.	0.130	0.854	1200.	0.064	0.928	1304.
-1.5	0.147	0.836	779.	0.107	0.879	1154	0.137	0.848	1191.	0.097	0.890	1250.	0.048	0.946	1329.
-1.0	0.098	0.889	856.	0.072	0.920	1234.	0.091	0.897	1260.	0.065	0.927	1302.	0.032	0.964	1354.
-0.5	0.049	0.944	938	0.036	0.960	1318.	0.046	0.949	1333.	0.032	0.965	1356.	0.016	0.982	1380.
0.0	0.000	1.000	1024.	0.000	1.000	1405.	0.000	1.000	1405.	0.000	1.000	1405.	0.000	1.000	1405.
$\sqrt{4at}$	10200.			13980.			10980.			15400.			31070.		
time in computation (yrs)	10.			18.8			11.6			22.8			92.8		
Actual time (yrs)	≈ 8.5			15.7			15.7			26.9			96.9		
	equation 20.17						equation 20.37								

Further, the computations for the row of table 20.3 for x = -2 km will be shown. Using (20.18):

$$u = \frac{2000}{13980.} = 0.143 \tag{20.67}$$

Θ can be evaluated using table 20.1*; its value is found to be:

$$\Theta = 0.841 \tag{20.68}$$

which yields a value of y of 1077. m when substituted into equation 20.17.

For times later than t = 18.8 years we must switch to the equation solution 20.37 but must remember to compute u based upon the shifted time scale shown in figure 20.8. For comparison purposes, the shoreline profile is computed for $t_2 = 0.617\ t_1$ - the point at which we change to the new solution in figure 20.8 as well as for the two times asked: 30 and 100 years. Note that these times must also be adjusted for use in the computations; the differential equation time values are listed in table 20.3 as well.

Comparison of the two beach lines for the time at which the accretion starts passing the tip show little significant variation.

Time corrections, based upon the volume of sand displaced by the harbor in our schematized model result in actual times needed to produce a given accretion being shorter than those computed via the solution to the differential equation. The actual times corresponding to the times, t, used in table 20.3 are also listed there.

Examination of the values of y versus x in table 20.3 confirms the statement (equation 20.24) that the accretion is essentially zero a distance $2.5L\ \pi/\phi'$ before the breakwater.

A plot of the accretion on an undistorted scale would be handy for showing the variations in the angle of attack, but impractical in light of the dimensions involved. Figure 20.10 shows the accretion plotted with a y axis distorted by a factor 10.

Examination of figure 20.10 shows dramatically how the accretion proceeds back along the shoreline as well as outward along the breakwater. An interesting but academic question is: what is the limit situation at $t = \infty$? The coast will, of course, ultimately become parallel to the original coast 1405 m seaward of its original location, at least theoretically. Actually, it will be more seaward with only part of the breaker zone being effectively blocked by the breakwater.

* A more complete table of the probability integral was used while compiling this example, however.

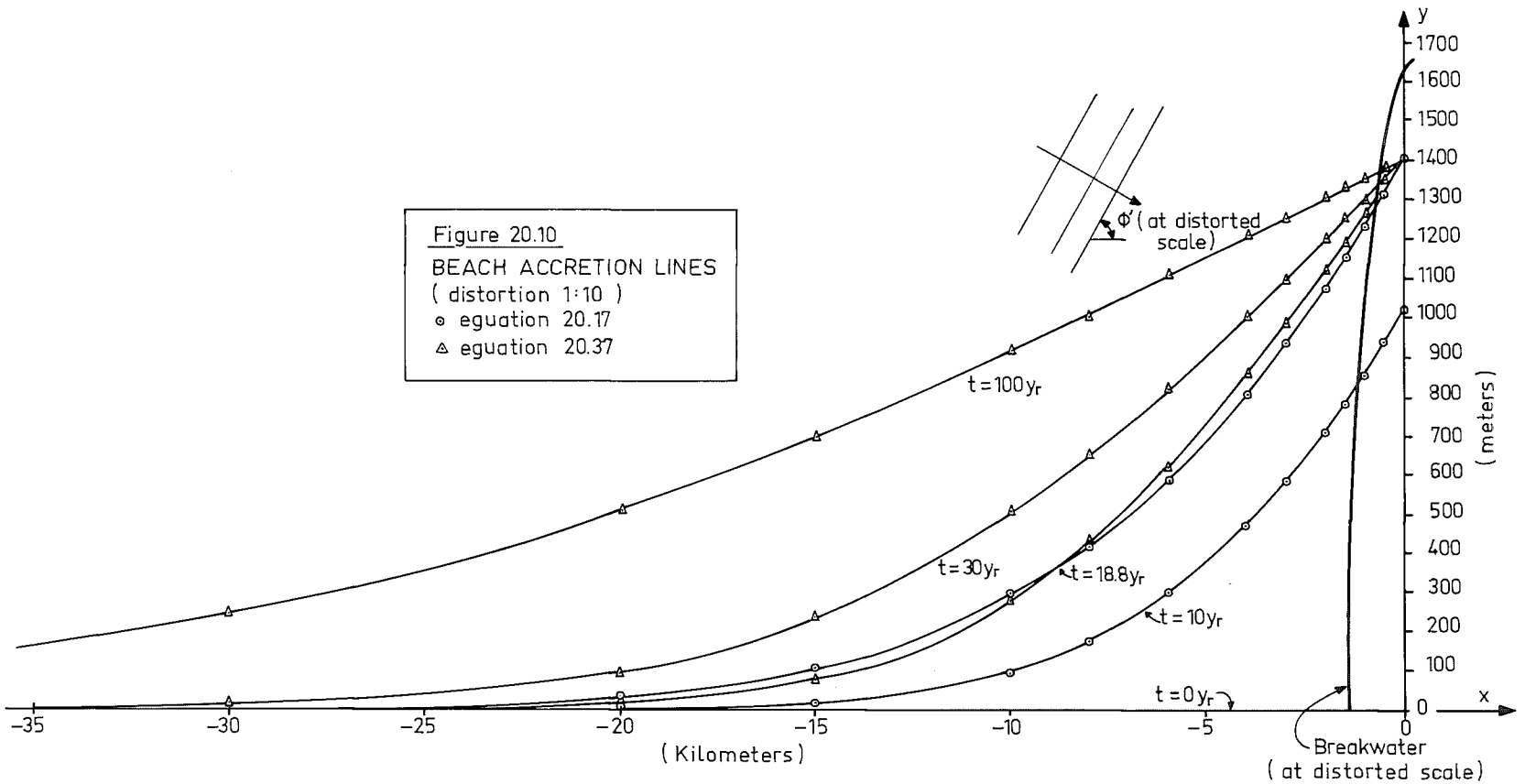
Figure 20.10
BEACH ACCRETION LINES
(distortion 1:10)
⊙ eguation 20.17
△ eguation 20.37
Φ' (at distorted scale)
t = 100 yr
t = 30 yr
t = 18.8 yr
t = 10 yr
t = 0 yr
y
x
1700
1600
1500
1400
1300
1200
1100
1000
900
800
700
600
500
400
300
200
100
0
(meters)
−35
−30
−25
−20
−15
−10
−5
0
(Kilometers)
Breakwater
(at distorted scale)

21. SAND TRANSPORT ALONG A BEACH PROFILE

J. v.d. Graaff

21.1 Introduction

Just as waves can contribute to a sediment movement along a coast, they can also contribute to a sediment movement along a beach profile perpendicular to a coast. As has been indicated already in chapter 18, waves can cause a net sand transport even when no other currents are present and the net mass transport of the waves is zero. This net transport results from a product of a time dependent sediment concentration and a time dependent velocity. Indeed, under some conditions - proper material grain size, for example - a negative - opposite the wave propagation direction - sand transport has been observed even when the long term average velocity has been positive. Of course, if such a resulting current in the direction of wave propagation is made large enough, a positive sand transport will result. Figure 21.1 shows a sample of test results from a laboratory flume in which a current was superimposed on the wave action. Positive sand transports and currents are in the direction of wave propagation. In this example, increasing the current, initially, causes the sand transport to become more negative and later to become positive and increase sharply.

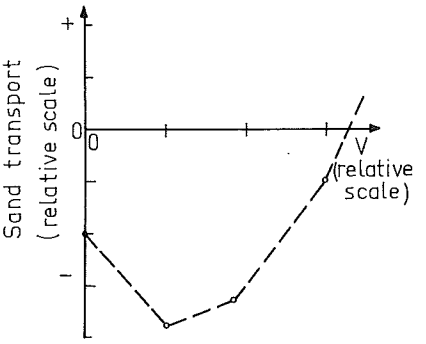

Figure 21.1
INFLUENCE OF CONSTANT CURRENT ON SAND TRANSPORT

The presence of the current paralleling the direction of wave propagation influences the eddy formation near the ripples directly as well as indirectly by influencing the wave length. In another field, this last influence is the basis for the design of air bubble curtain breakwaters - see volume III.

To make matters more complicated, the presence of a longshore current along a beach also influences the sand transport perpendicular to the beach. In light of the development of the longshore sand transport formulas which reflect an interaction of waves and current - chapters 16 and 19 - it is only logical to expect the presence of a longshore current to influence the on and offshore sediment transport caused by waves. If, indeed, the stirring up of bottom material depends upon the total bottom shear stress, as postulated in chapter 19, then the influence of this longshore current on the on and offshore transport is obvious.

Still another variable in the transport of material along a beach profile is the beach slope. It is conceivable that a component of the gravitational force now contributes to the transverse sediment transport. Perhaps even more important, the wave conditions vary from place to place as we proceed across the profile. This introduces even more complications.

Unfortunately, this was an underdeveloped research area until recently. Few model tests and even fewer dependable prototype measurements have been made. The mathematical descriptions available are, therefore, extremely primitive even when compared to the formulations available for longshore transport. Some of these primitive descriptions are presented in the following sections.

21.2 Two dimensional transverse transport

Bakker (1968) examined the transverse sand transport along a coast having groins extending only part way through the breaker zone. After observing that reasonably flat shore areas were built up by material supplied from offshore and steep beach profiles were flattened as material moved offshore, he proposed a simple transverse transport formula based upon the beach slope. He reasoned that for some equilibrium average beach slope, m_e, there would be no transverse sand transport; for other slopes, there would be a transport directly proportional to the difference between the actual and equilibrium slopes. Expressed as a formula:

$$S_y \alpha - (m - m_e) \tag{21.01}$$

where: m is the average beach slope, $\frac{dz}{dy}$,
m_e is the equilibrium beach slope,
S_y is the sand transport per unit width along the beach profile, and
α denotes "is proportional to".

The negative sign in (21.01) follows from the definition of the positive axes resulting in both m and m_e being usually negative while an offshore transport is considered positive in agreement with the positive y axis.

Since Bakker was interested in the sand transport along the beach profile partly blocked by a groin he chose to schematize the coast profile as shown in figure 21.2. In that figure, the point at which the transverse transport rate is desired is denoted by A and is located on the surface between the two schematizing "steps"*. Since the shaded areas are equal this implies that:

$$L_1 = \frac{1}{h_1} \int_{-h_1}^{0} y(z)\, dz \tag{21.02}$$

and

$$L_2 = \frac{1}{h_2} \int_{-h_2}^{-h_1} y(z)\, dz \tag{21.03}$$

where y(z) describes the actual profile.

The slope of this beach near point A can now be characterized by:

$$m = -2 \left(\frac{L_2 - L_1}{h} \right) \tag{21.04}$$

The distance $L_2 - L_1$ corresponding to the equilibrium slope is often referred to by a symbol, W, so that:

$$m_e = -2 \left(\frac{W}{h} \right) \tag{21.05}$$

---

* In Bakker's special case, this point was also the toe point of the groins.

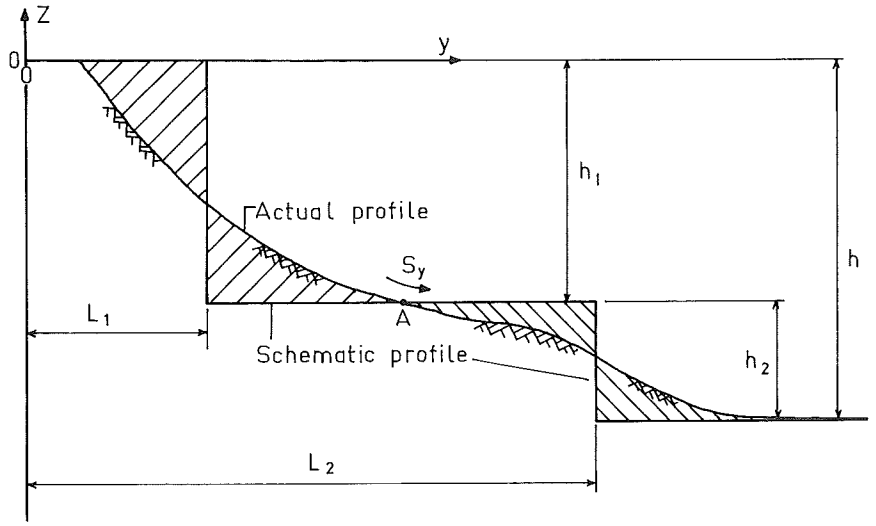

Figure 21.2
SCHEMATIZED BEACH PROFILE FOR TRANSVERSE TRANSPORT AT POINT A.
(hatched areas are equal)

Putting (21.04) and (21.05) into (21.01) and adding a proportionality constant, q_y, yields:

$$S_y = q_y (W - (L_2 - L_1)) \qquad (21.06)$$

This gives an equation of motion which is really much like that used by Pelnard - Considère - equation 20.05* .

The parameters q_y and W in equation 21.06 are both dependent upon many variables including the wave parameters, the sand parameters, and unfortunately, the position of the point A (fig. 21.2) along the beach profile. A dependence of the parameter, W, on the location of point A is obvious because of the relation between this location and the schematized slope. Indeed the slope of a beach is not constant but varies along the profile. The dependance of q_y on the location of A is less obvious but is apparently related to (among other things) the changes in the wave pattern occurring as the waves cross the beach.

Even so, Bakker assumed that the necessary parameters, q_y and W could relatively easily be determined: W from measurements on an existing equilibrium profile and q_y from field measurements.

* This comparison with equation 20.05 is not perfect. s_x in (20.05) represented the derivative of a sand transport with respect to an angle; here, q_y represents a derivative with respect to a distance. Granted, the constant depth, h, assumed makes it possible to interpret this distance as a slope angle.

Swart (1974) attempted to generalize the concept of Bakker (1968) for all locations along the beach profile and to determine values for q_y^* and W in terms of easily measured physical parameters. He carried out a large number of small scale model studies and a few laboratory studies at more-or-less prototype scale. These tests were all carried out with regular waves and erosion was taking place on all the beach profiles; these are serious limitations for the applicability of the results to prototype problems. Swart's results are a large number of emperical relationships involving non-dimensionless parameters.

Even so, there is nothing better available now (1977), and - subject to the restrictions already mentioned, Swart's emperical relations do make it possible to at least estimate transverse sediment transports past any given point on a profile as demonstrated in the following section.

As yet, not enough transverse sediment transport data caused by irregular waves have been collected in order to attempt a correlation with the work by Swart. The question of what characterizing wave best represents an irregular sea in a transverse transport computation has not been answered.

21.3 Example

This example illustrates the computation procedure proposed by Swart (1974) for the determination of the sand transport along the beach profile at a chosen location. The beach profile shown in figure 21.3 is subjected to regular waves approaching with crests parallel to the coast. The deep water wave height is 2.0 m and the wave period is 6.0 s. The beach has an average grain size of 225 μm and the still water level is 1.0 m above MSL as shown in the figure. The sand transport along the profile at point 0 (mean sea level) is desired.

We solve the problem using a two line coastal schematization with the evaluation separating the two zones at Mean Sea Level - the chosen elevation where the tranverse transport is to be determined. Thus, we are looking for S_y determined using an equation like (21.06).

In order to determine the value of $(L_2 - L_1)$, we must first determine the upper and lower limits of Swart's D profile. Using figure 21.4 and entering with:

$$\frac{H_o^{0.488}\, T^{0.93}}{D_{50}^{0.786}} = \frac{2^{0.488}\, 6^{0.93}}{(225\times10^{-6})^{.786}} = 5467 \qquad (21.07)$$

yields (indirectly):

---

* Swart chose his zone boundary more generally and generalized Bakker's q_y calling it s_y.

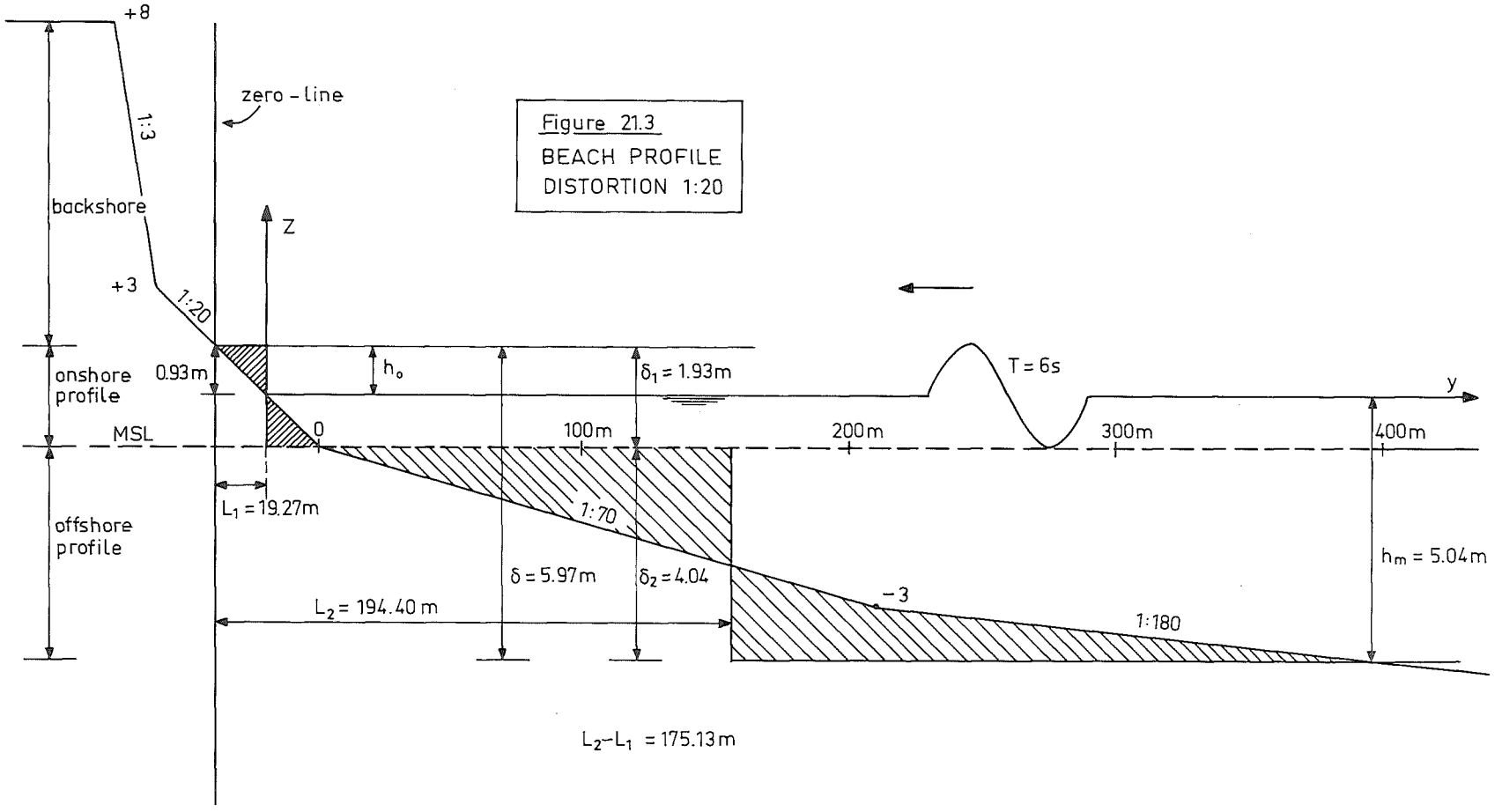

Figure 21.3
BEACH PROFILE
DISTORTION 1:20

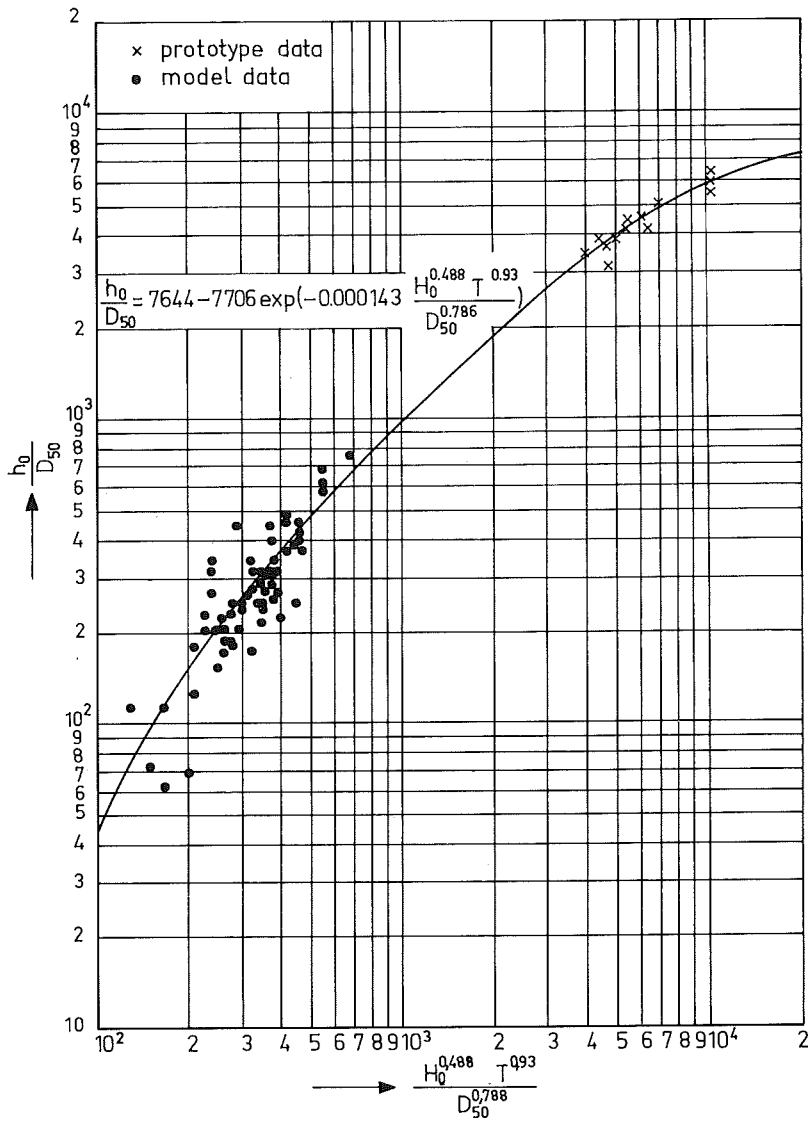

Figure 21.4
UPPER LIMIT OF D-PROFILE
h_0, H_0, D_{50} in m
T in sec.

h_0 = 0.93 m and *(21.08)

δ_1 = 1.93 m **(21.09)

The lower limit of the D profile is found using figure 21.5 entering with:

$$\frac{H_o^{0.473}}{T^{0.894} D_{50}^{0.093}} = \frac{2^{0.473}}{6^{0.894} (225 \times 10^{-6})^{0.093}} = 0.61 \qquad (21.10)$$

---

* The notation used by Swart is reasonably well adhered to in this section even though it is inconsistent with that used in the rest of these volumes. The subscript o here, has nothing to do with deep water, in general.

** Equivalent to h_1 in equation 21.02.

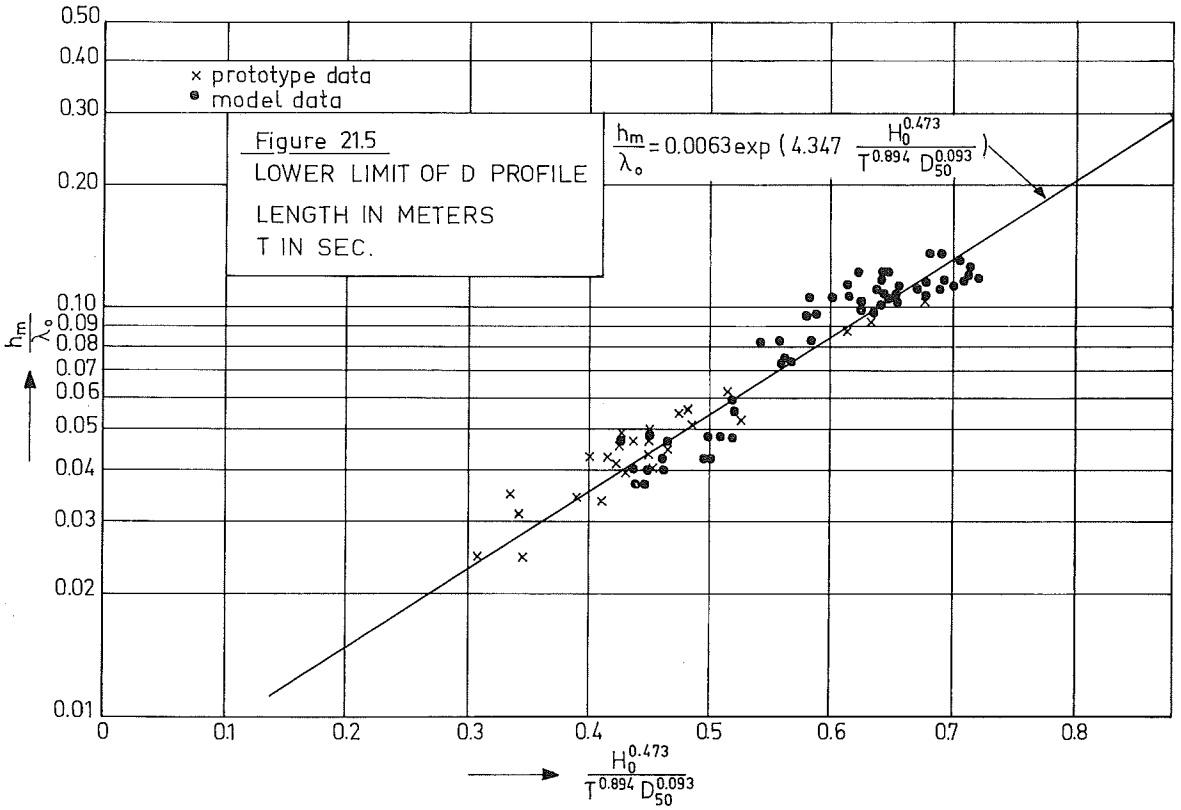

yields:

$$\frac{h_m}{\lambda_o} = 0.090 \qquad (21.11)$$

from which, with:

$$\lambda_o = 1.56\ T^2 = 56.2\ \text{m} \qquad (21.12)$$

$$h_m = 5.04\ \text{m and} \qquad (21.13)$$

$$\delta_2 = 4.04\ \text{m} \qquad (21.14)$$

These limits, then, yield the height of the D profile, δ, of:

$$\delta = \delta_1 + \delta_2 = h_o + h_m = 5.97\ \text{m} \qquad (21.15)$$

These limits are sketched in figure 21.3.

Knowing these limits, the distances L_1 and L_2 to the schematized shore steps can be computed using (21.02) and (21.03). This results in values for these parameters of 19.27 m and 194.40 m respectively. $L_2 - L_1$ is thus:

$$(L_2 - L_1) = 194.40 - 19.27 = 175.13\ \text{m} \qquad (21.16)$$

The following step is to evaluate the corresponding equilibrium distance, W, for the point in question. This cannot be done directly in Swart's method; instead, we determine, first, the W value for the still water level, W_r, using figure 21.6 entering with:

$$\frac{H_o^{0.132}}{\upsilon_{50}^{0.447}} \left(\frac{\lambda_o}{H_o}\right)^{0.717} = \frac{2^{0.132}}{(225\times10^{-6})^{0.447}} \left(\frac{56.2}{2}\right)^{0.717} = 512. \tag{21.17}$$

yields:

$$m_r \frac{H_o}{\lambda_o} = 6.49\times10^{-4} \tag{21.18}$$

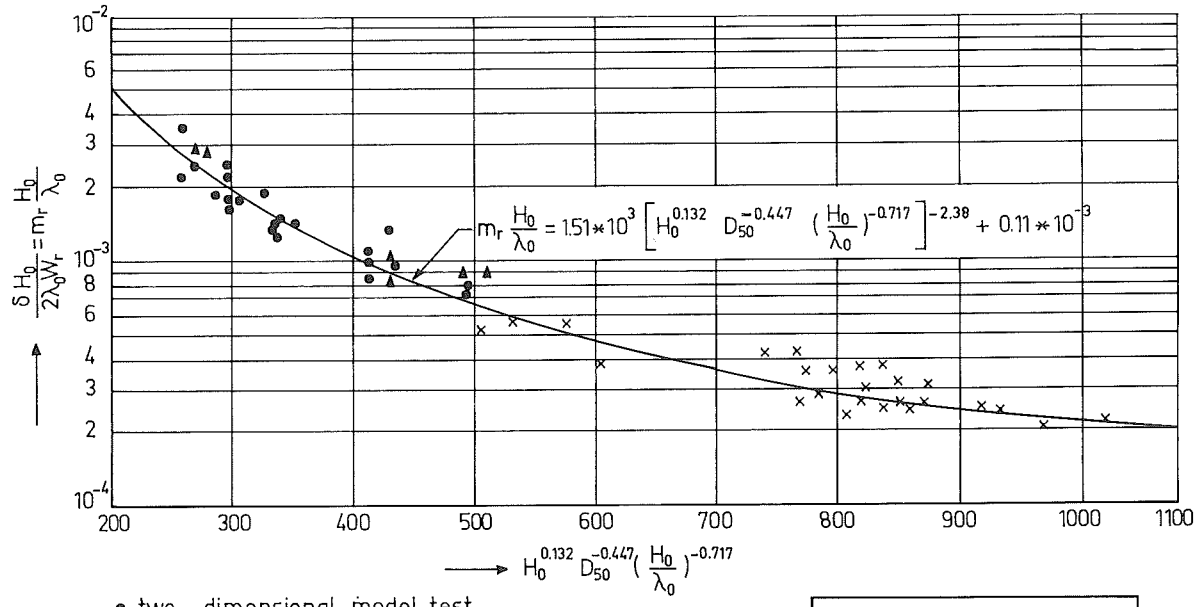

Figure 21.6
HORIZONTAL SCALE OF EQUILIBRIUM PROFILE
(lengths in meters)

from which:

$$W_r = \frac{\delta \quad H_o}{2\ \lambda_o\ 6.49\times10^{-4}} = \frac{(5.97)(2)}{(2)(56.2)(6.49\times10^{-4})} = 163.71 \tag{21.19}$$

is the equilibrium distance for the waterline.

The ratio, $\frac{W}{W_r}$, can be determined using figure 21.7. Here:

$$\Delta r = \frac{h_m - \delta_2}{\delta} = \frac{5.04-4.04}{5.97} = 0.168 \tag{21.20}$$

Then, entering that figure with:

$$\upsilon_{50}\ \Delta r^{0.68\times10^4} D_{50} = 225\times10^{-6}\ (0.168)^{(0.68\times10^4)(225\times10^{-6})}$$
$$= 1.47\times10^{-7} \tag{21.21}$$

(This is effectively zero).
yields:

$$\frac{W}{W_r} - 0.7\,\Delta r = 1.0 \qquad (21.22)$$

which, in turn yields:

$$W = [1 + (0.7)(0.168)]\ 163.71 = 184.35\ m \qquad (21.23)$$

Luckily, this value of W is greater than $(L_2 - L_1)$ indicating that an offshore sand transport can be expected - the only condition for which Swart's method has been checked.

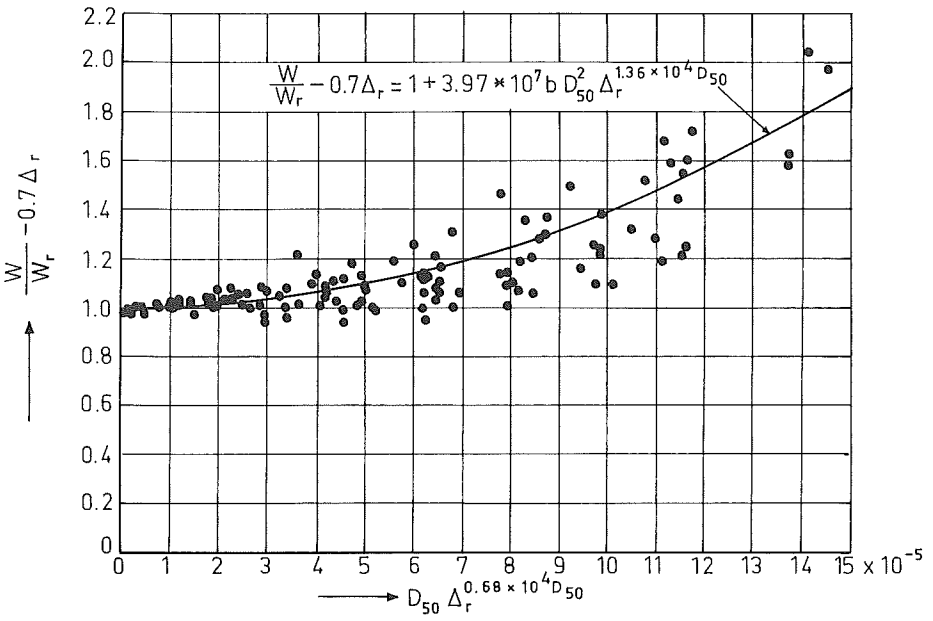

Figure 21.7
GENERAL RELATIONSHIP FOR W/W_r (TWO-DIMENSIONAL CASES)
D_{50} in meters
$b = 1$ for $\Delta_r > 0$
$b = 0$ for $\Delta_r < 0$

We now know values for $(L_2 - L_1)$ and W to substitute into equation 21.06; the only remaining problem is that of determining the value of s_y * for the desired location on the profile. Unfortunately, this value must also be found in a somewhat roundabout way.

---

* Corresponding to q_y in (21.06).

Using figure 21.8 entering with:

$$\left.\begin{aligned} x &= H_o^{1.68} \left(\frac{H_o}{\lambda_o}\right)^{-0.9} D_{50}^{-1.29} \left(\frac{H_o}{h_m}\right)^{2.66} \\ &= 2^{1.68} \left(\frac{2}{56.2}\right)^{-0.9} (225\times10^{-6})^{-1.29} \left(\frac{2}{5.04}\right)^{2.66} \\ &= 2.80\times10^{5} \end{aligned}\right\} \quad (21.24)$$

yields:

$$\frac{s_{ym}\, T}{D_{50}} = 0.972 \quad (21.25)$$

where s_{ym} is the maximum value of s_y occurring on the profile. Equation 21.25 then yields:

$$s_{ym} = (0.972)\,\frac{(225\times10^{-6})}{6} = 3.64\times10^{-5}\ \text{m/s} \quad (21.26)$$

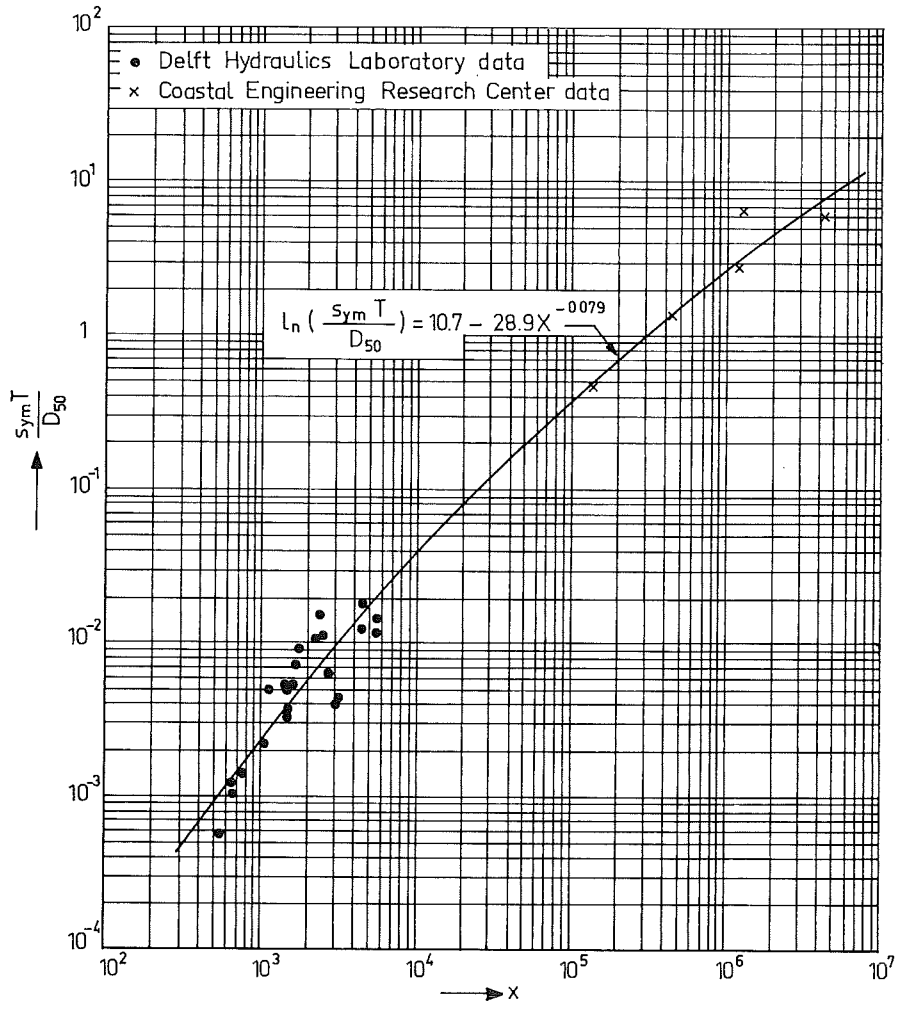

Figure 21.8
MAGNITUDE OF s_{ym}

REMARKS 1) $X = H_0^{1.68} \left(\frac{H_0}{\lambda_0}\right)^{-0.9} D_{50}^{-1.29} \left(\frac{H_0}{h_m}\right)^{2.66}$

2) $H_0, \lambda_0, h_m, D_{50}$ in m

3) T in sec

4) s_{ym} in m/sec

The location on the profile at which this maximum offshore transport takes place can be found using figure 21.9. Entering with:

$$H_o^{-0.55} \left(\frac{H_o}{h_m} \right)^{2.69} = (2)^{-0.55} \left(\frac{2}{5.04} \right)^{2.69} = 0.0568 \qquad (21.27)$$

yields:

$$\frac{\delta_{2m}}{\delta} = 0.737 \qquad (21.28)$$

where δ_{2m} is the δ_2 value at the point where s_{ym} occurs. This value of δ_{2m} turns out to be:

$$\delta_{2m} = (0.737)(5.97) = 4.40 \text{ m} \qquad (21.30)$$

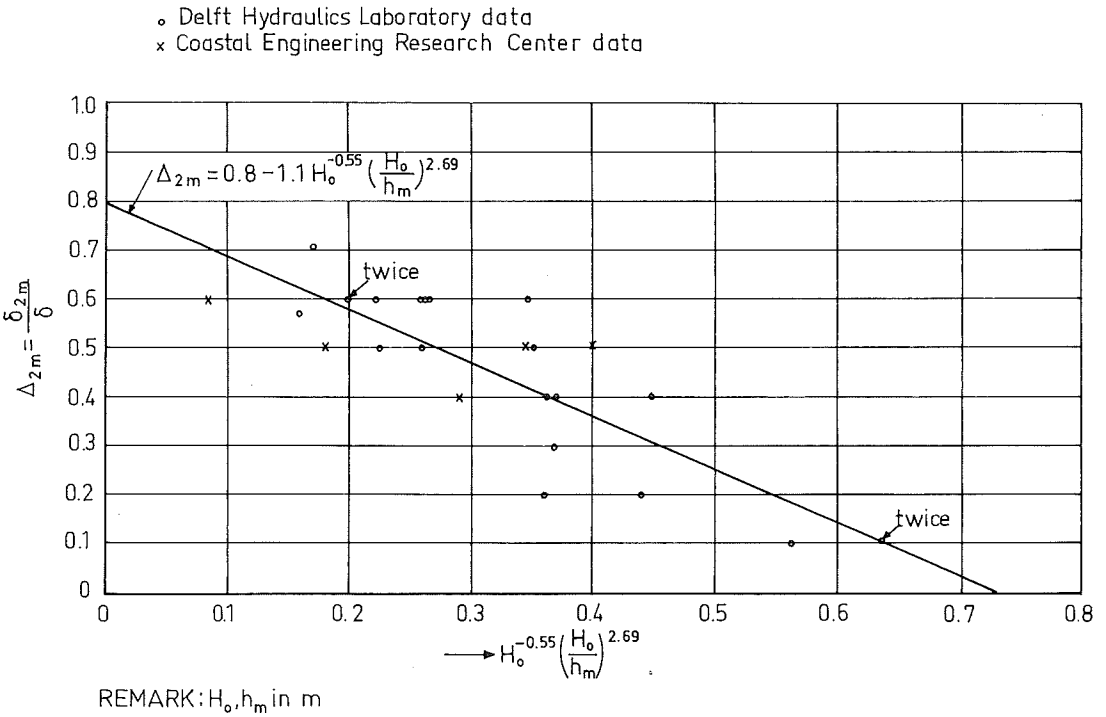

Figure 21.9
POSITION OF s_{ym}

This point is, thus, below the still water level but above (onshore from) the section where we wish to know the sand transport along the profile. ($|\delta_2 - \delta_{2m}| = |4.04 - 4.40| = 0.36$ m above mean sea level - figure 21.3.).

Figure 21.10 relates s_y - the desired value - to the maximum value s_{ym}. Entering with:

$$\left| \frac{\delta_2 - \delta_{2m}}{\delta} \right| \left(\frac{H_o}{h_m} \right)^2 \left(\frac{H_o}{\lambda_o} \right)^{-1} =$$

$$\left| \frac{4.04-4.40}{5.97} \right| \left(\frac{2}{5.04} \right)^2 \left(\frac{2}{56.2} \right)^{-1} = 0.267 \qquad (21.30)$$

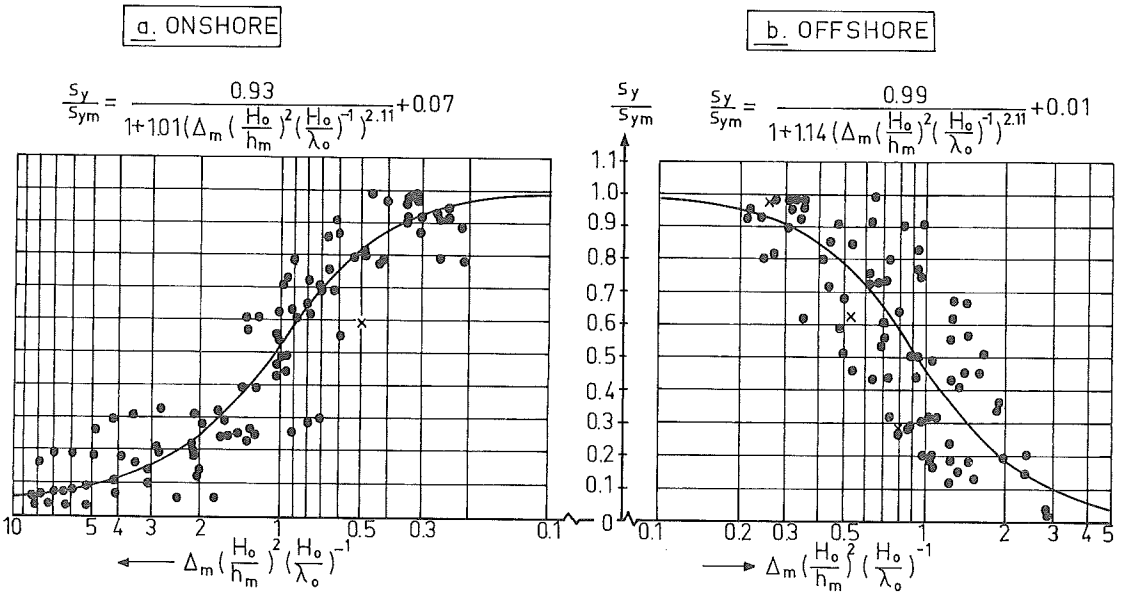

• Delft Hydraulics Laboratory data
× Coastal Engineering Research Center data

REMARKS: 1) H_o, λ_o, h_m in m
2) $\Delta_m = \left|\frac{\delta_2 - \delta_{2m}}{\delta}\right|$

Figure 21.10
DISTRIBUTION OF s_y / s_{ym}

yields, using figure 21.10b (we are offshore from the maximum):

$$\frac{s_y}{s_{ym}} = 0.935 \tag{21.31}$$

or:

$$s_y = (0.935)(3.64\times10^{-5}) = 3.40\times10^{-5} \text{ m/s} \tag{21.32}$$

We can now substitute values into equation 21.06. Using the results (21.16), (21.23), and (21.32):

$$\left.\begin{aligned} S_y &= (3.40\times10^{-5})(184.35 - 175.13) \\ &= 3.14\times10^{-4} \text{ m}^2/\text{s} \end{aligned}\right\} \tag{21.33}$$

or, on an hourly basis:

$$S_y = 1.13 \text{ m}^2/\text{hr}. \tag{21.34}$$

Thus a seaward sand transport of a bit more than one cubic meter per hour can be expected through each meter of coastline at mean sea level. This will not continue indefinitely, of course. The transport of material along the profile will modify the profile and change the parameters involved in this sand transport determination - especially the value $(L_2 - L_1)$.

21.4 Three dimensional transverse transport

When we allow a third dimension - along a coastline - to enter our discussion, we are immediately confronted by many additional resulting currents which further complicate the description of the transverse sand transport. As has already been indicated, longshore currents, whatever their cause - see chapters 12 through 16, will influence the transverse transport. Additional current components, such as rip currents, flowing along the beach profile perpendicular to the shore will obviously also be of direct influence.

A special case of current perpendicular to a coast occurs when a groin interrupts the longshore transport. Water flowing parallel to the coast toward the groin is deflected seaward along the groin. Continuity of the longshore current being re-established beyond the groin will lead to a shoreward current on the lee side of the groin. If this longshore current field normally extends seaward of the obstruction, as a tide current acts over a wide zone along a coast, then the flow around the tip of an obstruction will be more concentrated than would be the case if these longshore currents did not exist in the offshore area.

Unfortunately, the insight into the mechanism and characterizing parameters for these special types of currents is seriously lacking. Bowen (1969) has paid much attention to this problem. The incorporation of these currents in the determination of the transverse sediment transport still involves a lot of work.

Extra Notes

22. COASTAL CHANGES WITH MULTIPLE LINE THEORIES

E.W. Bijker

22.1 Introduction

The limitations of the single line shoreline development equations are numerous; collectively, they amount to too strong a schematization of reality. This can apply to initial and boundary conditions as well as the physical wave and beach characteristics. In particular, Bakker (1968) was concerned about a coast upon which the longshore sand transport is only partially blocked by groins which were shorter than the width of the breaker zone.

Bakker proposed a so-called two line theory for the solution of his problem; it turns out to be a special case of multiple line theories. Instead of schematizing a coastline with a single curve, a number of curves are used as explained in the following sections.

22.2 The schematization

Figure 22.1 shows beach profiles with one, two and three line schematizations. The choice of reference axis for the y distances is, of course arbitrary. The areas of each of the pairs of shaded "triangles" are equal. Each longshore transport S_{xi} is directed parallel to the coast out of the plane of the paper and describe the littoral sand movement in its zone. The horizontal planes are usually selected at elevations which correspond more or less to flat portions of the total profile. If special structures, such as groins, are involved in the schematization, the schematizing horizontal planes are often chosen so that the limits of the boundary conditions correspond to the limits of a transport zone. This is illustrated in the sketch in figure 22.2.

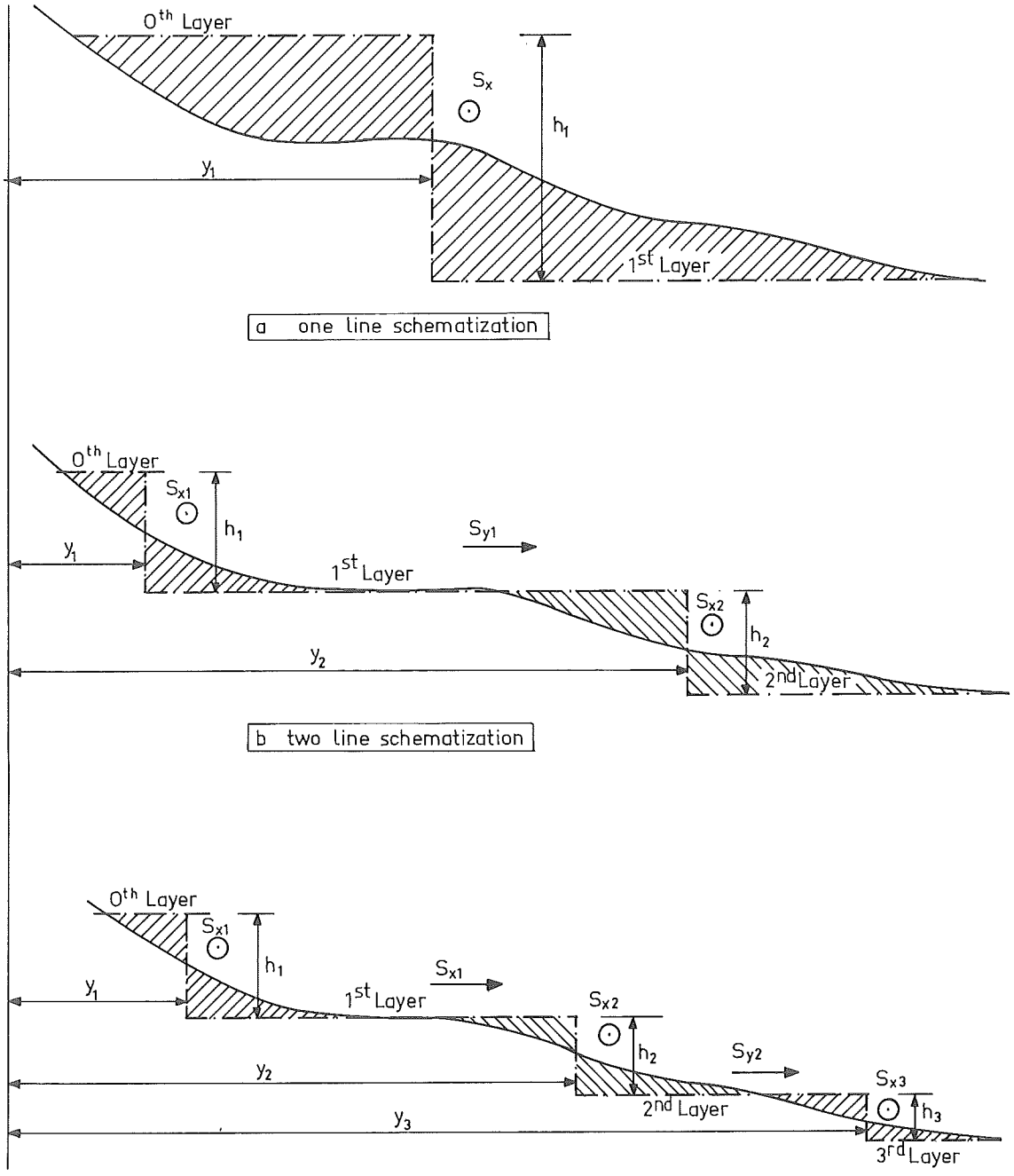

Figure 22.1

BEACH PROFILE WITH SCHEMATIZATIONS
(Pairs of cross hatched areas are equal)

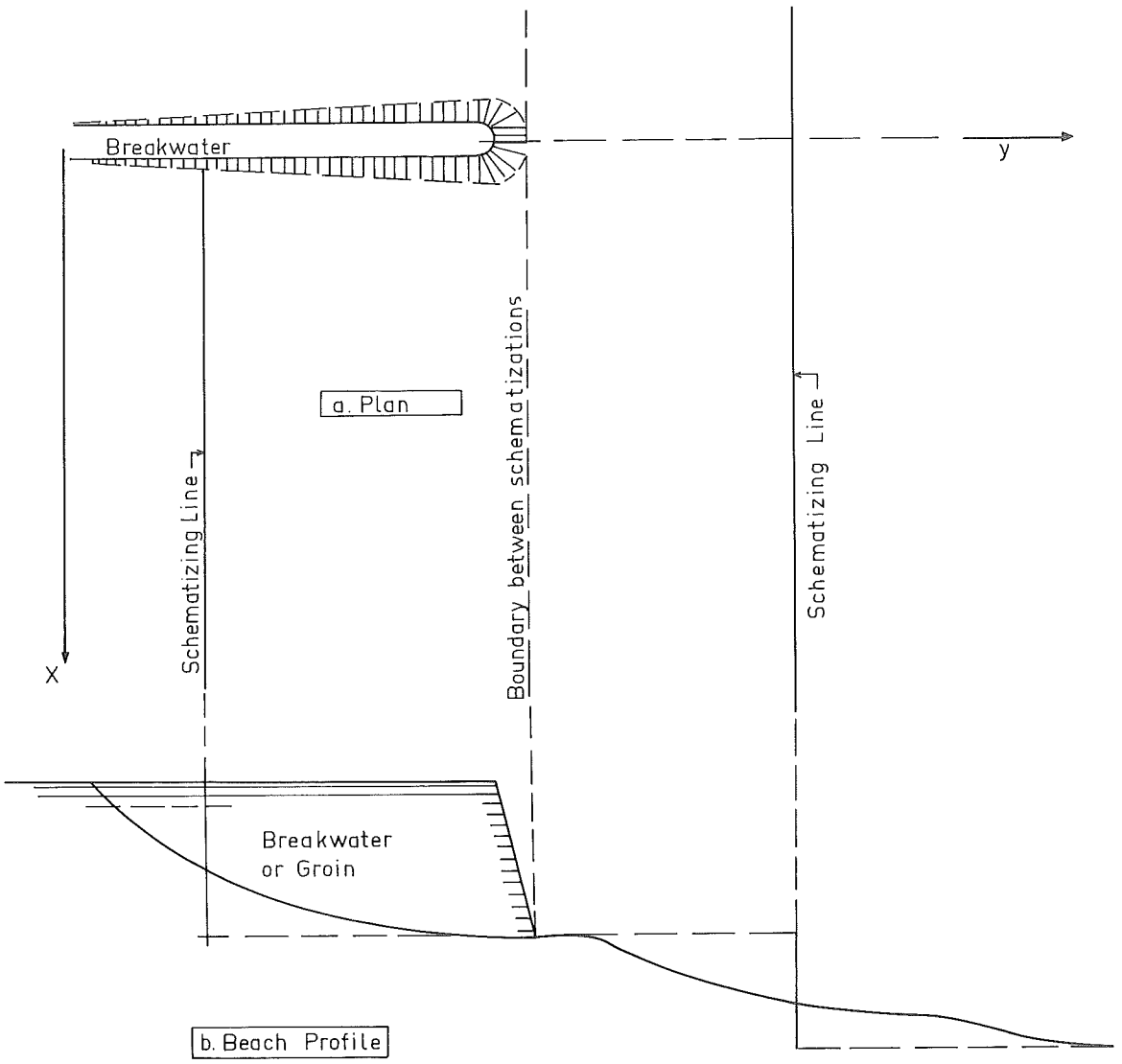

Figure 22.2
SHORE PLAN AND PROFILE
(two line schematization)

22.3 Equations of continuity and motion

Just as with the single - line approximation presented in chapter 20, it will be necessary to develop a continuity relationship and equations of motion for each of the schematization zones.

The equation of continuity is a bit more complex than that for a single line theory since there is now supply and removal of sand from two directions. Figure 22.3 shows an element in plan which can be compared to figure 20.2a. Once again, the net transport of material into the element is equal to the volume retained for each of the N elements - one for each line of the schematization. Thus, for i = 1 to N:

$$S_{xi}\,dt - (S_{xi} + dS_{xi})\,dt + S_{yi-1}\,dxdt - S_{yi}\,dxdt = dxdy\,h_i \quad (22.01)$$

No sand is transported transversely except between the zones so that:

$$S_{yo} = 0$$

$$S_{yN} = 0 \quad (22.02)$$

Figure 22.3
CONTINUITY EQUATION RELATIONSHIPS

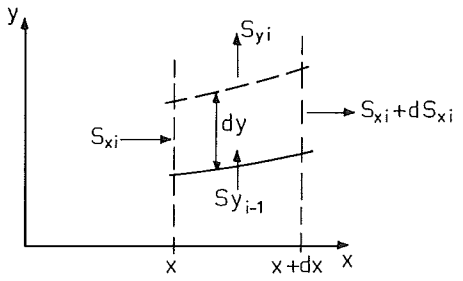

Using (20.02) and (20.03) which are still valid in (22.01), yields:

$$\frac{\partial S_{xi}}{\partial x} - S_{y(i-1)} + S_{yi} + h_i \frac{\partial y}{\partial t} = 0 \quad (22.03)$$

which can be compared to equation 20.04. It should be remembered in the above equations that S_{xi} is the longshore sand transport over the entire zone width, while S_{yi} is a transverse transport per unit length of beach. For N = 1 equation 22.03 degenerates to equation 20.04, Equation 22.03 is the general equation of continuity.

The terms $S_{y(i-1)}$ and S_{yi} in equation 22.03 can be evaluated using an equation such as 21.06 and the methods of the previous chapter. The method of Swart presented there yields, really, an equation of motion along the profile.

The rate of change of sand transport along the coastline, $\frac{\partial S_{xi}}{\partial x}$, can be found by extending the methods of section 20.3. Thus, referring to and extending the results there:

$$\frac{\partial S_{xi}}{\partial x} = \frac{\partial S_{xi}}{\partial \phi_i} \frac{\partial \phi_i}{\partial x} \quad (20.06) \quad (22.04)$$

and:

$$\frac{\partial \phi_i}{\partial x} = -\frac{\partial^2 y_i}{\partial x^2} \quad (20.07) \quad (22.05)$$

where ϕ_i is now the instantaneous angle of approach of the waves at the toe of each zone relative to the schematizing line for that zone. This angle of attack is thus:

$$\phi_i = \phi_i' - \frac{\partial y_i}{\partial x} \quad (22.06)$$

where ϕ_i' is the angle of wave approach at the toe of the ith zone measured relative to the x axis. The depth at this ith toe will be - from figure 22.1:

$$\sum_{n=1}^{i} h_n \qquad (22.07)$$

Obviously, the wave conditions should be evaluated at this same depth. In general, refraction, shoaling, and breaking will all have to be considered.

In practice, values of S_{xi} can be found by determining the longshore sand transport distribution across the beach using, for example, the Bijker method outlined in chapter 19. Integration of the resulting sand transport curve across each of the schematization zones independently yields a set of values for S_{xi}.

The derivative needed, $\frac{\partial S_{xi}}{\partial \phi_i}$, can then be evaluated approximately by evaluating sets of S_{xi} as outlined above for various slightly different values of ϕ_i'. The derivative in question is then approximated by:

$$\frac{\partial S_{xi}}{\partial \phi_i} \approx \frac{\Delta S_{xi}}{\Delta \phi_i'} \qquad (22.08)$$

22.4 Initial and boundary conditions

Just as with a one-line approach, appropriate initial and boundary conditions must be established consistent with the problem to be solved. Each line of the solution of an N line approach will need an initial and two boundary conditions. Further, boundary conditions for the transverse sediment transport must also be established. For example, a common physical boundary condition for the transverse transport is that no sand enters or leaves the schematized beach in the transverse direction; this led, in fact, to equation 22.02*. Since other initial and boundary conditions in the longshore direction look for each line much like those in chapter 20, they will not be elucidated further, here.

An additional advantage of the numerical solutions is that initial conditions can be much more flexible. For example, the initial condition implying that the beach be straight and of constant slope is no longer necessary. Now, the initial condition $y_i(x)\big|_{t=0}$ may describe the actual depth contours. This, of course, makes more realistic solutions possible.

* This boundary condition will be relaxed a bit in chapter 23.

22.5 Solution to the equations

Mathematicians have assured us that under appropriate conditions such as constant values for S_{xi}, S_{yi}, ϕ_i', and W_i and simple initial conditions $y_i(x)$ = constant at t = 0, an analytical solution exists to the equations of motion represented by (22.04) combined with the continuity relationship (22.03). Rather than find and use these analytical solutions, however, it has proven more popular and realistic to develop numerical integration schemes to solve the combination of equations 22.04 and 22.03 directly by approximate time-stepping techniques. The development of digital computer programs for this work is a major research activity within the Coastal Engineering Group at the Delft University of Technology.

22.6 Future developments

Progressing one step further in our numerical approximation, we can subdivide each of the schematizing lines of our beach into blocks along the beach; we are, then, placing a grid on the plan of the beach. - the x, y plane. Usually, these blocks elements will be relatively long (in the x direction) relative to its width. We can now compute wave, current, and sand transport conditions for each of these blocks at the start of the study and compute coastal changes occurring during some time. After some time, changes in either the coastal geometry or - more likely - the offshore wave and current conditions, will make it necessary for the computation parameters for each element to be recomputed. In this way, the development of a coastline and entire beach subjected to given storm conditions can be simulated. Indeed, even the effects of tides and other forces described previously in section 16.6 can also be included.

While all of this sounds very nice in principle, there remain several practical limitations. Continuity of water as well as sand must be provided, and transient situations such as the development of the longshore current on the lee side of a groin must also be accounted for. Perhaps most important, however, there remains an economic question involving the computation costs: "Will the increased accuracy of the solution justify the additional computational effort and cost?".

23. DUNE COASTS

E.W. Bijker
J. v.d. Graaff

23.1 Introduction

Dunes occur natueally in many parts of the world. In their most untamed state they are associated with exposed dry sand being transported by the wind. In this state, they can migrate with the wind, often becoming quite high and sometimes encroaching upon and disrupting the works of man. They have been known, for example, to cover highways and railroads and to destroy productive agricultural land - see figure 23.1.

Figure 23.1
DUNES ENCROACHING ON HIGHWAY
CAPE COD, U.S.A

While dunes occur throughout the world, they are actually quite frequent along coasts. The shore of The Netherlands is a splendid example of coastal dunes. They can also be found in many other parts of the world portions of the coast of Ghana, parts of the Oregon coast in the United States (volume I figures 25.4, 29.9 and 29.10, and figures 23.2 and 23.3 in this volume). The remains of an old transatlantic cable can be seen in the lower right in figure 23.3c. Isolated sand dunes are present along the mud coast of Suriname - Allersma (1968). Because of their height (usually), and thus volume of stored sand, coastal dunes can be utilized, where present, in a coastal protection scheme for the benefit of man. The remainder of this chapter will be devoted to the dynamics of a dune-protected coast such as is found in The Netherlands.

Figure 23.2
AERIAL PHOTO OF DUNE COAST
SANDY NECK, CAPE COD, U.S.A.

23.2 Dune formation

Two basic components are needed to form coastal dunes: a reasonably continuous, slow supply of sand, and a wind blowing at least somewhat toward the shore.

The sand is usually supplied by the sea - the waves - in one of two ways; either by transverse transport from deeper water or by accretion of a beach caused by a decreasing longshore sand transport along a coast. The first of these transport mechanisms is driven by the small net shoreward mass transport near the bottom in waves *outside* the breaker zone. (This is in *contrast* to the discussion of transverse mass transport *within* the breaker zone presented in section 11.5) Longuet Higgins (1953), Bijker, et al (1975) and Battjes (1976) discuss this mass transport in more detail. This is one of the predominant supplies of sand for the Dutch coast. These dunes generally grow slowly but rather steadily.

The second means of sand supply, a decreasing longshore transport, is a more obvious source of sand for dune buildup. Such a supply nourishes the dunes near the end of Cape Cod in The United States - see figure 23.1. Much more rapid dune growth can take place because of the larger supply.

a. ACCRETING DUNE COAST

b. STABLE DUNE COAST

c. ERODING DUNE COAST

Figure 23.3
THREE TYPES OF DUNES
CAPE COD, U.S.A

With either source of supply, the sand must become dry so that the wind can more easily pick it up for transport. (Wet, unsaturated sand has a fictive cohesion caused by the surface tension of the intergranular water. This surface tension can only be overcome by relatively strong winds). Tidal action can be sufficient to allow an upper layer of sand near the high tide line to dry and be transported by the wind. If the sea water is extremely saline the salts left behind as the water evaporates can be sufficient to cement the sand grains together so that they cannot be disturbed by the wind. Such a salt-cemented sand layer is often called caliche, but is not often found on the shores of the major oceans.

Figure 23.4 shows a sumewhat schematized cross-section of a dune-protected coast often found in The Netherlands. It compares well to that in volume I figure 25.1. The dry backshore tends to make the dunes appear to be very independent of the rest of the coast even though they are not. Except during storms, changes occur slowly, almost imperceptibly except to expert observers.

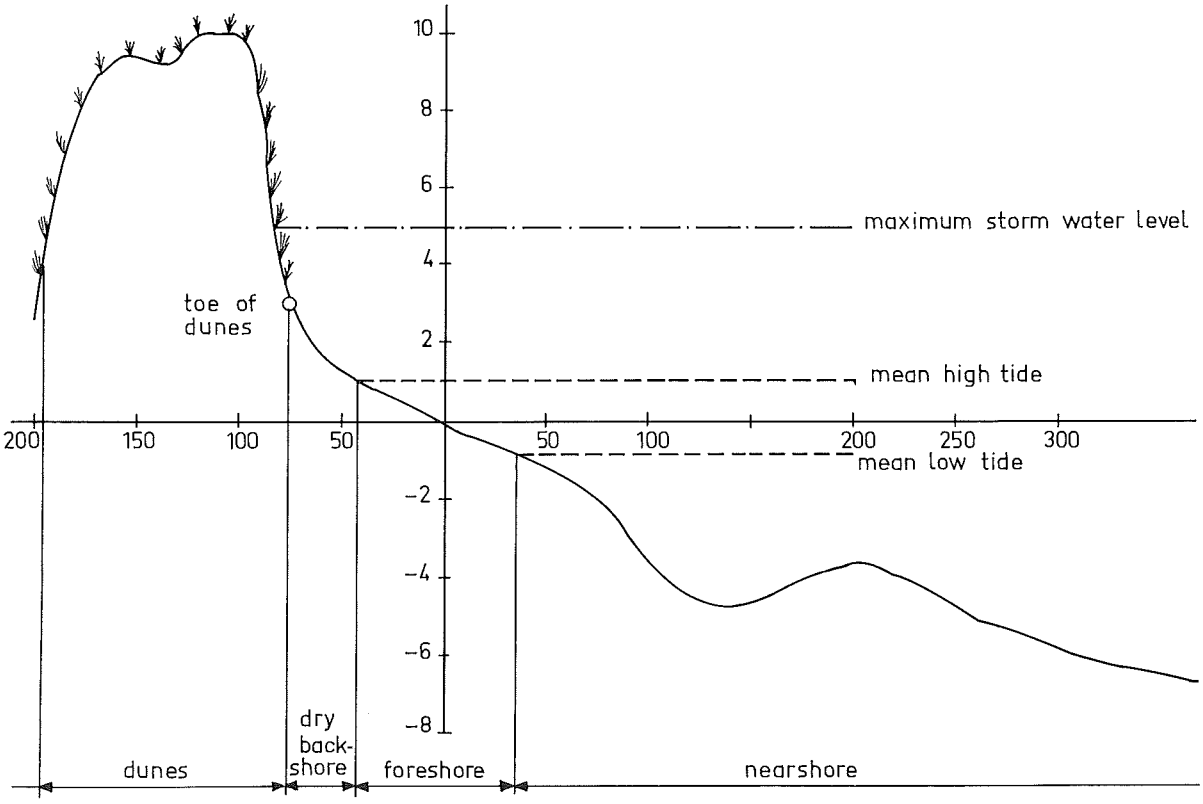

Figure 23.4
DUNE COAST PROFILE
(scale as shown)

This section has described how dunes are formed and nourished. A section in the following chapter will describe how dune forms can be modified for the benefit of man. The build-up process of a dune coast may, however, be interrupted from time to time by erosion. It is even possible that a dune coast is being more or less steadily eroded even though sand is also being supplied naturally from offshore. The condition necessary for this is that the erosion caused by an increasing longshore transport capacity more that offsets the supply of sand in the transverse direction. The following two sections will describe long and short term dune coastal changes based largely upon experience in The Netherlands.

23.3 Short term dune dynamics

During severe storms considerably higher water levels can be expected than under normal conditions*. Under superstorm conditions, as shown in figure 23.4, the dunes, themselves, are subjected to direct attack by the sea. Sand will be eroded from the dunes and transported primarily in the transverse direction - toward the sea along the beach profile. While there may, indeed, be a significant simultaneous longshore transport, this will not be of too much concern, especially if the conditions along the coast do not vary much from place to place and since the storm duration is relatively short. Even so, the changes in the coast profile can be spectacular during the short duration of a severe storm.

Even during the historic storm and flood of January-February 1953 in The Netherlands the damage to the dunes was not severe. In this storm which had an average frequency of intensity of about 1 into 250 years, most dune erosion amounted to about 100 m^3 of sand per meter beach length. This translates into a recession of the dune toe of a distance in the order of 20 to 30 meters.

Considerably more severe conditions for the Dutch coast can be conceived. There is, in fact, no limiting case; the probability of occurrance only becomes extremely small. The erosion of the dunes would likewise be much more severe. Indeed, most of the dune - protected areas of the Dutch coast can stand an erosion of more than 500 m^3 of sand per meter coastline and still prevent flooding of the hinterland. Unfortunately, a few portions of the coastline do not have such a generous reserve of sand in the dunes.

An extremely important question is, then, "How severe a storm can a given dune coast endure and not fail?" Many studies of this have been carried out in The Netherlands and studies are continuing. Some conclusions based upon both model and prototype studies complete this section.

---

* The extent of such a water level increase is dependent upon many factors. The Dutch coast is especially susceptible to such water level increases.

Since the transverse sediment transport dominates the coastal transport picture during dune erosion, the principle of continuity dictates that the sand eroded from the dunes must remain somewhere along the beach profile. Measurement made along the Dutch coast shortly before and soon after the storm in 1953 indicated that large portions of the coast had developed a so-called storm profile extending from the storm flood level to a depth more of less corresponding to the outer edge of the breaker zone. The profile was found to fit the emperical relationship:

$$z = -0.415\sqrt{y + 4.5} + 0.88 \qquad (23.01)$$

where y and z are defined in the usual way and are shown along with a profile in figure 23.5. Note that equation 23.01 is *not dimensionless* - metric units were used in its determination. This equation is published in an anonymous report by the Ministry of Public Works (1972) and is valid only for the profile below the still water level. Figure 23.5 shows such a profile. Continuity of sand dictates that the area of erosion equal the area of accretion in the figure.

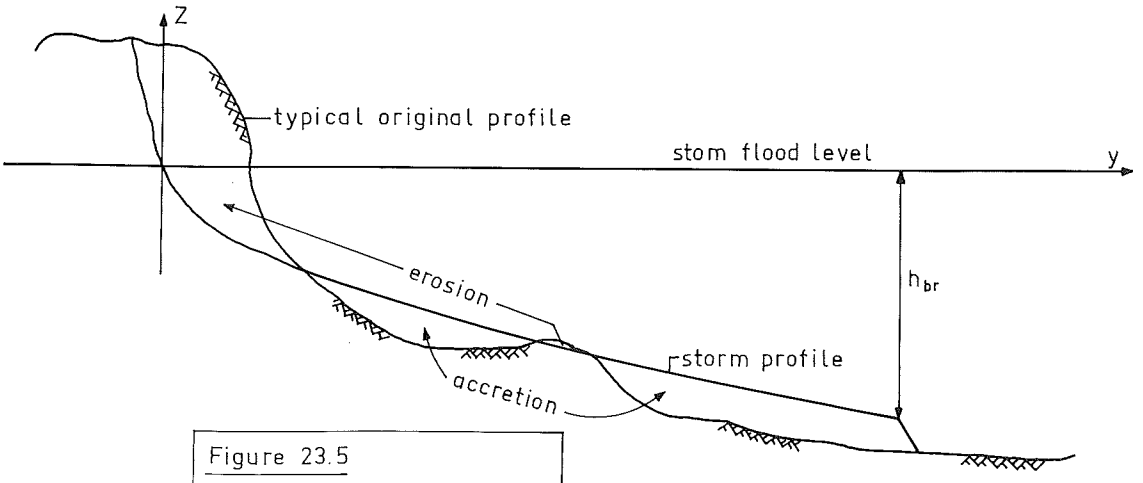

Figure 23.5
STORM PROFILE BY SWART
(distortion 1:25)

Unfortunately, no-one was brave enough to carry out measurements during the 1953 storm on the coast; we do not know, therefore, how the storm profile in figure 23.5 developed as a function of time. If the storm flood level is assumed to have been reached instantly and then maintained for some time during which the dune erosion takes place, then we can conclude from figure 23.5 that the breaker zone has become much wider during the erosion process. Further, since the storm beach profile is related to the storm flood still water level, the total quantity of dune material eroded is strongly dependent upon this storm level. The duration of the storm seems relatively less important; once the storm profile shown in figure 23.5 has been developed, further changes occur slowly unless the water level or wave height continues to increase. Emperical relationships have been developed, therefore, to predict dune erosion based upon the storm flood

level. Unfortunately, the large number of limiting assumptions involved in the method makes it more qualitative than quantitative in practice. Since the publication of the above mentioned work, further model studies carried out in the Delft Hydraulics Laboratory indicate that the computation may be a bit conservative - that less material will be eroded than is predicted.

Indeed, before further research has been completed we present here only the few rather qualitative results listed below, rather than the full set of emperical relations.

As stated above, the actual storm flood level is very important for the determination of the ultimate dune erosion. A small increase level can result in a large increase in erosion.

Relatively high dunes supply more sand for each meter of coastline erosion. The resulting coastline recession will be less, but the actual total volume of sand eroded will be more for a higher dune. This can be visualized by moving the storm profile to the right slightly in figure 23.5; the accretion volume increases rapidly. High dunes will minimize the coastal recession; low dunes will minimize the volume of eroded sand. This relation can be useful when artificially stimulating dune formation so that an optimum dune form can be approached.

A second storm occurring soon after an initial storm of equal intensity will cause relatively little additional damage to the dunes. Transverse sand transports of only 10 to 20 percent of that in the first storm have been experienced under the above conditions in The Netherlands.

Relatively severe storms, such as that in The Netherlands in 1953, do not move the dune sand very far; most of it remains within the breaker zone.

Dunes which are otherwise stable will be built up again over the succeeding years. This process is slow relative to the erosion in the storm, but recovery still only takes, at most a few years.

Usually the highest portion of a storm flood is of relatively limited duration. A major portion of the dune erosion takes place in that few hours, however. This in shown in figure 23.6.

23.4 Long term dune dynamics

A row of dunes protecting a coast needs to be stable over a period of years or decades in addition to being able to survive a severe storm. Slow but persistent coastal changes - especially erosion - must be determined and necessary allowances for these less spectacular but continuous processes must be made.

Since the dunes are so important to the coastal protection of The Netherlands, these slow changes in the dunes positions have been carefully followed for decades. Figure 23.7 shows the ten year average displacements of the toe of the dunes at four places along the Dutch coast during a bit more than a century. Only relative changes are shown in that figure; the zero point of the distance scale is quite arbitrary.

Figure 23.6
EFFECT OF STORM ON DUTCH COAST

Figure 23.7a, measured 10 km south of Den Helder shows a consistent erosion of about 1.3 m per year, while 31 km further south - figure 23.7b - the dunes have remained very stable. Near Bloemeldaal, 62 km south of Den Helder the dunes are accreting about 0.6 m per year - figure 23.7c. Just north of Scheveningen - figure 23.7d - an initial slow accretion became an erosion of about 1.4 m/year after about 1900. This is interesting in light of the fact that shore protection works - a seawall and groins - were built at Scheveningen around the turn of the century. The measurement point shown in the figure is about 2 km north of the end of those works.

Figure 23.8 shows the movement of the entire coastal region during one century. The letters a through d on the horizontal axis show the locations of the graphs in figure 23.7.

In contrast to the cause of dune erosion during storms, the coastal changes just described are caused primarily by longshore sediment movements. These coastal changes, then, imply a gradient in the longshore transport capacity along the coast. An accretion, obviously, results from a declining transport capacity; erosion implies an increasing longshore transport capacity. The changes just described in figures 23.7 and 23.8 for the toe of the dunes are typical, also, of the entire beach profile. If we assume that that total profile including the dunes is about 20 m high, then a beach and dune change of 1 m per year implies a gradient in the longshore transport capacity of about 20 000 cubic meters per year per kilometer. When this extends over a considerable distance a very large volume of sand can be involved. In 40 kilometers, for example, 1 m/year erosion implies an *increase* in sediment transport capacity of 800 000 m^3/year!

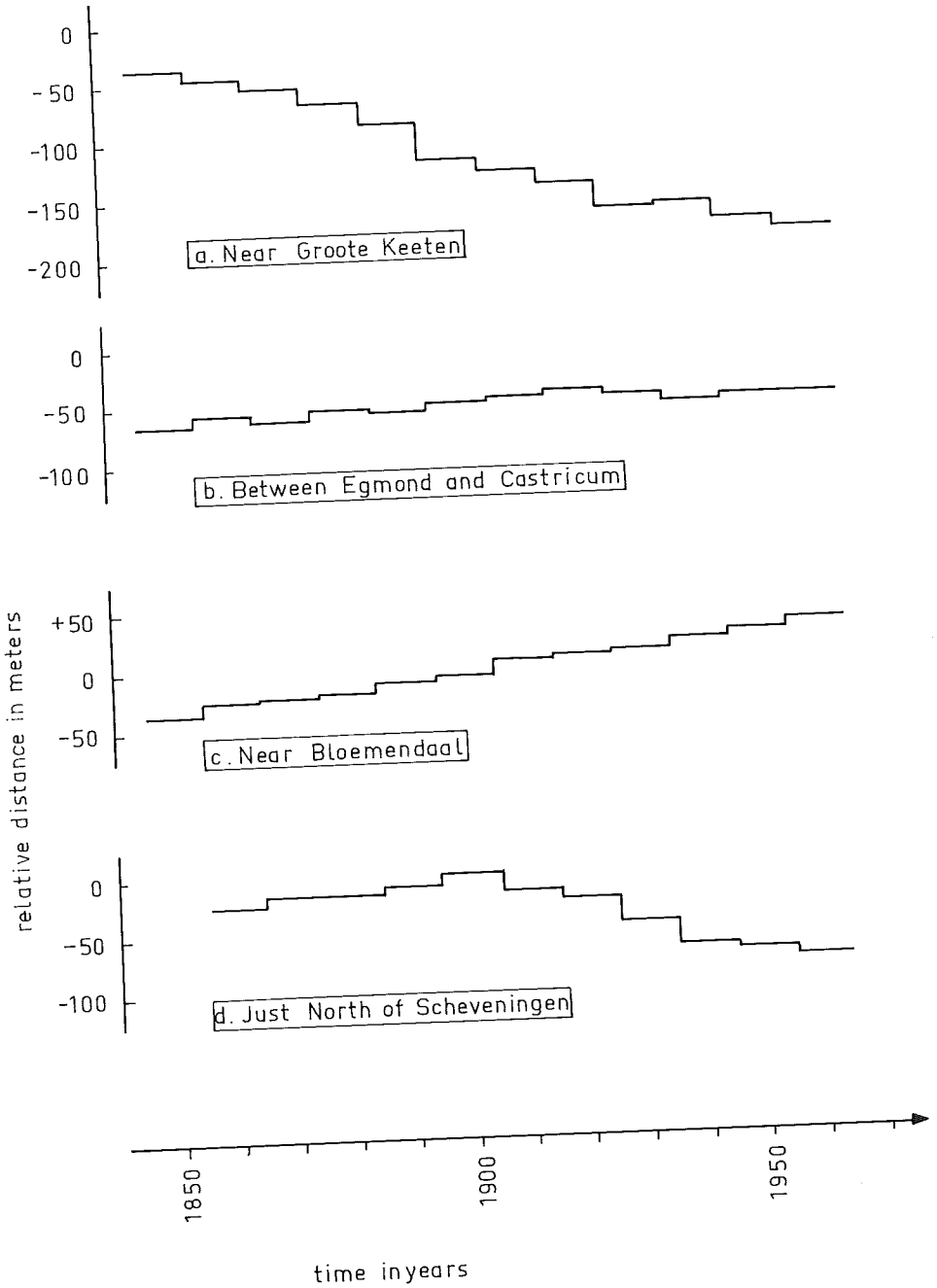

Figure 23.7
DUNE CHANGES AT 4 POINTS ON DUTCH COAST

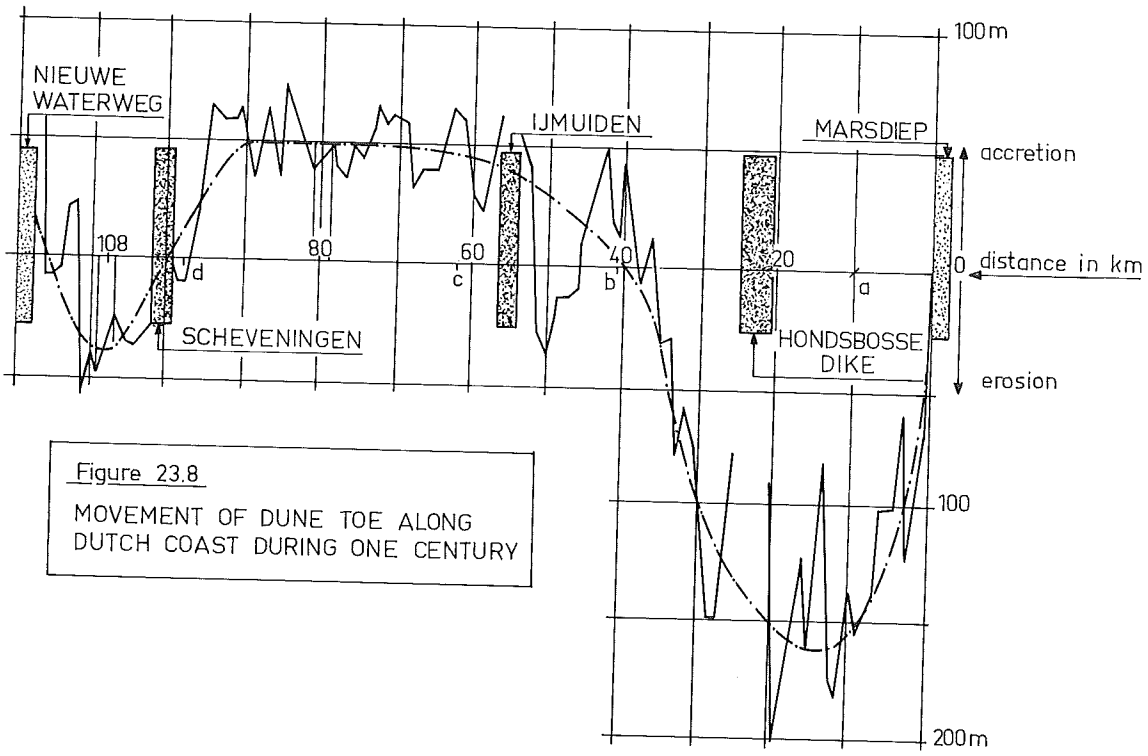

Figure 23.8
MOVEMENT OF DUNE TOE ALONG DUTCH COAST DURING ONE CENTURY

Erosion, especially, is of great importance for the long-term safety of a dune-protected coast. While we cannot always explain the reason for a slow coastal change or predict its magnitude exactly, it would seem logical, therefore, to attempt to determine existing tendencies, extrapolate them and attempt to cope with the eventual consequences. Often times, a further erosion, predicted sufficiently in advance, is no great problem; shoreline development can be planned with the possible coastal changes in mind. Problems become more difficult and often more emotional when it is too late to plan for natural coastal changes. Artificial shore protection works are then the most often considered solution. There is an alternative, however; abandonment of the area. This second alternative may be more economical on the long term in some situations.

Shore protection works will be discussed in depth in the following chapter. First, however, we conclude this chapter with a discussion of how to predict changes on dune-protected coasts.

23.5 Analysis method

The discussion in the previous sections of this chapter has been limited to the dune behavior at a single cross-section. Now, using an extension of the multiple line method of the previous chapter, we shall indicate how an entire dune coast might be analyzed.

Since the multiple line method involves both longshore and transverse sediment movement, it may be used succesfully either for long-term or short-term analysis. It may, however, be a bit combersome for a short-term analysis if the coastal morphology is dominated, then, by transverse transport.

The modification of the multiple line model method involves allowing sand to be added to the beach from the dunes. (We may remember from chapter 22 equations 22.02 that no sand was allowd to enter or leave the breaker zone in the transverse direction). We can now allow sand to enter the longshore transport zone nearest the dunes by removing the restriction that S_{yo} always be zero. This boundary condition must, however, be replaced by some feasable description of the dune modification process. This can, of course, be done based upon a slope just as with all of the other transverse transports*.
There are however, two important differences:
First, the dunes tend to "cave in" during erosion depositing a rather large volume of sand on the upper beach all at once. Our simulation model must do this, too. This can be done by stipulating, for example, that a given volume of sand be deposited upon the upper beach whenever the "slope" of the dunes becomes too great. This volume of sand can be related to the sand properties and dune height by an approximate slip circle analysis so familiar to foundation engineers. This yields an abrupt sand supply in contrast to Swart's concept.

The second problem, is that sand transport from the beach to the dunes is caused by an entirely different (and independent) phenomona, the wind. While a continuous type of transport function might be appropriate, too little is known about dune accretion to determine the necessary parameters for sand transport toward the dunes.

Studying an eroding coast, therefore, with a slip circle type of dune supply yields a mathematical description of S_{yo} with a special form. Extrapolating the notation of chapter 21, equation 21.06:

$$\text{If} \quad (W - (L_1 - L_o)) < 0$$
$$\text{then} \quad S_{yo} = 0 \tag{23.02}$$

$$\text{and if } (W - (L_1 - L_o)) > 0$$
$$\text{then} \quad S_{yo} = S_{dune} \tag{23.03}$$

where W_o is a distance corresponding to a "just stable" dune slope,
L_o is a distance characterizing the dune, and
S_{dune} is the volume of sand deposited on the upper beach during a single time interval via a "cave-in".

Since S_{dune} will normally be large, the upper (first) zone of the beach will "spring forward" as a result of the supply from the dunes. This will automatically restore the status (23.02) and initiate increased transverse transport to zones in deeper water. In a calm weather period during which sand supply from the beach rebuilds the dunes, a more continuous type of sand transport function - more like equation 21.06 - should be used instead of (23.02) and (23.03).

---

* Swart (1974) used this approach. It yields a continuous sand supply function.

Extra Notes

24. SHORE PROTECTION WORKS

E.W. Bijker
J. v.d. Graaff
W.W. Massie

24.1 Introduction

This chapter is concerned primarily with the various ways in which man can influence the natural processes occurring along a beach. The emphasis here will be on the morphological consequences of the various man-made changes rather than on the construction details of the structures themselves. This latter aspect, in general, belongs more to the field of hydraulic structures than to coastal engineering.

The principles of the morphological consequences of various man-made coastal changes are discussed in the following sections. Not suprisingly, most man-made changes involve beaches that are eroding. Indeed, accreting coasts seldom present problems.

24.2 Sand supply

Probably the simplest and most dependable means of maintaining an eroding beach is to supply sand to that beach from other sources; several methods are available.

The most straightforward seeming method is to move sand to a point shoreward of the breaker line via a dredging operation. Since the sand is to be discharged either into shallow water or upon the dry beach some form of hydraulic suction dredge capable of discharging through a pipeline seems most efficient - see volume I chapter 16. Sometimes, the sand supplied can come from a local excavation project carried out for another purpose; dredging to construct or enlarge a harbor is an excellent example of this. In this case the cost of the beach nourishment will probably be minimal since, at most, there will be only an extra cost for a possible longer pipeline.

Another source of supply often used is to dredge sand from a nearby accreting beach. (Oftentimes, erosion of one beach is accompanied by accretion of another local beach). Accretion and erosion on the two sides of a harbor entrance is an example of this. In the past, permanent fixed structures with dredging equipment mounted on them have been built on the accreting beach within the breaker zone to pick up sand moving along the beach and pump it to the eroding beach more or less continuously. At least one such sand by-passing installation is described in volume I of the *Shore Protection Manual*. Unfurtunately, such installations are often less than complete successes. They may not be properly located to obtain a sufficient supply of sand while a severe storm may cause them to "drown" in sand so that they can no longer operate. The discharge pipe from such an installation must often be permanently installed across a harbor entrance; the resulting submerged pipeline - a sort of U tube - can become plugged with sand in the event of an abrupt pumping failure with the discharge pipeline filled with sand-water mixture. Also, such fixed installations tie up quite a bit of investment capital for a single purpose.

It is often more economical and succesful, therefore, to move the sand using more conventional floating dredgers. These can then be utilized intermittently for by-passing while possibly doing other work at other times. It is not essential that the sand be picked up within the normal (calm weather) breakerzone. If a floating dredge makes either a deep pit or a trench parallel to the coast near but outside the calm weather breaker zone, sand will move to this pit as a result of the transverse sand transport along the beach profile. A multiple line transport theory may be used to study such a transport problem. If the pit is dredged more or less continuously, a solution boundary condition is that the coastal geometry at the pit does not change - any sand entering the pit area simply disappears. Likewise, a multiple line model can be used to simulate the behavior of the sand supplied to the eroding beach. If the necessary coefficients can be determined, it is possible via such a simulation to experiment by trial and error with various pick-up and discharge points in order to select the most favorable locations for these.

When no sand is available either on a beach or as part of other dredging operations, it is sometimes possible to dredge sand well offshore. The site must be selected far enough from the coast (usually a few nautical miles) so that the beach processes are not further affected. Often, the sand is dredged with trailing suction hopper dredges over a relatively large area so as to limit the effect on the offshore bathymetry. On the other hand, such a widespread dredging may increase the effect on the local fishery industry.

A disadvantage of any of the sand supply methods listed above is their long term character. Sand will have to be supplied at regular intervals effectively forever. While the initial capital investment can be very low, it may, conceivably, cost more total money in the long run.

Sand can also be supplied overland. While overland transport of sand can be prohibitively expensive on a continuous basis for supplying a slowly eroding beach, it can prove to be economical for the reinforcement of a dune-protected coast. Moving sand around on the dunes can, for example, lower and broaden their profile in order to make them more durable and minimize the possible future sand loss. Raising the dune crests by moving sand forward may be necessary, on the other hand, if the total coastline recession must be minimized - see chapter 23. Obviously, these measures are aimed only at a short-term beach improvement; it is usually too expensive on a long-term basis.

If the dunes along a coast are still slowly being built up by wind-blown sand, construction of wind breaks or the planting of various grasses can be successful in stimulating the dunes to take on or retain a desired form. Volume I of the *Shore Protection Manual* describes several types of dune protection and stimulation. Such protection methods may even be needed on an accreting shore in order to prevent the wind from transporting the sand inland from the beach where it could cause significant problems for other works of man such as agricultural lands or highways.

A distinct and very real advantage of all of the above beach nourishment schemes is inherent in beach nourishment itself; the operation is most like that of nature and the consequences of the operation for other nearby portions of the coast is probably the least of all the possible protection methods. The significance of this last remark will become more obvious later in this chapter.

24.3 Groins

Groins can prove to be very effective for stabilizing a coast being eroded as a result of a positive longshore sand transport gradient. The groins must extend entirely across the breaker zone with crests above the still water level to be completely effective. usually, however, only partial interruption of the longshore sediment transport is needed to acnieve beach stability; lower and shorter groins will then be acceptable. The groins at Scheveningen, The Netherlands, are of this latter type. During a severe storm there in January 1976 - figure 24.1 - the groins were completely submerged.

Figure 24.1
NORTH SEA STORM
SCHEVENINGEN, THE NETHERLANDS
JANUARY 1976.

The spacing of groins in conjunction with their height and length and the wave approach direction is also important for their effectiveness. Since the shore between the groins will orient itself more or less parallel to the approaching wave crests, beaches already subjected to nearly parallel approaching wave crests can be adequately protected by rather widely spaced groins. Figure 24.2 shows such a coast with the groins about 900 m apart. This spacing is extremely wide. Note how the beach between the groins is nearly straight but not parallel to the general coastline; The angle of wave attack (all waves come from one direction here) is obvious.

a. PLAN

b. OBLIQUE PHOTO

Figure 24.2
GROIN PROTECTED COAST, NEW JERSEY, U.S.A.

At the other extreme, groins must sometimes be placed at intervals along the shore about equal to their length. Since the construction of groins is expensive, it is of the utmost importance that they be properly designed themselves and be properly spaced. No simple rules of thumb can be given for the spacing of groins. We can, however, study the morphological consequences of various groin placement schemes using a multiple line simulation in order to determine optimum dimensions for a set of groins. If we wish to be accurate in our simulations, rather complete simulations will be needed; the influence of a groin on the approaching wave pattern will have to be included in the computation - see chapters 16 and 19.

Construction details of a wide variety of groin structures are given in volume I of the *Shore Protection Manual*. Many of the ideas of breakwater design in volume III of this Coastal Engineering Series can also be applied to the design of rubble mound groins.

What are the consequences of a row of groins for the remainder of a coastline? Sand approaching a set of groins from the "up drift" side along the beach will be stopped by the first groin; accretion can be expected there. After this accretion has reached the outer tip of the first groin, sand will begin passing into the space between the first and second groin, and so on. If the protected shore is very long, however, we can best not count on material being passed along in this way past the entire groin protected region for a very long time.

What, then, happens "downdrift" of the last groin? There, there will be an appreciable sand transport capacity in the breaker zone (remember, it was an increasing longshore sand transport capacity that eroded our beach in the first place, before we built groins) but no sand will be moving past the location of the last groin. Severe erosion will result; all of the sand which was originally picked up along the now-protected coast will be eroded from a relatively short portion of the coast just "downdrift" from the last groin. This eroding coast can, in turn, be protected by additional groins, but however many groins we build, we shall encounter an erosion problem somewhere. The groins simply displace a problem.

Still, it can be very useful to build groins. By stabilizing a portion of a beach the erosion problems can be concentrated in a smaller beach segment. Possibly, erosion of that particular segment is not detrimental. On the other hand, we might choose the location to be near a convenient outside source of sand for use in beach nourishment, there.

It is very important to remember that groins do little to prevent the transverse transport of sediment on or off shore. Indeed, transverse sand transport has caused severe erosion of parts of the Dutch coast during heavy storms even though groins were located at regular intervals along the shore. Structures to limit this transverse transport are discussed in the following section.

24.4 Sea walls

Sea walls are massive structures built parallel to a coastline to prevent the transverse transport of material from the coast toward deeper water. These structures are often monolithic structures such as that built along the Dutch coast at Scheveningen. Rubble protected slopes are also possible; the shore protection of the landfill area on the island of Jersey is an example of this. A special case of a seawall is one built within a row of dunes to limit the maximum extent of dune erosion.

An extremely important seawall design problem is that of predicting the maximum depth of erosion near the toe of such a structure. Such information is vital for the geotechnical analysis of the wall and embankment retained by it. How might we attack such a problem?

Figure 24.3 shows a sketch with a seawall embedded in a sand coast in order to limit the maximum erosion during a single very severe storm. In this case, the seawall has been built well back in the dunes and it will be attacked only after a considerable quantity of material has been eroded. The figure shows the same situation as that in the previous chapter - figure 23.5 - with a seawall added. Our problem is that of predicting the depth at the toe of the wall, h_t in the figure.

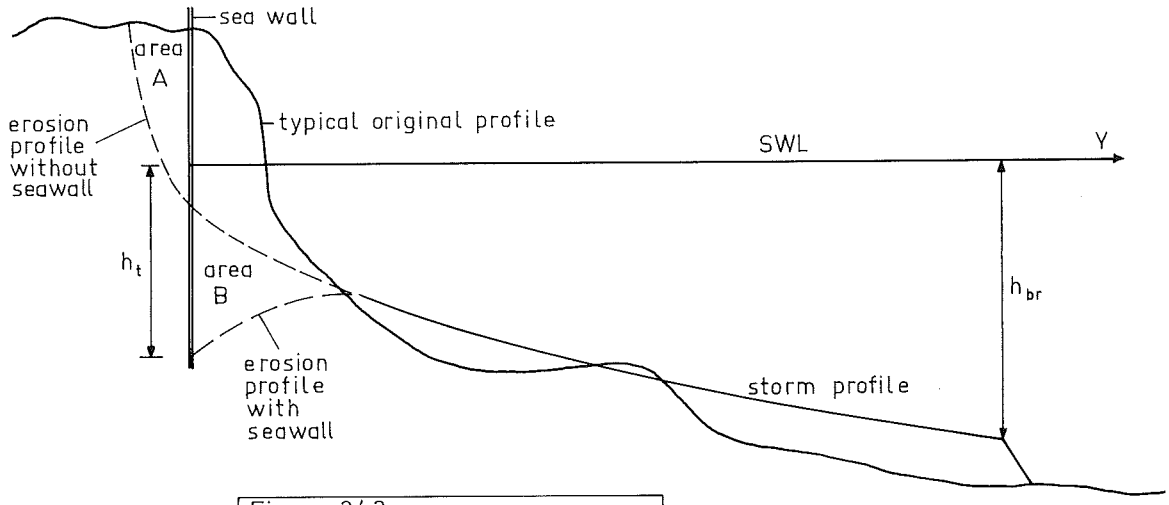

Figure 24.3
DUNES REINFORCED BY SEAWALL
(distortion 1:25)

One possible approach is to first assume that the seawall is not present. The erosion profile can then be computed via the emperical relation (23.01) provided that the design conditions correspond to those on the Dutch coast. The placement of the seawall would then prevent the erosion of a volume of material represented by area A in figure 24.3. If the storm profile were to be maintained, then the extra volume of material eroded from before the seawall - area B in the figure - would be equal to area A. The toe depth, h_t, can be determined, then, when some profile for the local erosion is assumed. Model studies carried out at the Delft Hydraulics Laboratory have indicated, however, that the extra volume of material eroded in front of the seawall - B in the figure - is greater than the volume A. The ratio of the volumes ranged between one and two. In order to maintain continuity of sand when B is larger than A, the entire storm profile apparently shifts slightly seaward. Unfortunately, all of the tests just mentioned were carried out with the seawall initially well buried in the dunes; the volume, A, was small compared to the total volume of sand moved. Extrapolation of these results to more exposed seawalls is, therefore most likely rather uncertain, at least until more experience is gained.

The slope of the seawall has been found to be an important parameter determining the toe erosion depth, h_t. Generally, the erosion depth before a vertical wall was found to be less than below a sloping wall. Most likely this is a result of the standing wave which forms against the vertical wall and the resulting low bottom velocities under the antinode present at the wall. Such a wall orientation may, however, increase the local dynamic forces acting on the wall; these will be more of importance for the structural design rather than the coastal morphology - see volume III for a discussion of these forces.

While theoretical predictions of erosion patterns before seawalls are not yet trustworthy, neither are model investigation techniques sufficiently developed to make dependable erosion predictions for specific cases. Too little is known of the actual processes involved to establish adequate scaling laws needed to relate model and prototype results. Until much further research has been completed, we can evaluate many sea wall type problems only in a qualitative way unless very extensive studies are carried out. Even so, many seawalls have been built in all parts of the world. Their failures can often be attributed to their design conditions being exceeded.

Not all seawalls protect sandy coasts. Figure 24.4 shows one protecting a solid rock coast in Helgoland, Germany.

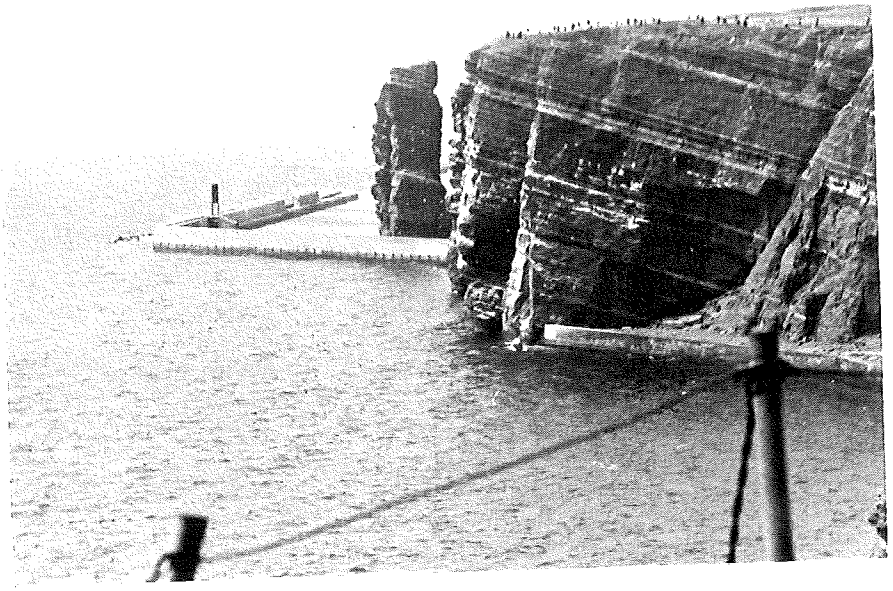

Figure 24.4 SEAWALL PROTECTING ROCK COAST HELGOLAND, GERMANY

Not all seawall designs are so uncertain, however, A rubble mound type seawall - a sort of heavy revetment - has been built on the island of Jersey as part of a landfill project. There, no erosion problems are present since the structure is founded upon solid rock. The only sand anywhere in the vicinity is that being used to make the fill behind the seawall! Even though there is most certainly a sand transport capacity of the waves, the bottom material is immovable and no problems have developed.

24.5 Detached breakwaters

The seawalls just described in the previous section were built on or behind the beach. Soemtimes, it is more desirable to build a series of detached breakwater segments offshore parallel to the coast. Detached in the context used here refers to their lack of connection to the land rather than their possible subdivision into segments. Figure 28.7 of volume I and 24.5, here, show a series of such breakwater segments built on the United States coast in the decade of the thirties. Portions of the coast of Israel have been similarly protected more recently. How do such breakwaters change the coastal processes?

The group of breakwater segments do not obstruct the longshore current or sand transport as such in a direct way as would groins. Instead, they modify the wave pattern between them and the coast; this influences both the current pattern and the longshore and transverse sand transport components. Since wave heights are reduced behind the breakwater segments by diffraction and later also by refraction, the sand transport capacity behind the breakwater is reduced leading to the deposition of material supplied from "updrift" in the lee of the breakwater. Further, the refraction and diffraction patterns behind the breakwater also modify the angle at which the waves approach a given segment of coast. Indeed, waves may approach from several directions simultaneously as waves diffracting around each end of a breakwater segment "collide" in the shadow zone.

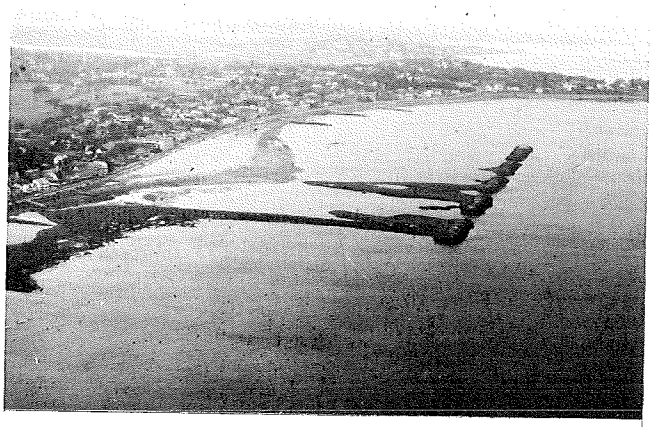

Figure 24.5
DETACHED BREAKWATER SEGMENTS
WINTHROP BEACH, U.S.A.

The transverse movement of sand will also be restricted in most cases. This has happened, for example, near detached breakwaters on the coast of Israel near Tel Aviv.

In principle, it should be possible to compute coastal changes in such a case using a multiple line simulation. The task is not easy, however. The rapidly changing wave conditions will require an extensive force balance to compute proper longshore current velocities - see section 16.6. Also, it will be difficult to properly modify the bottom friction in a sediment transport formula when a confused wave pattern is present. Lastly, the beach changes, themselves, will influence refraction patterns making repeated computation of the wave conditions necessary.

Another approach is to use a physical model study. This, too, will not be without problems. In order to reproduce the phenomona involved correctly, an undistorted model must be used. Unless such a model is very large, however, other scale effects will present problems.

Under certain conditions which are difficult to predict except via an extensive study, sand will accrete behind a breakwater segment until it reaches the breakwater itself and forms a tombolo - see figure 24.5. These "certain conditions" involve the wave climate as well as the breakwater segment lengths, gap widths, and distance from the original coast. If the accretion reaches the breakwater, then all longshore currents behind the breakwater are stopped. This can lead to an accumulation of floating trash which will degrade any recreational value of the beach. On the other hand, when a coast has accumulated nearly to a breakwater - has not reached it - the resulting longshore current concentration can result in a locally steep beach which can be dangerous for bathers.

In some cases, tombolos do not even extend above the water nor do their "breakwaters". Figure 24.6 shows such a natural tombolo near Plymouth, Massachusetts in the United States. The shoal extending outward and the irregularity in the otherwise straight coastline both result from the submerged rocky outcrop - High Pine Ledge - offshore.

24.6 Accretion control

The previous sections of this chapter have been concerned primarily with eroding coasts and measures to stabilize them. Not all problems originate with erosion, however. Occasionally accretion needs to be controlled in order to prevent its "spilling over" into areas where accretion would be detrimental. An excellent example of this "spilling over" is the movement of sand past the end of a breakwater built to protect a dredged harbor entrance channel. Methods to predict the quantity of sand passing the breakwater using a single-line simulation model were presented in chapter 20. What, however, is the best method to prevent this undesired movement of sand?

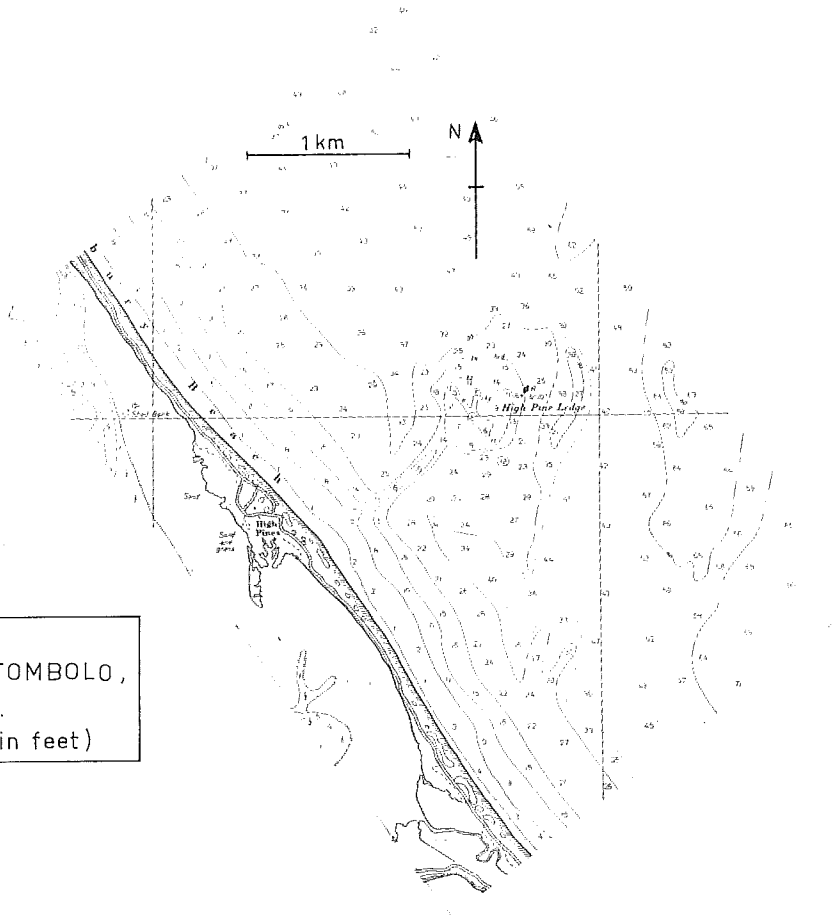

Figure 24.6
SUBMERGED, NATURAL TOMBOLO, PLYMOUTH, MASS., U.S.A.
(scale as shown, depths in feet)

Such a problem is illustrated somewhat schematically in figure 24.7. There, accretion has progressed to the point where sand is already by-passing the end of the breakwater at A. This is evidenced by the fact that the angle of the accreted beach is less than ϕ' at that point - see chapter 20.

One possible but rather uninspired method to halt the sand by-passing would be to simply extend the breakwater seaward at A as indicated by the dashed lines there in figure 24.7. This extention might even have been suggested when the original breakwater was built, but discarded because of the high construction cost in the relatively deep water. Such an extension at A would, of course, halt the by-passing immediately and remain effective until the accretion area had once again built out to the new breakwater tip. Figure 24.8 shows the development of the sand transport past the breakwater tip calculated using equation 20.49 in conjunction with table 20.2. If we assume that a breakwater extension at A is long enough to stop sand transport past the breakwater tip until a time equal to 1.5 times the original t_1, then a new curve labeled A in figure 24.8 can be computed using new time scale values in a way exactly similar to that used to compute the first curve shown.

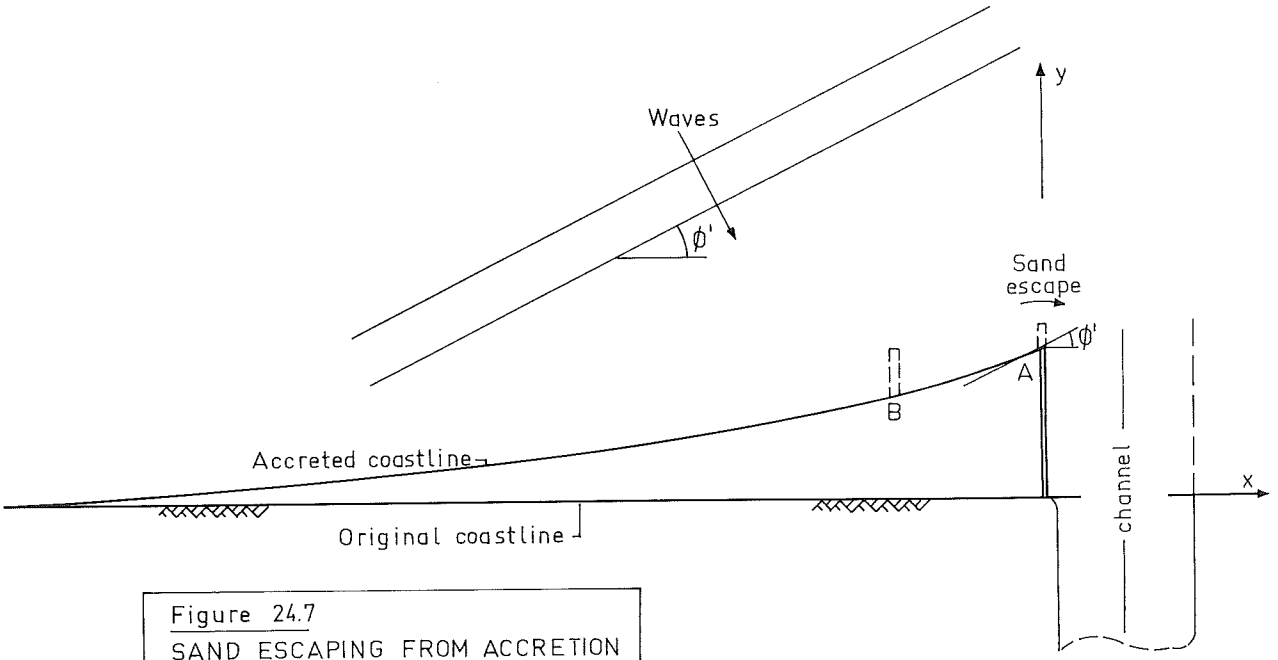

Figure 24.7
SAND ESCAPING FROM ACCRETION AREA WITH POSSIBLE COUNTER-MEASURES. (no scale)

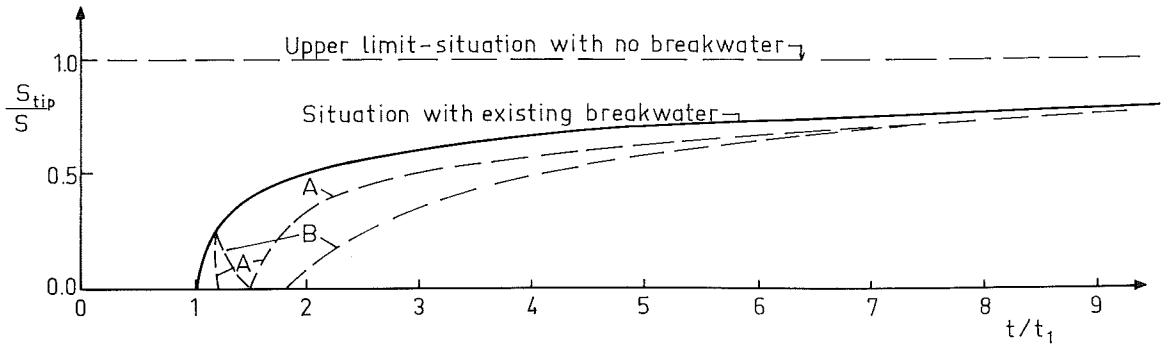

Figure 24.8
DEVELOPMENT OF SAND TRANSPORT PAST BREAKWATER TIP

A more inspired solution to the problem might be to construct a sort of groin on the beach somewhere "updrift" from the breakwater on the accreting beach - point B in figure 24.7. Construction of such a groin will immediately stop the sand transport past point B, but not past point A, as shown for the first, declining part of curve B in figure 24.8. That sand passing A is being eroded from the beach segment between B and A until the angle of the beach at A is once again equal to ϕ'. Ultimately, of course, sand will pass by the groin tip at B but not all of this sand will pass point A; some of it will be

retained between A and B rebuilding that coastline segment. The increasing portion of curve B in figure 24.8 lies below curve A, therefore. In contrast to the other curves, curve B is shown only qualatatively in figure 24.8; the precise form of the curve depends upon the time at which the extra groin is built ($t/t_1 = 1.20$ is shown), the length of the groin, and the distance A-B. The multiple line simulation method already presented can be used to predict the exact behavior, however.

25. CHANNEL SEDIMENTATION

E.W. Bijker
W.W. Massie

25.1 Introduction

All of the morphology problems discussed so far have involved rather slowly varying parameters; the gradients of wave height, or even sand transport with respect to position were small. Except for these slowly varying conditions, our problems have involved only abrupt boundary conditions such as the fact that the sand transport was stopped completely by a breakwater. How, now, must we approach a channel sedimentation problem?

To make the discussion more specific, consider, for example, the sand escaping around the tip of the breakwater, A, in figure 24.7 of the previous chapter. The theory of the previous chapters has been concentrated so far on answering the question of what happens to that accreting beach and how much sand escapes. Indeed, any reader should be able to answer that question by now. Our problem, now, however, is: What is happening with the sand passing around the breakwater tip, A, in figure 24.7? How much of that sand falls into our channel, and how much, if any, of that sand passes across to the other side where it will ostensibly be carried further? The answers to these questions are sought in the remainder of this chapter.

25.2 Physical changes

The physical parameter variations which influence the sediment transport after passing the tip of the breakwater in figure 24.7 are much more, now, than a change in the angle of the shore relative to the approaching wave crests. The most striking additional changes which occur are that the depth increases rather rapidly and the wave conditions change as we cross the channel; additional current components are also present. Generally the channel will be too deep for wave breaking to occur within it. Figure 25.1 illustrates the parameter changes more clearly. The location of a profile drawn *along* the beach within the breaker zone and *across* the channel is indicated by the dashed line C D in figure 25.1a. This profile, itself, is shown in figure 25.1b. Note that the depths on each side of the channel are unequal in figure 25.1b; this reflects the influence of the accretion of sand to the left of the breakwater. The depth corresponding to the outer edge of the breaker zone, h_{br}, is also shown in the longshore profile. Figure 25.1b shows a very abrupt change in water depth on each slope of the channel. Also, all wave breaking ceases in the area of interest to the right of the breakwater location. These changes have a multitude of consequences for the sediment transport along and across the channel.

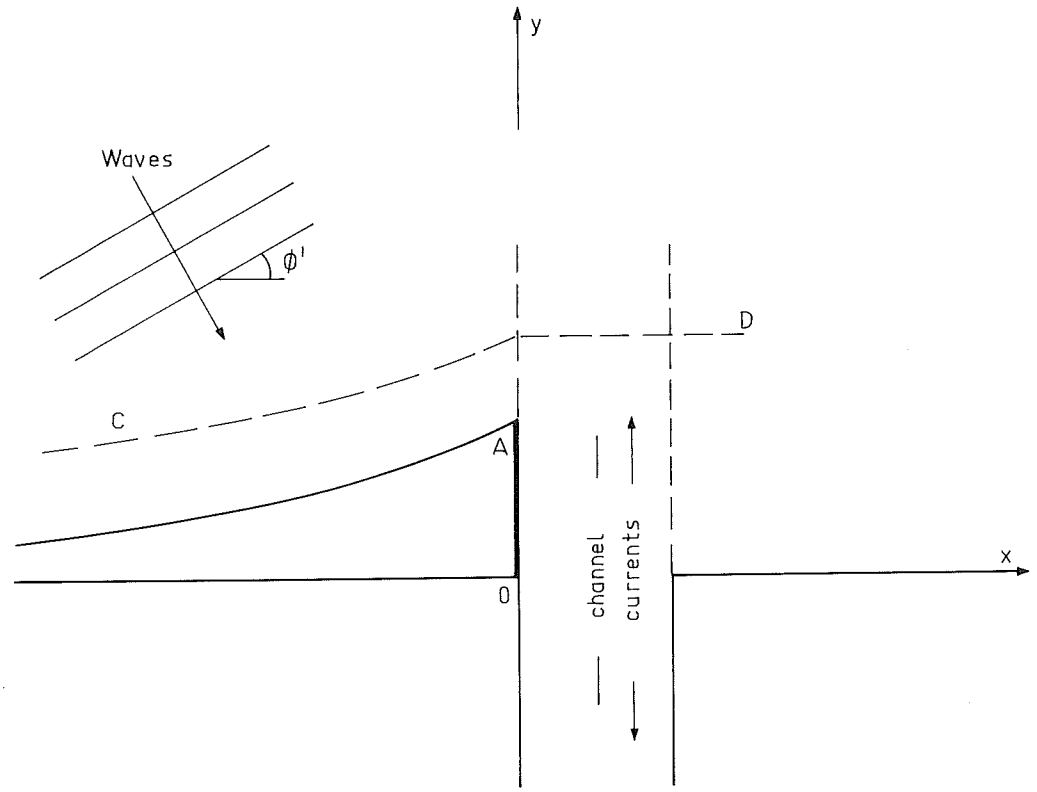

a. Plan adapted from figure 24.7

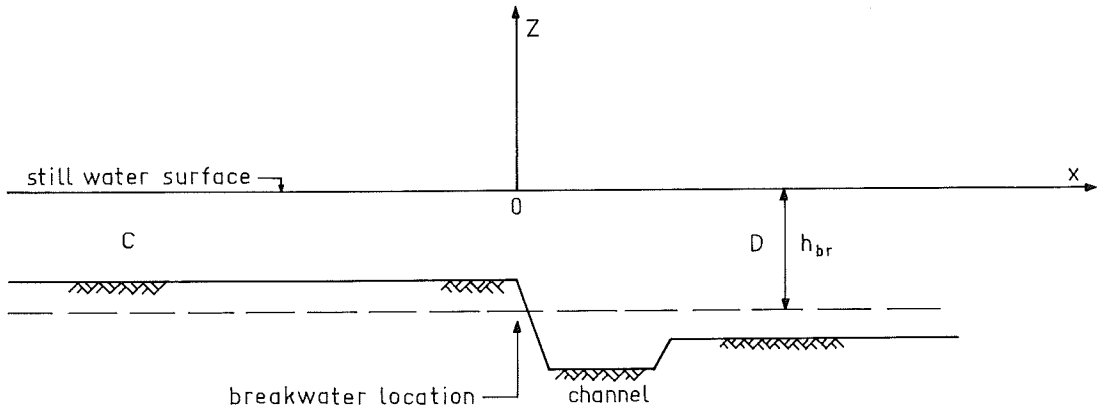

b. Profile C D (vertical scale distorted)

Figure 25.1
SHORE PLAN AND LONGSHORE PROFILE

A purely physical change is an altered current pattern in and beyond the channel. As soon as the breaker zone ends near the breakwater tip, the driving force for the longshore current - at least the shear stress gradient in the radiation stress - disappears - see chapter 12. A rapid change in wave set-up as well as set-down will also occur between the accreting beach and the channel. This will yield force components along the longshore profile whose direction depends upon the resulting water surface slope direction. - see section 16.6.

Further, wave height changes will occur along profile C-D to the right of the breakwater location. These changes, both in direction of approach and height, are caused by variations in refraction and shoaling resulting from the bathymetry differences. This means, then, that all of the radiation stress componenets will be changing quite rapidly near the channel.

The physical result of all this is that the physical cross-channel driving force component will certainly not look anything like equation 12.15 which was based only upon a radiation shear stress gradient. A new force balance will have to be formulated in order to determine the current.

Even though the waves are no longer breaking in the channel, the waves will still influence the bottom friction since they still cause velocity components at the sea bed except in very deep water - see chapter 5 of volume I. Equation 15.28 can still be used to evaluate the friction force since the derivation of the friction relationship in chapter 15 is general up to that point. Of course, the correct velocity, V, must be included in that equation. Not only friction and transverse gradients determine this velocity; longitudinal force gradients are very important as well and may even cause a channel velocity to be nearly parallel to the channel axis. The most obvious longitudinal driving force would result for the combined effects of tides and possible fresh water discharge. The force balance needed to predict the velocity distribution is too complex for theoretical treatment here.

An additional physical complication for the currents results from the fact that conditions vary quickly over short distances. This means that currents will be accelerating and decelerating in the area of the breakwater tip; inertia influences will also have to be included in a force balance. These have been avoided completely until now by stipulating that changes occur only slowly so that inertia influences could be neglected.

How does all of this affect the sediment transport? The effects on the two components of sediment transport, bed load, and suspended load, are indicated in the next sections.

25.3 Bed load transport

Bed load sediment transport responds very quickly to changes in physical conditions. The bed load transport is determined almost exclusively by the local conditions of velocity and bed shear stress. The repeated stirring up and re-settlement of sand grains near the bottom during a single wave period are evidence of this - refer to chapter 18.

This "lack of inertia" of the bed load implies that bed load transport rates can be computed relatively easily at any chosen location once the current and wave conditions have been determined. The Bijker approach reflected in equations 19.34 can be used. These relationships are independent of wave breaking and, therefore, may be used anywhere in the region of interest.

Once the bed load transport rate is known as a function of position we might compute bed load erosions and sedimentations. While this would be easy, it would only be of practical value when the suspended load transport remained either neglible or constant. This is the topic of the next section.

25.4 Suspended load transport

Suspended load presents considerably more of a problem than does the bed load. The suspended load is, of course, distributed over the entire depth at any location. Since suspended material will settle out no faster than its fall velocity (it reaches this speed only in perfectly still water) any settling or suspending process will occur gradually. The suspended sediment concentration at some given point will, therefore, be dependent upon the immediately local conditions of turbulence and bed load as well as the past history of these; the suspended sediment transport *does* demonstrate "inertia".

Since Einstein developed his formula - equation 19.17 - for a steady state condition, the relationships for suspended load transport developed in chapter 19 will be incorrect, now, in this typically non-steady state problem. In general, changes in suspended load transport will occur more slowly than equations such as (19.17) might lead the user to expect.

While it would, in principle, be possible to derive proper transient state concentration and suspended sediment relationships, the effort would not justify the reward; a simpler, more approximate approach is outlined below.

25.5 An approximate solution

In order to arrive at a workable solution to a channel siltation problem, the following crude method is suggested. Instead of obtaining a single approximate sedimentation value, we shall determine limits between which the channel morphological changes must lie. This will be based upon the sediment transport equations already developed for steady state conditions.

The first step in the procedure is to evaluate the physical conditions at several critical places. Several points just outside the channel and a few points spaced along the channel axis should be sufficient to predict channel morphological changes near the breakwater tip.

The second step is to evaluate the bed load transport and suspended load transport separately at each of the points just chosen. This is done under the incorrect assumption that the situation is only slowly changing.

The sedimentation or erosion of an area by bed load transport can be found rather accurately by examining the changes in transport rates between the chosen points in and around that area - the points chosen in step one. Since bed load transport demonstrates little "inertia", this result is probably quite accurate.

If deposition of suspended material is expected (the suspended sediment transport decreases) then the *maximum* deposition of this material can be found by comparing the two steady-state suspended sediment transport rates. Similarly, a *maximum* suspended load erosion can be found by comparing these steady state rates where erosion by suspended material transport is expected. These rates of deposition or erosion are maximum values by virtue of the "inertia" effect of the suspended sediment transport; the actual suspended load transport changes cannot be more than these. Therefore, the bed load transport change plus the maximum suspended load transport change will yield the upper limit erosion or deposition.

At the other extreme and especially with deposition, no significant actual change in suspended load transport may take place until well beyond the channel. This would become more true as the grain size of the suspended sediment or channel width decreased. Thus, a lower limit on erosion or deposition could be found by considering only bed load transport changes.

Unfortunately, no moer specific information can be given; much research in this area is needed in order to sort out the multitude of parameters involved and to determine their functional relationships.

Extra Notes

SYMBOLS AND NOTATION W.W. Massie

The symbols used in this set of notes are listed in the table. International standards of notation have been used where available except for occasional uses in which direct conflict of meaning would result. Certain symbols have more than one meaning, however this is only allowed when the context of a symbol's use is sufficient to define its meaning explicitly. For example, T is used to denote both wave period and temperature.

Functions are denoted using the British and American notation. The major discrepancy with European continental notation occurs with the inverse trigonometric functions. Thus, the angle whose sine is y is denoted by:

$\sin^{-1} y$ instead of arc sin y.

Possible confusion is avoided in these notes by denoting the reciprocal of the sine function by the cosecant function, csc, or by $\frac{1}{\sin}$. This same rule applies to the other trigonometric and hyperbolic functions as well.

In the table a meaning given in capital letters indicates an international standard. The meaning of symbols used for dimensions and units are also listed toward the end of the table.

Roman letters

Symbol	Definition	Equation	Dimensions	Units
A	energy density	fig. 3.5	$L^2 T^{-1}$	m^2/s
	coefficient	17.01	$M^{-1} L^2 T^2$	
	dimensionless roughness	19.18	--	--
a	amplitude of orbital displacement	15.16	L	m
	integration limit	19.10	L	m
	coefficient	20.11	$L^2 T^{-1}$	m^2/s
B	ship's beam	3.04	L	m
	distance from course line	5.01	L	m
	coefficient	19.01	--	--
b	distance between wave orthogonals	12.02	L	m
C	Chézy friction coefficient	13.01	$L^{1/2} T^{-1}$	$m^{\frac{1}{2}}/s$
C'	Chézy friction coefficient	19.46	$L^{1/2} T^{-1}$	$m^{\frac{1}{2}}/s$
C_B	block coefficient	3.04	--	--
c	wave celerity	3.02	$L T^{-1}$	m/s
	concentration	9.01	--	--
D	ship draft	3.04	L	m
	particle grain size	19.01	L	μm
D_{90}	particle grain size	19.46	L	μm
DWT	deadweight tonnage	ch.3	M	kg

Symbol	Definition	Equation	Dimensions	Units
E	chance or probability	4.13	--	--
	wave energy per unit surface area	10.02	$M\ T^{-2}$	N/m
e	BASE OF NATURAL LOGARITHMS	4.07	--	--
F_{tide}	tidal force per unit area	13.02	$M\ L^{-1}\ T^{-2}$	N/m^2
f	friction factor	15.15	--	--
g	ACCELERATION OF GRAVITY	10.02	$L\ T^{-2}$	m/s^2
H	wave height	4.23	L	m
h	water depth	4.01	L	m
	height of schematizing layer	20.04	L	m
h'	wave set-up	11.01	L	m
I	extra channel depth allowance	4.01	L	m
	Einstein integral values	19.18	--	--
i	interest rate	4.26	--	--
K	wave number of tide	13.04	L^{-1}	m^{-1}
K_r	refraction coefficient	17.07	--	--
k	wave number	10.01	L^{-1}	m^{-1}
L	ship length	3.04	L	m
	water level	4.01	L	m
	effective breakwater length	20.22	L	m
	distance to beach schematization	21.02	L	m
L_c	channel length	4.09	L	m
ℓ	mixing length	14.02	L	m
M	coefficient	20.30	L	m
M'	maximum number of ships	4.14	--	--
m	index counter	4.17	--	--
	beach slope	12.15	--	--
m'	accretion beach slope	20.26	--	--
N	number of waves encountered	4.12	--	--
	number of extreme values	5.03	--	--
n	wave velocity ratio	10.03	--	--
n	number of payments	4.26	--	--
pwf	present worth factor	4.26	--	--
Q	integral value	19.20	--	--
q	rate of change of sand transport per unit width	21.06	$L\ T^{-1}$	m/s
	dummy variable	4.07	--	--
R	response transfer function	fig. 3.5	--	--
R'	roughness allowance	4.01	L	m

Symbol	Definition	Equation	Dimensions	Units
S	radiation stress component	10.01	$M T^{-2}$	N/m
	sediment transport	17.08	$L^3 T^{-1}$	m^3/yr
	sediment transport per unit width	9.01	$L^2 T^{-1}$	m^2/yr
s	instantaneous ship position	4.02	L	m
	rate of change of sediment transport	20.05 21.06	$L^3 T^{-1}$ $L T^{-1}$	m^3/yr m/s
T	wave PERIOD	4.27	T	s
T'	tide PERIOD	13.03	T	s
T_e	PERIOD of encounter	3.03	T	s
t	TIME	4.02	T	s
U'	Wave "energy component"	17.01	MLT^{-3}	N/s
u	velocity component in X direction	15.17	$L T^{-1}$	m/s
	dummy parameter	20.18	--	--
u'	velocity fluctuation in x direction	14.01	$L T^{-1}$	m/s
V	VELOCITY	13.01	$L T^{-1}$	m/s
V_r	resultant VELOCITY	15.22	$L T^{-1}$	m/s
V_*	"shear" VELOCITY	15.04	$L T^{-1}$	m/s
v	VELOCITY component in Y direction			
	volume of sand accumulated	20.41	L^3	m^3
v'	VELOCITY fluctuation in y direction	14.01	$L T^{-1}$	m/s
v_s	ship VELOCITY	3.02	$L T^{-1}$	m/s
W	equilibrium width of schematized beach	21.06	L	m
	sediment particle fall velocity	19.12	$L T^{-1}$	m/s
X	COORDINATE in direction of wave propagation	10.01	L	m
x	COORDINATE along channel	4.02	L	m
	COORDINATE in direction of sand transport	9.01	L	m
x	COORDINATE along coast	13.01	L	m
	dummy variable	4.07	--	--
Y	COORDINATE along wave crest	10.04	L	m
y	COORDINATE perpendicular to coast	14.01	L	m
Z	vertical COORDINATE		L	m
	tide level	13.03	L	m
	ship squat plus trim	4.01	L	m
z	vertical COORDINATE	9.01	L	m
z'	vertical COORDINATE	15.02	L	m
z'_o	elevation for zero velocity	15.04	L	m
z'_t	elevation for velocity profile tangency	15.09	L	m
z^*	dimensionless depth	19.15	--	--

Greek letters

Symbol	Definition	Equation	Dimensions	Units
α	angle of approach of waves relative to ship	3.02	--	--
β	angle of accretion at breakwater tip	20.39	--	--
γ	wave breaking index	11.04	--	--
Δ	relative density of sediment	19.01	--	--
δ	parameter	21.09	L	m
ε	spectrum width parameter	ch 5	--	--
	eddy viscosity	14.01	$L^2\ T^{-1}$	m^2/s
	turbulent diffusion coefficient	19.12	$L^2\ T^{-1}$	m^2/s
η	water surface elevation	9.01	L	m
Θ	angle relative to principal plane	10.06	--	--
	value of integral	20.19	--	--
κ	Von Kármán coefficient	15.04	--	--
λ	WAVE LENGTH	10.01	L	m
μ	ripple factor	19.45	--	--
ξ	parameter	15.29	--	--
π	constant = 3.1415926536	3.03	--	--
ρ	mass density of (sea) water	3.04	$M\ L^{-3}$	kg/m^3
σ	standard deviation	4.03	depend upon problem	
τ	shear stress	14.01	$M\ L^{-1}\ T^{-2}$	N/m^2
ϕ	angle of wave approach relative to instantaneous coast	12.01	--	--
ϕ'	angle of wave approach relative to initial coast	20.08	--	--
Ω	tidal wave frequency	13.03	T^{-1}	1/s
ω	surface wave frequency	3.02	T^{-1}	1/s
ω_e	wave encounter frequency	3.02	T^{-1}	1/s

Special symbols

Symbol	Definition
$\overline{\ldots\ldots}$	time average of ....
$.\hat{.}.$	amplitude of ....
α	is proportional to
Δ	change in ....
∞	infinity

Subscripts

Symbol	Definition
b	bottom
bc	bottom, current
br	breaker line
c	keel clearance
cr	critical
cw	current and wave
i	counter index
L	still water level
m	maximum
min	minimum
o	deep water (except ch. 21)
p	particle
r	roughness
	resultant
	refraction
rms	root-mean-square
s	ship
sig	significant
t	at point of tangency
tip	tip of breakwater
w	wave
x	x component
xx	x component of normal stress
xy	x component of shear stress
y	y component
yx	y component of shear stress
yy	y component of normal stress
η	wave, water surface
1	
2	used to distinguish similar values actual meaning
3	from context

Functions

Notation	Meaning
cos ( )	cosine of the angle ( )
cosh ( )	hyperbolic cosine of ( )
exp ( )	e raised to the power ( )
f ( )	general function of ( )
ln ( )	natural logarithm of ( )
P ( )	chance of exceedance of ( )
p ( )	chance of occurrance in interval characterized by ( )
sin ( )	sine of the angle ( )
sinh ( )	hyperbolic sine of ( )
tan ( )	tangent of the angle ( )
tanh ( )	hyperbolic tangent of ( )
Δ	change in
Π ( )	product of ( )
$\sum$ ( )	sum of ( )

Dimensions and units

Symbol	Definition
cm	centimeter
ft	foot
h	hour
kg	KILOGRAM
km	kilometer
kt	knot = nautical miles per hour
L	LENGTH DIMENSION
M	MASS DIMENSION
m	METER
mm	milimeter = 10^{-3} m
µm	micrometer = 10^{-6} m
N	newton
rad	radian
s	second
T	TIME DIMENSION
yr	year
o	degree angle

REFERENCES

The following list includes bibliographic data on most (and hopefully all) of the references used in the previous chapters. Works are listed in alphabetical order by first author and in sequence of publication.

Ackers, P.; White, W.R. (1973): Sediment Transport: New Approach and Analysis: *Journal of the Hydraulics Division*: American Society of Civil Engineers: volume 99, number HY 11, November: pp 2041-2060.

Allersma, E. (1968): Mud on the Oceanic Shelf off Guiana: *Symposium on Investigations and Resources of the Caribbean Sea and Adjacent Regions*: Willemstad, Curaco, 18-26 November: pp 193-203, FAO, UNESCO.

——; Massie, W.W. (1973): *Statistical Description of Ocean Waves*: Coastal Engineering Group, Department of Civil Engineering, Delft University of Technology, Delft, The Netherlands.

Anonymous (1972): *Method for Computing Dune Erosion Resulting from A Severe Storm*: Technical Advisory Commission for Flood Prevention, Ministry of Public Works (Rijkswaterstaat), The Hague, The Netherlands.
In Dutch, original title: *Richtlijn voor de Berekening van Duinafslag ten gevolge van een Stormvloed.*

—— (1973): *Shore Protection Manual*: U.S. Army, Coastal Engineering Research Center: published by U.S. Government Printing office, Washington D.C., U.S.A.

—— (1974): Problems of Large Vessels in Shallow Water: *The Motor Ship*: number 648, pp 573-575, July.

——;(1976): *Computation of Longshore Transport*; Delft Hydraulics Laboratory report R968 part 1, September; Delft, The Netherlands.

Baker, Elijah, III (1952): *Introduction to Steel Shipbuilding*: second edition: Mc Graw-Hill Book Company, New York, U.S.A.

Bakker, W.T. (1968): The Dynamics of A Coast with A Groyne System: *Proceedings: 11th Coastal Engineering Conference*: volume I, chapter 31: London.

——(1971): *The Influence of the Longshore Variation of the Wave Height on the Littoral Current*: Study Report WWK 71-19: Ministry of Public Works (Rijkswaterstaat), The Hague, The Netherlands.

Battjes, J.A. (1974): *Computation of Set-Up, Longshore Currents, Run-Up and Overtopping due to Wind-Generated Waves*: Delft University of Technology Communications on Hydraulics, number 74-2. Department of Civil Engineering.

——(1975): Modeling of Turbulence in the Surf Zone: *Proceedings of Symposium on Modelling Techniques*: San Francisco: American Society of Civil Engineers: pp 1050-1061.

——(1976): *Radiation Stress*: Lecture notes for course on short waves: Fluid Mechanics Group, Department of Civil Engineering, Delft University of Technology, Delft, The Netherlands.
In Dutch, original title: *Golfspanning*.

——;Roos, A. (1976): Characteristics of Flow in Run-Up of Periodic Waves: *Proceedings of 15th Coastal Engineering Conference*: Honolulu, July.

Bijker, E.W. (1967): *Some Considerations about Scales for Coastal Models with Movable Bed*: Doctorate Dissertation, Delft University of Technology.
Also appeared as: Publication number 50, Delft Hydraulics Laboratory, Delft, The Netherlands.

——(1968): *Littoral Drift as A Function of Waves and Current*: Delft Hydraulics Laboratory publication number 58, 1969.
An extended summary also appears in: *Proceedings of the 11th Coastal Engineering Conference*: London, 1968.

——; Kalkwijk, J.; Pieters, T. (1975): *Mass Transport in Gravity Waves on A Sloping Bottom*: report 75-1, Department of Civil Engineering, Delft University of Technology, Delft, The Netherlands. Also appears in: *Proceedings of the 14th Coastal Engineering Conference*: Copenhagen, Denmark, June 1974.

Bowen, A.J. (1969): The Generation of Longshore Currents on A Plane Beach; *Journal of Marine Research*: volume 27, number 2, pp 206-215.

——;RipCurrents: *Journal of Geophysical Research*: volume 73, number 23, pp 5467-5490.

Chow, Ven Te (1959): *Open Channel Hydraulics*: Mc Graw - Hill Book Company, New York, U.S.A.

Comstock, John P - editor - (1967): *Principles of Naval Architecture*: The Society of Naval Architects and Marine Engineers, New York, U.S.A.

Dorrestein, R. (1961): On the Deviation of the Average Pressure at A Fixed Point in A Moving Fluid from its "Hydrostatic" Value: *Applied Scientific Research*, volume 10, section A, pp 384-392.

Eden, Edwin W. Jr. (1971): Vessel Controllability in Restricted Waters: *Journal of the Waterways, Harbors, and Coastal Engineering Division*: volume 97, number WW3, pp 475-490, August: American Society of Civil Engineers, New York, U.S.A.

Einstein, H.A. (1950): *The Bed-Load Function for Sediment Transportation in Open Channel Flows*: United States Department of Agriculture, Soil Conservation Service, Technical Bulletin number 1026.

Engelund, F.; Hansen, F. (1967): *A Monograph on Sediment Transport in Alluvial Channels*: Teknisk Forlag, Copenhagen, Denmark.

Frijlink, H.C. (1952): Discussion of the Sediment Transport Formulas of Kalinske, Einstein, and Meyer-Peter and Mueller in relation to recent Sediment Transport Measurements in Dutch Rivers: *2 me Journal Hydraulique*: Soc. Hydraulique de France, Grenoble: pp 98-103.
In French, original title: Discussion des Formules de Débit Solide de Kalinske, Einstein, et Meyer-Peter et Mueller compte tenue des mesures récentes de transport dans les rivières Néerlandaises.

van Hijum, E. (1972): *Skew Coastal Accretion Near A Breakwater*: unpublished research manuscript, Coastal Engineering Group, Delft University of Technology.
In Dutch, original title: *Kustaangroei voor een Dam bij Niet-Evenwijdige Aangroei*.

Jonsson, I.G. (1975): *The Wave Friction Factor Revisited*: Progress Report number 37, pp 3-8. Institute for Hydrodynamics and Hydraulic Engineering, Technical University of Denmark, Lyngby, Denmark.

Kalinske, A.A. (1947): Movement of Sediment as Bed Load in Rivers: *Transactions of the American Geophysical Union*, volume 28, number 4, pp 615-620.

von Kármán, Theodore (1930): Mechanical Similarity and Turbulence: *Proceedings of 3rd International Congress of Applied Mechanics*: volume I, pp 85-92: Stockholm, Sweden.
In German, original title: Mechanische Äehnlichkeit und Turbulenz.

Kennedy, J.F.; Locher, F.A. (1971): Sediment Suspension by Water Waves: *Waves on Beaches and Resulting Sediment Transport*: Proceedings of an Advanced Seminar, Mathematics Research Center Publication number 28, pp 249-295: University of Wisconsin, Madison, Wisconsin, U.S.A.

Komar, P.D. (1976): Evaluation of Wave-Generated Longshore Current Velocities and Sand Transport Rates on Beaches: article in: *Beach and Nearshore Sedimentation* (R.A. Davis, Jr. and R.L. Ethington, editors): Special Publication number 24: Society of Economic Paleontologists and Mineralologists.

Kray, Casimir, J. (1973): Design of Ship Channels and Maneuvering Areas: *Journal of the Waterways, Harbors and Coastal Engineering Division*: volume 99, number WW1, February, pp 89-110. American Society of Civil Engineers, New York, U.S.A.

Kroese, G.M.; Nieuwenhuyse, P. (1974): *Possibility to Use Tugboats to Assist Large Ships in Exposed Channels*: Student Thesis, Coastal Engineering Group, Department of Civil Engineering, Delft University of Technology.
In Dutch, original title: *Bijdrage tot het onderzoek naar de Mogelijkheid van het met Behulp van Grote Havensleepboten te Assisteren bij de Besturing van Mammoetschepen in een Scheepvaartgeul Buitengaats.*

Longuet-Higgins, M.S. (1953): Mass Transport in Water Waves: *Phil. Transactions Royal Society, London*: A., volume 245, number 903, pp 535-581.

——;Stewart, R.W. (1962): Radiation Stress and Mass Transport in Gravity Waves, with Application to Surf Beats: *Journal of Fluid Mechanics*: volume 13, pp 481-504.

——;——(1963): A Note on Wave Set-Up: *Journal of Marine Research*: volume 21, pp 4-10.

——;——(1964): Radiation Stresses in Water Waves: A Physical Discussion with Applications: *Deep Sea Research*: volume 11, pp 529-562.

——;(1971): Recent Progress in the Study of Longshore Currents: *Waves on Beaches and Resulting Sediment Transport*: Proceedings of an Advanced Seminar, Mathematics Research Center Publication number 28, pp 203-248: University of Wisconsin, Madison, Wisconsin, U.S.A.

Moore, G.W.; Cole A.Y. (1960): Coastal Processes, Vicinity of Cape Thompson, Alaska: *Geologic Investigations of Cape Thompson, N.W. Alaska-Preliminary Report*: Trace Element Investigation Report 753, U.S. Geological Survey, Washington D.C., U.S.A.

Oldenkamp, I. (1973): Statistical Analysis of Ship's Manoeuvres: Prepints, Symposium on Ship Handling, Netherlands Ship Model Basin, Wageningen, The Netherlands.

Pelnard-Considère (1954): Essay on the Theory of the Evolution of the Form of Beaches and Bars: *Quatroème Journées de l'Hydraulique*, Paris; Question 3, Les Energies de la Mer.
In French, original title: Essai de Théorie à l'Evolution des Formes de Rivages en Plages de Sables et de Galets.

Prandtl, Ludwig (1926): On Fully Developed Turbulence: *Proceedings of the 2nd International Congress of Applied Mechanics, Zurich*: pp 62-74.
In German, original title: Über die Ausgebildete Turbulenz.

Svašek, J.N.; Bijker, E.W. (1969): Two Methods for Determination of Morphological Changes Induced by Coastal Structures: *Proceedings of the 22nd International Navigation Congress, Paris*: subject II-4 pp 181-202: Permanent International Association of Navigation Congresses, Brussels, Belgium.

Swart, D.H. (1974): *Offshore Sediment Transport and Equilibrium Beach Profiles*: Doctorate Dissertation, Department of Civil Engineering, Delft University of Technology.
Also: Publication number 131: Delft Hydraulics Laboratory.
And Also: Report M918, part 2: Delft Hydraulics Laboratory, Delft, The Netherlands.

Thornton, E.B. (1970): Variation of Longshore Current Across the Surf Zone: *Proceedings of the 12th Coastal Engineering Conference*: volume I, chapter 18, pp 291-308.

Wanhill, Stephen R.C. (1974): Further Analysis of Optimum Size Seaport: *Journal of the Waterways, Harbors and Coastal Engineering Division*: volume 100, number WW4, pp 377-383: American Society of Civil Engineers, New York, U.S.A.

Wiegel, Robert L. (1964): *Oceanographical Engineering*: Prentice-Hall, Inc.: London.

Hinze, J.O. (1962): *Momentum and Mechanical Energy Balance Equations for A Flowing Homeogeneous Suspension with Slip Between the Phases*: Applied Scientific Research, volume 33, number A 11.

Kerssens, P.J.M.; van Rijn, L.V. (1977): *Model for Non-Steady Suspended Sediment Transport*: Delft Hydraulics Laboratory Publication 191, also included in the Proceedings of 17th Congress of IAHR in Baden-Baden.

Swart, D.H. (1976): *Coastal Sediment Transport: Computation of Longshore Transport*: Delft Hydraulics Laboratory, Report of Investigation R968, part I.